



Modelling Moving Evaporation Fronts in Porous  
Media

Zafar Hayat Khan

Department of Mathematics and Statistics

University of Strathclyde

Glasgow, UK

December 2011

This thesis is submitted to the University of Strathclyde for the  
degree of Doctor of Philosophy in the Faculty of Science.

This thesis is the result of the authors original research. It has been composed by the author and has not been previously submitted for examination which has led to the award of a degree.

The copyright of this thesis belongs to the author under the terms of the United Kingdom Copyright Acts as qualified by University of Strathclyde Regulation 3.50. Due acknowledgement must always be made of the use of any material contained in, or derived from, this thesis.

Signed:

Date:

# Acknowledgements

First and foremost, I would like to thank my supervisor, David Pritchard and co-supervisor John Mackenzie for the invaluable advice and friendly support they have given me over the past three years. Without their enthusiasm for their work and guidance, this thesis would not have been possible. They deeply influenced me and profoundly changed my thinking in the most positive way imaginable.

I am always grateful to Waqar Ahmed Khan and Inayat Ali Shah for mentoring and support throughout my research career.

I acknowledge University of Malakand for the financial support throughout my postgraduate studies.

I would like to extend my appreciation to all my friends and colleagues, who have inspired me over the course of my stay in Glasgow. In particular, Adnan Khan, Franck Kalala Mutombo and Chanpen Phokaew for all their help and friendship. I have really enjoyed my very productive time at the Department of Mathematics and Statistics, University of Strathclyde. Special thanks goes to Richard Rankin for his sincere friendship and for making me feel so welcome.

My final acknowledgments are to my family who encouraged and accompanied me in every step of my life with great patience. I cannot repay them for their wholehearted support in every possible way.

# Abstract

Understanding vertical heat transfer and through flow in porous media such as geothermal reservoirs is of great interest. In a geothermal system, a denser layer of liquid water may overlie a less dense layer of water vapour. Vertical and horizontal thermal diffusion stabilises such configurations, but the buoyancy contrast can cause instability.

In this study, the mechanisms contributing to the stability and instability of such systems are analysed using a separate-phase model with a sharp interface between liquid and vapour. The governing equations representing incompressibility, Darcy's law and energy conservation for each phase are linearised about suitable base states and the stability of these states is investigated. We have considered two different thermal boundary conditions, both with and without a vertical through-flow.

In the first case, the boundaries above and below the layer of interest are assumed to be isothermal. We found that due to the competition between thermal and hydrostatic effects, the liquid–vapour interface may have multiple positions. A two-dimensional linear stability analysis of these basic states shows that the Rayleigh–Taylor mechanism is the dominant contributor to instability, but that there are circumstances under which the basic state may be stable, especially when the front is close to one of the boundaries.

In the second case, a constant heat flux is imposed at the liquid boundary and a fixed temperature at the vapour boundary. We have shown that competition between the effects of cooling and the viscosity difference between the fluid phases causes multiple liquid-vapour front positions, whether or not gravity is considered. The stability analysis has shown that along with the Rayleigh-Taylor (buoyancy-driven) mechanism, a Saffman-Taylor viscous fingering mechanism can also play an important role in the transition to instability.

# Contents

<b>1</b>	<b>Introduction</b>	<b>1</b>
1.1	The basics of geothermal reservoirs . . . . .	2
1.2	Approaches to geothermal modelling . . . . .	4
1.2.1	Large-scale simulation models . . . . .	5
1.2.2	Idealised models . . . . .	6
1.2.2.1	Mixed-phase models . . . . .	7
1.2.2.2	Separate-phase models . . . . .	8
1.3	Outline of thesis . . . . .	11
<b>2</b>	<b>Mathematical Modelling of a Porous Medium</b>	<b>13</b>
2.1	Porous Medium . . . . .	13
2.1.1	Porosity $\varphi$ . . . . .	15
2.2	Darcy's Law . . . . .	16
2.3	Mass Balance Equation . . . . .	17
2.4	Equation of State . . . . .	19
2.5	Energy Equation in Porous Media . . . . .	21
2.5.1	The Heat Diffusion Equation in the Solid Phase . . . . .	21
2.5.2	The Heat Diffusion Equation in the Fluid Phase . . . . .	23
2.5.3	Local Thermal Equilibrium . . . . .	24

2.5.3.1	Conduction in Parallel . . . . .	25
2.5.3.2	Conduction in Series . . . . .	25
2.5.4	Local Thermal Non-Equilibrium . . . . .	26
2.6	Heat, mass conditions at the liquid-vapour interface in porous media	27
2.6.1	Pressure/Temperature relation . . . . .	27
2.6.1.1	Heat jump condition at phase change interface . . .	28
2.6.1.2	Special cases . . . . .	31
2.6.1.3	Mass jump condition at phase change interface . .	33
2.7	Numerical data for the parameters and variables used . . . . .	35
<b>3</b>	<b>One Dimensional Phase Change Problems</b>	<b>38</b>
3.1	The steady-state through flow problem . . . . .	39
3.1.1	Isothermal Boundary Conditions . . . . .	42
3.1.2	Constant heat flux boundary condition . . . . .	52
3.1.3	Summary and conclusions . . . . .	56
3.2	Instantaneous change of surface temperature: similarity solution . .	58
3.2.1	Similarity solution . . . . .	59
3.2.2	Interpretation of Stefan number . . . . .	61
3.2.3	Effects of density change: similarity solution . . . . .	64
3.2.3.1	Similarity solution . . . . .	64
3.2.3.2	Asymptotic solution . . . . .	67
3.2.4	Summary and conclusions . . . . .	69
<b>4</b>	<b>Stability of Steady Solutions with Isothermal Boundary Condi-</b>	
	<b>tions</b>	<b>70</b>
4.1	Physical mechanisms that stabilise and destabilise the steady state	
	solution . . . . .	70

4.1.1	Rayleigh-Taylor instability in a porous medium . . . . .	73
4.2	Mathematical formulation of the stability problem . . . . .	75
4.2.1	Perturbed form of the problem . . . . .	78
4.2.2	Zeroth order problem . . . . .	80
4.2.3	First order problem . . . . .	81
4.3	Stability of the steady state with no through flow . . . . .	83
4.3.1	Steady state . . . . .	83
4.3.2	First order problem . . . . .	84
4.3.3	The eigenvalue problem . . . . .	85
4.3.4	Dispersion analysis . . . . .	87
4.3.5	Transition to instability . . . . .	89
4.3.5.1	Onset of instability when $l \rightarrow \infty$ . . . . .	89
4.3.5.2	Onset of instability when $l = 0$ . . . . .	92
4.3.6	Special cases . . . . .	92
4.3.6.1	The classical one . . . . .	93
4.3.6.2	Il'ichev and Tsyppkin (2005) revisited . . . . .	94
4.3.6.3	Perturbed vapour phase is affected by both advec- tion and conduction . . . . .	98
4.3.6.4	Perturbed liquid phase is affected by both advec- tion and conduction . . . . .	100
4.4	Stability of the steady state with through flow . . . . .	103
4.4.1	Steady state solution . . . . .	103
4.4.2	Perturbed state . . . . .	105
4.4.3	The eigenvalue problem . . . . .	105
4.4.4	Dispersion analysis . . . . .	108
4.4.5	Numerical and asymptotic methods . . . . .	109

4.4.5.1	Numerical methods . . . . .	109
4.4.5.2	Asymptotic analysis . . . . .	110
4.4.6	Numerical results for $\sigma(l)$ . . . . .	112
4.4.6.1	Stability analysis of the low branch front position .	112
4.4.6.2	Stability analysis of the middle branch front position	114
4.4.6.3	Stability analysis of the upper branch front position	116
4.4.7	Summary of our findings . . . . .	119
4.5	Summary and conclusions . . . . .	120
4.5.1	Isothermal interface with no through flow . . . . .	120
4.5.2	Isothermal interface with through flow . . . . .	121

**5 Stability of Steady Solutions with a Heat Flux Condition on the Surface** **122**

5.1	Non-dimensional form . . . . .	122
5.2	Stability when there is no through flow . . . . .	123
5.2.1	Steady state . . . . .	124
5.2.2	Perturbed state . . . . .	125
5.2.3	The eigenvalue problem . . . . .	126
5.2.4	Dispersion analysis . . . . .	127
5.2.5	Transition to instability . . . . .	128
5.2.5.1	Onset of instability due to short-wave perturbations	128
5.2.5.2	Onset of instability at $l = 0$ . . . . .	130
5.2.5.3	Onset of instability for medium wave numbers . . .	130
5.2.6	Special cases . . . . .	134
5.3	Stability with non-zero through flow . . . . .	140
5.3.1	Steady state solution . . . . .	140
5.3.2	Perturbed state . . . . .	141

5.3.3	The eigenvalue problem . . . . .	141
5.3.4	Dispersion analysis . . . . .	143
5.3.5	Asymptotic analysis . . . . .	144
5.3.6	Numerical results for $\sigma(l)$ . . . . .	145
5.3.6.1	Unstable low branch solution . . . . .	145
5.3.6.2	Unstable middle branch solution . . . . .	147
5.3.6.3	Stable upper branch solution . . . . .	149
5.3.7	Rubin and Schweitzer (1972) revisited . . . . .	150
5.3.8	Summary of our findings . . . . .	154
5.4	Summary and conclusions . . . . .	155
5.4.1	Basic state with no through flow . . . . .	155
5.4.2	Basic state with through flow . . . . .	155
<b>6</b>	<b>Conclusions and possible extensions</b>	<b>157</b>
6.1	Summary . . . . .	157
6.2	Possible extensions . . . . .	158
6.2.1	Numerical work . . . . .	158
6.2.2	Analytical work . . . . .	161
<b>A</b>	<b>Determination of minimum heat output</b>	<b>163</b>
<b>B</b>	<b>Derivation of Rayleigh-Taylor instability in a porous medium</b>	<b>165</b>
<b>C</b>	<b>Formulation of the basic state with specified mass flux</b>	<b>170</b>
<b>D</b>	<b>Pressure continuity condition at the phase change front</b>	<b>174</b>
<b>E</b>	<b>Procedure for continuation method in Maple</b>	<b>177</b>

# List of Figures

1.1	Schematic representation of a geothermal reservoir [16]. . . . .	3
1.2	Idealised one-dimensional models of a geothermal reservoir. The “bubbles” are for visualisation only and do not represent separate phases. . . . .	8
2.1	Some everyday examples of porous media, various images, various sources. . . . .	14
2.2	Control volume through which fluid flows. . . . .	18
2.3	Fluid flow in porous media. . . . .	19
2.4	Models for parallel and series conduction in a porous medium [40]. .	26
2.5	Energy balance at a vaporising interface [68]. . . . .	32
2.6	Mass balance at a liquid-vapour phase change interface [11, p. 108].	34
3.1	Diagram of through flow problem. . . . .	40
3.2	Temperature profile for isothermal conditions with temperature contrast ratio $\Theta_0 = 0.43$ , Rayleigh number $R_3 = -2.0 \times 10^{-10}$ , $G_1 = \pm 7.2 \times 10^{-10}$ and reference Peclet number $Pec_i = \pm 3.65$ . . . . .	46

3.3	(a) Steady-state front position $S^*$ ; (b) mass flux quantity $Pec_i F(S^*)$ vs ratio of temperature contrast $\Theta_0$ ; and (c) mass flux quantity $Pec_i F(S^*)$ vs implicit front position $S^*$ with $H_{liq} = 8.74$ , $R_1 = 0.0006$ , $R = 22.11$ and $C = 2.02$ . Note that $R_3 < 0$ , i.e., liquid is above vapour. Note also that, following Straus & Schubert [77] we have taken $R > 1$ ; the large value of $R$ is chosen for clarity of the plots but does not qualitatively affect the results. . . . .	47
3.4	(a) Steady-state front position $S^*$ vs ratio of temperature contrast $\Theta_0$ and (b) mass flux quantity $Pec_i F(S^*)$ vs $\Theta_0$ for higher Rayleigh numbers $ R_3 $ with $H_{liq} = 8.74$ , $R_1 = 0.0006$ , $R = 22.11$ and $C = 2.02$ . Note that liquid overlies vapour, i.e., $R_3 < 0$ . . . . .	49
3.5	(a) Steady-state front position $S^*$ and (b) mass flux quantity $Pec_i F(S^*)$ vs thermal conductivities ratio $k$ for higher Rayleigh numbers $ R_3 $ with $H_{liq} = 8.74$ , $R_1 = 0.0006$ , $R = 22.11$ and $C = 2.02$ . Note that $R_3 < 0$ (liquid above vapour). . . . .	50
3.6	(a) Steady-state front position $S^*$ and (b) mass flux quantity $Pec_i F(S^*)$ vs the reciprocal of the Stefan number for the liquid phase $H_{liq}$ with $R_1 = 0.0006$ , $R = 22.11$ and $C = 2.02$ . Note that $R_3 < 0$ (liquid above vapour). . . . .	51
3.7	(a) Steady-state interface position $S^*$ and (b) Mass flux quantity $Pec_i F(S^*)$ vs heat flux $Q_{liq}$ with zero gravity and $H_{vap} = 41.17$ , $R = 22.11$ , $R_1 = 0.0006$ , $C = 2.01$ and $k = 4$ . . . . .	54
3.8	(a) Steady-state interface position $S^*$ and (b) Mass flux quantity $Pec_i F(S^*)$ vs heat flux $Q_{liq}$ when the vapour phase is above the liquid phase with $H_{vap} = 41.17$ , $R = 22.11$ , $R_1 = 0.0006$ , $C = 2.01$ and $k = 4$ . . . . .	55

3.9	(a) Steady-state interface position $S^*$ and (b) Mass flux quantity $Pec_i F(S^*)$ vs heat flux $Q_{liq}$ when the liquid is above the vapour with $H_{vap} = 41.17$ , $R = 22.11$ , $R_1 = 0.0006$ , $C = 2.01$ and $k = 4$ . . .	56
3.10	Diagram of unsteady condensation problem. . . . .	58
3.11	Similarity solution temperature profile with $R_1 = 0.1$ , $H_{liq} = 1$ , $k = 1$ , $h_2 = 4.5$ , $E_1 = 1$ , $E_2 = 1$ , $\Theta_0 = 0.5$ and $\varphi = 0.38$ . . . . .	66
3.12	The similarity front parameter $\beta_2$ as a function of the diffusivity ratio $h_2$ and the density ratio $R_1$ , where $H_{liq} = 5$ , $k = 4$ , $E_1 = 1$ , $E_2 = 1$ , $\Theta_0 = 0.5$ , and $\varphi = 0.38$ . . . . .	68
3.13	The similarity front parameter $\beta_2$ as a function of the diffusivity ratio $h_2$ and the temperature contrast ratio $\Theta_0$ , where $H_{liq} = 5$ , $k = 4$ , $E_1 = 1$ , $E_2 = 1$ , $\Theta_0 = 0.5$ and $\varphi = 0.38$ . . . . .	69
4.1	The physical schematic diagram for an evaporation front in a steady state [57, p. 2]. . . . .	71
4.2	Schematic of a perturbed evaporation front when heat is supplied from the vapour side [57, p. 3]. . . . .	72
4.3	Schematic diagram for the physics of perturbed interface, when $R_3 > 0$ (vapour above liquid). . . . .	77
4.4	The transition to instability when the liquid-vapour phase change front is at the middle of the porous layer with $R_1 = 0.0056$ , $R_2 = 8.75$ , $E_1 = 1$ , $E_2 = 1$ , $C = 1.96$ , $k = 4$ , $H_{liq} = 5$ , $\Theta_0 = 4$ and $\varphi = 0.38$ . Log scale is used for clarity. Note that $R_3 < 0$ (liquid above vapour). . . . .	88

4.5	The transition to instability when the liquid-vapour phase change front is near to the upper boundary, i.e., $S_0^* < \frac{1}{2}$ , with $R_1 = 0.0056$ , $R_2 = 8.75$ , $E_1 = 1$ , $E_2 = 1$ , $C = 1.96$ , $k = 4$ , $H_{liq} = 5$ , $\Theta_0 = 12$ and $\varphi = 0.38$ . . . . .	90
4.6	The transition to instability when the liquid-vapour phase change front is near to the lower boundary, i.e., $S_0^* > \frac{1}{2}$ , with $R_1 = 0.0056$ , $R_2 = 8.75$ , $E_1 = 1$ , $E_2 = 1$ , $C = 1.96$ , $k = 4$ , $H_{liq} = 5$ , $\Theta_0 = 1$ and $\varphi = 0.38$ . . . . .	92
4.7	The dispersion curves $\sigma = \sigma(l)$ when the interface is near to the liquid boundary, i.e., $S_0^* < \frac{1}{2}$ , with $R_1 = 0.0056$ , $R_2 = 8.75$ , $E_1 = 1$ , $E_2 = 1$ , $C = 1.96$ , $k = 4$ , $H_{liq} = 5$ , $\Theta_0 = 12$ and $\varphi = 0.38$ . (b) shows that the instability is attained at infinite wave numbers, when the line $F(l) = F_1$ moves upward. (c) shows that the instability occurs at zero wave number, when the line $F(l) = F_2$ moves downward. Figures (b) and (c) are adapted from [31]. . . . .	97
4.8	The dispersion curves $\sigma = \sigma(l)$ when the interface is near to the lower boundary, i.e., $S_0^* > \frac{1}{2}$ , with $R_1 = 0.0056$ , $R_2 = 8.75$ , $E_1 = 1$ , $E_2 = 1$ , $C = 1.96$ , $k = 4$ , $H_{liq} = 5$ , $\Theta_0 = 1$ and $\varphi = 0.38$ . (b) shows that the instability is attained at zero wave number, when the line $F(l) = F_1$ moves upward. (c) shows that the instability occurs at infinite wave numbers, when the line $F(l) = F_2$ moves downward. Figures (b) and (c) are adapted from [31]. Log scale is used for clarity. . . . .	98
4.9	Growth rate vs wave number in the presence of advection and conduction in the vapour region only with $R_1 = 0.0056$ , $R_2 = 8.75$ , $E_1 = 1$ , $E_2 = 1$ , $C = 1.96$ , $k = 4$ , $H_{liq} = 5$ and $\varphi = 0.38$ . . .	99

4.10	The critical Rayleigh number for long wavelength verses (a) ratio of the temperature contrast and (b) ratio of the densities $R_1$ , where $R_2 = 8.75$ , $C = 1.96$ , $k = 4$ , $H_{liq} = 5$ . . . . .	102
4.11	A bifurcation diagram for the phase change front $S_0^*$ , where $R_1 = 0.0006$ , $R_2 = 8.75$ , $C = 2.01$ , $k = 4$ , $H_{liq} = 8.74$ , $Pec_i = -20$ , $\Theta_0 = 2$ , $R = 22.11$ and $R_3 \leq 0$ . The arrows represent the direction along with we will follow the solution curve. . . . .	104
4.12	Asymptotic solution for the low, middle and upper branch front positions. . . . .	112
4.13	The low branch solution and the corresponding schematic configuration. . . . .	113
4.14	Stability plots of the low branch condensation front, where $\varphi = 0.38$ , $R_1 = 0.0006$ , $R_2 = 8.75$ , $E_1 = 1$ , $E_2 = 1$ , $C = 2.02$ , $k = 4$ , $H_{liq} = 8.74$ , $\Theta_0 = 2$ , $R = 22.11$ and $R_3 \leq 0$ . . . . .	114
4.15	The middle branch solution. . . . .	115
4.16	Behaviour of the low and middle branches near the turning point at $ R_3  \approx 7.4666$ . . . . .	115
4.17	Stability plots of the middle branch position of the liquid-vapour front. . . . .	116
4.18	The upper branch solution and the corresponding schematic configuration. . . . .	117
4.19	Behaviour of the middle and upper branches near the turning point at $ R_3  \approx 0.67632$ . . . . .	117
4.20	Stability plots of the upper branch position of the isothermal liquid-vapour front. . . . .	118

4.21	Identification of stable and unstable behaviour of the isothermal liquid-vapour interface. . . . .	120
5.1	Steady liquid-vapour interface position vs dimensionless heat flux $Q_{liq}$ , where $Q_{liq}^{mini} = 1$ . . . . .	125
5.2	Short wave disturbances of the liquid-vapour interface with no through flow and a constant heat flux at the liquid boundary, where $R_1 = 0.0006$ , $R_2 = 8.75$ , $\varphi = 0.38$ , $H_{vap} = 41.17$ , $C = 2.02$ and $k = 4$ . . .	130
5.3	The difference between the critical Rayleigh numbers for zero and infinite wave numbers vs (a) the density ratio $R_1$ and (b) the dimensionless heat flux $Q_{liq}$ , where $R_2 = 8.75$ , $H_{vap} = 7$ , $C = 1.96$ , and $k = 4$ . Note that $R_3 < 0$ (liquid above vapour). . . . .	131
5.4	The critical Rayleigh number $R_3^{crit}$ verses wave number $l$ for the dimensionless heat flux $Q_{liq}$ , for various values of $R_1$ . Here $R_2 = 8.75$ , $H_{vap} = 7$ , $E_1 = 1$ , $E_2 = 1$ , $C = 1.96$ , $\varphi = 0.38$ and $k = 4$ . Note that $R_3 < 0$ (liquid above vapour). . . . .	132
5.5	Medium wavelength disturbances of the liquid-vapour interface with no through flow and a constant heat flux condition. . . . .	133
5.6	The long wavelength behaviour of the liquid-vapour interface with no through flow and a constant heat flux condition when the critical Rayleigh number $R_3^{crit} = R_{3,max}^{crit}$ . For $R_{3,max}^{crit}$ see the text. . . . .	134
5.7	The difference between the critical Rayleigh numbers for zero and infinite wave numbers vs (a) the density ratio $R_1$ and (b) the heat flux $Q_{liq}$ for the different modes of heat transport, where $R_2 = 8.75$ , $H_{vap} = 7$ , $C = 1.96$ , $k = 4$ and $\varphi = 0.38$ . . . . .	136

5.8	The dependence of $ R_3^{crit} $ on the wave number $l$ for the different modes of heat transport (see Table 5.1), where $R_1 = 0.04$ , $R_2 = 8.75$ , $H_{vap} = 7$ , $C = 1.96$ , $k = 4$ , $E_1 = 1$ , $E_2 = 1$ and $\varphi = 0.38$ . . . .	137
5.9	Medium wavelength disturbances of the system with and without advection and a fixed flux condition at the liquid boundary. The values of $ R_{3,mini}^{crit} $ , $Q_{liq}$ and the other parameters for (a), (b) and (c) are adapted from figure 5.8 (a), (b) and (c), respectively. . . . .	138
5.10	Long wavelength disturbances of the system with and without advection and a fixed flux condition at the liquid boundary. The critical values of $ R_{3,0}^{crit} $ and $Q_{liq}$ and the other parameters for (a), (b) and (c) are adapted from figure 5.8 (a), (b) and (c), respectively.	139
5.11	A bifurcation diagram for the liquid-vapour front $S_0^*$ with a constant heat flux at the liquid boundary, where $R_1 = 0.0006$ , $R_2 = 8.75$ , $C = 2.01$ , $k = 4$ , $H_{vap} = 41.17$ , $Pec_i = -160$ , $Q_{liq} = 1.45$ , $R = 22.11$ and $R_3 \leq 0$ . See text for explanation of arrows. . . . .	141
5.12	Asymptotic solution for the low and middle branch front positions.	145
5.13	Stability plots of the low branch solution of $S_0^*$ with a fixed flux condition. . . . .	146
5.14	Comparison between the numerical and asymptotic solutions for the low branch solution of $S_0^*$ with a fixed flux condition. . . . .	147
5.15	Behaviour of the low and middle branch near the turning point at $ R_3  \approx 34.093$ . The log scale is used for better visualisation. . . . .	147
5.16	Stability plots for the middle branch front position and comparison with asymptotic solution. . . . .	148
5.17	Stability plots of the upper branch front position with a fixed flux condition. . . . .	149

5.18	A horizontal configuration in which the porous layer is mostly filled with vapour. . . . .	150
5.19	The bifurcation diagram for the liquid-vapour interface $S_0^*$ , when $R_3 = 0$ and $Q_{liq}$ is the bifurcation parameter. . . . .	151
5.20	Stability plots of the low branch solution of $S_0^*$ when $R_3 = 0$ . . . . .	152
5.21	Stability plots of the middle branch solution of $S_0^*$ when $R_3 = 0$ . . . . .	153
5.22	Stability plots of the upper branch solution of $S_0^*$ when $R_3 = 0$ . . . . .	153
5.23	Identification of stable and unstable behaviour of the liquid-vapour interface with a fixed flux condition. . . . .	155
6.1	The negative jump of the enthalpy $\rho E$ as a function of temperature $T$ , where $\rho_{liq} = 1$ , $\rho_{vap} = 0.1$ , $c_{liq,vap} = 1$ , $\lambda = 1$ , $T_S = 1$ and $T_{ref} = 0$ . . . . .	161
A.1	Energy balance across a liquid-vapour interface. . . . .	163

# List of Tables

2.1	Numerical values for the parameters and variables used in our analysis.	36
2.2	List of the possible range of numerical values for the dimensionless parameters and quantities we have used in our study. Note that these dimensionless quantities will be defined in chapter 3-5. . . . .	37
4.1	List of problems under consideration . . . . .	93
4.2	List of critical Rayleigh numbers for long wavelength . . . . .	101
5.1	List of problems under consideration with fixed flux condition . . .	134
5.2	List of critical Rayleigh numbers for long-wave perturbations with fixed flux condition . . . . .	135

# Chapter 1

## Introduction

A familiar occurrence, especially in a cold moist climate like Scotland, is that water vapour condenses and forms liquid water on the inside of a cold window. Such phase change phenomena in which vapour condenses (or liquid evaporates) are known as liquid-vapour phase changes. The interest in the investigation of liquid-vapour phase change problems arises from their wide range of applications, such as drying processes [51, 74, p. 397-409], geothermal systems [8, 28, 33, 82, 94], heat pipes [85], film boiling [27, 47, 59] and nuclear safety analysis [17]. The additional heat which is absorbed or released in these processes during the transformation of one phase to another phase is known as the latent heat of evaporation or condensation.

In 1883 Lord Rayleigh described for the first time the instability of a dense fluid overlying a lower density fluid in a gravitational field, which is known as the Rayleigh-Taylor instability [66]. The transitions to instability at fluid-fluid interfaces are of great interest on account of their above mentioned applications. These instabilities can often occur at a phase change interface between liquid and vapour. There is much need for the better understanding of the different physical phenom-

ena involved with liquid-vapour phase changes, and this is the focus of our study. In particular, we are interested in instabilities related to the Rayleigh-Taylor instability when they occur in porous media. The commonest such context is geothermal reservoirs, so we will now provide some background on geothermal reservoirs.

## 1.1 The basics of geothermal reservoirs

In 1904 geothermal energy was used for the first time to produce electricity in Lardarello, Italy [23, p. 1]. Apart from power production, greenhouseing, soil warming, aquaculture are other direct uses of geothermal resources [43, 44]. Reviews of geothermal systems and their characteristics can be found in [23, 39].

The geothermal energy is due to the natural heat content of the earth. A geothermal system has three key components:

1. **Heat source:** The main heat source in a geothermal system is the magmatic body present in the earth's crust, where the temperature exceeds 600 °C.
2. **Heat carrier:** Heat in a geothermal system is generally transported, by convection or conduction, through water occupying the pore space in the rock. Such water usually originates as rainwater, which seeps into the earth from the surface.
3. **Structure:** The structure deep in the earth varies: in some areas it is fractured rocks, in others a mixture of sand and fractured rocks and so it can be technically considered as a porous medium.

A visualisation of a geothermal reservoir is given in Figure 1.1. In a geothermal reservoir, the fluid near to the magmatic body exists in the form of vapour, while further away from the heat source it is liquid.

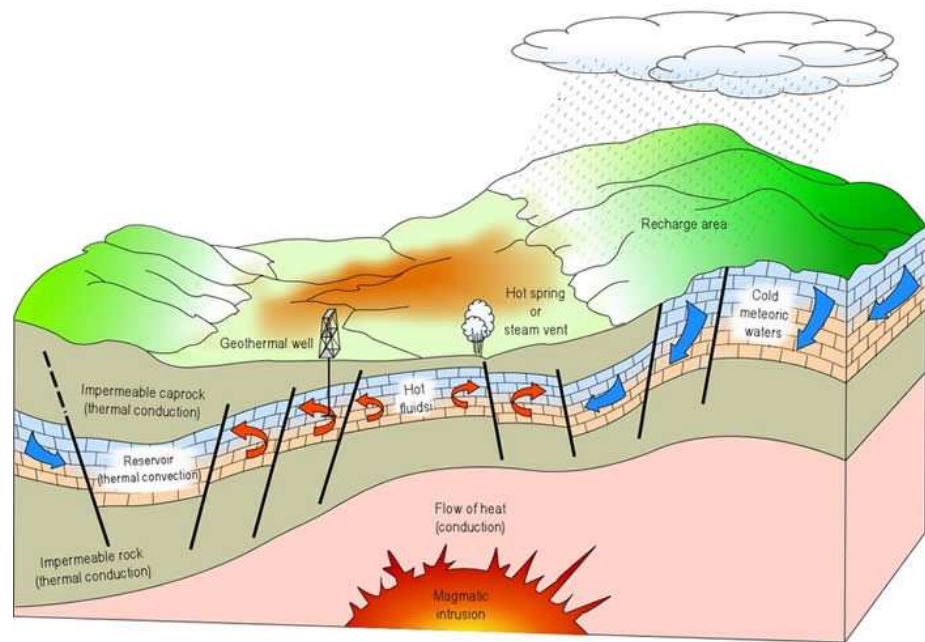


Figure 1.1: Schematic representation of a geothermal reservoir [16].

Geothermal systems can be classified into two main types.

1. **Water dominated:** In water-dominated systems, the fluid is mostly present in a hot liquid phase. A well-known example is Wairakei geothermal field in New Zealand [22]. Typical temperatures in these systems are  $300\text{ }^{\circ}\text{C}$  or higher, while typical pressures are also high ( $> 100\text{ bar}$ ).
2. **Vapour dominated:** In vapour-dominated systems, the fluid is mostly present in a vapour phase. These systems are regarded as the best ones for extracting energy from. Well-known vapour dominated geothermal reservoirs are the Larderello field in Italy [50] and the Geysers field in the USA [78]. Typical temperatures are again  $300\text{ }^{\circ}\text{C}$  or higher, while pressures are typically lower ( $< 100\text{ bar}$ ) than in water-dominated systems.

The vapour dominated reservoirs are preferable as they have fewer fluid production problems than hot water dominated reservoirs [82]. In vapour dominated systems,

a continual upward flow of fluid yields a high-quality super heated vapour phase which can be easily extracted for production [23, p. 21-27]. In this thesis, we will aim to improve the understanding of some of the physical mechanisms associated with a vapour dominated system.

In particular, White et al.'s [92] and Truesdell & White's [82] analyses of natural geothermal systems showed that the fluid phases in a great number of reservoirs can be visualised as

*“a water layer of considerable thickness located over a layer of super heated vapour”* Tsyarkin & Il'ichev [83].

Grant [20], while studying the vapour dominated Kawah Kamojang reservoir in West Java, asked: if a heavier fluid (water) overlies lighter fluid (vapour) then

*is the phase change interface between the two phases in such configurations gravitationally unstable?*

This is the key question that this thesis will address. Grant [20] proposed the answer that the system will be stable if there is no direct contact between the condensate layer (hot liquid water zone) and the vapour zone. Analogous problems have been studied without porous media, for example in film boiling problems where a thin vapour film separates a liquid from a heating plate [27, 47, 59]. In a geothermal context, various approaches are adopted to answer the above question.

## **1.2 Approaches to geothermal modelling**

Geothermal reservoirs are very complex in nature. Firstly, they have a very complicated geometry and within that geometry, a complicated permeability structure. Secondly, there are different hydrothermal processes related to different phases

of a single fluid. The key aim of geothermal modelling is to predict heat and mass transport within the system. This information helps engineers to assess the geothermal potential of the area under observation. We will discuss two types of models which are widely used.

### 1.2.1 Large-scale simulation models

The aim of geothermal system simulation is to develop a mathematical model of a reservoir which can provide quantitative predictions. Large-scale simulation models of a geothermal reservoir try to capture the real world three-dimensional geometry and permeability structure, and to represent all the physical and chemical aspects of a reservoir [64]. Such models have been developed over many decades [21, 56] and are now extremely complex: a good example is the **TOUGH+**<sup>1</sup> simulation program developed at the Lawrence Berkeley National Laboratory in the USA. Descriptions of how such models may be developed for particular geothermal systems are given by O’Sullivan et al. [56] for the Wairakei system in New Zealand, and by Blocher et al. [7] for the Gross Schoenbeck system in Germany. The complexity of such models means that large quantities of historical data and detailed monitoring are essential in order to calibrate them [22, 60].

As well as their role in site-specific modeling, large-scale simulation models have been used to address more general issues such as the stability of water-over-steam configurations. Ingebritsen & Sorey [33] presented two-dimensional simulations of a vapour dominated geothermal system. They investigated three different configurations of the natural state. In the first model, the natural state had an extensive vapour phase compared to the liquid phase, and the liquid through flow was assumed to be slow. The second and third models were distinct from the first model

---

<sup>1</sup><http://esd.lbl.gov/tough+/index.html>

in that in their natural states the vapour phase was small compared to the liquid phase, with significant liquid through flow. Ingebritsen & Sorey [33] concluded that for the existence of a vapour dominated zone there should be a permeability contrast between the groundwater aquifer and the geothermal aquifer (caprock hypothesis condition) as was suggested by Straus & Schubert [78]. Building on Ingebritsen & Sorey's [33] second case, Yano & Ishido [93] carried out numerical simulations of the Ginyu reservoir of the Kirishima field, Japan. They showed that for the support of a vapour dominated zone, a minimum rate of mass recharge is required, if the permeability of the caprock is high.

Although such studies suggest general conclusions, the large quantities of data they required and the complexity of the processes they model can make the essential mechanisms of stability or instability hard to identify. In order to obtain more generic insight, it is necessary to employ more highly idealised models of geothermal systems.

### 1.2.2 Idealised models

The idealised models always simplify the complex porous structure and the phase behaviour in a reservoir. In idealised models, various fluid phases are considered to be distinct fluids with individual thermodynamics and transport properties. The heat and mass transport processes for each phase are mathematically described on the basis of conservation of mass and energy, separately. Such models can be categorized into two types on the basis of phase distribution. Figure 1.2 illustrates the fact that the main difference between these models is whether they have a mixed liquid-vapour phase or a sharp interface separating the liquid and the vapour phases.

### 1.2.2.1 Mixed-phase models

Udell [85] carried out a one-dimensional study and investigated the configuration of fluid phases in a porous layer, while the layer was heated from the top and kept cool from below. He showed that in the steady state, there are three distinct regions in the porous layer: a conduction dominated vapour phase near to the heated boundary, an isothermal mixed-phase region in which the pores are filled with a mixture of liquid and vapour, and a conduction dominated liquid phase near to the cool boundary. A flow of liquid towards the heated layer and of vapour towards the cooled layer occurs in the isothermal mixed-phase region, which is known as counterflow. The upward liquid flow is driven by capillary forces and the downward vapour flow is driven by a pressure gradient. Udell's [84] experiment in a porous pack suggests that in the mixed-phase region, evaporation occurs near the heated boundary (upper) and condensation occurs at the cool boundary (lower). Later on, Torrance [80] re-visited Udell's [84] model assuming the porous layer is heated from below and cooled from above, this analysis is relevant to geothermal systems. He concluded with complete agreement on the configuration of the three distinct regions and counterflow within the mixed-phase region as was shown by Udell [84]. Satik et al. [72] studied two main cases related to liquid-vapour counterflow in porous media: the geothermal case driven by gravity [48, 73] and the heat pipe case driven by capillary pressure [2]. For zero net mass flux, the solutions were vapour dominated.

Amili & Yortsos's [1] linear stability analysis of a vapour-liquid counterflow region (mixed-phase region) overlying a super heated vapour phase or underlying a liquid phase, showed that the system is unstable for intermediate wave numbers above some critical Rayleigh number. Recently, Sahli et al. [70] studied the stability of boiling in fluid-saturated horizontal porous layers heated from below and

cooled from above, originally proposed by Ramesh & Torrance [65]. Both liquid and vapour dominated mixed-phase regions were considered. In liquid dominated systems (where the mixed-phase region contains mostly liquid), the convective instability is mainly driven by buoyancy gradients within the liquid region. In vapour dominated systems (where the mixed-phase region contains mostly vapour), the instability is mainly driven by the density difference between the liquid and mixed-phase regions.

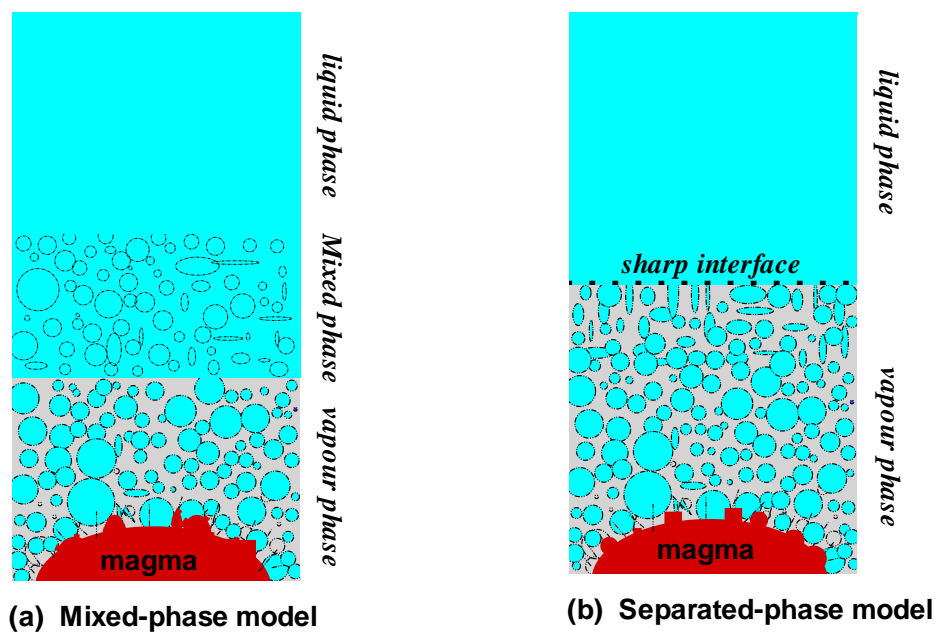


Figure 1.2: Idealised one-dimensional models of a geothermal reservoir. The “bubbles” are for visualisation only and do not represent separate phases.

### 1.2.2.2 Separate-phase models

In a vapour dominated reservoir, the dominance of vapour in the mixed-phase region leads to the consideration that the liquid and the vapour phases are separated by an interface of very small thickness. Models which treat the liquid-vapour

interface as having negligible thickness will be referred as separate-phase models (see Figure 1.2).

Rubin & Schweitzer [68] analysed two phase horizontal flow in a porous medium. A sharp phase change interface separating a vapour region from the liquid region was induced by heating one end of the porous medium above the vaporizing temperature of the liquid. They showed that if a constant temperature is prescribed on both boundaries, there is only one steady-state interface position; but if the heat flux is prescribed on the liquid boundary and constant temperature on the vapour boundary, there may be three steady-state positions. A quasi one-dimensional stability analysis of the latter case showed that the middle front position is unstable. Straus & Schubert [77] carried out a linear stability analysis of the phase change front in a vapour dominated system. In the basic (unperturbed) state, the fluid phases were considered to be static with the assumption that there is no net mass flux across the phase change interface; they showed that the phase change interface is gravitationally unstable for medium wavelength. Furthermore, if net mass flux is allowed through the interface then the stability of the system is permeability dependent. Later, Straus & Schubert [78] illustrated that a vapour dominated system can develop, if the phase change interface exists in a low permeability layer. Eastwood & Spanos [19] showed that if the phase change interface is sharp and there is a zero net mass flux across the interface then the system is unstable for long wavelength. In the case, when phase transition (net mass flux is allowed) is permitted then neutral stability can be predicted for a critical wave number.

Tsyarkin & Il'ichev [83] showed that the multiple locations of the phase change front are permeability dependent and suggested that the middle front is always unstable, whereas the other two positions may be stable or unstable. Later, the same authors categorized three different cases of transition to instability of the

stationary vertical phase change flow under the condition that conduction dominates over advection [29, 31]. It was shown that if the interface is equidistant from the liquid and vapour boundaries then there is a spontaneous transition to instability (all wave numbers become unstable at the same value of the controlling parameter). The remaining two cases were: that the transition to instability occurs first at zero wave number if the interface is near to the vapour boundary, whereas instability occurs first at infinite wave numbers if the interface is near to the liquid boundary. Il'ichev & Tsyarkin [28] concluded that the most unstable mode of transition happens for zero wave number, when a water phase overlies an air-vapour mixture phase. Most recently, Il'ichev & Tsyarkin [30] studied the stability of water over steam with an advective-conductive basic state. The interface has a unique position for isothermal boundary conditions. For an arbitrary value of the permeability a vapour dominated phase may exist and be stable.

The large-scale simulation and mixed-phase modeling of liquid-vapour (multi-phase) flow in a porous structure faces far greater challenges than that of a separate-phase model. The challenges associated with separate-phase models are mainly due to the discontinuous variations in heat and mass transport across the interface between the liquid and the vapour phases. Apart from the advantages and disadvantages of each of the above modeling approaches, the separate-phase model gives the cleanest understanding of the instability mechanism of the phase change interface. We will use the separate-phase model to understand the physics of a natural state of a vapour dominated system and will identify the mechanisms associated with the stability of the sharp phase change front.

### 1.3 Outline of thesis

The remaining chapters are organized as follows:

Chapter 2 is a brief introduction to porous media. We establish the fundamental governing equations of motion for a fluid in a porous medium, including Darcy's law, the continuity equation and the equation of state. Under the assumption of local thermal equilibrium, we derive a one-equation model for heat transfer in a porous medium. In a situation in which local thermal equilibrium does not hold, we develop separate heat transport equations for each phases (solid and liquid), which is known as the two-equation model. Finally we develop the famous Stefan condition in generalized form, analyzing the phase change interface and discuss some special cases already used in the literature.

Chapter 3 focuses on one-dimensional problems of phase change (evaporation and condensation) in a porous medium. We discuss first steady solutions, and then the similarity solutions to a phase change problem with an instantaneous change in surface temperature.

Chapter 4 describes the stability of a steady-state phase change front in a porous medium with isothermal boundaries. We start with the physical mechanism, discussing three different types of stabilising and destabilising factors. The classical Rayleigh-Taylor instability is revisited to provide a basis for the analysis of evaporation front stability in the presence of gravity. We discuss the two-dimensional linear stability of the phase change interface and derive four special cases, among which one is the work of Il'ichev & Tsypkin [31].

Chapter 5 is an extension of Chapter 4. We consider a constant heat flux condition at the liquid boundary of the porous layer which will yield multiple positions of the phase change front. We analyse the stability of each of the locations of the front.

Finally, in Chapter 6 we summarise the key points of our findings and discuss some possible directions for future work.

# Chapter 2

## Mathematical Modelling of a Porous Medium

In this chapter the basic definition of a porous medium and porosity are introduced, along with the derivation of Darcy's law, which describes the fluid flow process in a porous medium. We develop the differential equations that must be satisfied, when there is heat and mass transfer between the fluid and the porous medium. From the conservation of mass principle, we develop the continuity equation for a porous medium. We derive energy equations for the solid and liquid phases of the porous medium, from the conservation of energy principle, under the assumptions of local and local thermal non-equilibrium. Finally we develop the famous Stefan condition in generalised form, analysing the phase change interface, and discuss some special cases already used in the literature.

### 2.1 Porous Medium

Soil, fissured rock, cemented sandstone, limestone, sand, foam rubber, bread, concrete, bricks, paper towels, lungs and kidneys are just a few examples of the large

variety of porous materials experienced in practice [4]. All of these materials have common properties that lead us to classify them into a single class: porous media. By a porous medium we mean a material medium made of heterogeneous or multiphase matter. At least one of the considered phases is solid and at least one is not. The solid phase is usually called the solid matrix. The space within the porous medium domain that is not part of the solid matrix is named void space or pore space. The flow of one or more fluids occurs in the interconnected pores through the material. In single phase flow the pores are filled by a single fluid. In a complex situation (two phase flow) the pores are occupied by gas and liquid phases or possibly by two distinct liquid or gas phases, e.g. oil and water.



Figure 2.1: Some everyday examples of porous media, various images, various sources.

Due to the complex nature of the porous medium it is very difficult to describe it at the pore level or at the molecular level. So we will treat the porous medium as a continuum at scales much greater than the pore scale by averaging. The important

aspect of averaging is that it will enable us to get an adequate description of the fluid phases and their interaction with the solid matrix. In the literature, there are two major ways to do averaging: spatial and statistical. The spatial averaging is often referred to as the Representative Elementary Volume (REV) approach: it enables us to define an appropriate space domain over which the microscopic properties of the porous medium will be integrated, which leads to a continuum approach. In the statistical approach, as stated in the literature [55, p. 1], the averaging is over a group of macroscopic equivalent pore structures. If we ignore the fluctuations in the space averaged quantities, then the two approaches end with the same results. These two approaches are discussed in great detail by Bear [3, p. 15].

### 2.1.1 Porosity $\varphi$

The void space distributed within the solid matrix is characterized by the porosity of the porous medium. The porosity  $\varphi$  is defined as the total void volume divided by the total volume occupied by the solid matrix and void volumes. Mathematically

$$\varphi = \frac{\Lambda_{void}}{\Lambda_{total}}, \quad (2.1)$$

where  $\Lambda_{void}$  and  $\Lambda_{total}$  are the volume of void space and the total volume of the material, respectively. Pores may be connected to other pores, in which case they are said to be interconnected. On the other hand some pores may appear in isolation, so that they are not connected to other pores. It is clear that flow will occur through the interconnected pores. We therefore define the effective porosity as

$$\varphi_{eff} = \frac{\Lambda_{connected\ void}}{\Lambda_{total}}, \quad (2.2)$$

where  $\Lambda_{connected\ void} \leq \Lambda_{void}$  is the volume of the connected pores only. We will assume below that  $\varphi_{eff} = \varphi$ .

## 2.2 Darcy's Law

Fluid flow in a porous medium is described by Darcy's law, which was formulated by Henry Darcy in 1856 while investigating water flow through beds of sand connected with the fountains of the city of Dijon, France [14].

In Darcy's experiment, fluid is made to flow through a porous medium of cross sectional area  $A$  and length  $L$  with a rate  $\vec{Q}$ . When a steady state is achieved, the pressure gradient  $\nabla P$  is related to  $\vec{Q}$  by the empirical formula

$$\vec{Q} = -\frac{A}{\mu} K \cdot \nabla P, \quad (2.3)$$

where  $\mu$  is the dynamic viscosity of the fluid and  $K$  is a second order permeability tensor which is independent of the fluid nature but depends on the geometry of the medium [3, p. 119-125]. If we define  $\vec{v} = \vec{Q}/A$  as the Darcy velocity then (2.3) yields

$$\vec{v} = \frac{-K \cdot \nabla P}{\mu}. \quad (2.4)$$

The above expression (2.4) describes a steady flow of a Newtonian fluid that is only driven by a pressure gradient. In the case when the fluid is driven by other forces than the pressure gradient, we can include them in our analysis by replacing  $\nabla P$  with the sum of all driven forces  $\mathbb{F}$  per unit volume. The most common case encountered is a fluid driven by gravity  $\vec{g}$  and pressure gradient, i.e,  $\nabla (P + \rho g x)$  where  $x$  is the vertical axis and  $\rho$  is the density,

$$(2.4) \quad \Rightarrow \quad \vec{v} = -\frac{K}{\mu} \cdot \left\{ \nabla (P + \rho g x) \right\}. \quad (2.5)$$

If the porous medium is isotropic, then permeability reduces to a scalar  $K$  and (2.5) simplifies to

$$\vec{v} = -\frac{K}{\mu} \left( \nabla P - \rho \vec{g} \right), \quad (2.6)$$

where  $\vec{g} = -g \hat{e}_x$  and we will write  $\vec{v} = (u, v, w)$ .

## 2.3 Mass Balance Equation

Let us consider a control volume  $\Lambda$  located in a fluid flow field as shown in Figure 2.2, with boundary  $\Omega$ . The law of conservation of mass for a homogeneous fluid with respect to the control volume is stated as

$$\left( \begin{array}{c} \text{rate of mass} \\ \text{accumulation} \end{array} \right) = \left( \begin{array}{c} \text{rate of} \\ \text{mass in} \end{array} \right) - \left( \begin{array}{c} \text{rate of} \\ \text{mass out} \end{array} \right) \quad (2.7)$$

The terms in equation (2.7) can be expressed as follows.

The rate of accumulation of mass in any volume  $d\Lambda$  is  $\frac{\partial \rho_f}{\partial t} d\Lambda$ , where  $\rho_f$  is the density of the fluid. The total rate of mass accumulation in the control volume  $\Lambda$  can be obtained by integrating  $\frac{\partial \rho_f}{\partial t}$  over  $\Lambda$ .

$$\frac{\partial}{\partial t} \int_{\Lambda} \rho_f d\Lambda. \quad (2.8)$$

The rate at which mass flows across an infinitesimal surface  $d\Omega$  in the control volume surface is equal to  $\rho_f \vec{V} d\Omega \cos \theta$ , where  $\theta$  is the angle between the velocity vector  $\vec{V}$  and the outward unit normal vector  $\vec{n}$  to  $d\Omega$ . Mathematically mass efflux is

$$\begin{aligned} \rho_f \vec{V} d\Omega \cos \theta &= \rho_f d\Omega |\vec{V}| |\vec{n}| \cos \theta, \\ &= \rho_f \vec{V} \cdot \vec{n} d\Omega. \end{aligned}$$

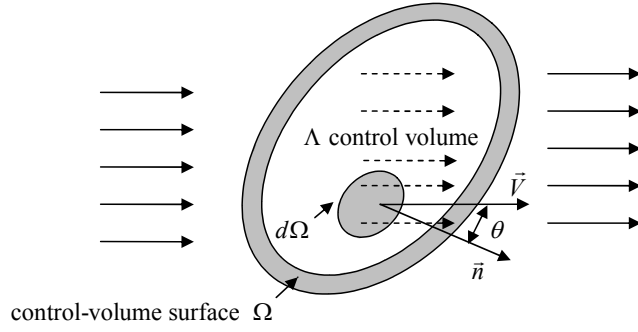


Figure 2.2: Control volume through which fluid flows.

The rate of mass flowing in through  $d\Omega$  is  $-\rho_f \vec{V} \cdot \vec{n} d\Omega$ , where the negative sign is because of the outward normal vector  $\vec{n}$ . The total net rate of mass influx into the control volume  $\Lambda$  can be obtained by integrating  $-\rho_f \vec{V} \cdot \vec{n} d\Omega$  over the control volume surface  $\Omega$  as

$$-\int_{\Omega} \rho_f \vec{V} \cdot \vec{n} d\Omega. \quad (2.9)$$

According to Gauss's divergence theorem, the surface integral (2.9) will be transformed into a volume integral as

$$-\int_{\Omega} \rho_f \vec{V} \cdot \vec{n} d\Omega = -\int_{\Lambda} \nabla \cdot (\rho_f \vec{V}) d\Lambda. \quad (2.10)$$

Substituting (2.8) and (2.10) into (2.7) gives

$$\begin{aligned} \int_{\Lambda} \left\{ \frac{\partial \rho_f}{\partial t} + \nabla \cdot (\rho_f \vec{V}) \right\} d\Lambda &= 0, \\ \Rightarrow \frac{\partial \rho_f}{\partial t} + \nabla \cdot (\rho_f \vec{V}) &= 0. \end{aligned} \quad (2.11)$$

This equation is called the continuity equation [38, p. 58].

Now we will use equation (2.11) to derive the mass balance equation or continuity equation for porous media. For this let us multiply equation (2.11) by the porosity  $\varphi$ , which is assumed to be constant in space, so we have

$$\varphi \frac{\partial \rho_f}{\partial t} + \nabla \cdot (\rho_f \varphi \vec{V}) = 0. \quad (2.12)$$

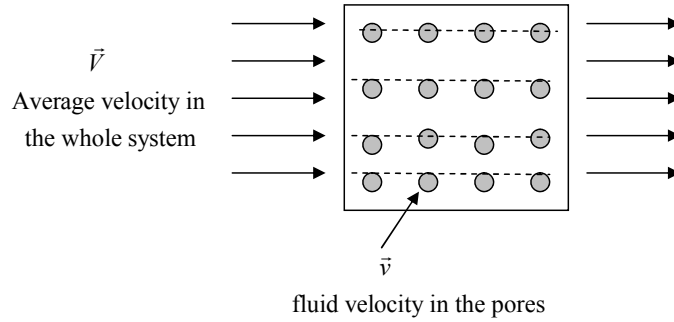


Figure 2.3: Fluid flow in porous media.

According to the Dupuit-Forchheimer relationship  $\vec{v} = \varphi \vec{V}$  [55, p. 5], where  $\vec{v}$  is the Darcy velocity (only in pores) and  $\vec{V}$  is the average velocity of the fluid in the whole system (solid matrix and voids, see Figure 2.3), then equation (2.12) will take the form

$$\varphi \frac{\partial \rho_f}{\partial t} + \nabla \cdot (\rho_f \vec{v}) = 0. \quad (2.13)$$

Note that  $\varphi$  is independent of time. The above equation is known as the continuity equation for a porous medium [55, p. 5]. As we are going to consider that the fluid in each phase is incompressible,  $\rho_f$  is a constant and (2.13) yields

$$\nabla \cdot \vec{v} = 0. \quad (2.14)$$

## 2.4 Equation of State

The equation of state relates the density of a fluid to the other thermodynamic properties: pressure, temperature and concentration of the system. A well known example of an equation of state is the gas law, which relates pressure, temperature and density by the gas constant. Similarly, a general equation of state for liquid systems can be formulated as

$$\rho = \rho(T, P), \quad (2.15)$$

where  $\rho$  is the density of the fluid and  $T$  is the temperature.

In case of incompressible fluid, the density of the fluid is independent of pressure, then (2.15) will be rewritten as

$$\rho = \rho(T). \quad (2.16)$$

The dependence of density on  $T$  is expressed through the value of the thermal expansion coefficient,  $\beta_T$ , where

$$\beta_T = -\frac{1}{\rho_0} \frac{\partial \rho}{\partial T}. \quad (2.17)$$

Here we have to note that  $\beta_T$  changes sign for temperatures less than the temperature of the density maximum. If the fluid under consideration is water then it has a density maximum at  $4^\circ C$ . The equation of state to express density in terms of  $\beta_T$  can be written as

$$\rho = \rho_0 (1 - \beta_T \Delta T), \quad (2.18)$$

where  $\Delta T = T - T_0$ , and the subscript zero refers to a reference state. Equation (2.18) is valid only when  $T$  is close to  $T_0$ . When  $\beta_T$  is assumed to be constant, then the resulting equation is called a linear equation of state. In order to account for parabolic temperature dependences, we may use a non-linear quadratic equation of state [81]:

$$\rho = \rho_0 \left[ 1 - \hat{\beta}_T (T - T_0)^2 \right], \quad (2.19)$$

where, as before,  $\rho_0$  is the fluid density at reference temperature  $T_0$  and where  $\hat{\beta}_T$  is a quadratic thermal expansion coefficient. Generally the differences in density between two phases (liquid and vapour) is much larger than the variations in density within a phase. Therefore, we will generally neglect changes of density within a phase and will take the density of each phase to be a (different) constant.

## 2.5 Energy Equation in Porous Media

### 2.5.1 The Heat Diffusion Equation in the Solid Phase

The conservation law of energy originates from the first law of thermodynamics. The law of energy conservation for a homogeneous, isotropic solid with heat generation can be expressed as:

$$\begin{pmatrix} \text{rate of energy} \\ \text{accumulation} \end{pmatrix} = \begin{pmatrix} \text{rate of energy in} \\ \text{by conduction} \end{pmatrix} + \begin{pmatrix} \text{rate of heat} \\ \text{generation} \end{pmatrix} \quad (2.20)$$

The various terms in this equation are evaluated as

$$\begin{pmatrix} \text{rate of energy} \\ \text{accumulation} \end{pmatrix} = \int_{\Lambda} (\rho c)_s \frac{\partial T_s(\vec{r}, t)}{\partial t} d\Lambda, \quad (2.21)$$

and

$$\begin{aligned} \begin{pmatrix} \text{rate of energy in} \\ \text{by conduction} \end{pmatrix} &= - \int_{\Omega} \vec{q}_s \cdot \vec{n} d\Omega \\ &= - \int_{\Lambda} \nabla \cdot \vec{q}_s(\vec{r}, t) d\Lambda. \end{aligned} \quad (2.22)$$

Here the subscript  $s$  refers to the solid phase in a porous medium,  $c$  is the specific heat,  $\rho$  is the density,  $T_s$  is the temperature of the solid,  $\vec{r} = (x, y, z)$  is the position vector,  $\vec{q}_s$  is the heat flux in the solid phase,  $\Omega$  is the surface area of the volume element  $\Lambda$ , and  $\vec{n}$  is the outward drawn normal unit vector to the surface element  $d\Omega$ : The minus sign is included to ensure that the heat flow is into the volume element  $\Lambda$ , and the divergence theorem is used to convert the surface integral to a volume integral.

The remaining term is evaluated as:

$$\begin{pmatrix} \text{rate of heat} \\ \text{generation} \end{pmatrix} = \int_{\Lambda} g_s(\vec{r}, t) d\Lambda, \quad (2.23)$$

where  $g_s[\text{W}/\text{m}^3]$  is the rate of heat generation per unit volume in the solid phase.

Substituting (2.21), (2.22) and (2.23) into (2.20) gives

$$\begin{aligned} \int_{\Lambda} (\rho c)_s \frac{\partial T_s(\vec{r}, t)}{\partial t} d\Lambda &= - \int_{\Lambda} \nabla \cdot \vec{q}_s(\vec{r}, t) d\Lambda + \int_{\Lambda} g_s(\vec{r}, t) d\Lambda. \\ \Rightarrow \int_{\Lambda} \left\{ (\rho c)_s \frac{\partial T_s(\vec{r}, t)}{\partial t} + \nabla \cdot \vec{q}_s(\vec{r}, t) - g_s(\vec{r}, t) \right\} d\Lambda &= 0. \end{aligned} \quad (2.24)$$

Eqn (2.24) is derived for an arbitrary volume element  $\Lambda$  within the solid, so we obtain

$$(\rho c)_s \frac{\partial T_s(\vec{r}, t)}{\partial t} = -\nabla \cdot \vec{q}_s(\vec{r}, t) + g_s(\vec{r}, t). \quad (2.25)$$

From Fourier's law

$$\vec{q}_s(\vec{r}, t) = -k_s \nabla T_s(\vec{r}, t). \quad (2.26)$$

Substituting (2.26) into (2.25), we get the following conduction equation in the solid phase,

$$(\rho c)_s \frac{\partial T_s(\vec{r}, t)}{\partial t} = \nabla \cdot (k_s \nabla T_s(\vec{r}, t)) + g_s(\vec{r}, t). \quad (2.27)$$

By multiplying (2.27) by  $(1 - \varphi)$ , we get the diffusion equation in the solid phase of the porous medium,

$$(1 - \varphi) (\rho c)_s \frac{\partial T_s(\vec{r}, t)}{\partial t} = (1 - \varphi) \nabla \cdot (k_s \nabla T_s(\vec{r}, t)) + (1 - \varphi) g_s(\vec{r}, t). \quad (2.28)$$

In (2.28),  $k_s \nabla T_s$  is the conductive heat flux through the solid and thus  $\nabla \cdot (k_s \nabla T_s)$  is the net rate of heat conduction into an infinitesimal volume of the solid. In (2.28) this appears multiplied by the factor  $(1 - \varphi)$ , which is the ratio of the cross-sectional area occupied by solid to the total cross-sectional area of the medium. The other two terms in (2.28) also contain the factor  $(1 - \varphi)$  because this is the ratio of the volume occupied by the solid to the total volume of the element.

### 2.5.2 The Heat Diffusion Equation in the Fluid Phase

The law of energy conservation for the fluid phase with temperature  $T_f$  can be expressed as:

$$\begin{aligned} \left( \begin{array}{c} \text{rate of energy} \\ \text{accumulation} \end{array} \right) &= \left( \begin{array}{c} \text{rate of energy in} \\ \text{by conduction} \end{array} \right) + \left( \begin{array}{c} \text{rate of energy in} \\ \text{by convection} \end{array} \right) \\ &+ \left( \begin{array}{c} \text{rate of heat} \\ \text{generation} \end{array} \right). \end{aligned} \quad (2.29)$$

All the terms in (2.29) are discussed in Section 2.5.1, except the convection term.

$$\begin{aligned} \left( \begin{array}{c} \text{rate of energy in} \\ \text{by convection} \end{array} \right) &= - \int_{\Omega} ((\rho c_p)_f T_f(\vec{r}, t)) (\vec{V} \cdot \vec{n}) d\Omega, \\ &= - \int_{\Lambda} (\rho c_p)_f (\vec{V} \cdot \nabla T_f(\vec{r}, t)) d\Lambda. \end{aligned} \quad (2.30)$$

Here the subscript  $f$  refers to the fluid phase,  $c_p$  is the specific heat at constant pressure of the fluid, and  $\rho_f$  is the density of the fluid. The fluid average velocity is denoted by  $\vec{V}$ .

Substituting (2.21), (2.22), (2.23) and (2.30) into (2.29) gives

$$\begin{aligned} \int_{\Lambda} \left\{ (\rho c_p)_f \frac{\partial T_f(\vec{r}, t)}{\partial t} + (\rho c_p)_f (\vec{V} \cdot \nabla T_f(\vec{r}, t)) + \nabla \cdot \vec{q}_f(\vec{r}, t) - g_f(\vec{r}, t) \right\} d\Lambda &= 0, \\ \Rightarrow (\rho c_p)_f \frac{\partial T_f(\vec{r}, t)}{\partial t} + (\rho c_p)_f (\vec{V} \cdot \nabla T_f(\vec{r}, t)) &= \nabla \cdot (k_f \nabla T_f(\vec{r}, t)) + g_f(\vec{r}, t). \end{aligned} \quad (2.31)$$

In the above equations,  $g_f$  is the rate of heat generation in the fluid phase and  $k_f$  is the thermal conductivity of the fluid phase.

Multiplying (2.31) by porosity  $\varphi$  we have

$$\varphi (\rho c_p)_f \frac{\partial T_f(\vec{r}, t)}{\partial t} + (\rho c_p)_f (\varphi \vec{V} \cdot \nabla T_f(\vec{r}, t)) = \nabla \cdot (\varphi k_f \nabla T_f(\vec{r}, t)) + \varphi g_f(\vec{r}, t).$$

From the Dupuit-Forchheimer relationship  $\vec{v} = \varphi \vec{V}$ . Then

$$\varphi (\rho c_p)_f \frac{\partial T_f(\vec{r}, t)}{\partial t} + (\rho c_p)_f \vec{v} \cdot \nabla T_f(\vec{r}, t) = \nabla \cdot (\varphi k_f \nabla T_f(\vec{r}, t)) + \varphi g_f(\vec{r}, t). \quad (2.32)$$

In (2.32), there also appears a convective term, due to the Darcy velocity. We recognize that  $\vec{v} \cdot \nabla T_f$  is the rate of change of temperature in the elemental volume due to the convection of the fluid into it, so this, multiplied by  $(\rho c_p)_f$ , must be the rate of change of thermal energy, per unit volume of fluid, due to the convection.

### 2.5.3 Local Thermal Equilibrium

Now we suppose that there is local thermal equilibrium in the porous medium. This means that there is no net heat flux between the solid and fluid phase. All the phases of the medium must be at the same temperature, and this temperature must be the same as that of its surrounding. Such medium is said to be in local thermal equilibrium. It will enable us to define only one local temperature  $T_s = T_f = T$ . The condition for local thermal equilibrium is that the time for heat to diffuse across the grains of a porous medium is much less than the time scale for the flow. Adding (2.28) and (2.32), we obtain a single model equation which will govern the porous medium under local thermal equilibrium [54]

$$\begin{aligned} & \left\{ (1 - \varphi) (\rho c)_s + \varphi (\rho c_p)_f \right\} \frac{\partial T(\vec{r}, t)}{\partial t} + (\rho c_p)_f \vec{v} \cdot \nabla T(\vec{r}, t) \\ & = \nabla \cdot (\{(1 - \varphi) k_s + \varphi k_f\} \nabla T(\vec{r}, t)) + \{(1 - \varphi) g_s(\vec{r}, t) + \varphi g_f(\vec{r}, t)\}. \end{aligned} \quad (2.33)$$

$$\text{Let } (\rho c)_m = (1 - \varphi) (\rho c_p)_s + \varphi (\rho c_p)_f, \quad (2.34)$$

$$k_m = (1 - \varphi) k_s + \varphi k_f, \quad (2.35)$$

$$g_m = (1 - \varphi) g_s + \varphi g_f. \quad (2.36)$$

Then (2.33) takes the form

$$(\rho c)_m \frac{\partial T(\vec{r}, t)}{\partial t} + (\rho c_p)_f \vec{v} \cdot \nabla T(\vec{r}, t) = \nabla \cdot (k_m \nabla T(\vec{r}, t)) + g_m(\vec{r}, t). \quad (2.37)$$

In above equations the subscripts  $s$ ,  $f$  and  $m$  refer to the solid, fluid and porous medium, respectively,  $c$  is the specific heat of the solid,  $c_p$  is the specific heat at constant pressure of the fluid,  $k_m$  is the thermal conductivity of a porous medium. Under the assumption of local thermal equilibrium between solid and fluid phases, it is convenient to define an effective thermal conductivity, which characterizes how the solid and fluid phases act together as a thermal conductor. The effective thermal conductivity depends in a complex way on the geometry of the porous medium. Here we will discuss two types of conduction in porous medium.

### 2.5.3.1 Conduction in Parallel

In the case of parallel conduction in a porous medium, the thermal flux  $\vec{q}$  goes simultaneously through both solid and fluid phases, as shown in Figure 2.4 (a). There is no net heat exchange between the phases. The effective thermal conductivity  $k_A^{parallel}$  is given by

$$k_A^{parallel} = \varphi k_f + (1 - \varphi) k_s. \quad (2.38)$$

Equation (2.38) can also be described as the arithmetic mean of the conductivities of the solid and fluid phases [53].

### 2.5.3.2 Conduction in Series

In the case of series conduction in the porous medium, the thermal flux  $\vec{q}$  cross successively both solid and fluid phases, as shown in Figure 2.4 (b). The effective thermal conductivity  $k_H^{series}$  is given by

$$\frac{1}{k_H^{series}} = \frac{\varphi}{k_f} + \frac{(1 - \varphi)}{k_s}. \quad (2.39)$$

In (2.39) the subscript  $H$  represents the harmonic mean of  $k_f$  and  $k_s$  [53]. It is obvious that parallel conduction offers less resistance to heat transfer in the porous

medium than conduction in series.

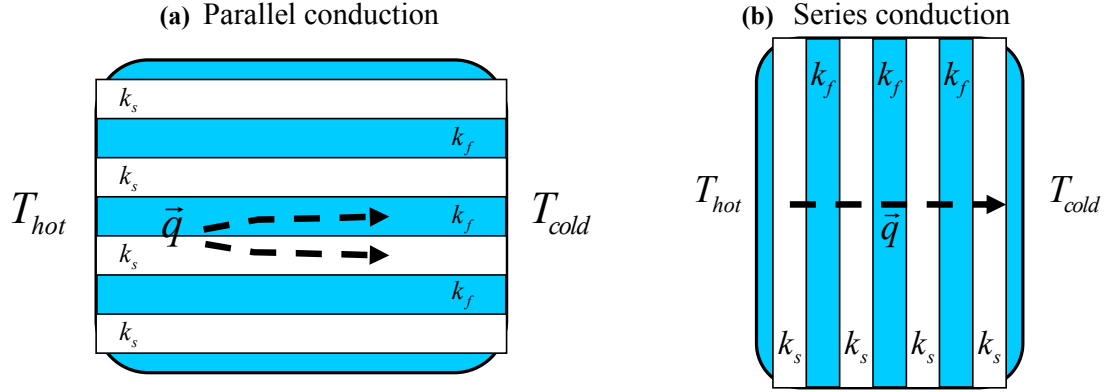


Figure 2.4: Models for parallel and series conduction in a porous medium [40].

#### 2.5.4 Local Thermal Non-Equilibrium

In certain situations the assumption of local thermal equilibrium between the solid and fluid phases is invalid. Such situations include those when there is significant heat generation in any of the phases, when the thermal properties of the two phases differ widely and when the particles or pores are not small enough in the porous medium.

When the assumption of local thermal equilibrium fails to be valid, one possible solution to model such cases is to develop separate transport equations for solid and fluid phases. This leads to a non-equilibrium model, and a two temperature model should be introduced for the energy equation [26, 54].

$$\left. \begin{aligned} (1 - \varphi) (\rho c_p)_s \frac{\partial T_s(\vec{r}, t)}{\partial t} &= (1 - \varphi) \nabla \cdot (k_s \nabla T_s(\vec{r}, t)) + (1 - \varphi) g_s(\vec{r}, t) \\ \varphi (\rho c_p)_f \frac{\partial T_f(\vec{r}, t)}{\partial t} + (\rho c_p)_f \vec{v} \cdot \nabla T_f(\vec{r}, t) &= \nabla \cdot (\varphi k_f \nabla T_f(\vec{r}, t)) + \varphi g_f(\vec{r}, t) \end{aligned} \right\} (2.40)$$

The two-equation model for heat transfer in porous medium is very difficult to apply. The reason is that the two equation model requires information on the effective conductivity values for solid and liquid phases, which can be determined

through experimental investigations. The solid to fluid heat transfer coefficient makes it hard to model the interface between the fluid and the solid matrix. The heat transfer coefficient can be determined either experimentally or using semi-theoretical work. Due to these difficulties, many investigators have used the so-called one-equation model described above for analysis of heat transfer in porous media [37, 86]. We will study phase change heat transfer in porous media using the one-equation model (2.37), while considering local thermal equilibrium across the solid-liquid interface.

## 2.6 Heat, mass conditions at the liquid-vapour interface in porous media

For the complete solution of the system of equations governing a liquid-vapour phenomena in a porous medium, the liquid-vapour interface must satisfy the heat and mass conservation principles. In this section we will determine the appropriate heat and mass flux conditions which apply at the interface between the vapour and liquid phases.

### 2.6.1 Pressure/Temperature relation

The contact between liquid and vapour means that the pressure and temperature at the front are related by  $T = T_S(P)$  or  $P = P_S(T)$ , where  $T_S$  and  $P_S$  are phase change temperature and pressure, respectively. This relation introduces an inherited non-linearity associated with phase change problems [23, p. 320]. Il'ichev & Tsyarkin [31] and Straus & Schubert [77] assumed that the temperature/pressure relationship determines the phase change condition. However, this assumption introduces a complicated empirical function, and it is not apparent that it is essential

to the physics of instability. In the interest of simplicity, then, we will assume that a constant temperature and a continuous pressure at the liquid-vapour interface are prescribed,

$$\text{at } x = S : \quad P_{liq} = P_{vap}, \quad T_{vap} = T_{liq} = T_S, \quad (2.41)$$

where  $S$  is an arbitrary horizontal position of the liquid-vapour interface and  $T_S$  is the prescribed temperature at the interface. The thermodynamic properties (density, specific heat, viscosity, thermal conductivity, permeability) of each phase will be assumed constant but different. Now we will derive the heat, mass jump conditions at the liquid-vapour interface.

### 2.6.1.1 Heat jump condition at phase change interface

Jozef Stefan studied the problem of thickness of polar ice: for this reason the freezing problem and phase-change problems more generally are referred as Stefan problems. Sarler [71] gives a detailed review of Stefan's achievements in the field of solid-liquid phase change problems, discussing eight different liquid-solid phase change problems published by Stefan between the years 1889 and 1891. The essential feature of Stefan problems is the existence of a moving interface of separation between the two phases, which is usually known as the liquid-solid phase change interface. The location of a phase change interface, which is not known beforehand, needs to be determined as part of the solution. The thermal energy balance condition at the phase change interface makes the solidification and melting Stefan problems non-linear; this condition is known as the Stefan condition.

It is important to note that the Stefan condition (energy condition) at the liquid-vapour interface will be derived under the assumption that the interface is at local thermodynamic equilibrium. This means that, while heat is being transferred across the interface, the internal processes occurring within the interface are fast enough

to keep the interface at equilibrium. Here we will formulate the Stefan condition at a moving interface in three dimensions. We will follow the same procedure as Gupta [24, p. 24-29]. We will start with the isothermal conditions at the interface  $\Phi(x, y, z, t) = 0$ ,

$$T_i = T_S, \quad i = liq, vap, \quad (2.42)$$

where the subscript  $i$  is for the two phases (liquid and vapour). The different notation  $\Phi$  for the interface is used for convenience.

The energy conservation (2.29) at the interface  $\Phi(x, y, z, t) = 0$  in vector form yields

$$[-\vec{q}]_{vap}^{liq} \cdot \vec{n} = \rho_{vap,liq} \lambda \left( \varphi \vec{\mathcal{U}} - \vec{v}_{vap,liq} \right) \cdot \vec{n}. \quad (2.43)$$

Here  $\vec{\mathcal{U}}$  is the velocity of the interface (which will be determined in terms of  $\Phi$  below), and  $\vec{q} = (q_1, q_2, q_3)$  is the diffusive heat flux vector which is defined as

$$q_\iota = - \sum_{j=1}^3 k_{m,\iota j} \frac{\partial T}{\partial x_j}, \quad \iota = 1, 2, 3, \quad (2.44)$$

where  $k_{m,\iota j}$  is the thermal conductivity tensor (the expression for thermal conductivity  $k_m$  in a porous medium is given by (2.35)),  $\vec{n}$  is the unit outward normal to the fluid at  $\Phi$ ,  $\vec{v}_{vap,liq}(u, v, w)$  is the Darcy velocity vector (see section 2.2) and  $\lambda_{vap} - \lambda_{liq} = \lambda$  is the latent heat.

The various terms in (2.43) are evaluated as follows

$$\begin{aligned} \vec{q}_i \cdot \vec{n} &= \vec{q}_i \cdot \frac{\nabla \Phi}{|\nabla \Phi|}, \quad i = liq, vap, \\ &= \frac{\left( q_{i,1} \frac{\partial \Phi}{\partial x} + q_{i,2} \frac{\partial \Phi}{\partial y} + q_{i,3} \frac{\partial \Phi}{\partial z} \right)}{|\nabla \Phi|}, \quad i = liq, vap, \\ &= \frac{- \sum_{j,k=1}^3 k_{m,ijk} \frac{\partial T^i}{\partial x_j} \frac{\partial \Phi}{\partial x_k}}{|\nabla \Phi|}, \quad i = liq, vap, \end{aligned} \quad (2.45)$$

The total derivative of  $\Phi(x, y, z, t)$  is

$$\begin{aligned}
\frac{d\Phi(x, y, z, t)}{dt} &= 0, \\
\Rightarrow \frac{\partial\Phi}{\partial t} + \frac{\partial\Phi}{\partial x} \frac{\partial x}{\partial t} + \frac{\partial\Phi}{\partial y} \frac{\partial y}{\partial t} + \frac{\partial\Phi}{\partial z} \frac{\partial z}{\partial t} &= 0, \\
\Rightarrow \frac{\partial\Phi}{\partial t} + (\vec{\mathcal{U}} \cdot \vec{n}) |\nabla\Phi| &= 0, \\
\Rightarrow \vec{\mathcal{U}} \cdot \vec{n} &= -\frac{1}{|\nabla\Phi|} \frac{\partial\Phi}{\partial t}. \tag{2.46}
\end{aligned}$$

This gives  $\vec{\mathcal{U}} \cdot \vec{n}$  (note that the velocity of a surface can be defined in the direction perpendicular to the surface), which is all we need in (2.43). Similarly

$$\vec{v}_{liq} \cdot \vec{n} = \frac{1}{|\nabla\Phi|} \left( u_{liq} \frac{\partial\Phi}{\partial x} + v_{liq} \frac{\partial\Phi}{\partial y} + w_{liq} \frac{\partial\Phi}{\partial z} \right), \tag{2.47}$$

or if the unit vector is normal to the vapour phase then

$$\vec{v}_{vap} \cdot \vec{n} = \frac{1}{|\nabla\Phi|} \left( u_{vap} \frac{\partial\Phi}{\partial x} + v_{vap} \frac{\partial\Phi}{\partial y} + w_{vap} \frac{\partial\Phi}{\partial z} \right), \tag{2.48}$$

where  $u$ ,  $v$  and  $w$  are the  $x$ ,  $y$  and  $z$  components of the Darcy velocity  $\vec{v}_{vap,liq}$ . Substituting (2.45), (2.46) and (2.47) into (2.43), we obtain the generalized form of the Stefan condition in porous media

$$\begin{aligned}
\sum_{j,k=1}^3 k_{m,liq,jk} \frac{\partial T_{liq}}{\partial x_j} \frac{\partial\Phi}{\partial x_k} - \sum_{j,k=1}^3 k_{m,vap,jk} \frac{\partial T_{vap}}{\partial x_j} \frac{\partial\Phi}{\partial x_k} \\
= \rho_{liq} \lambda \left\{ -\varphi \frac{\partial\Phi}{\partial t} - \left( u_{liq} \frac{\partial\Phi}{\partial x} + v_{liq} \frac{\partial\Phi}{\partial y} + w_{liq} \frac{\partial\Phi}{\partial z} \right) \right\}.
\end{aligned}$$

In the isotropic case  $k_{m,ijk} = k_{m,i} \delta_{jk}$ , where  $\delta_{jk}$  is the Kronecker delta function, we have

$$\begin{aligned}
\sum_{j=1}^3 \left\{ \sum_{k=1}^3 k_{m,liq} \delta_{jk} \frac{\partial\Phi}{\partial x_k} \right\} \frac{\partial T_{liq}}{\partial x_j} - \sum_{j=1}^3 \left\{ \sum_{k=1}^3 k_{m,vap} \delta_{jk} \frac{\partial\Phi}{\partial x_k} \right\} \frac{\partial T_{vap}}{\partial x_j} \\
= \rho_{liq} \lambda \left\{ -\varphi \frac{\partial\Phi}{\partial t} - \left( u_{liq} \frac{\partial\Phi}{\partial x} + v_{liq} \frac{\partial\Phi}{\partial y} + w_{liq} \frac{\partial\Phi}{\partial z} \right) \right\}.
\end{aligned}$$

Carrying out the summations, the above equation becomes

$$\begin{aligned}
& k_{m,liq} \left( \frac{\partial \Phi}{\partial x} \frac{\partial T_{liq}}{\partial x} + \frac{\partial \Phi}{\partial y} \frac{\partial T_{liq}}{\partial y} + \frac{\partial \Phi}{\partial z} \frac{\partial T_{liq}}{\partial z} \right) \\
& \quad - k_{m,vap} \left( \frac{\partial \Phi}{\partial x} \frac{\partial T_{vap}}{\partial x} + \frac{\partial \Phi}{\partial y} \frac{\partial T_{vap}}{\partial y} + \frac{\partial \Phi}{\partial z} \frac{\partial T_{vap}}{\partial z} \right) \\
& = \rho_{liq} \lambda \left\{ -\varphi \frac{\partial \Phi}{\partial t} - \left( u_{liq} \frac{\partial \Phi}{\partial x} + v_{liq} \frac{\partial \Phi}{\partial y} + w_{liq} \frac{\partial \Phi}{\partial z} \right) \right\}. \quad (2.49)
\end{aligned}$$

It will be helpful in subsequent chapters to write the interface condition as  $\Phi = 0$ , where

$$\begin{aligned}
\Phi(x, y, z, t) &= x - S(y, z, t) = 0 \\
\frac{\partial \Phi}{\partial t} &= -\frac{\partial S}{\partial t}, \quad \frac{\partial \Phi}{\partial x} = 1, \quad \frac{\partial \Phi}{\partial y} = -\frac{\partial S}{\partial y}, \quad \frac{\partial \Phi}{\partial z} = -\frac{\partial S}{\partial z}. \quad (2.50)
\end{aligned}$$

Substituting (2.50) into (2.49), we obtain

$$\begin{aligned}
& k_{m,liq} \left( \frac{\partial T_{liq}}{\partial x} - \frac{\partial S}{\partial y} \frac{\partial T_{liq}}{\partial y} - \frac{\partial S}{\partial z} \frac{\partial T_{liq}}{\partial z} \right) - k_{m,vap} \left( \frac{\partial T_{vap}}{\partial x} - \frac{\partial S}{\partial y} \frac{\partial T_{vap}}{\partial y} - \frac{\partial S}{\partial z} \frac{\partial T_{vap}}{\partial z} \right) \\
& \quad = \rho_{liq} \lambda \left\{ \varphi \frac{\partial S}{\partial t} - \left( u_{liq} - v_{liq} \frac{\partial S}{\partial y} - w_{liq} \frac{\partial S}{\partial z} \right) \right\}. \quad (2.51)
\end{aligned}$$

### 2.6.1.2 Special cases

Now we will derive the most commonly used forms of the Stefan condition found in the literature.

Rubin & Schweitzer [68] studied two phase flow in a porous medium. They assumed that liquid at a constant temperature enters the system from one end and at the opposite end the temperature of the system is raised above the evaporation point of the liquid by imposing a constant temperature in one case and in other case a constant heat flux. This causes an evaporation front separating a vapour region from a liquid region as shown in the figure below.

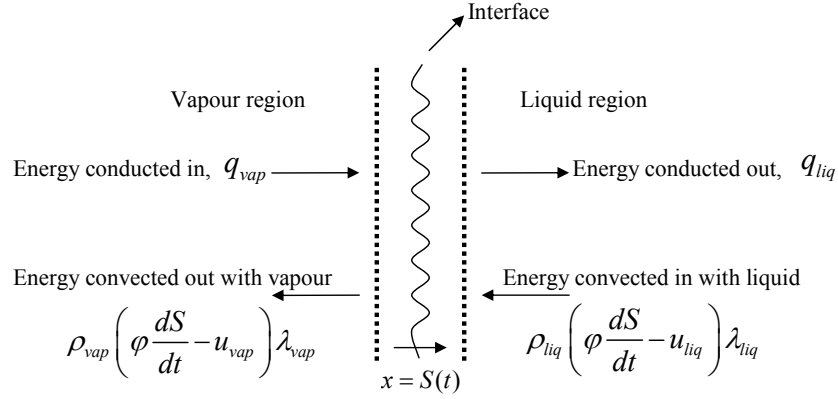


Figure 2.5: Energy balance at a vaporising interface [68].

In a geothermal context, Tsypkin & Il'ichev [83] also assumed that the movement of the interface  $S(t)$  was affected by the fluid motion and the phase change interface temperature depends on pressure. Both [68] and [83] assumed that the interface was moving in the  $x$  direction and also affected by the fluid motion in the  $x$  direction only,  $u_{liq} \neq 0$ ,  $v_{liq} = w_{liq} = 0$ . Under these assumptions (2.51) will take the form

$$k_{m,liq} \frac{\partial T_{liq}}{\partial x} - k_{m,vap} \frac{\partial T_{vap}}{\partial x} = \rho_{liq} \lambda \left( \varphi \frac{dS}{dt} - u_{liq} \right), \quad \text{at } x = S(t), \quad (2.52)$$

where  $u_{liq}$  is the  $x$  component of the Darcy velocity of the liquid.

In one-dimensional melting/freezing problems of the kind originally studied by Stefan, the interface is located at  $x = S(t)$ , so there is no variation in the  $y$  and  $z$  directions. The interface motion is not due to the motion of the fluid,  $u_{liq} = v_{liq} = w_{liq} = 0$ , and system under consideration is not porous,  $\varphi = 1$ , so (2.51) will take the form

$$k_s \frac{\partial T_s}{\partial x} - k_{liq} \frac{\partial T_{liq}}{\partial x} = \rho \lambda \frac{dS}{dt}, \quad \text{at } x = S(t), \quad (2.53)$$

where  $k_s$  is the thermal conductivity of the solid. The above equation is widely used in the literature [9, 34, 36, 42, 90].

A two dimensional melting process in an isotropic porous medium was studied by

Nield & Bejan [55, p. 305-330], considering local thermal equilibrium between the phase change material and the porous medium. The thermal properties of the two phases were assumed to be constant and identical. The solid and liquid phases were separated by a sharp interface. The interface position  $x = S$  changes with time  $t$  and  $y$  coordinate. In the light of this description, (2.51) will take the form

$$\frac{\partial S}{\partial t} = -\frac{k}{\rho\lambda} \left( \frac{\partial T}{\partial x} - \frac{\partial S}{\partial y} \frac{\partial T}{\partial y} \right). \quad (2.54)$$

The heat flux conditions (2.52), (2.53) and (2.54) at a phase change interface are just three examples depending upon the configurations under consideration. We will use (2.52) as a energy jump condition at the phase change interface separating the vapour phase from liquid phase.

### 2.6.1.3 Mass jump condition at phase change interface

A mass jump condition can be derived in the same way as the energy jump condition (see Section 2.6.1.1) at the interface. We present the derivation (for mass conservation at the interface) only in one dimension, because our interest is in situations where the interface is almost flat and the effects of any 2D perturbation end up being of higher order than we need for the analyses.

At the liquid-vapour interface, the system under consideration must satisfy the principle of mass conservation (2.7). The mass balance across the liquid-vapour interface in a porous medium is illustrated in Figure 2.6. Figure 2.6 shows that fluid (vapour) flows towards or away from the liquid-vapour interface with a velocity  $u_{vap}$ , where  $u_{vap}$  is the  $x$  component of the Darcy velocity.

Also the interface is moving with a velocity  $dS/dt$  and since the actual flow is in the pores, the vapour mass flux per unit time through the moving liquid-vapour

interface equals

$$\rho_{vap} \left( \varphi \frac{dS}{dt} - u_{vap} \right),$$

which must be equal to the liquid mass flux at the liquid-vapour interface,

$$\rho_{vap} \left( \varphi \frac{dS}{dt} - u_{vap} \right) = \rho_{liq} \left( \varphi \frac{dS}{dt} - u_{liq} \right), \quad (2.55)$$

where  $\rho_{liq,vap}$  is the density,  $\varphi$  is the effective porosity. Rearranging (2.55) yields

$$\varphi (\rho_{liq} - \rho_{vap}) \frac{dS}{dt} = \rho_{liq} u_{liq} - \rho_{vap} u_{vap}. \quad (2.56)$$

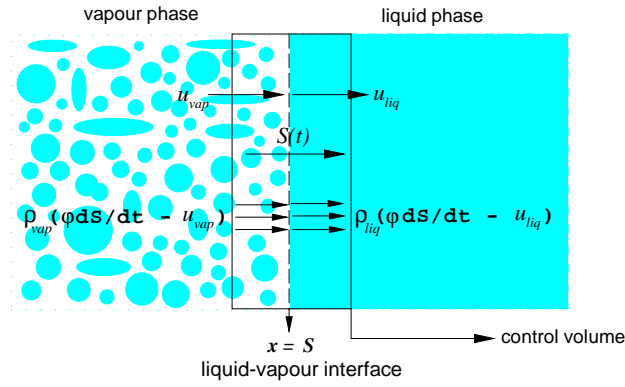


Figure 2.6: Mass balance at a liquid-vapour phase change interface [11, p. 108].

A comprehensive discussion of the mass balance (2.56) at a liquid-vapour interface can be found in [63], [25] and [11, p. 107-112].

Now substituting the  $x$  component of the Darcy velocity (2.6) for the liquid and vapour phases into the mass jump condition (2.56) yields

$$\varphi \left( 1 - \frac{\rho_{vap}}{\rho_{liq}} \right) \frac{dS}{dt} = \frac{\rho_{vap}}{\rho_{liq}} \frac{K}{\mu_{vap}} \frac{dP_{vap}}{dx} \Big|_{x=S} - \frac{K}{\mu_{liq}} \frac{dP_{liq}}{dx} \Big|_{x=S} - \frac{K g \rho_{liq}}{\mu_{liq}} \left( 1 - \frac{\rho_{vap}^2 \mu_{liq}}{\rho_{liq}^2 \mu_{vap}} \right), \quad (2.57)$$

where  $g$  is acting in the negative  $x$  direction. The above equation (2.57) has been used as a standard mass jump condition at the liquid-vapour interface [28–31, 77, 83] with the notational difference that in our case gravity is acting in the negative  $x$  direction.

## 2.7 Numerical data for the parameters and variables used

Now it is important to discuss the numerical values of the dimensional and dimensionless quantities of interest in our study. We will employ data from three sets of sources. The first set is taken from, Tsyarkin & Il'ichev's [83] and Straus & Schubert's [77] analyses of a separate-phase model (sharp interface). The second set of data is taken from Udell's [84] fluid flow experiments in a porous medium heated from below (mixed-phase model). The third set of data for parameters and variables is that used by Carey [11, p. 727] while studying the basic thermophysics and transport principles that underlie the mechanisms of condensation and vaporisation processes. Tables 2.1 and 2.2 represents the numerical values for the dimensional and dimensionless quantities, respectively, which we require in our analysis. Note that some quantities, in particular the permeability  $K$  of the porous medium and  $L$ , the layer thickness, may vary by many orders of magnitude. It is, therefore, important to investigate the behaviour of the model over a wide range of parameter values.

Symbol	Tsyarkin & Il'ichev's [83] numerical values	Carey [11, p. 727] numerical values	Straus & Schubert's [77] numerical values	Udell's [84] numerical values	Units (SI)
$\rho_{vap}$	4.82	0.597	178	1	kg/m <sup>3</sup>
$\rho_{liq}$	888.66	958.3	858	10 <sup>3</sup>	kg/m <sup>3</sup>
$c_{vap}$	1	2.03	3.6	1	kJ/kg K
$c_{liq}$	1	4.22	4.5	4.3	kJ/kg K
$\mu_{vap}$	15.80	12.55	15.90	22	$\mu$ Ns/m <sup>2</sup>
$\mu_{liq}$	148	277.53	130	250	$\mu$ Ns/m <sup>2</sup>
$k_{vap}$	$2 \times 10^3$	25	$4 \times 10^3$	10 <sup>3</sup>	mW/m K
$k_{liq}$	$2 \times 10^3$	679	$4 \times 10^3$	$2.5 \times 10^3$	mW/m K
$\lambda$	2000	2256.7	1700	2500	kJ/kg
$g$	9.8	9.8	9.8	9.8	m/s <sup>2</sup>
$T$	440 - 460	300 - 400	293 - 600	360 - 390	K
$T_S$	450	373.15	515	380	K
$L$	20	10	400	0.254	m
$K$	$10^{-17}$	$10^{-17}$	$2-4 \times 10^{-14}$	$6.4 \times 10^{-12}$	m <sup>2</sup>

Table 2.1: Numerical values for the parameters and variables used in our analysis.

Symbol	Interpretation	Carey's numerical values	Tsyarkin & Il'ichev's numerical values	Straus & Schubert's numerical values	Udell's numerical values
$\varphi$	porosity	-	0.03	0.05	0.38
$C$	specific heat ratio	2.02	1	0.8	4.3
$k$	thermal conductivity ratio	27.16	1	1	2.5
$R$	kinematic viscosity ratio	0.0138	0.050	1.69	0.011
$R_1$	density ratio	0.000623	0.0054	0.207	0.001
$R_2$	dynamic viscosity ratio	22.11	9.31	8.17	11.36
$H_{liq}$	Stefan number for liquid	8.74	200	2.13	29.06
$H_{vap}$	Stefan number for vapour	41.17	200	2.04	250
$\Theta_0$	Temperature contrast	0.37	1	0.83	0.50

Table 2.2: List of the possible range of numerical values for the dimensionless parameters and quantities we have used in our study. Note that these dimensionless quantities will be defined in chapter 3-5.

## Chapter 3

# One Dimensional Phase Change

## Problems

The simplest mathematical models of a real world problem are often restricted, for example to one-dimensional and steady-state behaviour. For example, the natural state of a geothermal system is often assumed to be steady-state [31, 68, 78, 95]. The overwhelming practice of beginning with a one-dimensional mathematical model of a geothermal reservoir can be justified by the fact that the problem has few unknown parameters and quantities which can be found easily. From another angle, one-dimensional models are regarded as an approximate representation of a three-dimensional model, and are considered a good starting point for the visualisation of the big picture. A one-dimensional state will only be seen if it is stable to multi-dimensional perturbations. A good mathematical understanding of a basic state (one-dimensional) of an evaporation/condensation phase change problem, especially the phase change interface (the core of such problems), will provide a good foundation for the better understanding of a more complex real world multi-dimensional geothermal model.

In this chapter, we study one-dimensional steady and moving interface problems. We will formulate these problems mathematically, and discuss analytical solutions.

### 3.1 The steady-state through flow problem

Rubin & Schweitzer [68] studied horizontal flow and heat transport in a porous medium. In their problem, liquid flows from a reservoir of constant temperature into one end of the porous medium and the other end is maintained at constant temperature or a constant heat flux is imposed. They assumed a constant temperature at the vapour boundary greater than the evaporation point of the liquid, which causes the formation of an evaporation front separating the liquid and vapour regions. They obtained exact solutions for the steady state problem.

We will now extend the analysis of Rubin & Schweitzer [68] and will consider one-dimensional steady-state vertical flow and heat transport because we are interested in buoyant effects. Figure 3.1 illustrates the flow configuration. In a geothermal reservoir, the fluid near to the magmatic body exists in the form of vapour (say at a temperature  $T_V$ ), while further away from the heat source it is liquid (say at a temperature  $T_L (< T_V)$ ). The fundamental variables describing the flow of the liquid and the vapour are the pressures in each region. The mass fluxes of the liquid and vapour regions are related to the pressure gradients through Darcy's law. If we ignore gravity then the flow direction is determined by the imposed pressure gradient across the reservoir. But in the presence of gravity, the direction of the flow is determined by both the imposed pressure gradient and the gravitational acceleration. If the phase change temperature  $T_S$  lies between the temperatures at the boundaries then a phase change front forms within the medium, separating a vapour region from a liquid region. The pressure difference across the liquid-vapour

interface due to the density difference is assumed small compared to  $(P_V - P_L)$  so that we may take  $P_{liq} = P_{vap}$  at  $x = S$ .

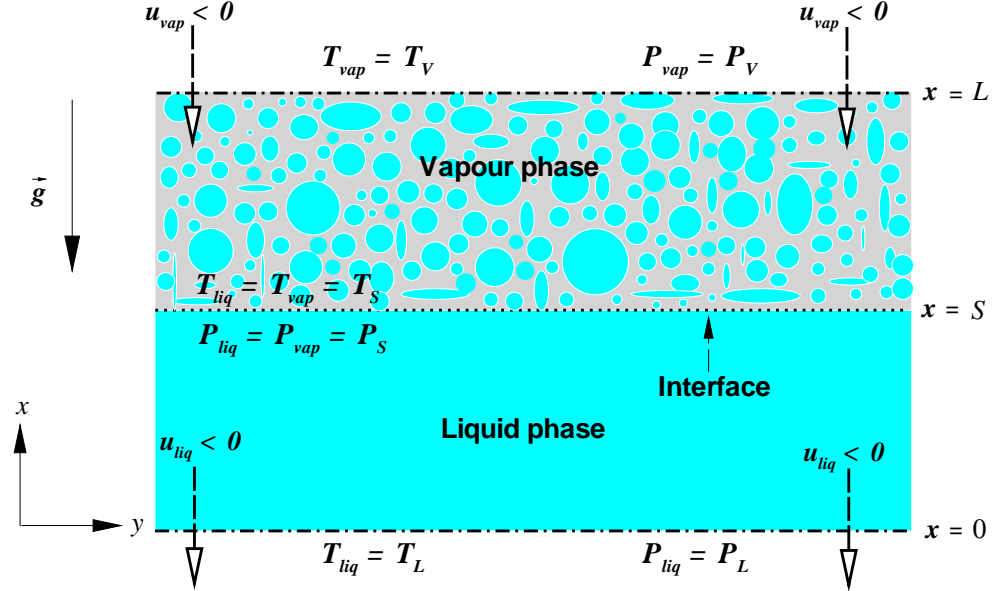


Figure 3.1: Diagram of through flow problem.

According to the above assumptions, the equations (2.6), (2.14) and (2.37) governing the mass and heat flow in a porous medium for this model will take the following form:

$$\text{Mass Balance: (2.14)} \Rightarrow \frac{d}{dx} (u_{liq,vap}) = 0, \quad (3.1)$$

$$\text{Darcy's Law: (2.6)} \Rightarrow u_{liq,vap} = -\frac{K}{\mu_{liq,vap}} \left\{ \frac{dP_{liq,vap}}{dx} + \rho_{liq,vap} g \right\}, \quad (3.2)$$

$$\text{Heat Equation: (2.37)} \Rightarrow k_m \frac{d^2 T_{liq,vap}}{dx^2} - (\rho c_p u)_{liq,vap} \frac{dT_{liq,vap}}{dx} = 0. \quad (3.3)$$

(Recall that the Darcy velocity  $\vec{v}_{liq,vap} = (u_{liq,vap}, v_{liq,vap})$ , where  $u_{liq,vap}$  is the  $x$ -component of the fluid velocity.)

The important point to note is the sign of the gravitational acceleration  $g$ : if  $g$  is positive then the lighter fluid (vapour) is above the heavier fluid (liquid) as sketched in Figure 3.1, whereas if  $g$  is negative then the heavier fluid (liquid) is

above the lighter fluid (vapour). The appropriate boundary conditions for this problem are

$$\text{at } x = 0 : P_{liq} = P_L, \quad (3.4)$$

$$\begin{cases} \text{case}(a) : T_{liq} = T_L, \\ \text{case}(b) : q_{liq} = -k_{m,liq} \frac{dT_{liq}}{dx}, \end{cases} \quad (3.5)$$

$$\text{at } x = L : P_{vap} = P_V, \quad T_{vap} = T_V, \quad (3.6)$$

where  $T_L$  and  $q_{liq}$  are specified, as are  $P_L$  and  $P_V$ . At the phase change front

$$x = S : P_{vap} = P_{liq}, \quad T_{vap} = T_{liq} = T_S, \quad (3.7)$$

where the phase change temperature  $T_S$  is prescribed (see Section 2.6.1). Now, since the interface position  $S$  is an unknown in the problem, we require further conditions at the interface. Energy should be conserved across the phase change interface. On  $S$ , the Stefan jump condition (2.52) holds,

$$k_{m,liq} \frac{dT_{liq}}{dx} \Big|_{x=S} - k_{m,vap} \frac{dT_{vap}}{dx} \Big|_{x=S} = -\lambda \rho_{liq} u_{liq}, \quad (3.8)$$

where  $\lambda = \lambda_{vap} - \lambda_{liq}$  is the latent heat of condensation. The jump at  $x = S$  is taken from liquid to vapour because of the heat flux difference in the both phases.

The mass conservation equation across the interface is

$$\rho_{liq} u_{liq} = \rho_{vap} u_{vap}. \quad (3.9)$$

For constant properties of the fluid, it is possible to obtain the mass flux as a function of the condensation front position  $S$ . Substituting Darcy's velocity (3.2) into the continuity equation (3.1) gives

$$\frac{d^2 P_{liq,vap}}{dx^2} = 0. \quad (3.10)$$

Solving (3.10) subject to the pressure boundary conditions (3.4)-(3.7) and combining the results with Darcy's law (3.2) gives the mass flux for the vapour and the liquid phases

$$\dot{m}_{vap} = -\frac{K}{\nu_{vap}} \left\{ \frac{(P_V - P_S)}{(L - S)} + \rho_{vap} g \right\}, \quad (3.11)$$

$$\dot{m}_{liq} = -\frac{K}{\nu_{liq}} \left\{ \frac{(P_S - P_L)}{S} + \rho_{liq} g \right\}, \quad (3.12)$$

where  $\dot{m}_{vap,liq} = (\rho u)_{vap,liq}$  is the mass flux and  $\nu_{vap,liq} = \frac{\mu_{vap,liq}}{\rho_{vap,liq}}$  is the kinematic viscosity. It is assumed that the pressures at the upper and lower boundaries are known and constant but the pressure  $P_S$  at the condensation front is unknown, and can be found in terms of the front position  $S$  by substituting (3.11) and (3.12) into the mass conservation equation (3.9)

$$P_S = \frac{R S P_V + P_L (L - S)}{R S + L - S} - \frac{g S (L - S)(\rho_{liq} - \rho_{vap} R)}{R S + L - S}, \quad (3.13)$$

where  $R = \frac{\nu_{liq}}{\nu_{vap}}$  is the ratio of the kinematic viscosities. The mass flux in the entire medium is obtained by substituting the pressure  $P_S$  at the front into (3.11) or (3.12)

$$\dot{m}_{vap} = \dot{m}_{liq} = -\frac{K}{\nu_{vap}} \left\{ \frac{(P_V - P_L)}{R S + L - S} + \frac{g [(\rho_{liq} - \rho_{vap}) S + \rho_{vap} L]}{R S + L - S} \right\}. \quad (3.14)$$

The temperature distribution  $T(x)$  and the condensation front position  $S$  will be obtained for two different sets of boundary conditions: (i) constant temperature at the lower boundary  $x = 0$  and (ii) constant heat flux  $q_{liq}$  at  $x = 0$ .

### 3.1.1 Isothermal Boundary Conditions

In this case, a constant temperature  $T_L$  will be imposed at the lower boundary  $x = 0$  with the restriction that  $T_L < T_S < T_V$ . So that the vaporisation temperature lies between the temperatures at the lower and upper layers. The following

dimensionless quantities will be used to non-dimensionalise (3.3)-(3.8) and (3.14):

$$\begin{aligned}
x^* &= \frac{x}{L}, & S^* &= \frac{S}{L}, & k &= \frac{k_{m,liq}}{k_{m,vap}}, & C &= \frac{c_{p,liq}}{c_{p,vap}}, & \Theta_{liq}(x^*) &= \frac{T_{liq}(x) - T_L}{T_S - T_L}, \\
\Theta_{vap}(x^*) &= \frac{T_V - T_{vap}(x)}{T_V - T_S}, & \Theta_0 &= \frac{T_V - T_S}{T_S - T_L}, & P^* &= \frac{K \rho_{liq} c_{p,liq} P}{\mu_{liq} k_{m,liq}}, \\
u_{liq,vap}^* &= \frac{L \rho_{liq,vap} c_{p,liq,vap} u_{liq,vap}}{k_{m,liq,vap}}, & v_{liq,vap}^* &= \frac{L \rho_{liq,vap} c_{p,liq,vap} v_{liq,vap}}{k_{m,liq,vap}}, \\
H_{liq} &= \frac{\lambda}{c_{p,liq} (T_S - T_L)}, & Pec_{liq} &= \frac{\dot{m}_{liq} c_{p,liq} L}{k_{m,liq}}, & Pec_{vap} &= \frac{\dot{m}_{vap} c_{p,vap} L}{k_{m,vap}}, \quad (3.15)
\end{aligned}$$

where  $H_{liq}$  is the reciprocal of the Stefan number for the liquid region, and represents the ratio of the latent heat  $\lambda$  to the sensible heat  $(T_S - T_L)$  [71, p. 91]. The Peclet numbers  $Pec_{liq,vap}$  are defined in terms of Darcy's velocity, the characteristic length-scale (set by the depth of the porous medium) and the fluid thermal diffusivity [55, p. 25]. The Peclet numbers  $Pec_{liq,vap}$  are not parameters, since the mass flux has to be found as part of the solution. Furthermore,  $Pec_{liq,vap}$  are just the base-state values of  $u_{liq,vap}^*$ . The Darcy's velocities in both phases (liquid and vapour) are scaled in terms of the length-scale and the thermal diffusion (the time scale is set by thermal diffusion). The pressure scale is based on these characteristic velocities and the resistance of the medium to liquid flow. The ratio of the temperature contrasts across the liquid and vapour layers is denoted by  $\Theta_0$ .

If the phase change front is at  $x = 0$ , then  $S = 0$ , i.e., the medium is filled with vapour only. Eqn (3.14) gives the following reference flow rate based on a layer entirely filled with vapour,

$$\dot{m}_i = -\frac{K}{\nu_{vap}} \left\{ \frac{(P_V - P_L)}{L} + \rho_{vap} g \right\}. \quad (3.16)$$

On the basis of flow rate (3.16) the reference Peclet number is defined as

$$Pec_i = \frac{\dot{m}_i c_{p,vap} L}{k_{m,vap}}. \quad (3.17)$$

The energy equations (3.3) for each phase, using the normalised quantities (3.15) and (3.17) take the form

$$\frac{d^2\Theta_{liq}}{dx^{*2}} - \frac{C Pec_i F(S^*)}{k} \frac{d\Theta_{liq}}{dx^*} = 0, \quad 0 \leq x^* \leq S^*, \quad (3.18)$$

$$\frac{d^2\Theta_{vap}}{dx^{*2}} - Pec_i F(S^*) \frac{d\Theta_{vap}}{dx^*} = 0, \quad S^* \leq x^* \leq 1. \quad (3.19)$$

The remaining dimensionless quantities involved in the above equations (3.18) and (3.19) are

$$F(S^*) = \frac{\dot{m}_{liq,vap}}{\dot{m}_i} = F_1(S^*) [1 - R G_1 S^*], \quad F_1(S^*) = \frac{1}{R S^* + 1 - S^*},$$

$$R_1 = \frac{\rho_{vap}}{\rho_{liq}}, \quad R_3 = \frac{K \rho_{liq}^2 c_{pliq} g L}{\mu_{liq} k_{m,liq}}, \quad G_1 = \frac{R_3 k(1 - R_1)}{C Pec_i}. \quad (3.20)$$

The Rayleigh number  $R_3$  is the ratio of the stabilising time to the destabilising time. Its interpretation is the same as that of the conventional Rayleigh number [55, p. 81], but its form is somewhat different.

$$\text{Rayleigh number } R_3, \text{ represents } \left\{ \begin{array}{l} \text{vapour above liquid, if } R_3 \text{ is positive,} \\ \text{liquid above vapour, if } R_3 \text{ is negative.} \end{array} \right.$$

The dimensionless quantity  $G_1$  is the ratio of the hydrostatic to the externally imposed pressure difference across the porous layer. The normalised forms of the boundary conditions (3.5), (3.7) and (3.8) are

$$\left. \begin{array}{l} \text{at } x^* = 0 : \Theta_{liq} = 0, \\ \text{at } x^* = 1 : \Theta_{vap} = 0, \end{array} \right\} \quad (3.21)$$

$$\text{at } x^* = S^* \left\{ \begin{array}{l} \Theta_{liq} = \Theta_{vap} = 1, \\ \frac{d\Theta_{liq}}{dx^*} + \frac{\Theta_0}{k} \frac{d\Theta_{vap}}{dx^*} = -\frac{H_{liq} C Pec_i F(S^*)}{k}. \end{array} \right. \quad (3.22)$$

The solutions of (3.18) and (3.19) for the temperature distribution in the liquid and in the vapour phase subject to the boundary conditions (3.21) and (3.22) are

$$\Theta_{liq}(x^*) = \frac{1 - \exp\left[\frac{C Pec_i F(S^*)}{k} x^*\right]}{1 - \exp\left[\frac{C Pec_i F(S^*)}{k} S^*\right]}, \quad 0 \leq x^* \leq S^*, \quad (3.23)$$

$$\Theta_{vap}(x^*) = \frac{1 - \exp[Pec_i F(S^*) (x^* - 1)]}{1 - \exp[Pec_i F(S^*) (S^* - 1)]}, \quad S^* \leq x^* \leq 1. \quad (3.24)$$

Substituting (3.23) and (3.24) into the energy jump condition (3.22) yields a transcendental equation for the position of the phase change front in terms of the independent parameters  $C$ ,  $H_{liq}$ ,  $\Theta_0$ ,  $Pec_i$ ,  $k$  and  $R$ ,

$$\frac{\Theta_0}{C} = \{\exp[Pec_i F(S^*) (1 - S^*)] - 1\} \left\{ H_{liq} + \frac{1}{1 - \exp\left[-\frac{C F(S^*) Pec_i S^*}{k}\right]} \right\}. \quad (3.25)$$

In the problem description, we have mentioned that in the presence of gravity, the flow direction depends on the pressure gradient and on gravity. So, it is important to note that

$$\text{Flow direction} = \begin{cases} \text{negative } x\text{-direction (vapour to liquid) if } Pec_i F(S^*) < 0, \\ \text{positive } x\text{-direction (liquid to vapour) if } Pec_i F(S^*) > 0. \end{cases}$$

The quantity  $Pec_i F(S^*)$  is the scaled version of the mass flux, which determines the flow direction. Since  $F(S^*)$  may be either positive or negative, depending on the sign and magnitude of  $G_1$ , the mass flux does not necessarily have the same sign as  $Pec_i$ .

The asymptotic solution of the transcendental equation (3.25) for the interface position  $S^*$  for small reference Peclet number  $Pec_i$  is

$$S^* \sim \frac{k}{k + \Theta_0} + O(Pec_i), \quad \text{as } Pec_i \rightarrow 0. \quad (3.26)$$

Equation (3.26) tells us that, in the absence of net flow in the reservoir, the front position depends on the ratio of the temperature contrast ( $\Theta_0$ ) and the ratio of thermal conductivities ( $k$ ) of the two phases. This result corresponds to equation (33a) of Rubin & Schweitzer [68], allowing for a trivial change to the coordinate system. In Section 4.3, we will extensively discuss the stability of the interface position  $S^*$  given by (3.26).

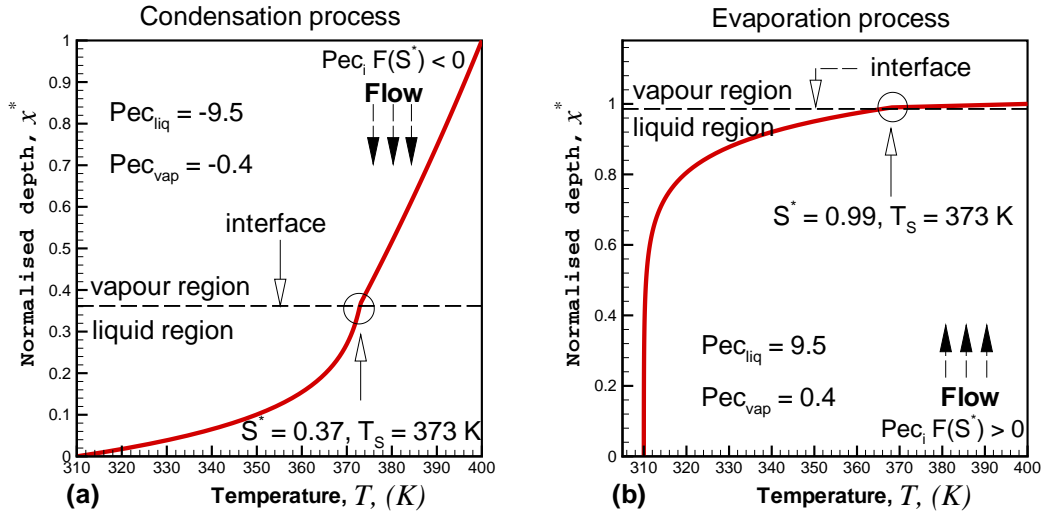


Figure 3.2: Temperature profile for isothermal conditions with temperature contrast ratio  $\Theta_0 = 0.43$ , Rayleigh number  $R_3 = -2.0 \times 10^{-10}$ ,  $G_1 = \pm 7.2 \times 10^{-10}$  and reference Peclet number  $Pec_i = \pm 3.65$ .

Figure 3.2 (a) shows a typical temperature distribution for the condensation process in the porous medium with  $H_{liq} = 8.74$ . The fluid flow is from the vapour to the liquid region ( $Pec_i F(S^*) < 0$ ) and the heavier fluid is above the lighter fluid ( $R_3 < 0$ ). For this particular plot, we have found that  $Pec_i F(S^*) = -0.415$ , for the front position  $S^* = 0.37$ , which is obtained as a part of the solution. Figure 3.2 (b) shows that the fluid flow is in the positive  $x$ -direction (liquid to vapour), i.e.,  $Pec_i F(S^*) > 0$ . For this particular plot  $Pec_i F(S^*) = 0.167$  when  $S^* = 0.99$ . As we know, the Peclet number is the ratio of the diffusive to the advective time

scales. The higher the Peclet number, the more dominance of advection over conduction can be observed. In the vapour phase the temperature profile is nearly linear with small vapour Peclet number  $|Pec_{vap}|$ , which shows that conduction dominates over advection. In the liquid phase the liquid Peclet number  $|Pec_{liq}|$  is higher than that in the vapour phase, advection dominates, and the temperature profile is exponential. Figures 3.2 (a) and (b) show that a boundary layer forms at the downstream end of the domain (near to the liquid boundary in Figure 3.2 (a), and near to the vapour boundary in Figure 3.2 (b)). This boundary layer becomes sharper for larger Peclet numbers.

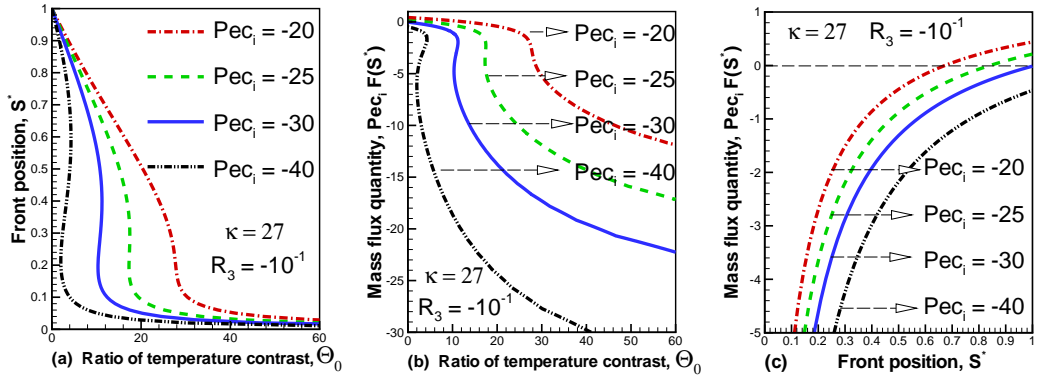


Figure 3.3: (a) Steady-state front position  $S^*$ ; (b) mass flux quantity  $Pec_i F(S^*)$  vs ratio of temperature contrast  $\Theta_0$ ; and (c) mass flux quantity  $Pec_i F(S^*)$  vs implicit front position  $S^*$  with  $H_{liq} = 8.74$ ,  $R_1 = 0.0006$ ,  $R = 22.11$  and  $C = 2.02$ . Note that  $R_3 < 0$ , i.e., liquid is above vapour. Note also that, following Straus & Schubert [77] we have taken  $R > 1$ ; the large value of  $R$  is chosen for clarity of the plots but does not qualitatively affect the results.

Figure 3.3 (a) illustrates the fact that for smaller Peclet numbers  $Pec_i$ , the front position  $S^*$  is monotonically decreasing as  $\Theta_0$  increases. Physically, as the temperature difference across the vapour region  $|T_V - T_S|$  gets large relative to the tem-

perature difference across liquid region  $|T_S - T_L|$ , the phase change front “wants” to be closer to the liquid boundary so that the conductive heat fluxes across these regions are the same.

Figure 3.3 (c) shows that as the front position gets closer to  $S^* = 1$  (the vapour boundary), the mass flux decreases. The porous layer becomes more and more saturated with liquid (heavy fluid), so more of the imposed pressure difference is used up supporting the weight of the liquid (i.e., more is used on hydrostatic pressure). When the front position  $S^*$  is sufficiently close to the vapour boundary (i.e.,  $S^* = 1$ ) and the reference Peclet number  $Pec_i$  is small enough (i.e., small imposed pressure difference), the mass flux reverses and we have downward flow (i.e.,  $Pec_i F(S^*) > 0$ ), see the top left hand corner of Figure 3.3 (b) and the top right hand corner of Figure 3.3 (c).

Moreover, the larger the reference Peclet number, the larger the upward flow rate (i.e.,  $Pec_i F(S^*) < 0$ , flow from vapour into liquid). For the larger values of  $Pec_i$ , there are some values of the temperature contrast ratio  $\Theta_0$  for which up to three phase change front positions exist. This interesting phenomenon arises from the competition between the thermal and the fluid-flow effects. As the temperature difference across the liquid region  $|T_S - T_L|$  gets large compared to that across the vapour region  $|T_V - T_S|$  (i.e. as  $\Theta_0$  decreases), conduction moves the front closer to the vapour boundary. But the closer the front is to the vapour boundary the greater the weight of the liquid in the system. This means a reduction in mass flux, and thus reduces the advective heat flux from vapour to liquid. This tends to move the front further from the vapour boundary. These competing effects lead to the multiple front positions in this region.

Figure 3.4 (a) illustrates the effects of gravity on the front position. The larger values of the Rayleigh number  $|R_3|$  correspond to a greater fluid weight effect,

which cause multiple front positions. Figure 3.4 (b) shows the dominance of the downward flow (flow from liquid into vapour, i.e.,  $Pec_i F(S^*) > 0$ ) for larger  $|R_3|$ .

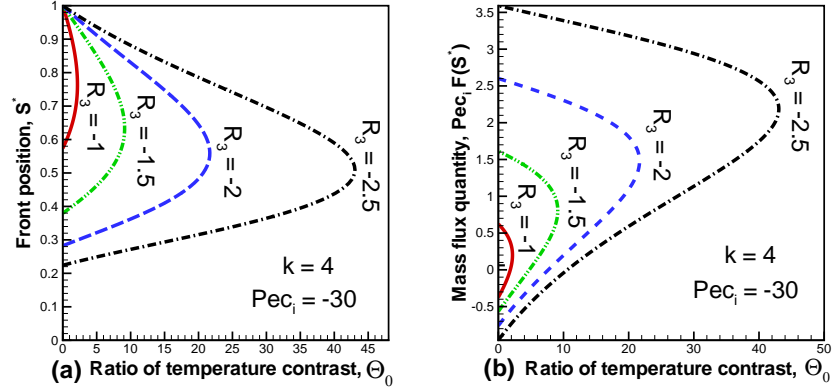


Figure 3.4: (a) Steady-state front position  $S^*$  vs ratio of temperature contrast  $\Theta_0$  and (b) mass flux quantity  $Pec_i F(S^*)$  vs  $\Theta_0$  for higher Rayleigh numbers  $|R_3|$  with  $H_{liq} = 8.74$ ,  $R_1 = 0.0006$ ,  $R = 22.11$  and  $C = 2.02$ . Note that liquid overlies vapour, i.e.,  $R_3 < 0$ .

It is important to have an accurate range for the ratio of the thermal conductivities  $k$ , especially when there is a gravitational effect. Figure 3.5 (a) shows that for a given value of  $k$ , the phase change front has multiple steady-state positions. In the absence of gravity the front has a unique position (see the curve for  $R_3 = 0$  in Figure 3.5 (a)), which is in complete agreement with Rubin & Schweitzer's [68] horizontal flow results. As we have already noted, in the absence of gravity, the direction of flow is based on the pressure gradient across the porous layer. For the particular case  $R_3 = 0$ , the fluid flow is from vapour into liquid, i.e.,  $Pec_i F(S^*) < 0$ , and is determined only by the pressure difference. Figure 3.5 (b) shows that the various solutions for  $S^*$  (for a given  $k$ ) correspond to different up/downflow rates. The low- $S^*$  solution corresponds to a strong flow from vapour

to liquid (negative  $x^*$ -direction, i.e.,  $Pec_i F(S^*) < 0$ ); the high- $S^*$  solution corresponds to a flow from liquid to vapour (positive  $x^*$ -direction, i.e.,  $Pec_i F(S^*) > 0$ ), and the intermediate solution generally corresponds to a weak flow from vapour to liquid.

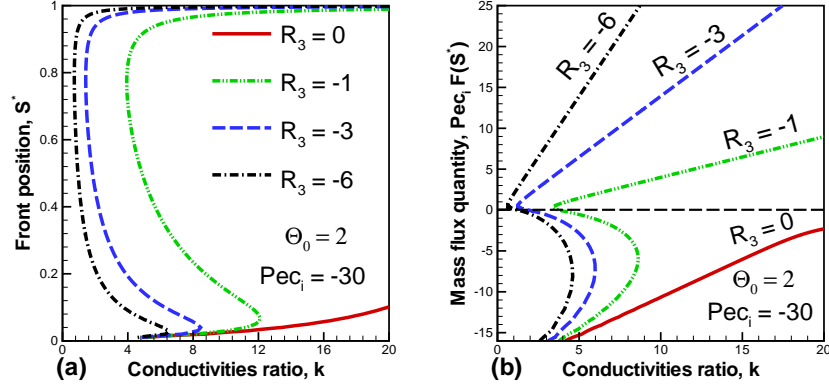


Figure 3.5: (a) Steady-state front position  $S^*$  and (b) mass flux quantity  $Pec_i F(S^*)$  vs thermal conductivities ratio  $k$  for higher Rayleigh numbers  $|R_3|$  with  $H_{liq} = 8.74$ ,  $R_1 = 0.0006$ ,  $R = 22.11$  and  $C = 2.02$ . Note that  $R_3 < 0$  (liquid above vapour).

As we have seen earlier, the competition between the thermal and fluid-flow effects causes multiple positions of the steady-state front. Figure 3.6 (a) demonstrates that for a given value of the reciprocal of the Stefan number  $H_{liq}$ , there are up to three front positions. It helps to divide the range of  $S^*$  into three regions

1. **Region i:** This region is defined as when  $S^*$  is small. As  $H_{liq}$  increases, the front comes closer to the liquid boundary and gives an advection dominated solution with high mass flux from vapour into liquid, i.e. a large negative Peclet number  $Pec_i F(S^*)$  (see Figure 3.6 (b)). The same behaviour has been seen when  $\Theta_0$  increases, see Figure 3.3 (a).

2. **Region ii:** This region is defined as when  $S^*$  approaches 1. As  $H_{liq}$  increases, conduction moves the front closer to the vapour boundary and gives a conduction dominated solution with small mass flux. In Figure 3.3 (a) we have seen that when  $\Theta_0$  decreases the front gets closer to the vapour boundary. Figure 3.6 (b) illustrates that in region ii the mass flux is from liquid into vapour ( $x^*$ -direction, i.e.  $Pec_i F(S^*) > 0$ ).
3. **Region iii:** Everything between region i and region ii has been labeled as region iii. Figures 3.6 (b) and 3.5 (b) indicate that a weak flow from vapour to liquid or liquid to vapour corresponds to an intermediate solution for  $S^*$ .

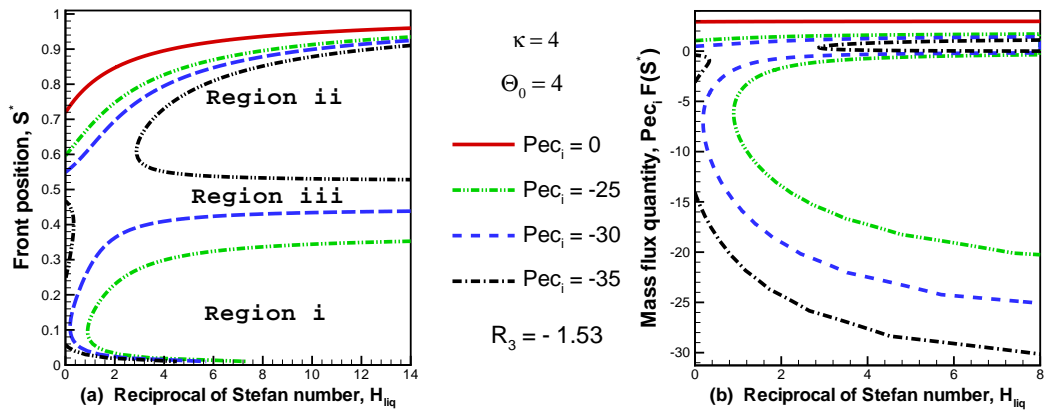


Figure 3.6: (a) Steady-state front position  $S^*$  and (b) mass flux quantity  $Pec_i F(S^*)$  vs the reciprocal of the Stefan number for the liquid phase  $H_{liq}$  with  $R_1 = 0.0006$ ,  $R = 22.11$  and  $C = 2.02$ . Note that  $R_3 < 0$  (liquid above vapour).

### 3.1.2 Constant heat flux boundary condition

For this case, constant heat flux  $q_{liq}$  is applied at  $x = 0$ . The necessary minimum heat flux required to condense the vapour at  $x = 0$  is found to be (see Appendix A)

$$q_{liq}^{min} = \frac{Pec_i k_{vap}}{c_{p,vap} L} \left[ \lambda + \frac{c_{p,vap}(T_V - T_S)}{1 - \exp(Pec_i)} \right]. \quad (3.27)$$

Now since we have considered a constant heat flux at the liquid boundary, we cannot use the dimensionless parameter (3.15) for the temperature profile in the liquid region because the temperature at the liquid boundary is unknown. So we will redefine the dimensionless parameters in the following way.

$$\Theta_{liq}(x^*) = \frac{T_{liq}(x) - T_V}{T_S - T_V}, \quad \Theta_{vap}(x^*) = \frac{T_{vap}(x) - T_V}{T_S - T_V},$$

$$H_{vap} = \frac{\lambda}{c_{p,vap}(T_V - T_S)}, \quad Q_{liq} = \frac{q_{liq}}{q_{liq}^{min}} \geq 1, \quad (3.28)$$

where  $H_{vap}$  is the reciprocal of the Stefan number for the vapour region. It is important to note that if  $Pec_i < 0$ , then the actual heat flux is negative, i.e.,  $q_{liq}^{min} < 0$  and this corresponds to  $Q_{liq} > 0$ . The governing energy equations for this case are identical to equations (3.18) and (3.19). The corresponding boundary conditions in dimensionless form, using the normalised quantities (3.15) and (3.28) are

$$\left. \begin{aligned} \text{at } x^* = 0 : \frac{d\Theta_{liq}}{dx^*} &= \frac{Q_{liq} Pec_i}{k} \left[ H_{vap} + \frac{1}{1 - \exp(Pec_i)} \right], \\ \text{at } x^* = 1 : \Theta_{vap} &= 0, \end{aligned} \right\} \quad (3.29)$$

$$\text{at } x^* = S^* \left\{ \begin{aligned} \Theta_{liq} &= \Theta_{vap} = 1, \\ \frac{d\Theta_{liq}}{dx^*} - \frac{1}{k} \frac{d\Theta_{vap}}{dx^*} &= \frac{H_{vap} Pec_i F(S^*)}{k}. \end{aligned} \right. \quad (3.30)$$

The solution for the temperature distribution in the vapour phase  $\Theta_{vap}(x^*)$  is the same as (3.24). The dimensionless temperature distribution for the liquid phase

subject to the boundary conditions (3.29) and (3.30) is

$$\begin{aligned} \Theta_{liq}(x^*) &= 1 + \frac{Q_{liq}}{F(S^*)C} \left\{ H_{vap} + \frac{1}{1 - \exp(Pec_i)} \right\} \\ &\times \left\{ \exp\left(\frac{C Pec_i F(S^*)}{k} x^*\right) - \exp\left(\frac{C Pec_i F(S^*)}{k} S^*\right) \right\}. \end{aligned} \quad (3.31)$$

Substituting (3.24) and (3.31) into the energy jump condition at the phase change interface (3.30) yields a transcendental equation for the interface position  $S^*$ ,

$$\begin{aligned} &\left\{ \frac{Q_{liq}}{F(S^*)} \left\{ H_{vap} + \frac{1}{1 - \exp(Pec_i)} \right\} \exp\left[\frac{C Pec_i F(S^*) S^*}{k}\right] \right. \\ &\left. - H_{vap} \right\} \times \{1 - \exp[Pec_i F(S^*) (1 - S^*)]\} = 1. \end{aligned} \quad (3.32)$$

The asymptotic solution of the transcendental equation (3.32) for small reference Peclet number  $Pec_i$  is

$$S^* \sim \frac{Q_{liq} - 1}{Q_{liq}} + O(Pec_i), \quad \text{as } Pec_i \rightarrow 0. \quad (3.33)$$

Equation (3.33) shows that, in the absence of net flow in the reservoir, the front position depends only on the dimensionless heat flux  $Q_{liq}$ . This result corresponds to equation (40a) of Rubin & Schweitzer [68]. In Section 5.2, we will extensively discuss the stability of the interface position  $S^*$  given by (3.33).

Figure 3.7 (a) shows typical results for the front position  $S^*$  as a function of the dimensionless constant heat flux  $Q_{liq}$  for different reference Peclet numbers  $Pec_i$ . It can be seen that there are three steady-state interface positions. We have shown in Section 3.1.1 that if there is a constant temperature at the boundaries and gravity is neglected then there is only one interface position. In contrast, for prescribed heat flux at the liquid boundary then there may be more than one front position. Figure 3.7 (b) shows that for  $Pec_i < 0$ , we have flow from vapour into liquid and  $Q_{liq} > 0$  corresponds to the actual heat flux being negative at the liquid boundary,

so we are cooling the reservoir from the liquid side. In fact  $Q_{liq}$  can be described as a dimensionless cooling flux. Furthermore, as  $Q_{liq}$  increases, we strengthen the cooling and the liquid region gets wider, i.e.,  $S^*$  increases. But as the liquid region gets wider, the mass flux decreases. The liquid has higher viscosity than the vapour ( $\mu_{liq} > \mu_{vap}$ ), so there is more resistance to flow in the presences of more liquid in the reservoir. As the liquid region gets wider, resistance to flow increases so through flow decreases as does advective heat flux. Moreover, the cooling at the liquid boundary depends on both an advective and a conductive flux, so as the thickness of the liquid layer increases, the advective heat flux becomes weak and thus conduction dominates.

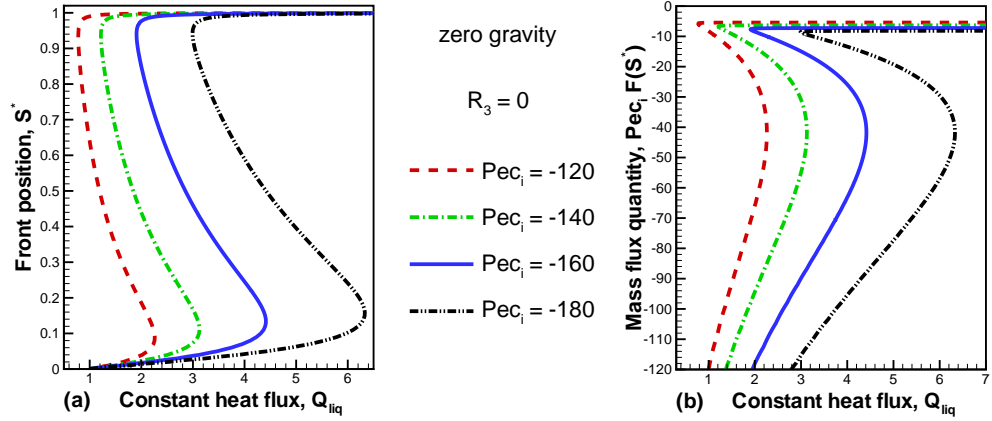


Figure 3.7: (a) Steady-state interface position  $S^*$  and (b) Mass flux quantity  $Pec_i F(S^*)$  vs heat flux  $Q_{liq}$  with zero gravity and  $H_{vap} = 41.17$ ,  $R = 22.11$ ,  $R_1 = 0.0006$ ,  $C = 2.01$  and  $k = 4$ .

Figure 3.7 (b) shows that the various solutions for  $S^*$  (for a given  $Q_{liq}$ ) again correspond to different flow rates. The low and intermediate solutions for  $S^*$  (in the range  $0 < S^* \lesssim 0.5$ ) correspond to a strong flow from vapour to liquid, whereas the intermediate and high- $S^*$  solutions (in the range  $0.5 \lesssim S^* < 1$ ) correspond

to a weak upflow rate.

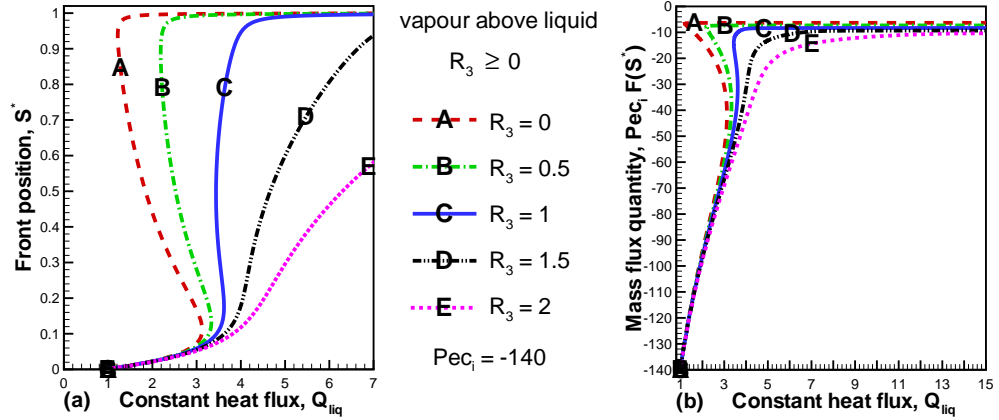


Figure 3.8: (a) Steady-state interface position  $S^*$  and (b) Mass flux quantity  $Pec_i F(S^*)$  vs heat flux  $Q_{liq}$  when the vapour phase is above the liquid phase with  $H_{vap} = 41.17$ ,  $R = 22.11$ ,  $R_1 = 0.0006$ ,  $C = 2.01$  and  $k = 4$ .

Figure 3.8 (a) shows the results for the dependence of the phase change front  $S^*$  on the constant heat flux  $Q_{liq}$  and on Rayleigh number  $R_3$ , when the lighter fluid (vapour) is above the heavier fluid (liquid). As  $R_3$  and  $Q_{liq}$  become larger the front ceases to have multiple positions. In the isothermal problem (Section 3.1.1), we also found that, large positive  $R_3$  (vapour above liquid) led to single front position, because for large  $R_3$  which corresponds to the weight of the fluid measure the same way as conduction.

Figure 3.9 (a) represents the influence of Rayleigh number  $|R_3|$  on the front position, when the heavier fluid is above the lighter fluid ( $R_3 < 0$ ). The competition between the effects of cooling and the viscosity difference (see Figure 3.7), with the addition of the weight effect on the front, causes multiple front positions. The larger values of  $|R_3|$  correspond to a greater fluid weight effect on the front, which we have discussed in Section 3.1.1.

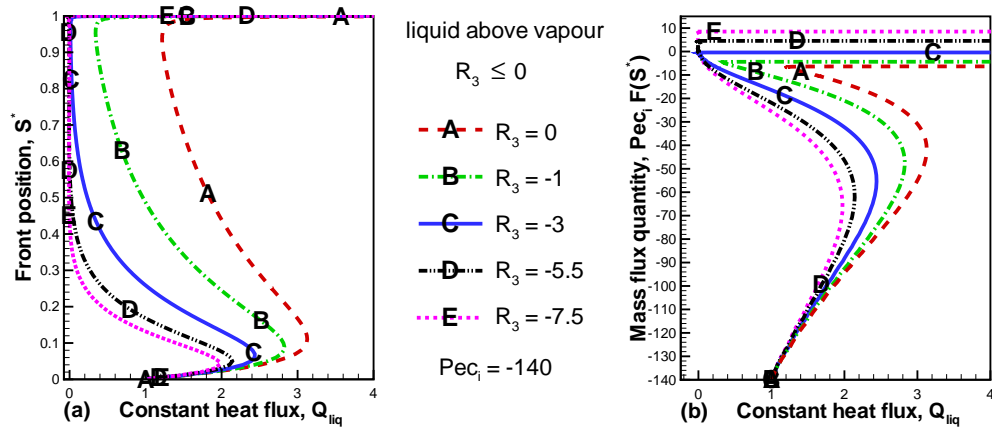


Figure 3.9: (a) Steady-state interface position  $S^*$  and (b) Mass flux quantity  $Pec_i F(S^*)$  vs heat flux  $Q_{liq}$  when the liquid is above the vapour with  $H_{vap} = 41.17$ ,  $R = 22.11$ ,  $R_1 = 0.0006$ ,  $C = 2.01$  and  $k = 4$ .

### 3.1.3 Summary and conclusions

We have studied two phase through flow in a porous medium considering two different types of boundary conditions. The temperature difference across the porous layer is such that a phase change interface exists, separating the liquid phase from the vapour phase. The flow behaviour is determined by the imposed pressure gradient and gravity.

#### Isothermal conditions

In the first case we considered prescribed temperature at the boundaries. Rubin & Schweitzer [68] showed that the steady-state front has only one position if a constant temperature is prescribed on the boundaries, while considering horizontal mass flow. In contrast, we have shown that if we consider the gravity factor but hold the pressure difference across the layer fixed then there may be multiple

steady-state front positions. We have discussed in detail how the competition between the thermal and fluid-flow effects causes multiple positions of the steady-state front (see Figures 3.3, 3.4, 3.5 and 3.6). Rubin & Schweitzer's [68] results are obtained as a special case.

### **Constant heat flux condition**

In the second type of boundary condition, we assumed constant heat flux at the liquid boundary. We confirmed Rubin & Schweitzer's [68] results that, for prescribed heat flux and in the absence of gravity, there are up to three front positions (see Figure 3.7). We have shown that if the lighter fluid is above the heavier fluid then large values of  $R_3$  give a unique front position (see Figure 3.8). But if the heavier fluid is above the lighter fluid then large values of the Rayleigh number  $R_3$  give multiple front positions (see Figure 3.9).

### 3.2 Instantaneous change of surface temperature: similarity solution

We consider an unsteady condensation problem. A material which exists in two phases (liquid and vapour) fills the half space  $x \geq 0$  (see Figure 3.10). For time  $t \leq 0$  the material is in the vapour phase at a constant temperature  $T_V > T_S$ , where  $T_S$  is the phase change temperature. At time  $t = 0$  the temperature of the surface  $x = 0$  is instantaneously lowered and maintained at  $T_L < T_S$ . This will cause a layer of liquid to be formed adjacent to the surface  $x = 0$  and as time increases this layer will expand into the vapour. We first assume that the densities are same in the liquid and vapour regions, which will ensure no flow. In Section 3.2.3 we will assume that the densities no longer remain the same, i.e.,  $\rho_{liq} \neq \rho_{vap}$ . This is more realistic, but also more complicated mathematically. The phase change temperature  $T_S$  is assumed to be constant.

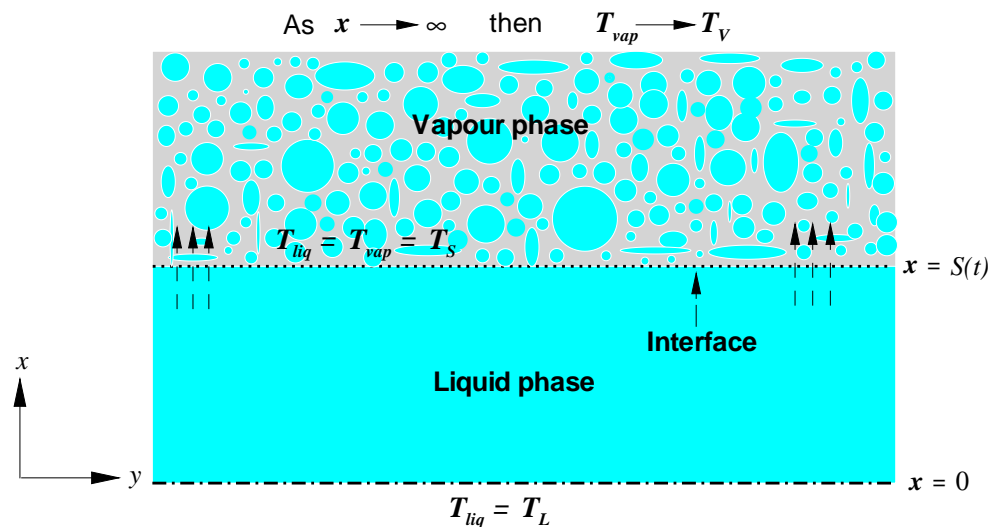


Figure 3.10: Diagram of unsteady condensation problem.

Assuming that the heat transfer is only due to conduction, the problem can be described by a pair of Fourier heat conduction equations. The detailed derivation of the governing energy equation is discussed in Section 2.5. According to the above assumptions, the energy equation (2.37) and the corresponding boundary conditions for this model will take the following form:

$$\left. \begin{aligned} (\rho c_p)_{m,liq} \frac{\partial T_{liq}}{\partial t} &= k_{m,liq} \frac{\partial^2 T_{liq}}{\partial x^2}, \quad \text{for } t > 0, \quad 0 < x < S(t), \\ T_{liq}(0) &= T_L, \quad T_{liq}(S) = T_S, \\ (\rho c_p)_{m,vap} \frac{\partial T_{vap}}{\partial t} &= k_{m,vap} \frac{\partial^2 T_{vap}}{\partial x^2}, \quad \text{for } t > 0, \quad S(t) < x, \\ T_{vap}(S) &= T_S, \quad \text{as } x \rightarrow \infty \text{ then } T_{vap} \rightarrow T_V. \end{aligned} \right\} \quad (3.34)$$

The heat flux condition is to be applied at the unknown position of the interface  $S(t)$ . Conservation of heat requires that the latent heat of condensation be diffused away from the interface so that

$$\varphi \lambda \rho_{liq} \frac{dS(t)}{dt} = k_{m,liq} \frac{\partial T_{liq}}{\partial x} \Big|_{x=S} - k_{m,vap} \frac{\partial T_{vap}}{\partial x} \Big|_{x=S}. \quad (3.35)$$

The above heat flux condition is a special form of (2.52) under the assumption that there is no flow of liquid, i.e.,  $u_{liq} = 0$ .

### 3.2.1 Similarity solution

In a similarity solution a similarity variable, combining the space and time variables, is sought that transforms the governing partial differential equations into a set of ordinary differential equations with the similarity variable as the independent variable [12, 49, p. 143-160]. Let us introduce the dilation transformation

$$m = \varepsilon^a x, \quad n = \varepsilon^b t, \quad Y(m, n) = \varepsilon^c T(\varepsilon^{-a} m, \varepsilon^{-b} n). \quad (3.36)$$

Using the transformation (3.36), the heat equation becomes

$$\varepsilon^{b-c} \frac{\partial Y(m, n)}{\partial n} = \varepsilon^{2a-c} \alpha_{m,liq,vap} \frac{\partial^2 Y(m, n)}{\partial m^2} \quad (3.37)$$

Now if  $b - c = 2a - c$ , (i.e.,  $b = 2a$ ) then the heat equation (3.34) in both phases (liquid and vapour) is invariant under the dilation transformation (3.36), i.e., if  $T(x, t)$  is the solution of the heat equation in the variables  $x$  and  $t$ , then for  $m, n$ ,  $Y(m, n)$  given by (3.36),  $Y(m, n)$  solves the heat equation in the variables  $m$  and  $n$ . Note that

$$Y n^{-c/b} = (\varepsilon^c T)(\varepsilon^b t)^{-c/b} = T t^{-c/b},$$

and

$$\frac{m}{n^{a/b}} = \frac{\varepsilon^a x}{(\varepsilon^a t)^{a/b}} = \frac{x}{t^{a/b}},$$

so both groupings of variables are invariant under the transformation (3.36) for all choices of  $a, b, c$ . This suggests that we look for a solution for (3.34) that is of the form

$$T(x, t) = t^{c/b} F(\eta) \quad \text{for} \quad \eta = \frac{x}{t^{a/b}} = \frac{x}{\sqrt{t}} \quad \text{since} \quad b = 2a. \quad (3.38)$$

Now using the transformation (3.38), we will have

$$\frac{\partial T_{liq,vap}}{\partial t} = t^{c/2a-1} \left\{ \frac{c}{2a} F_{liq,vap}(\eta) - \frac{\eta}{2} \frac{dF_{liq,vap}(\eta)}{d\eta} \right\}, \quad (3.39)$$

and

$$\frac{\partial^2 T_{liq,vap}}{\partial x^2} = t^{c/2a-1} \frac{d^2 F_{liq,vap}(\eta)}{d\eta^2}. \quad (3.40)$$

Substituting (3.39) and (3.40) into the heat equation (3.34), we have

$$t^{c/2a-1} \left\{ \alpha_{m,liq,vap} \frac{d^2 F_{liq,vap}(\eta)}{d\eta^2} + \frac{\eta}{2} \frac{dF_{liq,vap}(\eta)}{d\eta} - \frac{c}{2a} F_{liq,vap}(\eta) \right\} = 0. \quad (3.41)$$

Now we will transform the boundary conditions using the transformation (3.38), since  $T_{liq}(0, t) = T_L$  then  $T_{liq}(0, t) = t^{c/b} F_{liq}(0)$  and this can equal the constant  $T_L$  if and only if  $c = 0$ . The same is true for  $T_{liq,vap}(S, t) = t^{c/b} F_{liq,vap}(S/\sqrt{t}) = T_S$

and finally  $T_{vap}(\infty, t) = t^{c/b} F_{vap}(\infty) = T_V$ . In this case when  $c = 0$  the problem for  $T(x, t)$  reduces to

$$\left. \begin{aligned} \frac{d^2 F_{liq}}{d\eta^2} + \frac{\eta}{2\alpha_{m,liq}} \frac{dF_{liq}}{d\eta} &= 0, \\ F_{liq}(0) = T_L, \quad F_{liq,vap}(S/\sqrt{t}) &= T_S, \\ \frac{d^2 F_{vap}}{d\eta^2} + \frac{\eta}{2\alpha_{m,vap}} \frac{dF_{vap}}{d\eta} &= 0, \\ F_{vap} \rightarrow T_V \text{ as } \eta \rightarrow \infty, \end{aligned} \right\} \quad (3.42)$$

where  $\alpha_m$  is the thermal diffusivity. The solution of (3.42) with the appropriate boundary conditions is

$$T_{liq}(x, t) = T_L - (T_L - T_S) \frac{\operatorname{erf}\left(\frac{x}{2\sqrt{\alpha_{m,liq}t}}\right)}{\operatorname{erf}(\beta)}, \quad (3.43)$$

$$T_{vap}(x, t) = T_V + (T_S - T_V) \frac{\operatorname{erfc}\left(\frac{x}{2\sqrt{\alpha_{m,vap}t}}\right)}{\operatorname{erfc}(\hbar_1 \beta)}, \quad (3.44)$$

where  $\beta = \frac{S(t)}{2\sqrt{\alpha_{m,liq}t}}$  and  $\hbar_1 = \sqrt{\frac{\alpha_{m,liq}}{\alpha_{m,vap}}}$ . We seek a similarity solution in which the interface position is given by

$$S(t) = 2\beta \sqrt{\alpha_{m,liq}t}. \quad (3.45)$$

Putting (3.43), (3.44) and (3.45) into (3.35) gives

$$\varphi \sqrt{\pi} \beta H_{liq} = E_1 \left( \frac{\exp(-\beta^2)}{\operatorname{erf}(\beta)} - \frac{\Theta_0}{k} \hbar_1 \frac{\exp(-\beta^2 \hbar_1^2)}{\operatorname{erfc}(\beta \hbar_1)} \right), \quad (3.46)$$

where  $E_1 = \frac{(\rho c_p)_{m,liq}}{(\rho c_p)_{liq}}$ . The above equation has been dimensionlised by using  $t = \frac{L^2 \rho_{liq} c_{p,liq} t^*}{k_{m,liq}}$  and (3.15).

### 3.2.2 Interpretation of Stefan number

Solomon [76] has shown for a specific melting process that the ratio of sensible to latent heat is independent of time and can be related to the Stefan number.

We will now follow the same procedure while considering the condensation phase change problem.

First we note that the latent heat stored at time  $t$  is

$$\text{LH} = \varphi \rho_{liq} \lambda S(t) = 2 \varphi \beta \rho_{liq} \lambda \sqrt{\alpha_{m,liq} t}. \quad (3.47)$$

The total heat (TH) removed from the system is the time integral of the surface heat flux which is

$$\text{TH} = k_{m,liq} \int_0^t \frac{dT_{liq}(0, t)}{dx} dt = \frac{2 k_{m,liq} (T_S - T_L) \sqrt{t}}{\sqrt{\alpha_{m,liq} \pi} \text{erf}(\beta)}. \quad (3.48)$$

We know that total heat is the sum of sensible heat and latent heat

$$\begin{aligned} \text{TH} &= \text{SH} + \text{LH}, \\ \Rightarrow \frac{\text{SH}}{\text{LH}} &= \frac{\text{TH}}{\text{LH}} - 1. \end{aligned}$$

Now from (3.47) and (3.48) we get

$$\frac{\text{TH}}{\text{LH}} = \frac{c_{p,liq} (T_S - T_L) (\rho c_p)_{m,liq}}{\varphi \sqrt{\pi} \lambda \beta \text{erf}(\beta) (\rho c_p)_{liq}} = \frac{E_1}{\varphi H_{liq} \sqrt{\pi} \beta \text{erf}(\beta)}. \quad (3.49)$$

Finally we have

$$\frac{\text{SH}}{\text{LH}} = \frac{\text{TH}}{\text{LH}} - 1 = \frac{E_1}{\varphi \sqrt{\pi} H_{liq} \beta \text{erf}(\beta)} - 1. \quad (3.50)$$

It is clear from (3.50) that the ratio SH/LH is independent of time.

If the temperatures at the phase change front and in the vapour phase are the same, i.e.,  $T_S = T_V$  then the ratio of the temperature contrast  $\Theta_0$  becomes zero.

In this case, (3.46) and (3.50) yields

$$\frac{\text{SH}}{\text{LH}} = \exp(\beta^2) - 1. \quad (3.51)$$

In the limit in which  $H_{liq}$  is large (small Stefan number), the root  $\beta$  is very small, so (3.46) yields

$$\beta \simeq \sqrt{\frac{E_1}{2 \varphi H_{liq}}}. \quad (3.52)$$

Hence

$$\exp(\beta^2) \simeq 1 + \beta^2 \simeq 1 + \frac{E_1}{2\varphi H_{liq}}. \quad (3.53)$$

Finally substituting (3.53) into (3.51) we get

$$\frac{SH}{LH} \simeq \frac{E_1}{2\varphi H_{liq}}, \quad (3.54)$$

where  $E_1 = (\rho c_p)_{m,liq} / (\rho c_p)_{liq}$ ,  $\varphi$  is the porosity and  $H_{liq}$  is the reciprocal of the Stefan number (for the liquid phase,  $Ste_{liq} = c_{p,liq} (T_S - T_L) / \lambda$ ). If we assume that  $E_1 / \varphi = 1$  then (3.54) yields

$$\frac{SH}{LH} \simeq \frac{Ste_{liq}}{2}, \quad (3.55)$$

(3.55) shows that for this particular condensation problem Stefan number  $Ste_{liq}$  is approximately twice the ratio  $SH/LH$ , which is also independent of time.

### 3.2.3 Effects of density change: similarity solution

This problem is the extension of the problem considered in Section 3.2, by considering advective heat transfer in the vapour region only, and a density difference between the two phases (liquid and vapour). The density difference means that although the liquid is static there is flow in the vapour region. Usually the density of the liquid is greater than the vapour, i.e.,  $\rho_{liq} > \rho_{vap}$ . To illustrate the effects of the density change, we consider the one dimensional condensation problem illustrated in Figure 3.10. In the light of the above assumptions the governing energy equation (2.37) will take the form

$$\begin{aligned} (\rho c_p)_{m,liq} \frac{\partial T_{liq}}{\partial t} &= k_{m,liq} \frac{\partial^2 T_{liq}}{\partial x^2}, \quad \text{for } t > 0, \quad 0 < x < S(t), \\ T_{liq}(0) &= T_L, \quad T_{liq}(S) = T_S, \\ (\rho c_p)_{m,vap} \frac{\partial T_{vap}}{\partial t} + (\rho c_p)_{vap} u_{vap} \frac{\partial T_{vap}}{\partial x} &= k_{m,vap} \frac{\partial^2 T_{vap}}{\partial x^2}, \quad \text{for } t > 0, \quad S(t) < x, \\ T_{vap}(S) &= T_S, \quad \text{as } x \rightarrow \infty \text{ then } T_{vap} \rightarrow T_V. \end{aligned} \quad (3.56)$$

In the absence of any driving force, the velocity of the vapour  $u_{vap}$  has to be determined by the mass balance at the interface [12]. Mass conservation (2.56) across the liquid-vapour interface  $S(t)$  yields

$$u_{vap} = \varphi \left( 1 - \frac{1}{R_1} \right) \frac{dS(t)}{dt}, \quad \text{where } R_1 = \frac{\rho_{vap}}{\rho_{liq}}, \quad (3.57)$$

There is also an energy flux condition to be applied at the unknown position of the liquid-vapour interface  $S(t)$ . The heat jump condition (2.52) gives

$$\lambda \rho_{vap} \left( \varphi \frac{dS(t)}{dt} - u_{vap} \right) = k_{m,liq} \frac{\partial T_{liq}}{\partial x} \Big|_{x=S} - k_{m,vap} \frac{\partial T_{vap}}{\partial x} \Big|_{x=S}. \quad (3.58)$$

#### 3.2.3.1 Similarity solution

The similarity transformation  $\eta = \frac{x}{2\sqrt{\alpha_{m,vap}t}}$  will give the following set of ordinary differential equations with the appropriate boundary conditions. We will seek

solutions of the form  $T_{liq}(x, t) = F_{liq}(\eta)$  for the liquid region and  $T_{vap}(x, t) = F_{vap}(\eta)$  for the vapor region.

$$\left. \begin{aligned} \frac{d^2 F_{liq}}{d\eta^2} + 2\eta \frac{\alpha_{m,vap}}{\alpha_{m,liq}} \frac{dF_{liq}}{d\eta} &= 0, \\ F_{liq}(0) = T_L \quad \text{and} \quad F_{liq,vap}(\beta_2) &= T_S, \\ \frac{d^2 F_{vap}}{d\eta^2} &= 2 \left\{ \frac{\varphi}{E_2} \left( 1 - \frac{1}{R_1} \right) \beta_2 - \eta \right\} \frac{dF_{vap}}{d\eta}, \\ \text{as } \eta \rightarrow \infty \quad \text{then} \quad F_{vap} &\rightarrow T_V, \end{aligned} \right\} \quad (3.59)$$

where  $E_2 = \frac{(\rho c_p)_{m,vap}}{(\rho c_p)_{vap}}$  and the liquid-vapour front has the position

$$S(t) = 2\beta_2 \sqrt{\alpha_{m,vap} t}, \quad (3.60)$$

where the constant  $\beta_2$  is to be determined. The heat jump condition (3.58) in terms of the similarity variable is

$$\varphi \lambda \rho_{liq} \beta_2 \alpha_{m,vap} = \frac{k_{m,liq}}{2} \frac{dF_{liq}}{d\eta} \Big|_{\eta=\beta_2} - \frac{k_{m,vap}}{2} \frac{dF_{vap}}{d\eta} \Big|_{\eta=\beta_2}. \quad (3.61)$$

The solution of (3.59) is

$$F_{liq}(\eta) = T_L - (T_L - T_S) \frac{\text{erf}(\hbar_2 \eta)}{\text{erf}(\hbar_2 \beta_2)}, \quad \eta < \beta_2, \quad (3.62)$$

$$F_{vap}(\eta) = T_V + (T_S - T_V) \frac{\text{erfc} \left\{ \frac{\varphi \beta_2}{E_2} \left( \frac{1}{R_1} - 1 \right) + \eta \right\}}{\text{erfc} \left\{ \beta_2 \left( 1 - \frac{\varphi}{E_2} \left( 1 - \frac{1}{R_1} \right) \right) \right\}}, \quad \eta > \beta_2, \quad (3.63)$$

where  $\hbar_2 = \sqrt{\frac{\alpha_{m,vap}}{\alpha_{m,liq}}}$ . Substituting (3.62) and (3.63) into (3.61) gives

$$\sqrt{\pi} \varphi \beta_2 H_{liq} = \frac{E_1}{\hbar_2} \left\{ \frac{\exp(-\hbar_2^2 \beta_2^2)}{\text{erf}(\hbar_2 \beta_2)} - \frac{\Theta_0}{k} \frac{1}{\hbar_2} \frac{\exp \left\{ -\beta_2^2 \left( 1 - \frac{\varphi}{E_2} \left( 1 - \frac{1}{R_1} \right) \right)^2 \right\}}{\text{erfc} \left\{ \beta_2 \left( 1 - \frac{\varphi}{E_2} \left( 1 - \frac{1}{R_1} \right) \right) \right\}} \right\}. \quad (3.64)$$

The above equation (3.64) represents the most general eigenvalue relationship for  $\beta_2$  in transcendental form. A special case of this result has appeared previously: if  $R_1 = 1$ , which implies that the densities of the two phases are the same, then (3.64) reduces to (3.46).

A typical temperature distribution in the liquid-vapour regions with  $\alpha_{m,liq} = 0.12$  and  $\alpha_{m,vap} = 2.4$  is shown in Figure 3.11. Pure conduction takes place in the liquid region, thus the temperature profile in the liquid region is nearly linear. In the vapour region the exponential behaviour of the temperature shows convection dominating over conduction. The two regions are separated at  $\beta_2 = 0.24$  at interface temperature  $T_S = 10$ . The interface is moving right into the vapour region with time  $t$ , which indicates that condensation is taking place.

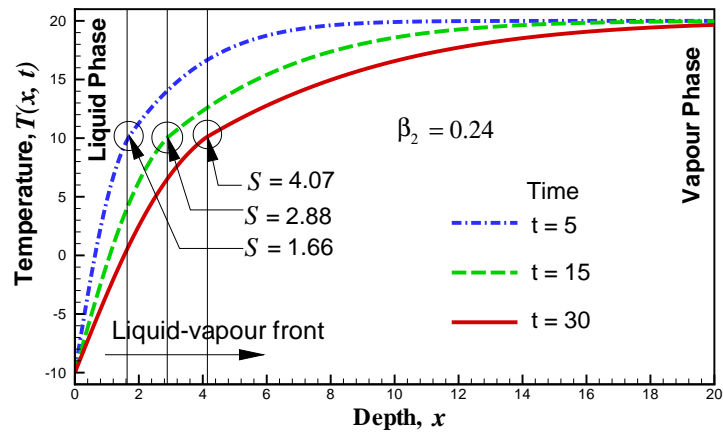


Figure 3.11: Similarity solution temperature profile with  $R_1 = 0.1$ ,  $H_{liq} = 1$ ,  $k = 1$ ,  $\bar{h}_2 = 4.5$ ,  $E_1 = 1$ ,  $E_2 = 1$ ,  $\Theta_0 = 0.5$  and  $\varphi = 0.38$ .

### 3.2.3.2 Asymptotic solution

The error functions and exponential terms in the transcendental equation (3.64) have the following asymptotic expansions

$$\begin{aligned} \operatorname{erf}(\hbar_2\beta_2) &= \frac{2}{\sqrt{\pi}} \left\{ \hbar_2\beta_2 - \frac{(\hbar_2\beta_2)^2}{3} + \frac{(\hbar_2\beta_2)^5}{10} + O(\hbar_2\beta_2)^6 \right\}, \\ \frac{e^{-(\hbar_2\beta_2)^2}}{\operatorname{erf}(\hbar_2\beta_2)} &= \frac{\sqrt{\pi}}{2\hbar_2\beta_2} \left\{ 1 + \frac{(\hbar_2\beta_2)^2}{3} + \frac{(\hbar_2\beta_2)^4}{90} + O(\hbar_2\beta_2)^6 \right\} \\ &\quad \times \left\{ 1 - (\hbar_2\beta_2)^2 + \frac{(\hbar_2\beta_2)^4}{2!} + O(\hbar_2\beta_2)^6 \right\}, \\ \frac{e^{-(\hbar_2\beta_2)^2}}{\operatorname{erf}(\hbar_2\beta_2)} &= \frac{\sqrt{\pi}}{2\hbar_2\beta_2} \left\{ 1 - \frac{2}{3}(\hbar_2\beta_2)^2 + \frac{4}{15}(\hbar_2\beta_2)^4 + O(\hbar_2\beta_2)^6 \right\}, \end{aligned} \quad (3.65)$$

also

$$\operatorname{erfc} \left\{ \beta_2 \underbrace{\left( 1 - \frac{\varphi}{E_2} \left( 1 - \frac{1}{R_1} \right) \right)}_{=\hbar_3} \right\} = 1 - \frac{2}{\sqrt{\pi}} \left\{ \beta_2 \hbar_3 - \frac{1}{3} (\beta_2 \hbar_3)^3 + \frac{1}{10} (\beta_2 \hbar_3)^5 + O(\beta_2 \hbar_3)^7 \right\}, \quad (3.66)$$

and

$$\begin{aligned} \frac{e^{-(\beta_2 \hbar_3)^2}}{\operatorname{erfc}(\beta_2 \hbar_3)} &= \left\{ 1 - (\beta_2 \hbar_3)^2 + \frac{1}{2} (\beta_2 \hbar_3)^4 + O(\beta_2 \hbar_3)^6 \right\} \\ &\quad \times \left\{ 1 + \frac{2}{\sqrt{\pi}} (\beta_2 \hbar_3) + \frac{4}{\pi} (\beta_2 \hbar_3)^2 - \frac{2(\pi+2)}{3\pi\sqrt{\pi}} (\beta_2 \hbar_3)^3 + O(\beta_2 \hbar_3)^4 \right\}, \\ \frac{e^{-(\beta_2 \hbar_3)^2}}{\operatorname{erfc}(\beta_2 \hbar_3)} &= \left\{ 1 + \frac{2}{\sqrt{\pi}} (\beta_2 \hbar_3) + \left( \frac{4}{\pi} - 1 \right) (\beta_2 \hbar_3)^2 + O(\beta_2 \hbar_3)^3 \right\}. \end{aligned} \quad (3.67)$$

Substitution of (3.65) and (3.67) into (3.64) gives

$$\begin{aligned} \sqrt{\pi} \varphi \beta_2 H_{liq} &= \frac{E_1}{\hbar_2^2} \left[ \frac{\sqrt{\pi}}{2\beta_2} \left\{ 1 - \frac{2}{3}(\hbar_2\beta_2)^2 + \frac{4}{15}(\hbar_2\beta_2)^4 + O(\hbar_2\beta_2)^6 \right\} \right. \\ &\quad \left. - \frac{\Theta_0}{k} \left\{ 1 + \frac{2}{\sqrt{\pi}} (\beta_2 \hbar_3) + \left( \frac{4}{\pi} - 1 \right) (\beta_2 \hbar_3)^2 + O(\beta_2 \hbar_3)^3 \right\} \right]. \end{aligned} \quad (3.68)$$

If the Stefan number ( $Ste_{liq} = 1/H_{liq}$ ) for the liquid phase is close to zero, then the root  $\beta_2$  is very small, so ignoring the higher order terms in (3.68) we get

$$\sqrt{\pi} \varphi \beta_2 H_{liq} = \frac{E_1}{h_2^2} \left[ \frac{\sqrt{\pi}}{2\beta_2} - \frac{\Theta_0}{k} \left\{ 1 + \frac{2\beta_2}{\sqrt{\pi}} \left( 1 - \frac{\varphi}{E_2} \left( 1 - \frac{1}{R_1} \right) \right) \right\} \right]. \quad (3.69)$$

Figures 3.12 (a) and (b) compare the numerical values of  $\beta_2$  with those given by the asymptotic expansion (3.68). In the liquid phase the error is  $O(\beta_2 h_2)^6$ ; if the diffusivity ratio of the two phases  $h_2 > 0.5$  then the error due to the solution in the liquid phase is reduced (see Figure 3.12 (a)). Figure 3.12 (b) shows that an error of magnitude  $O\left(\beta_2 \left(1 - \frac{\varphi}{E_2} \left(1 - \frac{1}{R_1}\right)\right)\right)^2$  in the vapour phase is an insignificant error in the interface energy balance.

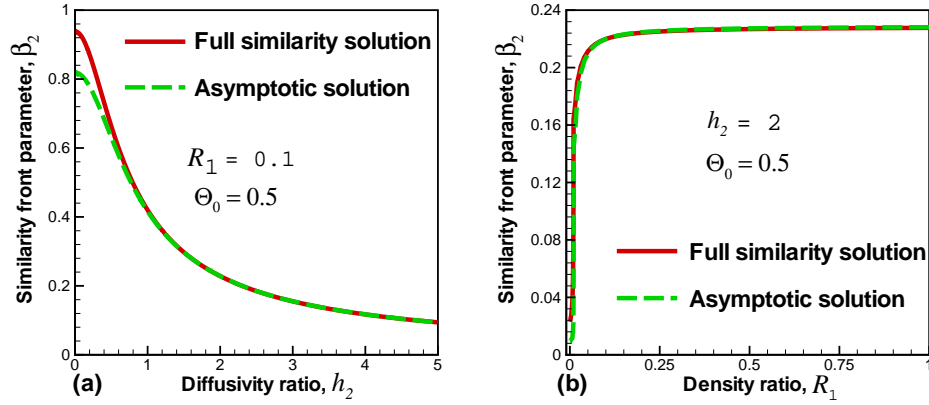


Figure 3.12: The similarity front parameter  $\beta_2$  as a function of the diffusivity ratio  $h_2$  and the density ratio  $R_1$ , where  $H_{liq} = 5$ ,  $k = 4$ ,  $E_1 = 1$ ,  $E_2 = 1$ ,  $\Theta_0 = 0.5$ , and  $\varphi = 0.38$ .

In Figure 3.13 (a) and (b), the similarity front parameter  $\beta_2$  is plotted against the diffusivity ratio  $h_2$  and temperature contrast  $\Theta_0$ , for various values of the density ratio  $R_1$ . The results for the special case (same density ratio,  $R_1 = 1$  in the transcendental equation (3.46)) also presented in Figure 3.13. Figures 3.13 (a) and (b) show that as either the diffusivity ratio  $h_2$  or the temperature contrast

ratio  $\Theta_0$  increases, the similarity front parameter  $\beta_2$  decreases and thus the liquid-vapour front moves more slowly.

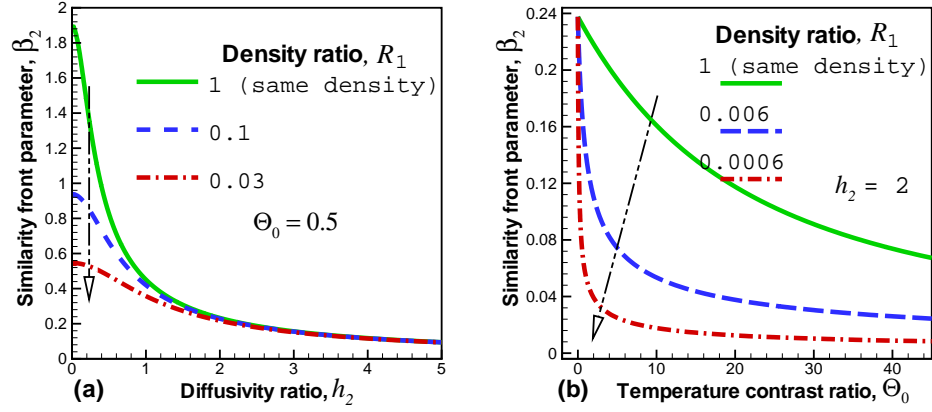


Figure 3.13: The similarity front parameter  $\beta_2$  as a function of the diffusivity ratio  $h_2$  and the temperature contrast ratio  $\Theta_0$ , where  $H_{liq} = 5$ ,  $k = 4$ ,  $E_1 = 1$ ,  $E_2 = 1$ ,  $\Theta_0 = 0.5$  and  $\varphi = 0.38$ .

### 3.2.4 Summary and conclusions

We have studied an unsteady two phase flow problem in a porous medium. The similarity solution assumes that when time  $t = 0$ , the porous layer is filled with one phase (vapour). As the process starts, heat transport (conduction and advection in the vapour phase) takes place and the vapour temperature decreases with time, the liquid-vapour interface starts to exist. The interface moves forward into the vapour phase with time, which indicates that condensation takes place. The liquid-vapour interface position is found to be  $S(t) = 2\beta_2\sqrt{\alpha_{m,vap}t}$ , where  $\beta_2$  is a similarity front parameter depending on the other parameters of the problem and  $\alpha_{m,vap}$  is the thermal diffusivity of the vapour phase.

# Chapter 4

## Stability of Steady Solutions with Isothermal Boundary Conditions

In this chapter, we will begin by giving a brief description of the physical stabilising or destabilising mechanisms acting on a steady condensation or evaporation front of the kind discussed in Chapter 3. The classical Rayleigh-Taylor instability, which occurs when a higher density fluid is above a lower density fluid in a gravitational field, is discussed as a reference case. We will use the work of Il'ichev & Tsykin [31] as a basis; we will discuss five different cases regarding the stability of a steady front with no through flow; and then we will extend the analysis by considering through flow.

### 4.1 Physical mechanisms that stabilise and destabilise the steady state solution

To start with, we will review the mechanisms that are known to act to stabilise/destabilise the liquid-vapour front.

We consider a porous layer of infinite extension bounded by two horizontal, much more permeable layers separated by a low-permeability layer. The upper and lower highly permeable layers are filled either with vapour and liquid, respectively or liquid and vapour, respectively. In the low-permeability layer there exists a phase change front which separates the liquid phase from the vapour phase. The liquid side is kept cool, whereas the vapour side is hot. Also gravity is considered to act across the layer. The highly permeable layers will allow us to impose constant pressures at both sides.

In the steady state the phase change front is flat and it is the stability of this state that is in question. Figure 4.1 shows a constant influx and efflux in the steady state and this may be zero. The adjustment of pressure at the boundaries will allow us to achieve any required rate of flow through the medium: zero flow rate is a special case. The heat needed for evaporation is supplied from the vapour side.

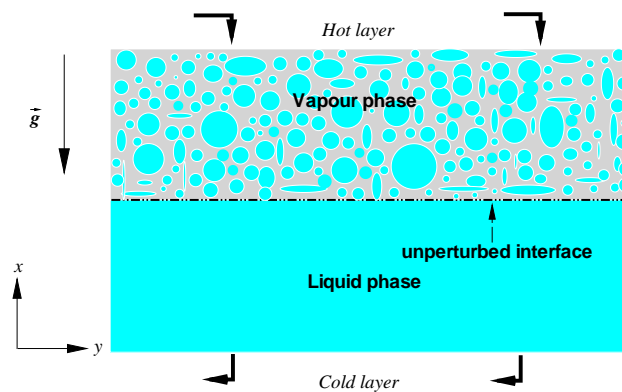


Figure 4.1: The physical schematic diagram for an evaporation front in a steady state [57, p. 2].

The dotted wave in Figure 4.2 represents the perturbed interface. At a trough the front is closer to the cold boundary (liquid boundary), and at a crest it is closer to the hot boundary (vapour boundary).

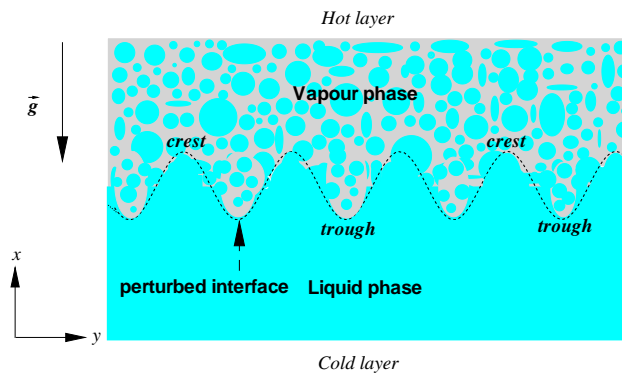


Figure 4.2: Schematic of a perturbed evaporation front when heat is supplied from the vapour side [57, p. 3].

Three different types of mechanisms are able to stabilise or destabilise the system.

### 1. Vertical Diffusion

When the front is perturbed, the crest is closer to the heat source (vapour boundary). At the crest the vertical thermal gradient on the vapour side gets sharper whereas the vertical thermal gradient on the liquid side becomes less sharp. Due to the vertical thermal gradient more heat is transferred to the crest and less heat is taken away from it. This in turn tends to vaporise the liquid, so the displacement of the crest is decreased and the front is stabilised. This is the dominant stabilising mechanism for long waves.

### 2. Horizontal Diffusion

A second stability mechanism is provided by the horizontal thermal gradient, which eliminates the variations in the horizontal direction: this has a stabilising effect. For short waves, the horizontal thermal gradient is greater which implies that the horizontal diffusion is stronger and thus the stabilising effect is strongest for short waves.

### 3. Buoyancy Force

The third mechanism is the buoyancy force (Rayleigh-Taylor mechanism): if the lighter fluid is above the heavier fluid then gravity has a stabilising effect by pulling the perturbed interface back to its original position. If the heavier fluid is above the lighter fluid then the density difference (buoyancy) causes instability. The classical Rayleigh-Taylor analysis [66] shows that the buoyancy force is strongest for short waves. The Rayleigh-Taylor instability in a porous medium is discussed in detail in Section 4.1.1.

A comprehensive discussion of the physics of these stabilising and destabilising mechanisms can be found in [58].

#### 4.1.1 Rayleigh-Taylor instability in a porous medium

Saffman & Taylor [69] analysed the stability of a horizontal interface between two superposed viscous fluids which are forced by gravity and an imposed pressure gradient through a porous medium. The basic state is of uniform motion with vertically upward velocity  $V$ . We have re-visited Saffman & Taylor's [69] linear stability analysis of the above configuration in Appendix B. In this analysis the interface acts as a material surface which moves with the fluid, there is no fluid flux across it and there is no thermal effects. It has been shown that the growth rate  $\hat{\sigma}$  of infinitesimal disturbances must satisfy

$$\hat{\sigma} = \left\{ \frac{R_2 - 1}{R_2 + 1} V^* - \frac{1 - R_1}{1 + R_2} R_2 R_3 \right\} \frac{\hat{l}}{\varphi}, \quad (4.1)$$

When the basic state has no through flow and the interface is stationary (i.e.  $V^* = 0$ ), then (4.1) takes the form

$$\hat{\sigma} = -\frac{1 - R_1}{1 + R_2} \frac{R_2 R_3 \hat{l}}{\varphi}. \quad (4.2)$$

It is clear from (4.1) that the growth rate  $\hat{\sigma}$  is directly proportional to the wave number  $\hat{l}$ . It also follows from (4.1) that the interface is unstable to infinitesimal perturbations if

$$\frac{1}{\varphi(1+R_2)} \left\{ (R_2 - 1)V^* - (1 - R_1)R_2R_3 \right\} > 0, \quad (4.3)$$

where  $\varphi$  is the porosity,  $V^*$  is the dimensionless velocity,  $R_2 = \mu_{liq}/\mu_{vap}$  is the ratio of the dynamic viscosities,  $R_1$  is the density ratio. The Rayleigh number  $R_3$ , if  $< 0$ , represents a configuration with liquid above vapour. Equation (4.3) represents two destabilising mechanisms.

### 1. Viscous fingering

If we consider that the basic flow is free of gravity (i.e.  $R_3 = 0$ ) or if the densities are equal (i.e.  $R_1 = 1$ ), then the stability criterion (4.3) becomes

$$(R_2 - 1)V^* > 0, \quad (4.4)$$

which shows that viscosity contrast is essential for instability if gravity is neglected. This type of instability is known as viscous fingering [67, 69].

### 2. Density contrast

If we assume that the second term in (4.3) is dominant or if the viscosities are equal (i.e.  $R_2 = 1$ ), then the stability criterion (4.3) becomes

$$(1 - R_1)R_3 > 0, \quad (4.5)$$

which shows that if the denser fluid is above less dense fluid ( $R_3 < 0$ , liquid above vapour) then the system is unstable. (Recall that  $R_1 < 1$  from (3.20)). This type of instability has been discussed in Section 4.1, where we referred to it as buoyant instability.

## 4.2 Mathematical formulation of the stability problem

Now we will present all the governing equations and interfacial conditions which will be used to analyse the physical mechanisms associated with the problem defined at the start of Section 4.1. The governing equations have already been derived in Chapter 2 in a general form, but here we will recall them in the form most suitable to the problem. The continuity equation (2.14), Darcy's law (2.6) and the energy transport equation (2.37) are made non-dimensional using the same dimensional quantities as (3.15) and (3.20).

### Continuity equation

The continuity equation (2.14) takes the dimensionless form

$$\frac{\partial u_{liq,vap}^*}{\partial x^*} + \frac{\partial v_{liq,vap}^*}{\partial y^*} = 0. \quad (4.6)$$

We consider that the densities of the liquid and vapour are constant but different.

### Darcy's law

The equations that model the fluid physics in a porous structure are given by Darcy's equation in each phase. The equations may be written in scaled form as

$$\left. \begin{aligned} u_{liq}^* &= - \left( \frac{\partial P_{liq}^*}{\partial x^*} + R_3 \right), & u_{vap}^* &= - \frac{R_1 R_2 k}{C} \left( \frac{\partial P_{vap}^*}{\partial x^*} + R_1 R_3 \right), \\ v_{liq}^* &= - \frac{\partial P_{liq}^*}{\partial y^*}, & v_{vap}^* &= - \frac{R_1 R_2 k}{C} \frac{\partial P_{vap}^*}{\partial y^*}. \end{aligned} \right\} \quad (4.7)$$

In the equations above,  $R_3$  is the Rayleigh number which has been defined (also see (3.20)) as

$$R_3 = \frac{K \rho_{liq}^2 c_{p,liq} g L}{\mu_{liq} k_{m,liq}},$$

where  $K$  is the permeability of the homogeneous medium and  $g$  is the acceleration due to gravity with  $x^*$ -axis negative downwards. The Rayleigh number  $R_3$  will be our key quantity for understanding the Rayleigh-Taylor instability in a geothermal system.

### Energy equation

We will use the one-equation model to describe the heat transport in the porous medium assuming local thermal equilibrium (see Section 2.5.3). In dimensionless form, the equations in the liquid and vapour regions become

$$\left. \begin{aligned} E_1 \frac{\partial \Theta_{liq}}{\partial t^*} + u_{liq}^* \frac{\partial \Theta_{liq}}{\partial x^*} + v_{liq}^* \frac{\partial \Theta_{liq}}{\partial y^*} &= \frac{\partial^2 \Theta_{liq}}{\partial x^{*2}} + \frac{\partial^2 \Theta_{liq}}{\partial y^{*2}}, \\ \frac{E_2 k R_1}{C} \frac{\partial \Theta_{vap}}{\partial t^*} + u_{vap}^* \frac{\partial \Theta_{vap}}{\partial x^*} + v_{vap}^* \frac{\partial \Theta_{vap}}{\partial y^*} &= \frac{\partial^2 \Theta_{vap}}{\partial x^{*2}} + \frac{\partial^2 \Theta_{vap}}{\partial y^{*2}}. \end{aligned} \right\} \quad (4.8)$$

It can be seen from the above equations that the energy transport is coupled with the mass transport, which introduces non-linearities. But this is not the only reason for the inherited non-linearities. The other reason is the coupling of the interface position with the heat and mass transport equation which has been discussed in Section 3.1.

### Interfacial mass and energy jump conditions

The most important aspect of phase change problems is the energy and mass balance at the interface of the two phases, which makes the problem non-linear. We derived the possible generalised form of the energy balance at the phase change interface in Section 2.6.1.1. The energy jump condition (2.51) at the interface  $x = S(y, t)$  is scaled with the same dimensional quantities as (3.15) and (3.20), to

yield

$$\varphi H_{liq} \frac{\partial S^*}{\partial t} = \left\{ \frac{\partial \Theta_{liq}}{\partial x^*} - \frac{\partial S^*}{\partial y^*} \frac{\partial \Theta_{liq}}{\partial y^*} \right\}_{x^*=S^*} + \frac{\Theta_0}{k} \left\{ \frac{\partial \Theta_{vap}}{\partial x^*} - \frac{\partial S^*}{\partial y^*} \frac{\partial \Theta_{vap}}{\partial y^*} \right\}_{x^*=S^*} - H_{liq} \left( \frac{\partial P_{liq}^*}{\partial x^*} + R_3 \right). \quad (4.9)$$

This energy jump condition shows that the liquid-vapour interface position depends on the temperature distributions in both phases as well as on the transfer of fluid across the front (evaporation or condensation).

Furthermore the mass jump condition at the interface (2.57) is also coupled with the velocity profiles in both phases, giving in scaled form

$$\varphi (1 - R_1) \frac{\partial S^*}{\partial t^*} = R_1 R_2 \left. \frac{\partial P_{vap}^*}{\partial x^*} \right|_{x^*=S^*} - \left. \frac{\partial P_{liq}^*}{\partial x^*} \right|_{x^*=S^*} - R_3 (1 - R_1^2 R_2). \quad (4.10)$$

To examine the stability of the liquid-vapour interface, an infinitesimal disturbance is applied to the basic state. The aim is to linearise the above governing equations and boundary conditions about the basic state and to study the behaviour of the perturbed interface (see Figure 4.3).

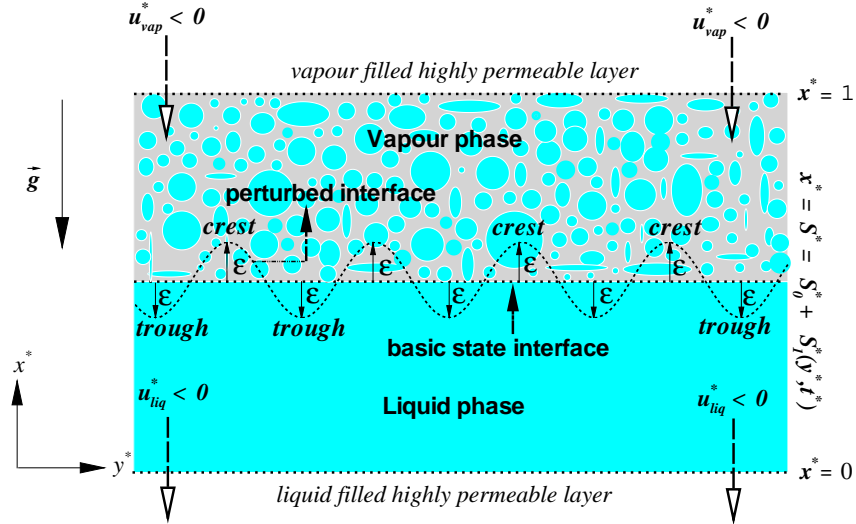


Figure 4.3: Schematic diagram for the physics of perturbed interface, when  $R_3 > 0$  (vapour above liquid).

### 4.2.1 Perturbed form of the problem

The temperature, velocity, pressure field both in the liquid and vapour regions and the liquid-vapour phase change front are expanded in the following manner

$$\begin{aligned}
 \Theta_{liq} &= \Theta_{liq}^0(x^*) + \epsilon \Theta_{liq}^1(x^*, y^*, t^*), & \Theta_{vap} &= \Theta_{vap}^0(x^*) + \epsilon \Theta_{vap}^1(x^*, y^*, t^*), \\
 u_{liq}^* &= \omega_0 + \epsilon \omega_1, & u_{vap}^* &= \Omega_0 + \epsilon \Omega_1, & v_{liq}^* &= \Gamma_0 + \epsilon \Gamma_1, & v_{vap}^* &= \Upsilon_0 + \epsilon \Upsilon_1, \\
 P_{liq}^* &= \Lambda_0 + \epsilon \Lambda_1, & P_{vap}^* &= \Pi_0 + \epsilon \Pi_1, & S^* &= S_0^* + \epsilon S_1^*(y^*, t^*),
 \end{aligned} \tag{4.11}$$

and only the first order terms in  $\epsilon$  are retained [18, p. 48], where  $0 < \epsilon \ll 1$ . The small perturbation parameter  $\epsilon$  represents the magnitude of the deviation from the basic state (see Figure 4.3). The subscript and superscript 0 and 1 denote the steady state and perturbed state, respectively.

The perturbed forms of the equations governing the liquid region are

$$\left. \begin{aligned}
 \frac{\partial(\omega_0 + \epsilon \omega_1)}{\partial x^*} + \frac{\partial(\Gamma_0 + \epsilon \Gamma_1)}{\partial y^*} &= 0, \\
 \omega_0 + \epsilon \omega_1 &= - \left( \frac{\partial(\Lambda_0 + \epsilon \Lambda_1)}{\partial x^*} + R_3 \right), \\
 \Gamma_0 + \epsilon \Gamma_1 &= - \frac{\partial(\Lambda_0 + \epsilon \Lambda_1)}{\partial y^*}, \\
 E_1 \frac{\partial(\Theta_{liq}^0 + \epsilon \Theta_{liq}^1)}{\partial t^*} + (\omega_0 + \epsilon \omega_1) \frac{\partial(\Theta_{liq}^0 + \epsilon \Theta_{liq}^1)}{\partial x^*} \\
 + (\Gamma_0 + \epsilon \Gamma_1) \frac{\partial(\Theta_{liq}^0 + \epsilon \Theta_{liq}^1)}{\partial y^*} &= \nabla^{*2} (\Theta_{liq}^0 + \epsilon \Theta_{liq}^1).
 \end{aligned} \right\} \tag{4.12}$$

The perturbed equations governing the vapour region are

$$\left. \begin{aligned} \frac{\partial (\Omega_0 + \epsilon \Omega_1)}{\partial x^*} + \frac{\partial (\Upsilon_0 + \epsilon \Upsilon_1)}{\partial y^*} &= 0, \\ \Omega_0 + \epsilon \Omega_1 &= -\frac{R_1 R_2 k}{C} \left( \frac{\partial (\Pi_0 + \epsilon \Pi_1)}{\partial x^*} + R_1 R_3 \right), \\ \Upsilon_0 + \epsilon \Upsilon_1 &= -\frac{R_1 R_2 k}{C} \frac{\partial (\Pi_0 + \epsilon \Pi_1)}{\partial y^*}, \\ \frac{E_2 k R_1}{C} \frac{\partial (\Theta_{vap}^0 + \epsilon \Theta_{vap}^1)}{\partial t^*} + (\Omega_0 + \epsilon \Omega_1) \frac{\partial (\Theta_{vap}^0 + \epsilon \Theta_{vap}^1)}{\partial x^*} \\ + (\Upsilon_0 + \epsilon \Upsilon_1) \frac{\partial (\Theta_{vap}^0 + \epsilon \Theta_{vap}^1)}{\partial y^*} &= \nabla^{*2} (\Theta_{vap}^0 + \epsilon \Theta_{vap}^1). \end{aligned} \right\} \quad (4.13)$$

The energy and mass jump conditions (4.9) and (4.10) at the phase change interface in perturbed form are

$$\begin{aligned} \varphi H_{liq} \frac{\partial (S_0^* + \epsilon S_1^*)}{\partial t^*} &= \left\{ \frac{\partial (\Theta_{liq}^0 + \epsilon \Theta_{liq}^1)}{\partial x^*} - \frac{\partial (S_0^* + \epsilon S_1^*)}{\partial y^*} \frac{\partial (\Theta_{liq}^0 + \epsilon \Theta_{liq}^1)}{\partial y^*} \right\}_{x^*=S_0^*} \\ &+ \frac{\Theta_0}{k} \left\{ \frac{\partial (\Theta_{vap}^0 + \epsilon \Theta_{vap}^1)}{\partial x^*} - \frac{\partial (S_0^* + \epsilon S_1^*)}{\partial y^*} \frac{\partial (\Theta_{vap}^0 + \epsilon \Theta_{vap}^1)}{\partial y^*} \right\}_{x^*=S_0^*} \\ &- H_{liq} \left( \frac{\partial (\Lambda_0 + \epsilon \Lambda_1)}{\partial x^*} + R_3 \right), \end{aligned} \quad (4.14)$$

and

$$\varphi (1 - R_1) \frac{\partial (S_0^* + \epsilon S_1^*)}{\partial t^*} = R_1 R_2 \frac{\partial (\Pi_0 + \epsilon \Pi_1)}{\partial x^*} \Big|_{x^*=S_0^*} - \frac{\partial (\Lambda_0 + \epsilon \Lambda_1)}{\partial x^*} \Big|_{x^*=S_0^*} - R_3 (1 - R_1^2 R_2). \quad (4.15)$$

Now the first priority is to get the basic state which will describe the natural state of a geothermal system, from the above perturbed equations.

### 4.2.2 Zeroth order problem

The equations governing the mass flow in the liquid and in the vapour region after equating the terms proportional to  $\epsilon^0$  in (4.12) and (4.13), yield

$$\left. \begin{aligned} \frac{\partial \omega_0}{\partial x^*} + \frac{\partial \Gamma_0}{\partial y^*} &= 0, & \frac{\partial \Omega_0}{\partial x^*} + \frac{\partial \Upsilon_0}{\partial y^*} &= 0, \\ \omega_0 &= -\frac{\partial \Lambda_0}{\partial x^*} - R_3, & \Omega_0 &= -\frac{R_1 R_2 k}{C} \left\{ \frac{\partial \Pi_0}{\partial x^*} + R_1 R_3 \right\}, \\ \underbrace{\Gamma_0 = -\frac{\partial \Lambda_0}{\partial y^*}}_{\text{liquid phase}} &= 0, & \underbrace{\Upsilon_0 = -\frac{R_1 R_2 k}{C} \frac{\partial \Pi_0}{\partial y^*}}_{\text{vapour phase}} &= 0, \end{aligned} \right\} \quad (4.16)$$

where  $(\omega_0, \Gamma_0)$  is the velocity of the water (liquid) and  $(\Omega_0, \Upsilon_0)$  is the velocity of the vapour. The pressure conditions at the liquid and vapour boundaries and at the phase change front  $S_0^*$  are  $\Lambda_0(S_0^*) = \Pi_0(S_0^*) = P_{S^*}^*$ ,  $\Lambda_0(0) = P_L^*$ ,  $\Pi_0(1) = P_V^*$ . Equating the terms proportional to  $\epsilon^0$  in (4.15), the mass flux condition at the phase change interface becomes

$$\varphi(1 - R_1) \frac{\partial S_0^*}{\partial t^*} = R_1 R_2 \left. \frac{d\Pi_0}{dx^*} \right|_{x^*=S_0^*} - \left. \frac{d\Lambda_0}{dx^*} \right|_{x^*=S_0^*} - R_3 (1 - R_1^2 R_2). \quad (4.17)$$

For the heat transport in the whole system, after equating the terms proportional to  $\epsilon^0$  in (4.12) and (4.13), we obtain

$$\left. \begin{aligned} E_1 \frac{\partial \Theta_{liq}^0}{\partial t^*} + \omega_0 \frac{d\Theta_{liq}^0}{dx^*} &= \nabla^{*2} \Theta_{liq}^0, \\ \frac{E_2 k R_1}{C} \frac{\partial \Theta_{vap}^0}{\partial t^*} + \Omega_0 \frac{d\Theta_{vap}^0}{dx^*} &= \nabla^{*2} \Theta_{vap}^0. \end{aligned} \right\} \quad (4.18)$$

The corresponding perturbed temperature boundary conditions are

$$\left. \begin{aligned} \text{at } x^* = 0 : \Theta_{liq}^0 &= 0, \\ \text{at } x^* = 1 : \Theta_{vap}^0 &= 0, \end{aligned} \right\} \quad (4.19)$$

$$\text{at } x^* = S_0^* \left\{ \begin{aligned} \Theta_{liq}^0 &= \Theta_{vap}^0 = 1, \\ H_{liq} \varphi \frac{\partial S_0^*}{\partial t^*} &= \frac{d\Theta_{liq}^0}{dx^*} + \frac{\Theta_0}{k} \frac{d\Theta_{vap}^0}{dx^*} + H_{liq} \omega_0. \end{aligned} \right. \quad (4.20)$$



The Taylor-series expansion of the interface condition (4.14) about  $S_0^*$  gives

$$\varphi H_{liq} \frac{\partial S_1^*}{\partial t^*} = \left\{ S_1^* \frac{d^2 \Theta_{liq}^0}{dx^{*2}} + \frac{\partial \Theta_{liq}^1}{\partial x^*} \right\} + \frac{\Theta_0}{k} \left\{ S_1^* \frac{d^2 \Theta_{vap}^0}{dx^{*2}} + \frac{\partial \Theta_{vap}^1}{\partial x^*} \right\} - H_{liq} \frac{\partial \Lambda_1}{\partial x^*}. \quad (4.25)$$

Having completed the mathematical formulation of the problem, we will now carry out two dimensional stability analyses of the basic states which have been studied in detail in Section 3.1.1. The two basic states under consideration can be differentiated by fluid flow. In the first case, the base state has no through flow, though this does not mean that there is no flow in the perturbed state. In the second case, vertical through flow is allowed in both phases (liquid and vapour).

## 4.3 Stability of the steady state with no through flow

This is the basic state considered by Il'ichev & Tsypkin [31]: our analysis is similar to theirs except that we employ a simpler  $T_S(P)$  condition (see Section 2.6.1) and a more complete heat transport equation.

### 4.3.1 Steady state

The basic state of the system is assumed to be steady and independent of the horizontal variable  $y^*$ , so  $\Lambda_0$ ,  $\Theta_{liq}^0$ ,  $\Pi_0$  and  $\Theta_{vap}^0$  are all functions of  $x^*$  only. Also the fluid is stationary,  $\omega_0 = \Omega_0 = \Gamma_0 = \Upsilon_0 = 0$ . The temperature profile is assumed to be conductive and the phase change front is static, so (4.16) and (4.18) give

$$\text{pressure profile} \quad \left\{ \begin{array}{l} \frac{d\Lambda_0}{dx^*} = -R_3, \quad \Lambda_0(0) = P_L^*, \\ \frac{d\Pi_0}{dx^*} = -R_1 R_3, \quad \Lambda_0(S_0^*) = \Pi_0(S_0^*), \end{array} \right. \quad (4.26)$$

and

$$\text{temperature profile} \quad \left\{ \begin{array}{l} \frac{d^2\Theta_{liq}^0}{dx^{*2}} = 0, \quad \Theta_{liq}^0(0) = 0, \quad \Theta_{liq}^0(S_0^*) = 1, \\ \frac{d^2\Theta_{vap}^0}{dx^{*2}} = 0, \quad \Theta_{vap}^0(1) = 0, \quad \Theta_{vap}^0(S_0^*) = 1, \\ \frac{d\Theta_{liq}^0}{dx^*} + \frac{\Theta_0}{k} \frac{d\Theta_{vap}^0}{dx^*} = 0. \end{array} \right. \quad (4.27)$$

The stationary solutions of (4.26) and (4.27) give the linear pressure profile and the purely conductive temperature profiles in the liquid and the vapour regions

$$\left. \begin{array}{l} \Lambda_0 = P_L^* - R_3 x^*, \quad \Pi_0 = P_L^* + R_3 S_0^* (R_1 - 1) - R_1 R_3 x^*, \\ \Theta_{liq}^0 = \frac{x^*}{S_0^*}, \quad \Theta_{vap}^0 = \frac{x^* - 1}{S_0^* - 1}. \end{array} \right\} \quad (4.28)$$

The front position in the steady state is

$$S_0^* = \frac{k}{k + \Theta_0}. \quad (4.29)$$

The steady state liquid-vapour phase change front position (4.29) has been found as a limiting case (no flow in the steady state, i.e.,  $Pec_i \rightarrow 0$ ) in Section 3.1.1.

### 4.3.2 First order problem

At the first order, we assume that fluid flow is two dimensional and mass flux across the phase change front is time dependent. Equations (4.21) and (4.22) then give

$$\left\{ \begin{array}{l} \frac{\partial^2 \Lambda_1}{\partial x^{*2}} + \frac{\partial^2 \Lambda_1}{\partial y^{*2}} = 0, \quad \Lambda_1(0) = 0, \\ \frac{\partial^2 \Pi_1}{\partial x^{*2}} + \frac{\partial^2 \Pi_1}{\partial y^{*2}} = 0, \quad \Pi_1(1) = 0, \\ \Lambda_1(S_0^*) + S_1^* \frac{d\Lambda_0}{dx^*} \Big|_{x^*=S_0^*} = \Pi_1(S_0^*) + S_1^* \frac{d\Pi_0}{dx^*} \Big|_{x^*=S_0^*}, \\ \varphi(1 - R_1) \frac{dS_1^*}{dt} = R_1 R_2 \left\{ S_1^* \frac{d^2 \Pi_0}{dx^{*2}} + \frac{d\Pi_1}{dx^*} \right\} - \left\{ S_1^* \frac{d^2 \Lambda_0}{dx^{*2}} + \frac{d\Lambda_1}{dx^*} \right\}. \end{array} \right. \quad (4.30)$$

Il'ichev & Tsyarkin [31] assumed only transient conductive heat transfer at first order, but we will consider both advection and diffusion here, thus the energy equation (4.23) gives

$$\left. \begin{array}{l} E_1 \frac{\partial \Theta_{liq}^1}{\partial t^*} + \omega_1 \frac{d\Theta_{liq}^0}{dx^*} = \nabla^{*2} \Theta_{liq}^1, \\ \frac{E_2 k R_1}{C} \frac{\partial \Theta_{vap}^1}{\partial t^*} + \Omega_1 \frac{d\Theta_{vap}^0}{dx^*} = \nabla^{*2} \Theta_{vap}^1. \end{array} \right\} \quad (4.31)$$

The corresponding first order temperature boundary conditions are

$$\left. \begin{array}{l} \Theta_{liq}^1(0) = 0, \quad \Theta_{liq}^1(S_0^*) = -S_1^* \frac{d\Theta_{liq}^0}{dx^*} \Big|_{x^*=S_0^*}, \\ \Theta_{vap}^1(1) = 0, \quad \Theta_{vap}^1(S_0^*) = -S_1^* \frac{d\Theta_{vap}^0}{dx^*} \Big|_{x^*=S_0^*}. \end{array} \right\} \quad (4.32)$$

The heat flux at the phase change front is time dependent

$$\varphi H_{liq} \frac{\partial S_1^*}{\partial t^*} = \left\{ S_1^* \frac{d^2 \Theta_{liq}^0}{dx^{*2}} + \frac{\partial \Theta_{liq}^1}{\partial x^*} \right\} + \frac{\Theta_0}{k} \left\{ S_1^* \frac{d^2 \Theta_{vap}^0}{dx^{*2}} + \frac{\partial \Theta_{vap}^1}{\partial x^*} \right\} - H_{liq} \frac{\partial \Lambda_1}{\partial x^*}. \quad (4.33)$$

### 4.3.3 The eigenvalue problem

The equation which describes the relationship between the decay (or growth) rate  $\sigma$  and the wave number  $l$  is known as the dispersion equation. According to the classical procedure [18, p. 49], the pressure and temperature profiles in both regions (liquid and vapour) and the phase change interface location in the first order problem are expanded in normal modes,

$$(\Theta_{liq}^1, \Theta_{vap}^1, \Lambda_1, \Pi_1, S_1^*) = (\phi_{liq}(x^*), \phi_{vap}(x^*), \Psi(x^*), \Sigma(x^*), \Phi) \exp[\sigma t^* + i l y^*], \quad (4.34)$$

where  $\phi_{liq}$ ,  $\phi_{vap}$  and  $\Phi$  are the eigenfunctions of temperature in the liquid region, temperature in the vapour region and the interface location, respectively, and  $l$  and  $\sigma$  denote the wave number and the rate of growth (or decay) of the disturbance. The eigenfunctions of pressure in both phases (liquid and vapour) are denoted by  $\Psi$  and  $\Sigma$ , respectively. When the expansion (4.34) is substituted into (4.30) we obtain

$$\left. \begin{aligned} \frac{d^2 \Psi(x^*)}{dx^{*2}} - l^2 \Psi(x^*) &= 0, & \Psi(0) &= 0, \Sigma(1) = 0, \\ \frac{d^2 \Sigma(x^*)}{dx^{*2}} - l^2 \Sigma(x^*) &= 0, & \Psi(S_0^*) &= \Sigma(S_0^*) + \Phi R_3 (1 - R_1), \\ \varphi (1 - R_1) \sigma \Phi &= R_1 R_2 \left. \frac{d\Sigma}{dx^*} \right|_{x^*=S_0^*} - \left. \frac{d\Psi}{dx^*} \right|_{x^*=S_0^*}. \end{aligned} \right\} \quad (4.35)$$

The solutions of (4.35) are

$$\text{pressure profile} \left\{ \begin{aligned} \Psi(x^*) &= 2 C_1 \sinh(l x^*), \\ \Sigma(x^*) &= 2 C_2 \frac{\sinh(l(x^* - 1))}{\cosh(l) - \sinh(l)}, \end{aligned} \right. \quad (4.36)$$

where

$$C_1 = \frac{\Phi}{2l} \frac{1 - R_1}{\sinh(l S_0^*)} \left\{ \frac{\varphi\sigma + R_3 l \coth(l S_0^*)}{R_1 R_2 \coth(l(S_0^* - 1)) - \coth(l S_0^*)} + R_3 l \right\},$$

$$C_2 = \frac{\Phi}{2l} \frac{(1 - R_1) \{\varphi\sigma + l R_3 \coth(l S_0^*)\} \{\cosh(l) - \sinh(l)\}}{\{R_1 R_2 \cosh(l(S_0^* - 1)) - \coth(l S_0^*) \sinh(l(S_0^* - 1))\}}.$$

The normal mode expansion (4.34) of the first order temperature profiles (4.31) and of the corresponding boundary conditions (4.32) gives

$$\left. \begin{aligned} \left( \frac{d^2}{dx^{*2}} - E_1 \sigma - l^2 \right) \phi_{liq} + \frac{1}{S_0^*} \frac{d\Psi}{dx^*} &= 0, \\ \phi_{liq}(0) = 0, \quad \phi_{liq}(S_0^*) &= -\frac{\Phi}{S_0^*}, \\ \left( \frac{d^2}{dx^{*2}} - \frac{E_2 k R_1}{C} \sigma - l^2 \right) \phi_{vap} + \frac{1}{S_0^* - 1} \frac{R_1 R_2 k}{C} \frac{d\Sigma}{dx^*} &= 0, \\ \phi_{vap}(1) = 0, \quad \phi_{vap}(S_0^*) &= \frac{\Phi}{1 - S_0^*}. \end{aligned} \right\} \quad (4.37)$$

The solution of (4.37) for the eigenfunctions of the temperature profiles is

$$\begin{aligned} \phi_{liq}(x^*) &= \frac{C_1}{S_0^*} \frac{2l}{E_1 \sigma} \left[ \frac{\sinh(\gamma_1 x^*)}{\sinh(\gamma_1 S_0^*)} \{\cosh(\gamma_1 S_0^*) - \cosh(l S_0^*)\} \right. \\ &\quad \left. + \{\cosh(l x^*) - \cosh(\gamma_1 x^*)\} \right] - \frac{\Phi \sinh(\gamma_1 x^*)}{S_0^* \sinh(\gamma_1 S_0^*)}, \end{aligned} \quad (4.38)$$

$$\begin{aligned} \phi_{vap}(x^*) &= \frac{2l R_2 C_2}{(S_0^* - 1) E_2 \sigma \{\cosh(l) - \sinh(l)\}} \left\{ \frac{\sinh(\gamma_2(x^* - 1))}{\sinh(\gamma_2(S_0^* - 1))} \right. \\ &\quad \left. \{\cosh(\gamma_2(S_0^* - 1)) - \cosh(l(S_0^* - 1))\} \right. \\ &\quad \left. + \cosh(l(x^* - 1)) - \cosh(\gamma_2(x^* - 1)) \right\} \\ &\quad - \frac{\Phi \sinh(\gamma_2(x^* - 1))}{(S_0^* - 1) \sinh(\gamma_2(S_0^* - 1))}, \end{aligned} \quad (4.39)$$

where  $\gamma_1 = \sqrt{l^2 + E_1 \sigma}$  and  $\gamma_2 = \sqrt{l^2 + \frac{E_2 k R_1}{C} \sigma}$ .

### 4.3.4 Dispersion analysis

The relationship between the growth rate and wave number can be obtained using the energy balance across the liquid-vapour interface. Substituting (4.34) into (4.33) and removing the terms for the temperature gradient in the undisturbed temperature field leads to

$$\varphi H_{liq} \sigma \Phi = \left[ \left\{ \frac{d\phi_{liq}}{dx^*} + \frac{\Theta_0}{k} \frac{d\phi_{vap}}{dx^*} \right\} - H_{liq} \frac{d\Psi}{dx^*} \right]_{x^*=S_0^*}. \quad (4.40)$$

The substitution of (4.36), (4.38) and (4.39) into (4.40) gives the dispersion equation

$$\begin{aligned} \varphi H_{liq} \sigma \Phi &= \left[ \frac{C_1 2l}{S_0^* E_1 \sigma} \{ \gamma_1 \coth(\gamma_1 S_0^*) \{ \cosh(\gamma_1 S_0^*) - \cosh(l S_0^*) \} \right. \\ &+ \left. l \sinh(l S_0^*) - \gamma_1 \sinh(\gamma_1 S_0^*) \} - \frac{\Phi \gamma_1}{S_0^*} \coth(\gamma_1 S_0^*) \right] \\ &+ \frac{\Theta_0}{k} \left[ \frac{2l R_2 C_2}{(S_0^* - 1) E_2 \sigma \cosh(l) - \sinh(l)} \{ l \sinh(l(S_0^* - 1)) \right. \\ &- \left. \gamma_2 \sinh(\gamma_2(S_0^* - 1)) - \gamma_2 \coth(\gamma_2(S_0^* - 1)) \{ \cosh(l(S_0^* - 1)) \right. \\ &- \left. \cosh(\gamma_2(S_0^* - 1)) \} \} - \frac{\Phi \gamma_2}{(S_0^* - 1)} \coth(\gamma_2(S_0^* - 1)) \right] \\ &- H_{liq}(1 - R_1) \Phi \left\{ \frac{\{ \varphi \sigma + l R_3 \coth(l S_0^*) \}}{R_1 R_2 \coth(l(S_0^* - 1)) - \coth(l S_0^*)} + R_3 l \right\} \coth(l S_0^*). \end{aligned} \quad (4.41)$$

The growth rate  $\sigma$  in equation (4.41) has multiple solutions because  $\gamma_1$  and  $\gamma_2$  depend on  $\sigma$ ; this non-linear equation must be solved numerically for  $\sigma$ . For this, Maple's<sup>1</sup> `implicitplot`<sup>2</sup> routine has been used. In this case, this method is adequate, but in some related problems (discussed in Section 4.4) matters are not so simple. Some solutions of the dispersion equation (4.41) are shown in Figure

<sup>1</sup><http://www.maplesoft.com/products/Maple/index.aspx>

<sup>2</sup><http://www.maplesoft.com/support/help/Maple/view.aspx?path=plots/>

4.4, when the interface is at the middle of the porous layer, i.e.,  $S_0^* = \frac{1}{2}$ . The front becomes unstable first for zero wave number, when the Rayleigh number  $R_3$  crosses the critical value  $|R_{30}^{crit}| = 13.21$  (see Figure 4.4 (a)).

It is interesting to contrast these results with those of Il'ichev & Tsypkin [31]. They found that if  $S_0^* = \frac{1}{2}$  the transition to instability was “spontaneous”: all wave numbers become unstable at the same value of  $R_3$ . Meanwhile, short waves become unstable first if  $S_0^* < \frac{1}{2}$ , and long waves if  $S_0^* > \frac{1}{2}$ . This will be discussed further in Section 4.3.6.2. For short waves, the front position becomes unstable when  $|R_{3\infty}^{crit}| = 17.22$  (see Figure 4.4 (b)). The results in Figure 4.4 show that the transition to instability is not spontaneous as found by Il'ichev & Tsypkin [31], indicating that the interesting behaviour in their model is an artefact of taking a very simple model which neglected thermal advection. This motivates a more thorough investigation of the transition to instability.

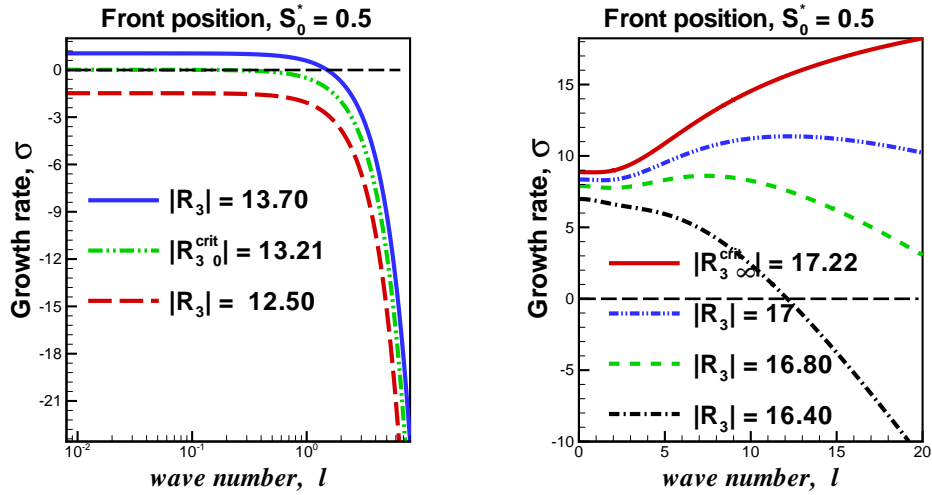


Figure 4.4: The transition to instability when the liquid-vapour phase change front is at the middle of the porous layer with  $R_1 = 0.0056$ ,  $R_2 = 8.75$ ,  $E_1 = 1$ ,  $E_2 = 1$ ,  $C = 1.96$ ,  $k = 4$ ,  $H_{liq} = 5$ ,  $\Theta_0 = 4$  and  $\varphi = 0.38$ . Log scale is used for clarity. Note that  $R_3 < 0$  (liquid above vapour).

### 4.3.5 Transition to instability

In this section, the possible types of transition to instability and the effect of the critical Rayleigh number on the stability of the front for short, medium and long wavelength disturbances will be discussed.

#### 4.3.5.1 Onset of instability when $l \rightarrow \infty$

We will use asymptotic analysis to help us locate the stability boundary in parameter space. We will focus in particular on the critical Rayleigh number for infinite wave number. For this let  $\sigma = \sigma^* l$  and  $\sigma^* = \sigma_0 + \frac{\sigma_1}{l} + O\left(\frac{1}{l^2}\right)$  and take  $l \rightarrow \infty$ ; then expanding (4.41) in asymptotic series in  $l$  gives

$$\begin{aligned} \varphi H_{liq} \sigma_0 l + \varphi \sigma_1 \sim & \left\{ -\frac{l}{S_0^*} + \frac{(\varphi \sigma_0 - R_1 R_2 R_3)(1 - R_1) - \sigma_0 E_1(R_1 R_2 + 1)}{2(R_1 R_2 + 1)S_0^*} \right\} \\ & + \frac{\Theta_0}{k} \left\{ \frac{l}{S_0^* - 1} + \frac{k R_1 R_2 (\varphi \sigma_0 + R_3)(1 - R_1) + \sigma_0 E_2(R_1 R_2 + 1)}{2(R_1 R_2 + 1)(S_0^* - 1)} \right\} \\ & + H_{liq} \left\{ \frac{(\varphi \sigma_0 - R_1 R_2 R_3)(1 - R_1)l}{R_1 R_2 + 1} + \frac{\varphi \sigma_1(1 - R_1)}{R_1 R_2 + 1} \right\} + O\left(\frac{1}{l^2}\right). \end{aligned} \quad (4.42)$$

Equating the terms proportional to  $l$ , (4.42) implies that

$$\sigma_0 \sim \underbrace{\frac{R_1 R_2 + 1}{\varphi H_{liq} R_1(R_2 + 1)} \left\{ -\frac{1}{S_0^*} - \frac{\Theta_0}{k} \frac{1}{1 - S_0^*} \right\}}_{\text{first term}} - \underbrace{\frac{1 - R_1 R_2 R_3}{R_2 + 1} \frac{1}{\varphi}}_{\text{second term}}. \quad (4.43)$$

From (4.43) it is clear that the first term has always negative sign because the dimensional parameters in the first term are all positive real numbers. So the first term, which represents the diffusive heat transport process, has a stabilising effect on the liquid-vapour phase change front (see Section 4.1).

Now here we have two different cases to discuss. If the lighter fluid is above the heavier fluid, i.e.,  $R_3 > 0$ , then the second term has a negative sign (recall that

$R_1 < 1$ ) and the front is stable for infinite wave numbers.

Alternatively, if  $R_3 < 0$ , which means that heavier fluid (liquid) is above the lighter fluid (vapour), then the second term in (4.43) has a positive sign and has a destabilising effect on the liquid-vapour phase change front. It is the competition between the first and second terms which will determine the nature of the liquid-vapour phase change front. Now we will find the critical Rayleigh number for infinite wave numbers. For this, in the case of marginal stability  $\sigma_0 = 0$ , and solving (4.43) for  $R_3$  and using the value of  $S_0^*$  from (4.29), we have

$$R_3^{crit} \sim R_{3,\infty}^{crit} = \frac{2(R_1 R_2 + 1)}{H_{liq} R_1 R_2 (R_1 - 1)} \frac{k + \Theta_0}{k}, \quad \text{as } l \rightarrow \infty. \quad (4.44)$$

When searching for the stability boundary we use this value (4.44) as a convenient starting point.

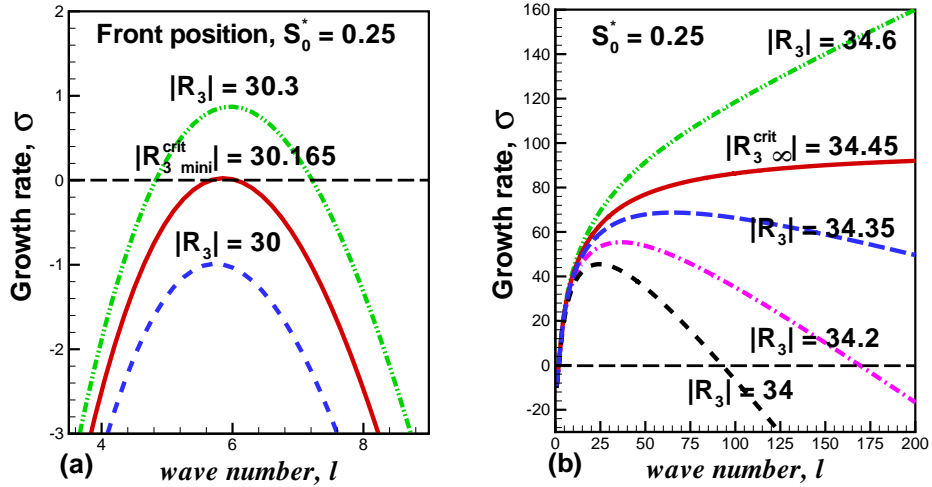


Figure 4.5: The transition to instability when the liquid-vapour phase change front is near to the upper boundary, i.e.,  $S_0^* < \frac{1}{2}$ , with  $R_1 = 0.0056$ ,  $R_2 = 8.75$ ,  $E_1 = 1$ ,  $E_2 = 1$ ,  $C = 1.96$ ,  $k = 4$ ,  $H_{liq} = 5$ ,  $\Theta_0 = 12$  and  $\varphi = 0.38$ .

Figure 4.5 provides a representative example of how the growth rate ( $\sigma$ ) varies with the wave number ( $l$ ), where the Rayleigh number  $R_3$  is the curve parameter and

the front is near to the liquid boundary,  $S_0^* < \frac{1}{2}$ . In the case when  $|R_3| < |R_3^\infty^{crit}|$  and  $R_3 < 0$ , both short and long wavelength disturbances are stable since  $\sigma < 0$ . Short wavelength disturbances (large  $l$ ) are stabilised by horizontal thermal diffusion which eliminates the variations in the horizontal direction of the perturbed front, whereas long wavelength disturbances (small  $l$ ) are stabilised by vertical diffusion. Medium wavelength disturbances become unstable as the Rayleigh number increases, through a Rayleigh-Taylor instability (see Section 4.1.1). When the Rayleigh number crosses the short-wave threshold, i.e.,  $|R_3| > |R_3^\infty^{crit}|$  and  $R_3 < 0$ , then the phase change front is unstable for short wavelength.

The reciprocal of the Stefan number,  $H_{liq} = \frac{\lambda}{c_{pliq}(T_S - T_L)}$ , it represents the ratio of the latent heat of liquid-vapour phase change ( $\lambda$ ) to the sensible heat ( $T_S - T_L$ ). If the latent heat is very large then the interface acts like a material surface. In the case when  $H_{liq} \rightarrow \infty$ , then the stability of the front depends on the buoyancy force only. In this limit, the first term on the right hand side of (4.43) tends to zero, leaving

$$\sigma_0 \sim -\frac{1 - R_1 R_2 R_3}{R_2 + 1} \frac{1}{\varphi}. \quad (4.45)$$

This recovers the Rayleigh-Taylor result (4.2). Now if the lighter fluid is above the heavier fluid, i.e.  $R_3 > 0$ , then it is clear from (4.45) that the liquid-vapour phase change front is always stable. In the case when the high density fluid (water) is above the low density fluid (vapour), i.e.  $R_3 < 0$ , then (4.45) shows that the front is unstable: this is the buoyancy instability which we have discussed in Section 4.1.1.

### 4.3.5.2 Onset of instability when $l = 0$

Assuming marginal stability ( $\sigma = 0$ ) and using  $S_0^*$  from (4.29), the critical Rayleigh number for zero wave number is obtained by taking the limit of (4.41) as  $l \rightarrow 0$ ,

$$R_{3,0}^{crit} \approx \frac{2C(kR_1R_2 + \Theta_0)}{\Theta_0 R_1 R_2 (R_1 - 1)(\Theta_0 + (2H_{liq} + 1)C)} \left( \frac{k + \Theta_0}{k} \right)^2. \quad (4.46)$$

Figure 4.6 illustrates that, if the liquid-vapour front is near to the vapour boundary, i.e.,  $S_0^* > \frac{1}{2}$ , then the front can become unstable first for zero wave number.

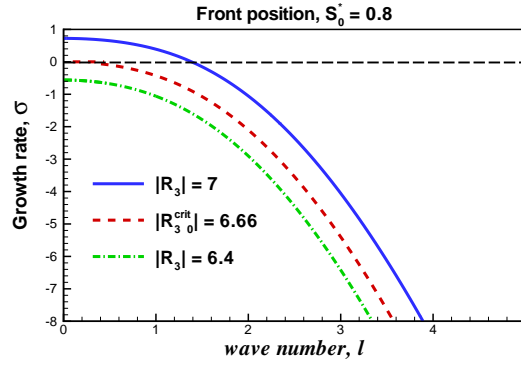


Figure 4.6: The transition to instability when the liquid-vapour phase change front is near to the lower boundary, i.e.,  $S_0^* > \frac{1}{2}$ , with  $R_1 = 0.0056$ ,  $R_2 = 8.75$ ,  $E_1 = 1$ ,  $E_2 = 1$ ,  $C = 1.96$ ,  $k = 4$ ,  $H_{liq} = 5$ ,  $\Theta_0 = 1$  and  $\varphi = 0.38$ .

### 4.3.6 Special cases

Finally we will consider some special cases of the dispersion equation (4.41). The different cases which we are going to deal with are given in the following table.

In Table 4.1 Diff(L) denotes diffusion in the liquid phase, adv(V) denotes advection and diffusion in the vapour phase,  $T$ ,  $P$ ,  $u$  are temperature, pressure and velocity, respectively.

Table 4.1: List of problems under consideration

Boundary conditions	Modes of heat transport		
	Diff(L)/diff(V)	Diff(L)/adv(V)	Adv(L)/diff(V)
$T$ fixed, $P$ fixed	4.3.6.2	4.3.6.4	4.3.6.3
$T$ fixed, $u$ fixed	4.3.6.1		

These special cases are motivated that we can relate our results to Il'ichev & Tsypkin's [31] work. Il'ichev & Tsypkin's [31] model has been revisited and then modified (possible extensions) to understand the more realistic problem.

#### 4.3.6.1 The classical one

This case is a standard one, in which we assume that the mode of heat transfer in the porous medium is pure conduction. We also assume that there is no flow, so gravity  $g$  does not affect the system. The boundaries are assumed to be isothermal. In the absence of any type of fluid flow, while the limit of  $C_1$  and  $C_2$  is assumed to be small, (4.41) yields

$$\varphi H_{liq} \sigma = -\frac{\gamma_1}{S_0^*} \coth(\gamma_1 S_0^*) - \frac{\Theta_0}{k} \frac{\gamma_2}{(1 - S_0^*)} \coth(\gamma_2(1 - S_0^*)), \quad (4.47)$$

where  $\gamma_1 = \sqrt{l^2 + E_1} \sigma$ ,  $\gamma_2 = \sqrt{l^2 + \frac{E_2 k R_1}{C} \sigma}$ .

From mathematical point of view, all the parameters involved are positive in (4.47), so the growth rate  $\sigma < 0 \forall l$ : this means that the system is stable. As we have discussed in Section 4.1, the diffusion stabilises the system and here we find the same type of stability. Moreover in any case whether the heavier fluid (liquid) is above the lighter fluid (vapour) or vapour above the liquid, if there is no flow in the system and the process of heat transfer is only governed by conduction, then the system will always be stable. This confirms the argument presented in Section

4.1.

#### 4.3.6.2 Il'ichev & Tsyarkin [31] revisited

This problem is the extension of the problem discussed in 4.3.6.1, by considering fluid flow, so the phase change interface is influenced by the flow; and gravity becomes important. The mode of heat transfer will remain conduction in the system and the same thermal boundary conditions apply. The same type of problem was studied by Il'ichev & Tsyarkin [31], with the extra assumption that the phase transition temperature depends on pressure (for discussion see Section 2.6.1). Since the heat transport in both phases is purely conductive, then in the absence of advection in both phases (setting  $d\Psi/dx^*$  and  $d\Sigma/dx^*$  equal to zero in (4.37), except at the liquid-vapour phase change front), by following the procedure as before, we obtain the dispersion relation

$$\begin{aligned} \varphi H_{liq} \sigma &= -\frac{\gamma_1}{S_0^*} \coth(\gamma_1 S_0^*) - \frac{\Theta_0}{k} \frac{\gamma_2}{(1 - S_0^*)} \coth(\gamma_2(1 - S_0^*)) \\ &- H_{liq}(1 - R_1) \left\{ R_3 l + \frac{\{\varphi\sigma + lR_3 \coth(lS_0^*)\}}{R_1 R_2 \coth(l(S_0^* - 1)) - \coth(lS_0^*)} \right\} \coth(lS_0^*). \end{aligned} \quad (4.48)$$

In the case of marginal stability,  $\sigma = 0$ , (4.48) takes the form

$$\begin{aligned} F^2(l) + \left\{ R_1 R_2 + \frac{S_0^*}{1 - S_0^*} \frac{\Theta_0}{k} + S_0^* H_{liq} R_1 R_2 R_3 (1 - R_1) \right\} F(l) \\ + \frac{S_0^*}{1 - S_0^*} \frac{\Theta_0}{k} R_1 R_2 = 0, \end{aligned}$$

where

$$F(l) = \frac{\coth(lS_0^*)}{\coth(l(1 - S_0^*))}. \quad (4.49)$$

The quadratic equation (4.49) has a solution of the form

$$F(l) = F_{1,2} = b \pm \sqrt{b^2 - c}, \quad (4.50)$$

where

$$b = -\frac{1}{2} \left\{ R_1 R_2 + \frac{S_0^*}{1 - S_0^*} \frac{\Theta_0}{k} + S_0^* H_{liq} R_1 R_2 R_3 (1 - R_1) \right\}, \quad (4.51)$$

$$c = \frac{S_0^*}{1 - S_0^*} \frac{\Theta_0}{k} R_1 R_2. \quad (4.52)$$

In order to obtain physically meaningful solutions for  $l$ , we require that  $F > 0$ , which is possible when  $b > 0$  and  $c > 0$ . The expression (4.52) shows that  $c > 0$  because  $R_1$ ,  $R_2$  and  $k$  are the ratio of the densities, viscosities and diffusivities of the liquid and vapour, respectively, so all these three ratios are positive. The location of the interface is denoted by  $S_0^*$ , which is in the range  $0 < S_0^* < 1$ . Finally the dimensionless parameter  $H_{liq}$ , which represents the reciprocal of the Stefan number for the liquid is positive, so  $c > 0$ .

A necessary and sufficient condition for  $b > 0$  is that (using the value of  $S_0^*$  from (4.29))

$$R_3^{crit} \sim R_{3,\infty}^{crit} = \frac{2(R_1 R_2 + 1)}{H_{liq} R_1 R_2 (R_1 - 1)} \frac{k + \Theta_0}{k}. \quad (4.53)$$

This tells us immediately that the instability can only occur for sufficiently large, negative values of the Rayleigh number  $R_3$ . The condition on critical Rayleigh number for infinite wave numbers (4.53) is the same as (4.44), because the horizontal diffusion dominates advection for short waves.

For the complete analysis we also need the critical Rayleigh number for zero wave number, which has been found by taking the limit of (4.48) as  $l \rightarrow 0$ , with  $(\sigma \rightarrow 0)$  and using  $S_0^*$  from (4.29)

$$R_{3,0}^{crit} \approx \frac{(k R_1 R_2 + \Theta_0)}{\Theta_0 H_{liq} R_1 R_2 (R_1 - 1)} \left( \frac{k + \Theta_0}{k} \right)^2. \quad (4.54)$$

Now we will discuss the possible types of transitions to instability depending upon the position of the liquid-vapour phase change front  $S_0^*$ .

**Front position**  $S_0^* = \frac{1}{2}$

Let us assume that the position of the liquid-vapour phase change front is the middle of the porous layer, i.e.,  $S_0^* = \frac{1}{2}$ , so (4.29) yields

$$k = \Theta_0. \quad (4.55)$$

Substituting (4.55) into the necessary conditions on the Rayleigh numbers for the short and long wavelengths, (4.53) and (4.54), respectively, gives

$$R_{3,0}^{crit} = \frac{4(R_1 R_2 + 1)}{H_{liq} R_1 R_2 (R_1 - 1)} = R_{3,\infty}^{crit}, \quad (4.56)$$

which shows that if  $|R_3| = |R_{3,0}^{crit}| = |R_{3,\infty}^{crit}|$  (recall  $R_3 < 0$ , liquid above vapour), then  $\sigma(l) = 0$ . The instability takes place spontaneously, in the sense that as  $|R_3|$  is increased, the system becomes unstable, i.e.  $\sigma(l) = 0$ , for all wave numbers  $l$  at once. The same type of transition to instability was found by Il'ichev & Tsytkin [31], while considering that the phase change temperature depends on pressure but we take the temperature at the interface as a constant. Furthermore, if  $|R_3| > |R_{3,\infty}^{crit}|$  then the system is unstable, at fixed values of the pressure and temperature on the upper and lower boundaries.

**Front position**  $S_0^* < \frac{1}{2}$

When the liquid-vapour phase change front is near to the liquid (upper) boundary, i.e.,  $S_0^* < \frac{1}{2}$ , then the critical Rayleigh numbers (4.53) and (4.54) for short and long wavelength are related by  $|R_{3,\infty}^{crit}| < |R_{3,0}^{crit}|$ . This relation suggests that the transition to instability happens first for short wavelengths. Figure 4.7 (a) shows that the onset of instability occurs for infinite wave numbers. In Figure 4.7 (b) and (c) the lines  $F(l) = F_1$  and  $F(l) = F_2$  represent the positive and negative roots of (4.50), respectively. When the line  $F(l) = F_1$  moves upward (see Figure

4.7 (b)), the positive root  $F_1$  of (4.50) causes instability for short waves.

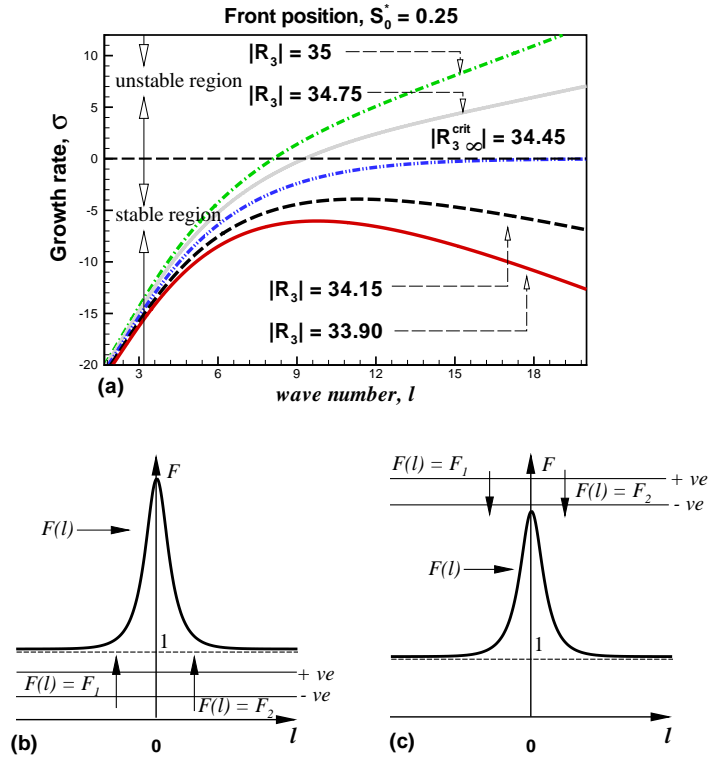


Figure 4.7: The dispersion curves  $\sigma = \sigma(l)$  when the interface is near to the liquid boundary, i.e.,  $S_0^* < \frac{1}{2}$ , with  $R_1 = 0.0056$ ,  $R_2 = 8.75$ ,  $E_1 = 1$ ,  $E_2 = 1$ ,  $C = 1.96$ ,  $k = 4$ ,  $H_{liq} = 5$ ,  $\Theta_0 = 12$  and  $\varphi = 0.38$ . (b) shows that the instability is attained at infinite wave numbers, when the line  $F(l) = F_1$  moves upward. (c) shows that the instability occurs at zero wave number, when the line  $F(l) = F_2$  moves downward. Figures (b) and (c) are adapted from [31].

**Front position  $S_0^* > \frac{1}{2}$**

The behavior of the dispersion relation (4.48), when the liquid-vapour phase change front is near to the vapour boundary, is illustrated in Figure 4.8. Figure 4.8 (b) shows that the transition to instability occurs for zero wave number when the

line  $F(l) = F_1$  moves upward. In this case when  $S_0^* > \frac{1}{2}$ , the front first becomes unstable for the positive roots of (4.50).

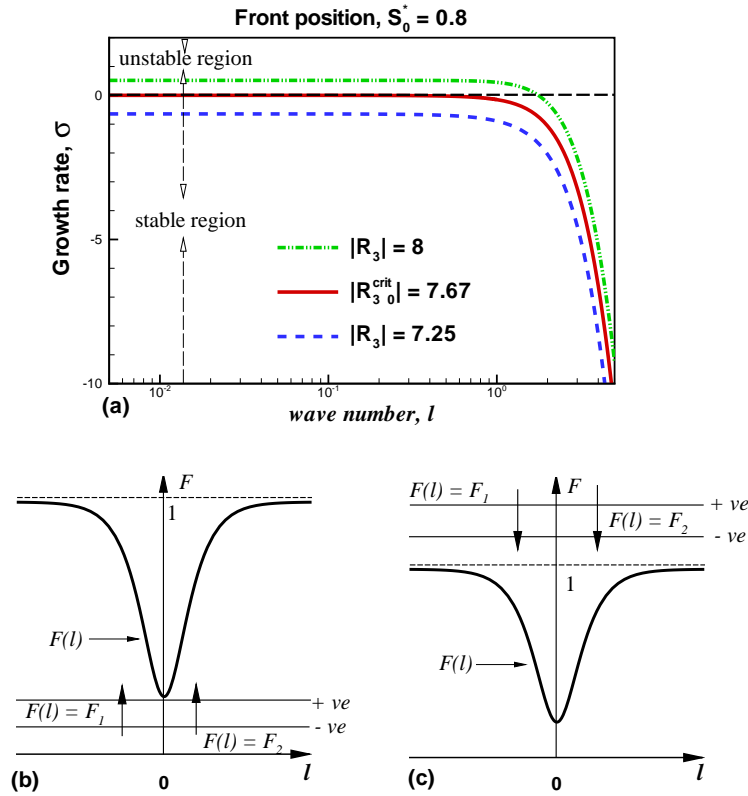


Figure 4.8: The dispersion curves  $\sigma = \sigma(l)$  when the interface is near to the lower boundary, i.e.,  $S_0^* > \frac{1}{2}$ , with  $R_1 = 0.0056$ ,  $R_2 = 8.75$ ,  $E_1 = 1$ ,  $E_2 = 1$ ,  $C = 1.96$ ,  $k = 4$ ,  $H_{liq} = 5$ ,  $\Theta_0 = 1$  and  $\varphi = 0.38$ . (b) shows that the instability is attained at zero wave number, when the line  $F(l) = F_1$  moves upward. (c) shows that the instability occurs at infinite wave numbers, when the line  $F(l) = F_2$  moves downward. Figures (b) and (c) are adapted from [31]. Log scale is used for clarity.

### 4.3.6.3 Perturbed vapour phase is affected by both advection and conduction

The problem discussed in 4.3.6.2 is now extended by assuming that the mode of heat transfer in the vapour region is both conduction and advection, while in the

liquid region the heat transport is by conduction only. The rest of the assumptions and the boundary conditions remain the same. Ignoring the advection term in the liquid phase (setting  $d\Psi/dx^*$  equal to zero in (4.37), except at the liquid-vapour phase change front), the dispersion relation can be obtained as

$$\begin{aligned}
\varphi H_{liq} \sigma \Phi &= \frac{\Theta_0}{k} \left[ \frac{2l R_2 C_2}{(S_0^* - 1) E_2 \sigma \cosh(l) - \sinh(l)} \frac{1}{\{l \sinh(l(S_0^* - 1)) \right.} \\
&- \left. \gamma_2 \sinh(\gamma_2(S_0^* - 1)) - \gamma_2 \coth(\gamma_2(S_0^* - 1)) \{ \cosh(l(S_0^* - 1)) \right. \\
&- \left. \cosh(\gamma_2(S_0^* - 1)) \} \} - \frac{\Phi \gamma_2}{(S_0^* - 1) \coth(\gamma_2(S_0^* - 1))} \right] \\
&- H_{liq} (1 - R_1) \Phi \left\{ \frac{\{\varphi \sigma + l R_3 \coth(l S_0^*)\}}{R_1 R_2 \coth(l(S_0^* - 1)) - \coth(l S_0^*)} + R_3 l \right\} \coth(l S_0^*) \\
&- \frac{\Phi \gamma_1}{S_0^*} \coth(\gamma_1 S_0^*). \tag{4.57}
\end{aligned}$$

Some solutions of the dispersion equation (4.57) are shown in figure 4.9, which will be discussed in the next section.

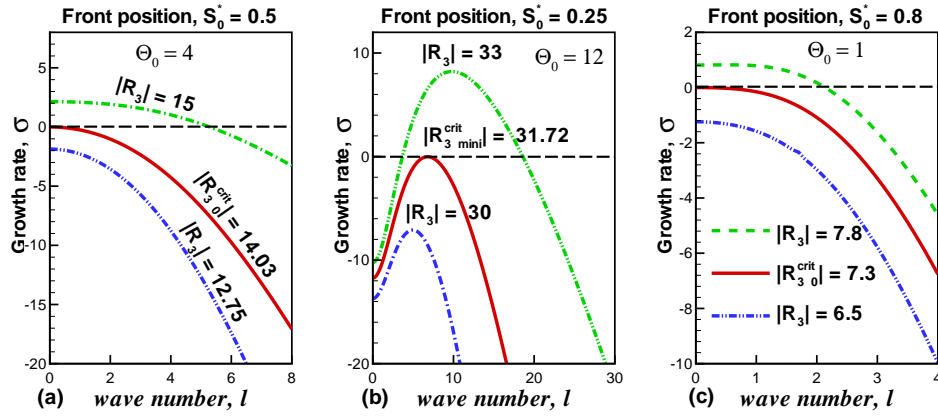


Figure 4.9: Growth rate vs wave number in the presence of advection and conduction in the vapour region only with  $R_1 = 0.0056$ ,  $R_2 = 8.75$ ,  $E_1 = 1$ ,  $E_2 = 1$ ,  $C = 1.96$ ,  $k = 4$ ,  $H_{liq} = 5$  and  $\varphi = 0.38$ .

#### 4.3.6.4 Perturbed liquid phase is affected by both advection and conduction

In this case the mode of heat transfer in the vapour region is assumed to be conduction only, while conduction and advection are both considered in the liquid region. The boundary conditions are the same as considered in 4.3.6.2 and 4.3.6.3. Ignoring the advection term for the vapour phase (setting  $d\Sigma/dx^*$  equal to zero in (4.37) only) or taking  $C_2 = 0$  in the dispersion equation (4.41) yields

$$\begin{aligned}
\varphi H_{liq} \sigma \Phi &= \left[ \frac{C_1 2l}{S_0^* E_1 \sigma} \{ \gamma_1 \coth(\gamma_1 S_0^*) \{ \cosh(\gamma_1 S_0^*) - \cosh(l S_0^*) \} \right. \\
&+ \left. l \sinh(l S_0^*) - \gamma_1 \sinh(\gamma_1 S_0^*) \} - \frac{\Phi \gamma_1}{S_0^*} \coth(\gamma_1 S_0^*) \right] \\
&- \frac{\Theta_0}{k} \frac{\Phi \gamma_2}{(S_0^* - 1)} \coth(\gamma_2 (S_0^* - 1)) - H_{liq} (1 - R_1) \Phi \{ R_3 l \\
&+ \left. \frac{\{ \varphi \sigma + l R_3 \coth(l S_0^*) \}}{R_1 R_2 \coth(l (S_0^* - 1)) - \coth(l S_0^*)} \right\} \coth(l S_0^*). \quad (4.58)
\end{aligned}$$

Now we are in a position to make some final comments about the stability of the steady liquid-vapour phase change front with no flow. Several important conclusions are as follows. In Section 4.3.6.2 we found that when the interface is at the middle of the porous layer, with the assumption that there is only pure conductive heat transfer in the entire system, then the transition to instability is spontaneous, which is completely in agreement with the results shown by Il'ichev & Tsytkin [31]. However, as we have seen in Figure 4.5 and again in Sections 4.3.6.3 and 4.3.6.4, when any advection is included the spontaneous transition no longer occurs.

In Section 4.1 we discussed three different types of mechanisms which stabilise or destabilise the liquid-vapour phase change front. The same three types can be seen from Figures 4.9 (b) and 4.5 (a), when the interface is near to the liquid boundary. The liquid-vapour phase change front is stable for both short and long wavelength.

The stability of long waves is due to vertical diffusion and the short wavelength disturbances are stabilised by horizontal diffusion. The front becomes unstable for medium wavelengths for higher Rayleigh numbers: this is a reflection of the buoyant instability, because the denser fluid (liquid) is above the less dense fluid (vapour). The condition on critical Rayleigh number for short wave disturbance for the different cases discussed in Sections 4.3.6.2, 4.3.6.3 and 4.3.6.4 is the same as (4.44), because the horizontal diffusion dominates advection for short waves.

Table 4.2: List of critical Rayleigh numbers for long wavelength

Critical Rayleigh number, $ R_{30}^{crit} $	Modes of heat transport
$\frac{(k R_1 R_2 + \Theta_0)}{\Theta_0 H_{liq} R_1 R_2 (R_1 - 1)} \left( \frac{k + \Theta_0}{k} \right)^2$	Conduction in the entire system
$\frac{2(k R_1 R_2 + \Theta_0)}{\Theta_0 R_1 R_2 (1 + 2 H_{liq})(R_1 - 1)} \left( \frac{k + \Theta_0}{k} \right)^2$	Adv & diff in the liquid phase
$\frac{2C(k R_1 R_2 + \Theta_0)}{\Theta_0 R_1 R_2 (\Theta_0 + 2C H_{liq})(R_1 - 1)} \left( \frac{k + \Theta_0}{k} \right)^2$	Adv & diff in the vapour phase
$\frac{2C(k R_1 R_2 + \Theta_0)}{\Theta_0 R_1 R_2 (R_1 - 1)(\Theta_0 + (2H_{liq} + 1)C)} \left( \frac{k + \Theta_0}{k} \right)^2$	Adv & diff in the entire system

The above different critical Rayleigh numbers for long wavelengths based on the different modes of heat transfer, are plotted in Figure 4.10 as function of the ratio of the temperature contrasts across the liquid and vapour layers  $\Theta_0$  and of the density ratio  $R_1$ . Figure 4.10 (a) shows that when  $\Theta_0$  is very large or very small the system is more stable than for intermediate values; this is because these limits correspond to a strong thermal gradient on one side or the other of the front, which has a stabilising effect through vertical diffusion (see Section 4.1). Furthermore, a system which is governed by both advection and conduction is more unstable for zero wave number than a purely conductive system. Figure 4.10 (b) surprisingly shows that the interface becomes more stable as  $R_1 \rightarrow 0$ ; because

the Rayleigh–Taylor mechanism is not effective for  $l = 0$ , and hence our physical intuition is misleading in this case.

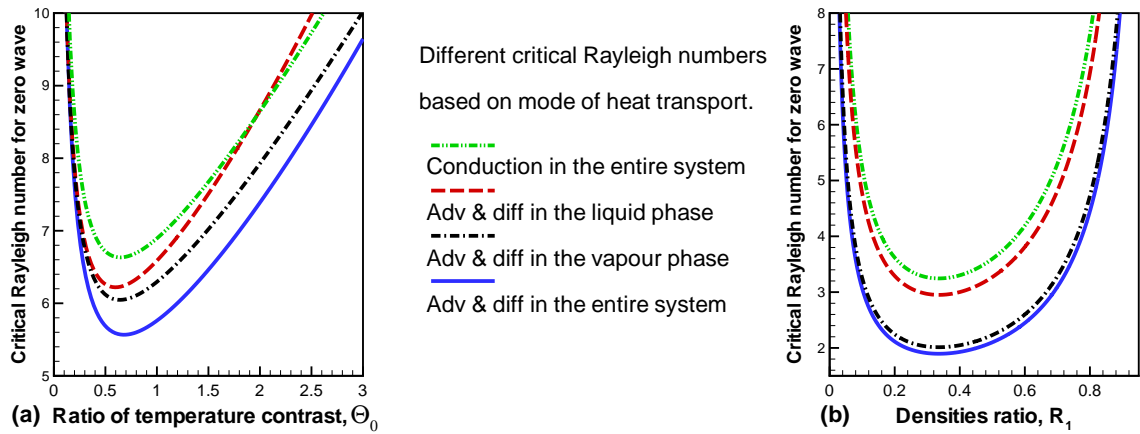


Figure 4.10: The critical Rayleigh number for long wavelength versus (a) ratio of the temperature contrast and (b) ratio of the densities  $R_1$ , where  $R_2 = 8.75$ ,  $C = 1.96$ ,  $k = 4$ ,  $H_{liq} = 5$ .

## 4.4 Stability of the steady state with through flow

In this section, we will discuss the stability of the steady state front in a geothermal system with through flow where the heavier fluid (water) overlies the lighter fluid (vapour) with isothermal boundary conditions. The competition between the thermal and fluid-flow effects in such configurations means that multiple positions of the phase change interface are possible (see Section 3.1.1). The multiple front positions make it necessary to investigate the stability of each position in order to determine which front positions, if any, may occur in practice.

### 4.4.1 Steady state solution

The mathematical conceptualisation of the problem with isothermal conditions and the possible physical mechanisms associated with instability have been discussed in Section 3.1.1. The transcendental equation which determines the phase change front position  $S_0^*$  has been obtained as

$$\frac{\Theta_0}{C} = \left\{ \exp [Pec_i F(S_0^*) (1 - S_0^*)] - 1 \right\} \left\{ H_{liq} + \frac{1}{1 - \exp \left[ -\frac{CF(S_0^*)Pec_i S_0^*}{k} \right]} \right\}. \quad (4.59)$$

In the basic state we are specifying the difference in pressures across the porous layer, so

$$\left. \begin{aligned} \omega_0 &= \frac{1}{k} Pec_i F(S_0^*) C, \\ \Omega_0 &= Pec_i F(S_0^*), \end{aligned} \right\} \quad (4.60)$$

where  $Pec_i$  is the reference Peclet number based on the basic flow rate. The full mathematical derivation of (4.60) has been given in Appendix C.

In Section 3.1.1, we have concluded that the transcendental equation (4.59) may have multiple solutions for  $S_0^*$ . If we ignore gravity, then the problem becomes one of horizontal flow [68], and the steady front has a unique position. The bifurcation diagram 4.11 shows that in the interval  $|R_3| \in [0, 0.676)$  the interface  $S_0^*$  has a unique low branch position. For  $|R_3| \approx 0.676$  and  $|R_3| \approx 7.47$  the transcendental equation (4.59) has two solutions which include both the low and upper branch solutions. In the interval  $|R_3| \in (0.676, 7.47)$  the liquid-vapour interface  $S_0^*$  has three different positions for the same isothermal conditions. The upper branch represents the only solution for  $S_0^*$  when  $|R_3| \gtrsim 7.47$ . Tsyarkin & Il'ichev [83] also discussed the multiple solutions of the isothermal interface with the exception that they considered permeability to be the controlling parameter. They showed that the unique position of the phase change front is always stable as long as advective heat transport is negligible. We will use the bifurcation diagram 4.11 and will follow the solution curve when analysing the stability of the unique and multiple solutions of (4.59).

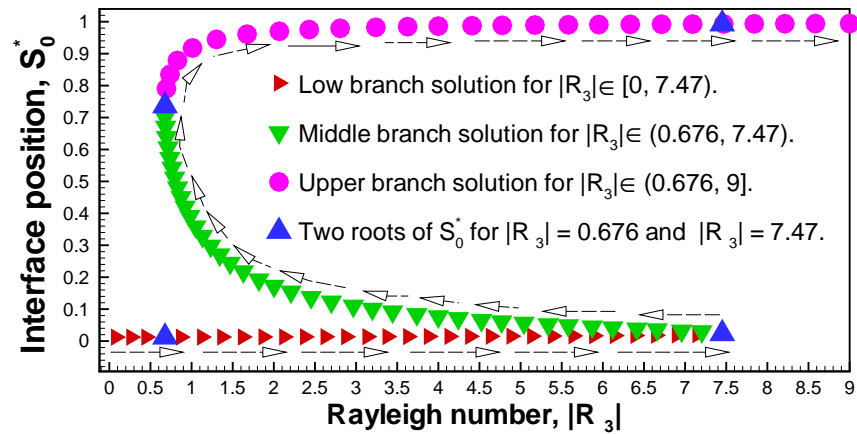


Figure 4.11: A bifurcation diagram for the phase change front  $S_0^*$ , where  $R_1 = 0.0006$ ,  $R_2 = 8.75$ ,  $C = 2.01$ ,  $k = 4$ ,  $H_{liq} = 8.74$ ,  $Pec_i = -20$ ,  $\Theta_0 = 2$ ,  $R = 22.11$  and  $R_3 \leq 0$ . The arrows represent the direction along with we will follow the solution curve.

### 4.4.2 Perturbed state

In the first order formulation, we assume two dimensional time-dependent flow. A time dependent mass flux is allowed across the phase change front. The mathematical formulation has been given in (4.30). The heat flow is time dependent, advective and diffusive in both phases (liquid and vapour), so (4.23) will take the form

$$\left. \begin{aligned} E_1 \frac{\partial \Theta_{liq}^1}{\partial t^*} + \omega_0 \frac{\partial \Theta_{liq}^1}{\partial x^*} + \omega_1 \frac{d\Theta_{liq}^0}{dx^*} &= \nabla^{*2} \Theta_{liq}^1, \\ \frac{E_2 k R_1}{C} \frac{\partial \Theta_{vap}^1}{\partial t^*} + \Omega_0 \frac{\partial \Theta_{vap}^1}{\partial x^*} + \Omega_1 \frac{d\Theta_{vap}^0}{dx^*} &= \nabla^{*2} \Theta_{vap}^1. \end{aligned} \right\} \quad (4.61)$$

The corresponding perturbed thermal boundary conditions and the time dependent heat jump condition at the phase change front will remain the same as (4.24) and (4.25).

### 4.4.3 The eigenvalue problem

The eigenvalue problem for the pressure profiles in both phases is the same as given in (4.35). However, the pressure continuity condition across the interface with advection in the basic state takes the form

$$\Psi(S_0^*) = \Sigma(S_0^*) + \Phi N_0, \quad (4.62)$$

where

$$N_0 = F_1(S_0^*) \frac{C}{k} \frac{Pec_i}{R} \left\{ (R-1) + \frac{k R R_3 (1-R_1)}{C Pec_i} \right\}.$$

The pressure continuity condition (4.62) across  $S_0^*$  has been derived in Appendix D. The solutions of (4.35) for the pressure eigenfunctions subject to the pressure continuity condition (4.62) are

$$\left. \begin{aligned} \Psi(x^*) &= 2 C_3 \sinh(l x^*), \\ \Sigma(x^*) &= 2 C_4 \frac{\sinh(l(x^* - 1))}{\cosh(l) - \sinh(l)}, \end{aligned} \right\} \quad (4.63)$$

where the constants of integration are

$$C_3 = \frac{1}{2} \frac{\Phi}{l} \left[ \frac{\left\{ \varphi \sigma (1 - R_1) + \coth(l(S_0^* - 1)) l N_0 \right\}}{\sinh(l S_0^*) \left\{ R \coth(l(S_0^* - 1)) - \coth(l S_0^*) \right\}} \right],$$

$$C_4 = \frac{1}{2} \frac{\Phi}{l} \left[ \frac{\left\{ \varphi \sigma (1 - R_1) + \coth(l S_0^*) l N_0 \right\} \left\{ \cosh(l) - \sinh(l) \right\}}{\sinh(l(S_0^* - 1)) \left\{ R \coth(l(S_0^* - 1)) - \coth(l S_0^*) \right\}} \right].$$

The normal mode expansion (4.34) of the first order temperature profiles (4.61) and of the corresponding boundary conditions (4.24) yields the eigenvalue problem for the temperature distributions,

$$\left. \begin{aligned} & \left( \frac{d^2}{dx^{*2}} - \omega_0 \frac{d}{dx^*} - E_1 \sigma - l^2 \right) \phi_{liq} + \frac{d\Theta_{liq}^0}{dx^*} \frac{d\Psi}{dx^*} = 0, \\ & \phi_{liq}(0) = 0, \quad \phi_{liq}(S_0^*) = -\Phi \left. \frac{d\Theta_{liq}^0}{dx^*} \right|_{x^*=S_0^*}, \\ & \left( \frac{d^2}{dx^{*2}} - \Omega_0 \frac{d}{dx^*} - \frac{E_2 k R_1}{C} \sigma - l^2 \right) \phi_{vap} + \frac{R_1 R_2 k}{C} \frac{d\Theta_{vap}^0}{dx^*} \frac{d\Sigma}{dx^*} = 0, \\ & \phi_{vap}(1) = 0, \quad \phi_{vap}(S_0^*) = -\Phi \left. \frac{d\Theta_{vap}^0}{dx^*} \right|_{x^*=S_0^*}. \end{aligned} \right\} (4.64)$$

Here  $d\Theta_{liq}^0/dx^*$  and  $d\Theta_{vap}^0/dx^*$  denote basic state vertical temperature gradients in the liquid and in the vapour phase, respectively, which can be obtained by differentiating (3.23) and (3.24) with respect to  $x^*$ :

$$\left. \begin{aligned} & \frac{d\Theta_{liq}^0}{dx^*} = N_1 \exp(\omega_0 x^*), \\ & \frac{d\Theta_{vap}^0}{dx^*} = N_2 \exp(\Omega_0 (x^* - 1)), \end{aligned} \right\} (4.65)$$

which leads to

$$\left. \frac{d\Theta_{liq}^0}{dx^*} \right|_{x^*=S_0^*} = N_3, \quad \text{and} \quad \left. \frac{d\Theta_{vap}^0}{dx^*} \right|_{x^*=S_0^*} = N_4, \quad (4.66)$$

where

$$\left. \begin{aligned} N_1 &= \frac{\omega_0}{\exp(\omega_0 S_0^*) - 1}, \quad N_2 = \frac{\Omega_0}{\exp(\Omega_0 (S_0^* - 1)) - 1}, \\ N_3 &= N_1 \exp(\omega_0 S_0^*), \quad N_4 = N_2 \exp(\Omega_0 (S_0^* - 1)). \end{aligned} \right\} \quad (4.67)$$

The solution of (4.64) for the eigenfunction of the liquid temperature distribution is

$$\begin{aligned} \phi_{liq}(x^*) &= \frac{C_3 l N_1}{f_1 f_4 f_5 f_6} \left\{ f_1 f_4 f_6 \exp(x^*(\omega_0 - 1)) + \left\{ 2 f_1 f_4 E_1 \sigma \cosh\left(\frac{\gamma_3 x^*}{2}\right) \right. \right. \\ &\quad \left. \left. - \left[ 2 f_1 f_2 E_1 \sigma + f_6 f_7 - f_3 f_5 \right] \sinh\left(\frac{\gamma_3 x^*}{2}\right) \right\} \exp\left(\frac{x^* \omega_0}{2}\right) \right. \\ &\quad \left. - f_1 f_4 f_5 \exp(x^*(\omega_0 + 1)) \right\} - \frac{\Phi N_3}{f_1 f_4} \exp\left(\frac{x^* \omega_0}{2}\right) \sinh\left(\frac{\gamma_3 x^*}{2}\right), \end{aligned} \quad (4.68)$$

where

$$\begin{aligned} \gamma_3 &= \sqrt{\omega_0^2 + 4 E_1 \sigma + 4 l^2}, \quad f_1 = \exp\left(\frac{\omega_0 S_0^*}{2}\right), \quad f_2 = \cosh\left(\frac{\gamma_3 S_0^*}{2}\right), \\ f_3 &= \exp((\omega_0 + l) S_0^*), \quad f_4 = \sinh\left(\frac{\gamma_3 S_0^*}{2}\right), \quad f_5 = (\omega_0 l + E_1 \sigma), \\ f_6 &= (\omega_0 l - E_1 \sigma), \quad f_7 = \exp(S_0^* (\omega_0 - l)). \end{aligned}$$

The solution of (4.64) for the vapour temperature distribution is

$$\begin{aligned} \phi_{vap}(x^*) &= \frac{1}{f_{10} f_{11} f_{12}} \left[ f_{19} \exp((\Omega_0 - l)x^* + 2l - \Omega_0) \right. \\ &\quad \left. - (f_{18} + 2f_{16}) \exp\left(\frac{1}{2}\Omega_0(x^* - 1)\right) \sinh\left(\frac{(x^* - 1)\gamma_4}{2C}\right) \right. \\ &\quad \left. + f_{20} \left\{ 2k \sigma E_2 R_1 \exp(l) \cosh\left(\frac{(x^* - 1)\gamma_4}{2C}\right) \right. \right. \\ &\quad \left. \left. - f_9 \exp((\Omega_0 + l)x^* - \Omega_0) \right\} \right], \end{aligned} \quad (4.69)$$

where

$$\begin{aligned}
\gamma_4 &= \sqrt{((\Omega_0^2 + 4l^2)C^2 + 4E_2\sigma CkR_1)}, \quad f_8 = (C\Omega_0l - kR_1E_2\sigma), \\
f_9 &= (C\Omega_0l + kR_1E_2\sigma), \quad f_{10} = (C^2\Omega_0^2l^2 - k^2R_1^2E_2^2\sigma^2), \\
f_{11} &= \exp\left(\frac{\Omega_0(S_0^* - 1)}{2}\right), \quad f_{12} = \sinh\left(\frac{\gamma_4(S_0^* - 1)}{2C}\right), \\
f_{13} &= \cosh\left(\frac{\gamma_4(S_0^* - 1)}{2C}\right), \quad f_{14} = \exp(\Omega_0(S_0^* - l) - lS_0^*), \\
f_{15} &= \exp(\Omega_0(S_0^* - 1) + l(S_0^* - 2)), \quad f_{16} = \left( lR_2k^2N_2C_4 \exp(l)f_{11}R_1^2E_2\sigma f_{13} \right. \\
&\quad \left. - \frac{1}{2}f_9R_1R_2kN_2C_4 \exp((\Omega_0 + l)S_0^* - \Omega_0)l + \frac{1}{2}f_8\Phi N_4f_9 \right), \\
f_{17} &= f_{12}N_2C_4lf_{11}k^2R_2\sigma E_2R_1^2 \exp(l), \quad f_{19} = f_{12}C_4lf_{11}N_2kR_1R_2f_8, \\
f_{18} &= R_1R_2klC_4N_2f_8 \exp((\Omega_0 - l)S_0^* + 2l - \Omega_0), \quad f_{20} = f_{11}C_4lf_{12}N_2kR_1R_2.
\end{aligned}$$

#### 4.4.4 Dispersion analysis

The normal mode expansion (4.34) of the energy jump condition (4.25) at  $x^* = S_0^*$  gives the dispersion equation in the form

$$\varphi\sigma H_{liq}\Phi = \left\{ \Phi \frac{d^2\Theta_{liq}^0}{dx^{*2}} + \frac{d\phi_{liq}}{dx^*} \right\} + \frac{\Theta_0}{k} \left\{ \Phi \frac{d^2\Theta_{vap}^0}{dx^{*2}} + \frac{d\phi_{vap}}{dx^*} \right\} - H_{liq} \frac{d\Psi_1}{dx^*}. \quad (4.70)$$

From the basic state we know that

$$\left. \begin{aligned}
\frac{d^2\Theta_{liq}^0}{dx^{*2}} \Big|_{x^*=S_0^*} &= N_3\omega_0, \\
\frac{d^2\Theta_{vap}^0}{dx^{*2}} \Big|_{x^*=S_0^*} &= N_4\Omega_0.
\end{aligned} \right\} \quad (4.71)$$

Substituting (4.71) into (4.70) yields

$$\varphi \sigma H_{liq} \Phi = \left\{ \frac{d\phi_{liq}}{dx^*} + \Phi N_3 \omega_0 \right\} + \frac{\Theta_0}{k} \left\{ \frac{d\phi_{vap}}{dx^*} + \Phi N_4 \Omega_0 \right\} - H_{liq} \frac{d\Psi_1}{dx^*}. \quad (4.72)$$

The complete solution for  $\sigma(l)$  has been obtained by substituting (4.63), (4.68) and (4.69) into (4.72) which is then solved numerically using [Maple](#), as described in the following section.

## 4.4.5 Numerical and asymptotic methods

### 4.4.5.1 Numerical methods

While plotting our results for the dispersion relation  $\sigma(l)$  (4.72), we encountered many difficulties when the wave number  $l$  became large, especially on the upper branch solution. The main reason is that the function  $\mathcal{A} \equiv \text{LHS}(4.72) - \text{RHS}(4.72)$  contains a large number of exponentials, which depend on  $l$  and  $\sigma$ . So when  $l$  and  $\sigma$  get large, these exponential terms are huge. Following are the two approaches we used in [Maple](#) to generate plots of the function  $\sigma(l)$ .

1. **Implicit plot:** Implicit plots in [Maple](#) are essentially contour plots of the zero contour of  $\mathcal{A}$ . But this is quite a crude method because [Maple's](#) `implicitplot` command relies on just evaluating  $\mathcal{A}$  on a grid and then interpolating it. For some of the plots that we generated using [Maple's](#) `implicitplot` command, there was evidence of numerical error effecting the solution branch. Therefore, we look for more accurate way for tracking that solution branch.
2. **Continuation method:** Once we know roughly where the solution branch is, we can track it more accurately using a continuation method. The continuation method requires an initial guess for  $\sigma$ ; it then increments  $l$  at each

step and searches for  $\sigma$  in an interval around the previous output value for  $\sigma$  (for [Maple](#) code see Appendix E). This method allowed us to extend the solution further along each branch.

#### 4.4.5.2 Asymptotic analysis

As we have mentioned earlier, for the high value of the front position  $S_0^*$ , it is quite hard to track down the roots of  $\sigma$  for large  $l$ . So to determine the behaviour of  $\sigma$  for large  $l$ , we have used asymptotic analysis.

The numerical results for  $\sigma(l)$  appear to be a straight line for large  $l$ . We therefore seek an asymptotic solution of the form  $\sigma \sim \sigma^* l$  as  $l \rightarrow \infty$ . The expression  $\mathcal{A}$ , of which we are trying to locate the roots, includes both exponentially and algebraically large and small terms. The [Maple](#) `asympt` routine in general cannot obtain the asymptotics for such expressions; however it is too large to simplify by hand. Therefore we have used Maple to carry out the asymptotic expansion in two stages.

In the first stage, we substitute the ansatz  $\sigma = \sigma^* l$  into  $\mathcal{A}$  and then rewrite all the exponential and hyperbolic expressions in terms of powers of  $\alpha_1 \equiv \exp(l)$  and  $\alpha_2 \equiv \exp(S_0^* l)$  multiplied by appropriate asymptotic expansions in powers of  $1/l$ . So, for example, we write

$$\begin{aligned} \sinh\left(\frac{1}{2} S_0^* \sqrt{\omega_0^2 + 4 E_1 \sigma + 4 l^2}\right) &\sim \frac{1}{2} \alpha_2 \exp\left(\frac{1}{2} S_0^* E_1 \sigma^*\right) \left(1 + O\left(\frac{1}{l}\right)\right) \\ &\quad - \frac{1}{2} \alpha_2^{-1} \exp\left(-\frac{1}{2} S_0^* E_1 \sigma^*\right) \left(1 + O\left(\frac{1}{l}\right)\right). \end{aligned}$$

While using Maple, we have retained more terms in the series of powers of  $1/l$  than have been shown here.

The next stage was to collect all the combinations of powers of  $\alpha_1$  and  $\alpha_2$ , which was done by repeated use of [Maple](#)'s `expand`, `series` and `collect` routines. Only

certain combinations of powers appeared, and it was necessary to determine which was dominant. For example,  $\alpha_1 > \alpha_2$  because  $S_0^* < 1$ . But in general it is not clear whether, for example,  $\alpha_1 > \alpha_2^2$ . So these types of combinations can not be determined automatically. The combinations of  $\alpha_1$  and  $\alpha_2$  which appear in the expansion of  $\mathcal{A}$  are  $\alpha_2^1 \alpha_1^5$ ,  $\alpha_2^2 \alpha_1^4$ ,  $\alpha_2^3 \alpha_1^3$ ,  $\alpha_2^3 \alpha_1^5$ ,  $\alpha_2^4 \alpha_1^3$ ,  $\alpha_2^4 \alpha_1^4$ ,  $\alpha_2^5 \alpha_1^3$ ,  $\alpha_2^5 \alpha_1^5$ ,  $\alpha_2^6 \alpha_1^3$ ,  $\alpha_2^6 \alpha_1^4$  and  $\alpha_2^7 \alpha_1^3$ . It is clear that the terms  $\alpha_2^1 \alpha_1^5$ ,  $\alpha_2^2 \alpha_1^3$ ,  $\alpha_2^2 \alpha_1^4$ ,  $\alpha_2^3 \alpha_1^3$ ,  $\alpha_2^3 \alpha_1^5$ ,  $\alpha_2^4 \alpha_1^3$ ,  $\alpha_2^4 \alpha_1^4$  and  $\alpha_2^5 \alpha_1^3$  compared to  $\alpha_2^5 \alpha_1^5$  are exponentially small. Comparing the remaining terms  $\alpha_2^5 \alpha_1^5$ ,  $\alpha_2^6 \alpha_1^3$ ,  $\alpha_2^6 \alpha_1^4$  and  $\alpha_2^7 \alpha_1^3$ , it is easy to see that the term  $\exp(5 S_0^* l) \exp(5 l)$  must be the largest since  $\alpha_1 > \alpha_2$ . Thus we discard the remaining terms and expand the coefficient of  $\exp(5 S_0^* l) \exp(5 l)$  in inverse powers of  $l$  using `asympt`. The leading term in this expansion is

$$\mathcal{A} \sim f(\sigma^*; \text{other parameters}) l \exp(5 S_0^* l) \exp(5 l).$$

Setting  $f$  equal to zero and solving for  $\sigma^*$  numerically using `fsolve`, we obtain the asymptotic results plotted in Figure 4.12. The asymptotic solutions for the three branches are plotted in Figure 4.12. As we have mentioned in Section 4.3.4, it was very hard to find the numerical solutions of  $\sigma$  on the upper branch front position for large  $l$ . But Figure 4.12 shows that there always exists an asymptotic solution for all the branch front positions. The low branch in the interval  $|R_3| \in (2.35, 7.47)$  is unstable to short-wave perturbations because  $\sigma^* > 0$  as  $l \rightarrow \infty$ . The middle branch when  $|R_3| \in (0.676, 7.47)$  is unstable for all wave numbers. Figure 4.12 (b) shows that the transition to short-wave instability on the upper branch happens when  $|R_{3,\infty}^{crit}| \approx 0.7665$ .

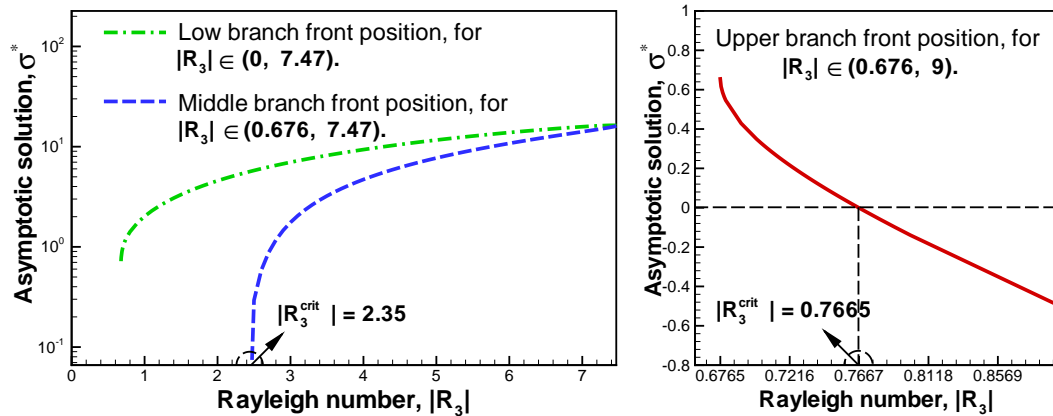


Figure 4.12: Asymptotic solution for the low, middle and upper branch front positions.

#### 4.4.6 Numerical results for $\sigma(l)$

In Section 3.1.1, we have found three solution branches, i.e. three possible values for  $S_0^*$ . These three possible front positions correspond to three different flow rates across the interface. In the following discussion, we restrict the analysis to  $|R_3| \in [0, 9]$  because for all higher values of  $|R_3|$  the transcendental equation (4.59) has only one solution for  $S_0^*$ .

##### 4.4.6.1 Stability analysis of the low branch front position

The bifurcation diagram 4.13 (a) shows that in the interval  $|R_3| \in [0, 7.47]$  the interface  $S_0^*$  has a low branch position. This low branch includes the only solution for  $S_0^*$  when  $|R_3| \in [0, 0.676)$ . The low- $S_0^*$  solution corresponds to a configuration in which the porous layer is mostly filled with vapour, and there is a strong flow from vapour into liquid with condensation occurring at the front (see the discussion in Section 3.1.1 and the schematic in Figure 4.13 (b)).

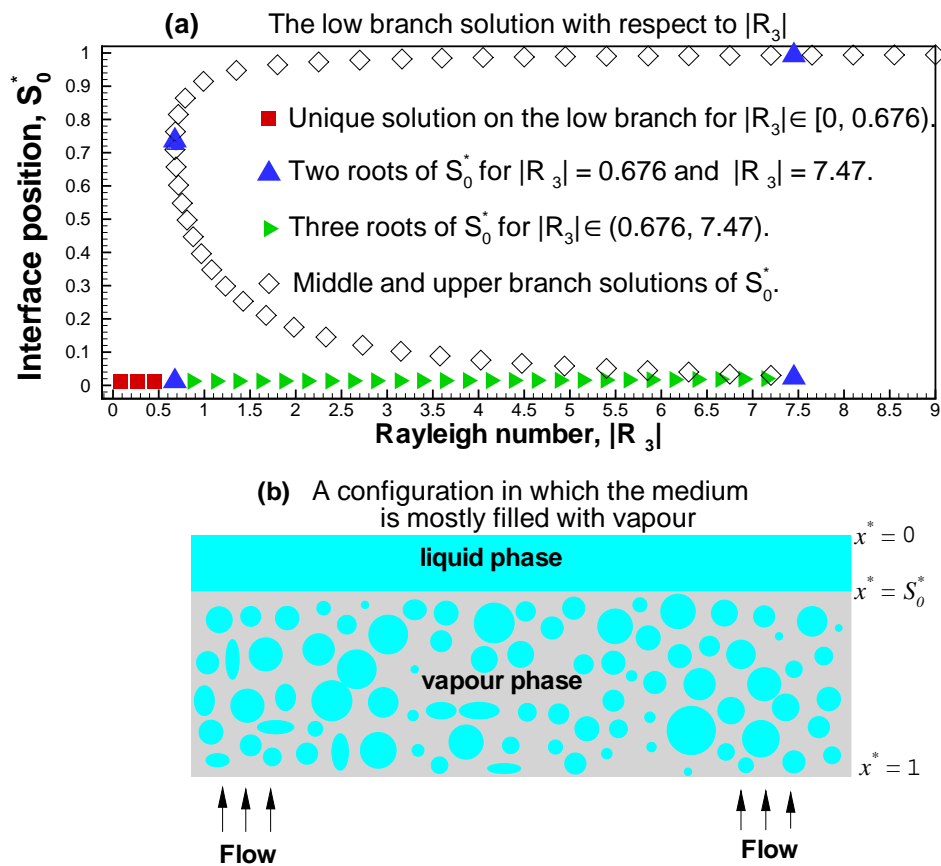


Figure 4.13: The low branch solution and the corresponding schematic configuration.

The stability analysis results in Figure 4.14 (a) shows that the unique low branch front position is stable. Loss of stability occurs first when  $|R_3| \approx 2.08125$ ; note that this Rayleigh number value is rather higher than the value at which this branch becomes non-unique. When the Rayleigh number crosses the medium-wave threshold, i.e.,  $|R_3| > |R_{3,mini}^{crit}| \approx 2.08125$  and  $R_3 < 0$ , then the condensation front becomes unstable to medium wave perturbations only (see Figure 4.14 (b)). Remaining on the low branch solution, the liquid-vapour interface becomes unstable to short-wave disturbances when  $|R_3| > |R_{3,\infty}^{crit}| \approx 2.35$  and  $R_3 < 0$  (see Figure 4.14 (c)).

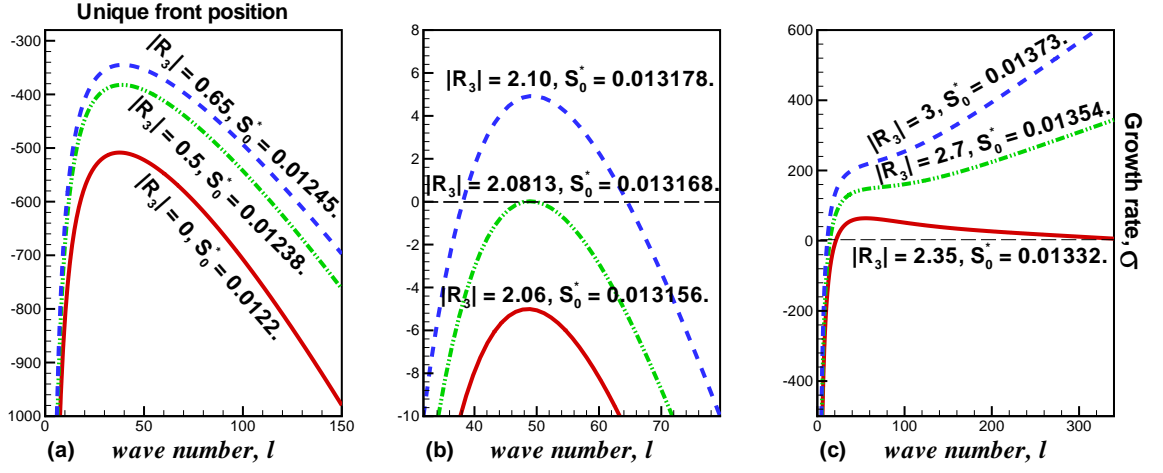


Figure 4.14: Stability plots of the low branch condensation front, where  $\varphi = 0.38$ ,  $R_1 = 0.0006$ ,  $R_2 = 8.75$ ,  $E_1 = 1$ ,  $E_2 = 1$ ,  $C = 2.02$ ,  $k = 4$ ,  $H_{liq} = 8.74$ ,  $\Theta_0 = 2$ ,  $R = 22.11$  and  $R_3 \leq 0$ .

#### 4.4.6.2 Stability analysis of the middle branch front position

The bifurcation diagram 4.15 (a) shows that in the interval  $|R_3| \in (0.676, 7.47)$  the interface  $S_0^*$  has three solutions, of which we will now discuss the middle branch in this section. The intermediate solution for the interface  $S_0^*$  corresponds to a slow flow either from vapour into liquid or from liquid into vapour (see Section 3.1.1).

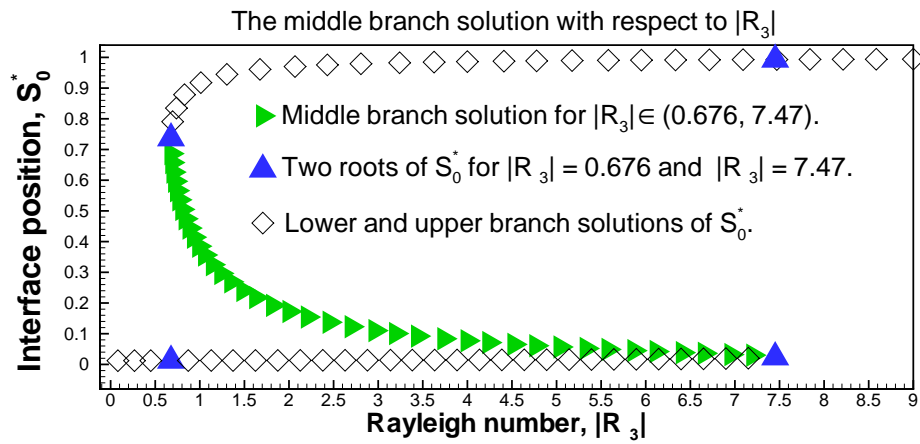


Figure 4.15: The middle branch solution.

Figures 4.16 and 4.17 show that the middle branch front position is unstable for all wave numbers. The turning point between the low and middle branches is at  $|R_3| \approx 7.47$ . The behaviour of the growth rate  $\sigma$  in the neighbourhood of the turning point (at  $|R_3| \approx 7.47$ ) is shown in Figure 4.16. Figure 4.16 (c) indicates that  $\sigma(l = 0)$  passes through zero precisely at the turning point. Figures 4.17 show that the asymptotic solutions and the numerical solutions of the dispersion equation (4.72) for the middle branch front position agree well.

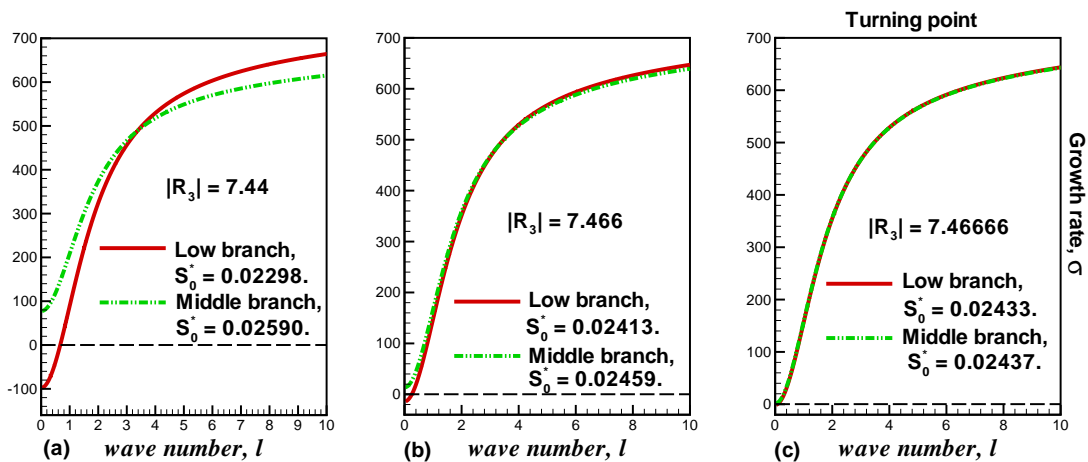


Figure 4.16: Behaviour of the low and middle branches near the turning point at  $|R_3| \approx 7.4666$ .

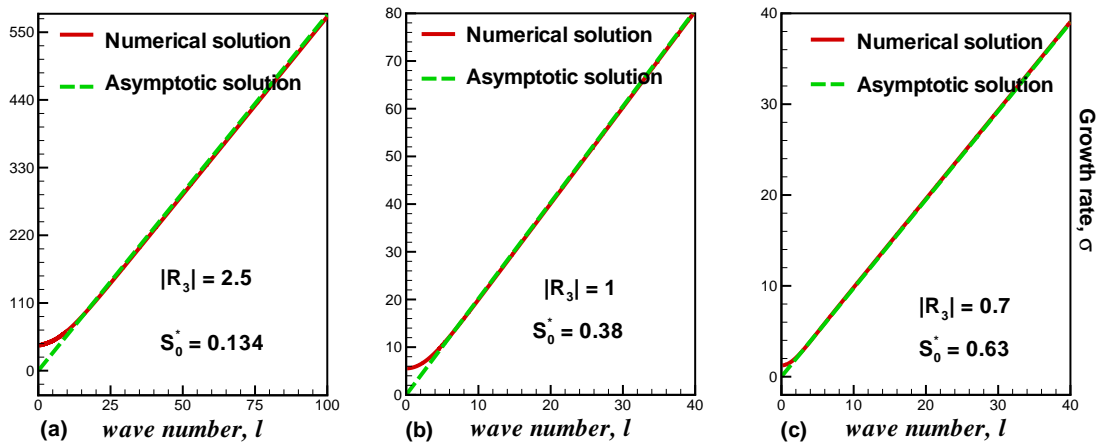
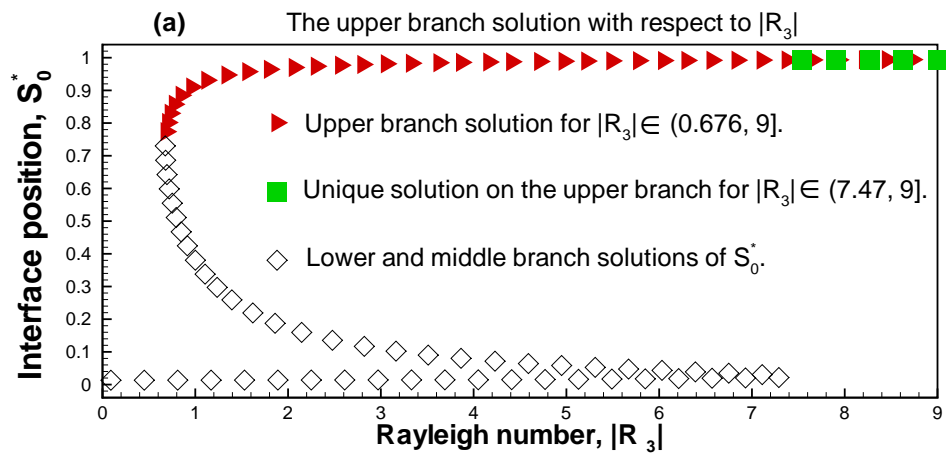


Figure 4.17: Stability plots of the middle branch position of the liquid-vapour front.

#### 4.4.6.3 Stability analysis of the upper branch front position

The bifurcation diagram 4.18 (a) shows that in the interval  $|R_3| \in (0.676, 9]$  the interface  $S_0^*$  has an upper branch position. This upper branch also represents the only solution for  $S_0^*$  when  $|R_3| \gtrsim 7.47$ . Figure 4.18 (b) shows that the high- $S_0^*$  solution corresponds to a configuration in which the porous layer is mostly filled with liquid, and there is a strong flow from liquid into vapour with evaporation occurring at the front (see the discussion in Section 3.1.1).



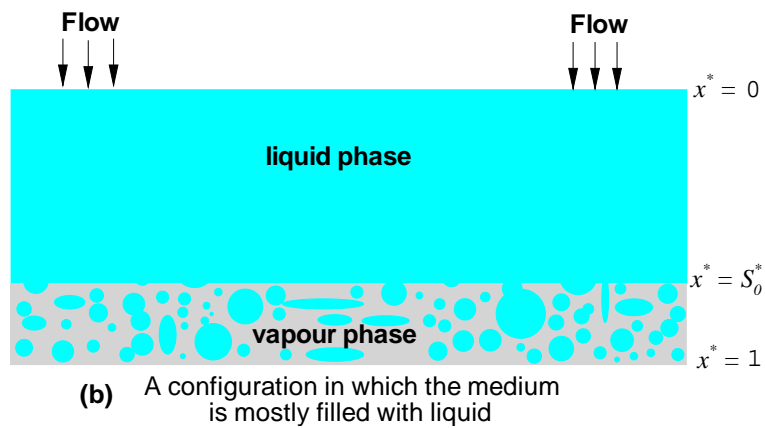


Figure 4.18: The upper branch solution and the corresponding schematic configuration.

The stability plots 4.19 illustrate the behaviour of the middle and upper branch near the turning point at  $|R_3| \approx 0.67632$ . The growth rate  $\sigma$  passes through zero for  $l = 0$  precisely at the turning point. Furthermore, the upper branch front position in the neighbourhood of the turning point becomes stable to long-wave perturbations only.

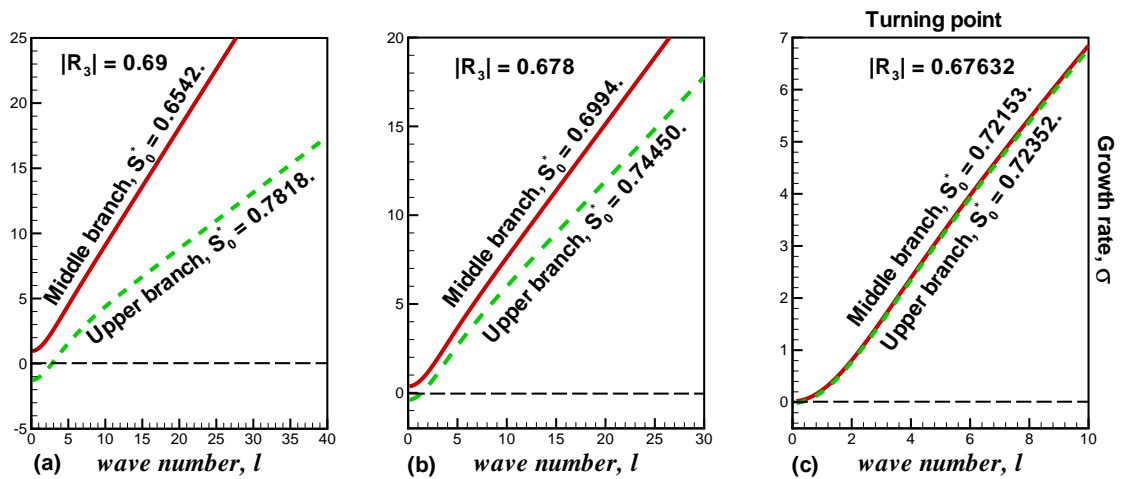


Figure 4.19: Behaviour of the middle and upper branches near the turning point at  $|R_3| \approx 0.67632$ .

Representative examples of the variations in growth rate  $\sigma$  with wave number  $l$  for the upper branch front position are given in Figure 4.20. The bifurcation parameter  $R_3$  is the curve parameter as before. Figure 4.20 (a) shows that the high- $S_0^*$  front position first becomes stable to very long (but finite) wavelength perturbations. When  $|R_3| < 0.7665$  then the upper branch is unstable to short-wave perturbations. Figure 4.20 shows that when  $0.7505 < |R_3| < 0.7665$  then the liquid-vapour interface is stable to both long and short-wave perturbations since  $\sigma < 0$ . As  $|R_3|$  increases in magnitude beyond 0.7505, the upper branch front position  $S_0^* \approx 1$  and the medium is almost entirely filled with liquid. It is not only liquid, as there is still a vapour region, but this is very thin. Essentially the front is “anchored” by the boundary conditions at  $x^* = 0$  and has very little space in which it can be perturbed.

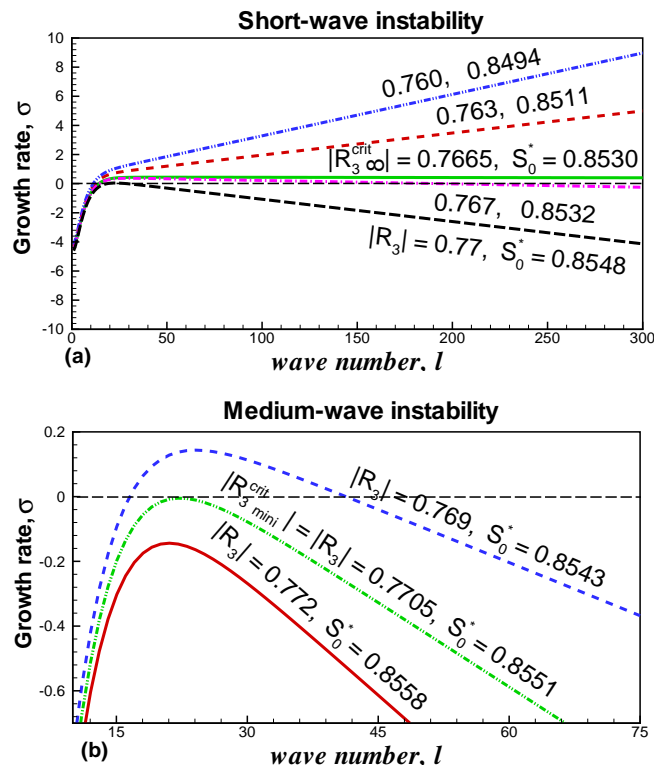


Figure 4.20: Stability plots of the upper branch position of the isothermal liquid-vapour front.

### 4.4.7 Summary of our findings

Finally, we are in a position to summarise our findings about the stability of the liquid-vapour interface. Figure 4.21 summarises our results.

- (i) For  $|R_3| \lesssim 0.676$  : There is only one front position, which is stable.
- (ii) When  $0.676 \lesssim |R_3| \lesssim 0.7705$  : There are three front positions and only the low- $S_0^*$  position is stable. The intermediate and the high- $S_0^*$  front positions are unstable.
- (iii) When  $0.7705 \lesssim |R_3| \lesssim 2.08$  : There are three front positions. The middle branch position is unstable to all wave numbers. The remaining two are stable.
- (iv) When  $2.08 \lesssim |R_3| \lesssim 2.35$  : There are three front positions. The low- $S_0^*$  position is unstable to medium-wave perturbations only. The middle branch is unstable to all waves, whereas the upper branch is stable.
- (v) When  $2.35 \lesssim |R_3| \lesssim 7.47$  : There are three front positions. The low- $S_0^*$  position is stable to very long (but finite) wavelengths. The middle branch is unstable to all wave numbers, whereas the upper branch is stable.
- (vi) For  $|R_3| \gtrsim 7.47$  : There is only one front position, which is stable.

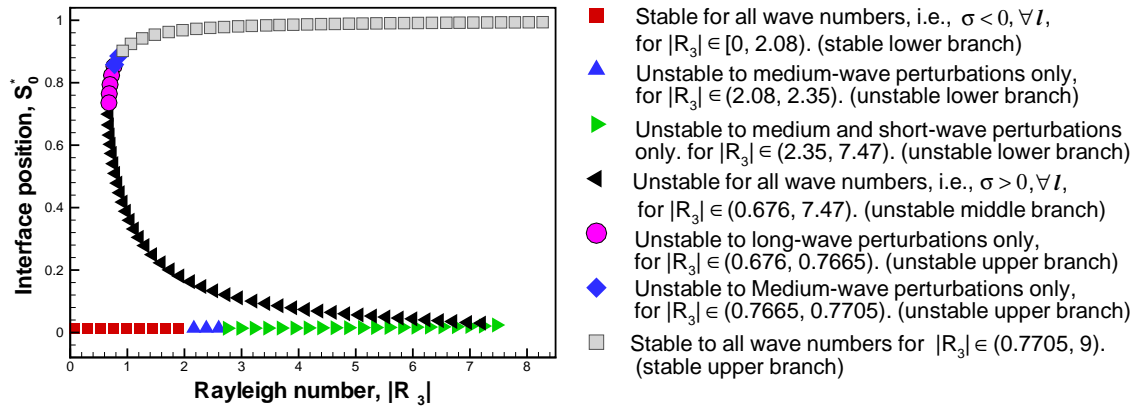


Figure 4.21: Identification of stable and unstable behaviour of the isothermal liquid-vapour interface.

## 4.5 Summary and conclusions

In this chapter we used linear stability methods to study the behaviour of the steady phase-change front between a liquid and its own vapour in a porous medium, where the boundaries were assumed to be isothermal. The unperturbed state was analysed with the assumption of no through flow then later on this assumption was relaxed.

### 4.5.1 Isothermal interface with no through flow

Two dimensional stability analysis was carried out of a base state with fixed temperatures at the top and bottom boundaries with no through flow. We concluded in Section 4.3.6.2 that when the liquid-vapour interface is at the middle of the porous layer with the assumption that there is only pure conductive heat transfer in the entire system then the transition to instability is spontaneous, which is completely in agreement with the results shown by Il'ichev & Tsypkin [31]. But if heat advection is included the results are different and there is no longer a spontaneous transition to instability when the front is at the middle of the porous layer.

### 4.5.2 Isothermal interface with through flow

In Section 4.4, we discussed the stability of the most interesting case, where the interface with through flow has multiple positions. We find ourselves in agreement with Il'ichev & Tsypkin [30] that a stable regime is possible when the water layer overlies the vapour layer, where the basic state is both advective and conductive. But Il'ichev & Tsypkin [30] analysis fails to consider the stability of the multiple basic states that are available at higher Rayleigh numbers  $|R_3|$ . Our approach throughout was to seek the most comprehensive analytical description of the multiple basic states phenomena. We show that the upper and middle solution branches for the front position are always subject to an instability of Rayleigh-Taylor type, which is particularly effective for short-wave perturbations.

# Chapter 5

## Stability of Steady Solutions with a Heat Flux Condition on the Surface

In this chapter, we will extend the problem studied in Chapter 4 by considering that heat is extracted at a constant rate at the liquid boundary, while the vapour boundary is kept isothermal. This problem can be expected to be richer than the problem with isothermal boundary conditions, because we have shown that the interface can have multiple locations both with and without gravity (see Section 3.1.2).

### 5.1 Non-dimensional form

For the proposed two dimensional stability problem, the dimensionless forms of the continuity equation, Darcy's law and the heat transport equation in both phases (liquid and vapour) are given in (4.6), (4.7) and (4.8). The dimensionless mass flux condition at the liquid-vapour interface will remain the same as (4.10).

But because of the fixed flux condition at the liquid boundary, the energy jump condition (2.51) after using the appropriate dimensionless quantities (3.15), (3.20) and (3.28) has a new dimensionless form

$$\begin{aligned} \varphi \frac{\partial (S_0^* + \epsilon S_1^*)}{\partial t^*} = & \left[ \frac{C}{H_{vap}} \left[ \frac{1}{k} \left\{ \frac{\partial (\Theta_{vap}^0 + \epsilon \Theta_{vap}^1)}{\partial x^*} - \frac{\partial (S_0^* + \epsilon S_1^*)}{\partial y^*} \frac{\partial (\Theta_{vap}^0 + \epsilon \Theta_{vap}^1)}{\partial y^*} \right\} \right. \right. \\ & \left. \left. - \left\{ \frac{\partial (\Theta_{liq}^0 + \epsilon \Theta_{liq}^1)}{\partial x^*} - \frac{\partial (S_0^* + \epsilon S_1^*)}{\partial y^*} \frac{\partial (\Theta_{liq}^0 + \epsilon \Theta_{liq}^1)}{\partial y^*} \right\} \right] \right. \\ & \left. - \left( \frac{\partial (\Lambda_0 + \epsilon \Lambda_1)}{\partial x^*} + R_3 \right) \right]_{x^*=S_0^*}. \end{aligned} \quad (5.1)$$

The fixed heat flux condition (3.29) at the liquid boundary  $x^* = 0$  in perturbed form is

$$\left. \frac{\partial (\Theta_{liq}^0 + \epsilon \Theta_{liq}^1)}{\partial x^*} \right|_{x^*=0} = \frac{Q_{liq} Pec_i}{k} \left\{ H_{vap} + \frac{1}{1 - \exp(Pec_i)} \right\}. \quad (5.2)$$

We will follow the same procedure as in Chapter 4 to obtain the zeroth and first order problems for the stability analysis (see Section 4.2.1). In Chapter 4, we have discussed the stability of the basic state with and without through flow. Here we will follow the same approach.

## 5.2 Stability when there is no through flow

In this section, we will discuss the stability of a steady liquid-vapour phase change front in a porous medium with heat extraction from the liquid boundary, with no through flow. The steady state has been discussed in Section 3.1.2 as a special case of a through flow problem. The two important parameters in this problem are the Rayleigh number ( $R_3$ ) which accounts for buoyancy effects, and the dimensionless heat flux ( $Q_{liq}$ ) at the liquid boundary.

### 5.2.1 Steady state

We have made the same assumptions as in Section 4.3.1. The governing equations for the pressure and the temperature profiles remain the same as (4.26) and (4.27), respectively. However, the temperature boundary conditions change, since we are considering a constant heat flux condition at the liquid boundary instead of the isothermal temperature. If we assume no through flow in the basic state, the state under consideration becomes a limiting case of the through flow problem discussed in Section 3.1.2. The limit of the fixed heat flux condition (3.29) as the reference Peclet number  $Pec_i \rightarrow 0$  yields

$$\left. \frac{d\Theta_{liq}^0}{dx^*} \right|_{x^*=0} \sim -\frac{Q_{liq}}{k} + O(Pec_i). \quad (5.3)$$

Equating the terms proportional to  $\epsilon^0$  in (5.1) gives the energy jump condition in the basic state

$$\frac{d\Theta_{liq}^0}{dx^*} - \frac{1}{k} \frac{d\Theta_{vap}^0}{dx^*} = 0. \quad (5.4)$$

The solution of (4.27) with the fixed heat condition (5.3) gives the conductive temperature profile in the liquid region

$$\Theta_{liq}^0 = \frac{Q_{liq}}{k} (S_0^* - x^*) + 1, \quad (5.5)$$

and the temperature profile in the vapour phase remains the same as (4.28). The front position  $S_0^*$  in the steady state with a fixed heat flux condition is obtained by substituting (4.28) (thermal gradient in the vapour phase only) and (5.5) into the energy jump condition (5.4), obtaining

$$S_0^* = \frac{Q_{liq} - 1}{Q_{liq}}. \quad (5.6)$$

The same expression as (5.6) for the steady front position has been found as a limiting case, when the fluid is stationary (see Section 3.1.2, equation (3.33)). The

dimensionless stationary front position  $0 \leq S_0^* \leq 1$ , so the expression for the minimum heat flux  $Q_{liq}$  is

$$Q_{liq}^{mini} = 1.$$

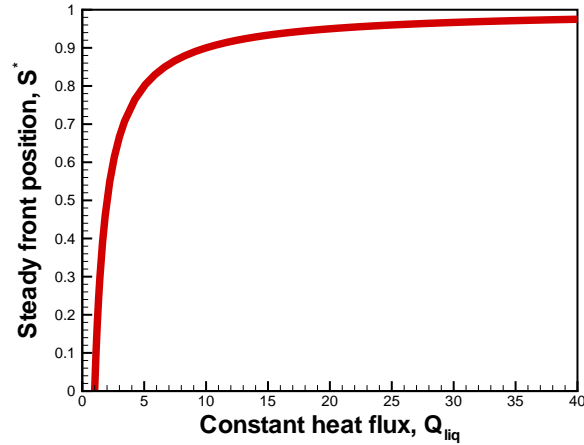


Figure 5.1: Steady liquid-vapour interface position vs dimensionless heat flux  $Q_{liq}$ , where  $Q_{liq}^{mini} = 1$ .

Figure 5.1 presents typical results for steady front position  $S_0^*$  as a function of dimensionless heat flux  $Q_{liq}$  with  $Q_{liq} \geq Q_{liq}^{mini}$ . It can be observed that the greater the heat flux at the upper (liquid) boundary, the closer the front moves to the lower (vapour) boundary, increasing the heat flux between vapour boundary and front to match  $Q_{liq}$ . Furthermore, the liquid-vapour interface has a unique position without through flow.

### 5.2.2 Perturbed state

The mathematical formulation of the two dimensional flow behaviour is the same as given in Section 4.3.2. The perturbed time dependent advective and diffusive

heat flow in both phases (liquid and vapour) is governed by

$$\left. \begin{aligned} E_1 \frac{\partial \Theta_{liq}^1}{\partial t^*} - \frac{\partial \Lambda_1}{\partial x^*} \frac{d\Theta_{liq}^0}{dx^*} &= \nabla^{*2} \Theta_{liq}^1, \\ \frac{E_2 k R_1}{C} \frac{\partial \Theta_{vap}^1}{\partial t^*} - \frac{R_1 R_2 k}{C} \frac{\partial \Pi_1}{\partial x^*} \frac{d\Theta_{vap}^0}{dx^*} &= \nabla^{*2} \Theta_{vap}^1. \end{aligned} \right\} \quad (5.7)$$

The corresponding first order temperature boundary conditions are

$$\left. \begin{aligned} \frac{\partial \Theta_{liq}^1}{\partial x^*} \Big|_{x^*=0} &= 0, \quad \Theta_{liq}^1(S_0^*) = -S_1^* \frac{d\Theta_{liq}^0}{dx^*} \Big|_{x^*=S_0^*}, \\ \Theta_{vap}^1(1) &= 0, \quad \Theta_{vap}^1(S_0^*) = -S_1^* \frac{d\Theta_{vap}^0}{dx^*} \Big|_{x^*=S_0^*}. \end{aligned} \right\} \quad (5.8)$$

Equating the terms proportional to  $\epsilon$  in equation (5.1) gives the first order heat jump condition at the phase change front,

$$\varphi \frac{\partial S_1^*}{\partial t^*} = \left[ \frac{C}{H_{vap}} \left[ \frac{1}{k} \left\{ S_1^* \frac{d^2 \Theta_{vap}^0}{dx^{*2}} + \frac{\partial \Theta_{vap}^1}{\partial x^*} \right\} - \left\{ S_1^* \frac{d^2 \Theta_{liq}^0}{dx^{*2}} + \frac{\partial \Theta_{liq}^1}{\partial x^*} \right\} \right] - \frac{\partial \Lambda_1}{\partial x^*} \right]_{x^*=S_0^*}. \quad (5.9)$$

### 5.2.3 The eigenvalue problem

The eigenvalue problem and its solution for the pressure profiles in the liquid and in the vapour regions has been already given in Section 4.3.3. The normal mode expansion (4.34) of the first order temperature profiles (5.7) and of the corresponding boundary conditions (5.8) gives

$$\left. \begin{aligned} \left( \frac{d^2}{dx^{*2}} - E_1 \sigma - l^2 \right) \phi_{liq} + \frac{d\Theta_{liq}^0}{dx^*} \frac{d\Psi}{dx^*} &= 0, \\ \frac{d\phi_{liq}}{dx^*} \Big|_{x^*=0} &= 0, \quad \phi_{liq}(S_0^*) = -\Phi \frac{d\Theta_{liq}^0}{dx^*} \Big|_{x^*=S_0^*}, \end{aligned} \right\} \quad (5.10)$$

$$\left. \begin{aligned} \left( \frac{d^2}{dx^{*2}} - \frac{E_2 k R_1}{C} \sigma - l^2 \right) \phi_{vap} + \frac{R_1 R_2 k}{C} \frac{d\Theta_{vap}^0}{dx^*} \frac{d\Sigma}{dx^*} &= 0, \\ \phi_{vap}(1) &= 0, \quad \phi_{vap}(S_0^*) = -\Phi \frac{d\Theta_{vap}^0}{dx^*} \Big|_{x^*=S_0^*}, \end{aligned} \right\} \quad (5.11)$$

where  $d\Theta_{liq}^0/dx^*$  and  $d\Theta_{vap}^0/dx^*$  denote basic state vertical temperature gradients in the liquid and in the vapour phase, respectively, which can be obtained by differentiating (5.5) and (4.28) with respect to  $x^*$ ,

$$\frac{d\Theta_{liq}^0}{dx^*} = -\frac{Q_{liq}}{k}, \quad \frac{d\Theta_{vap}^0}{dx^*} = \frac{1}{S_0^* - 1}. \quad (5.12)$$

The solution of (5.10) for the liquid phase temperature eigenfunction is

$$\begin{aligned} \phi_{liq}(x^*) &= \frac{2l Q_{liq} C_1}{E_1 k \sigma} \left\{ \frac{\cosh(\gamma_1 x^*) \cosh(l S_0^*)}{\cosh(\gamma_1 S_0^*)} - \cosh(l x^*) \right\} \\ &+ \frac{Q_{liq} \Phi \cosh(\gamma_1 x^*)}{k \cosh(\gamma_1 S_0^*)}. \end{aligned} \quad (5.13)$$

In the above equation, the expressions for  $\gamma_1$  and  $C_1$  are given in Section 4.3.3. The solution of (5.11) for the vapour phase temperature eigenfunction will remain the same as (4.39).

#### 5.2.4 Dispersion analysis

The relationship between the growth rate and wave number is obtained by substituting (4.34) into (5.9) which yields

$$\varphi \sigma \Phi = \left\{ \frac{C}{H_{vap}} \left\{ \frac{1}{k} \frac{d\phi_{vap}}{dx^*} - \frac{d\phi_{liq}}{dx^*} \right\} - \frac{d\Psi}{dx^*} \right\}_{x^*=S_0^*}. \quad (5.14)$$

Substituting (4.36), (4.39) and (5.13) into (5.14) gives the dispersion equation

$$\begin{aligned} \varphi \sigma \Phi &= \frac{C}{H_{vap}} \left\{ - \left[ \frac{2l Q_{liq} C_1}{E_1 k \sigma} \{ \gamma_1 \tanh(\gamma_1 S_0^*) \cosh(l S_0^*) - l \sinh(l S_0^*) \} \right. \right. \\ &+ \left. \frac{Q_{liq} \Phi}{k} \tanh(\gamma_1 S_0^*) \right] + \frac{1}{k} \left[ \frac{2l R_2 C_2}{(S_0^* - 1) E_2 \sigma \cosh(l) - \sinh(l)} \right. \\ &\times \{ l \sinh(l(S_0^* - 1)) - \gamma_2 \sinh(\gamma_2(S_0^* - 1)) - \gamma_2 \coth(\gamma_2(S_0^* - 1)) \\ &\times \{ \cosh(l(S_0^* - 1)) - \cosh(\gamma_2(S_0^* - 1)) \} \} - \left. \left. \frac{\Phi \gamma_2}{(S_0^* - 1)} \coth(\gamma_2(S_0^* - 1)) \right] \right\} \\ &- (1 - R_1) \Phi \left\{ \frac{\{ \varphi \sigma + l R_3 \coth(l S_0^*) \}}{R_1 R_2 \coth(l(S_0^* - 1)) - \coth(l S_0^*)} + R_3 l \right\} \coth(l S_0^*). \end{aligned} \quad (5.15)$$

## 5.2.5 Transition to instability

In this section, the possible types of transition to instability will be discussed but before that it is important to find out the critical Rayleigh numbers for both zero wave number and infinite wave numbers, which play important roles in the changeover of the stable system to unstable.

### 5.2.5.1 Onset of instability due to short-wave perturbations

The asymptotic analysis of (5.15) is used to find the parameters, especially the critical Rayleigh number, which control the instability for infinite wave numbers. For this let  $\sigma = \sigma^* l$  and  $\sigma^* = \sigma_0 + \frac{\sigma_1}{l} + O\left(\frac{1}{l^2}\right)$  and take  $l \rightarrow \infty$ , then using the asymptotic series of (5.15) gives

$$\begin{aligned} \varphi \sigma_0 l + \varphi \sigma_1 &\sim \frac{C}{H_{vap}} \left[ \frac{1}{k} \left\{ \frac{k R_1 R_2 (\varphi \sigma_0 + R_3) (1 - R_1) + \sigma_0 E_2 (R_1 R_2 + 1)}{2 (R_1 R_2 + 1) (S_0^* - 1)} \right. \right. \\ &+ \left. \left. \frac{l}{S_0^* - 1} \right\} - \left\{ \frac{Q_{liq} l}{k} - Q_{liq} \left\{ \frac{(1 - R_1) (\varphi \sigma_0 - R_1 R_2 R_3)}{2 k (R_1 R_2 + 1)} \right. \right. \right. \\ &- \left. \left. \left. \frac{\sigma_1 \sigma_0}{2 k (R_1 R_2 + 1)} \right\} \right\} \right] + \left\{ \frac{(\varphi \sigma_0 - R_1 R_2 R_3) (1 - R_1) l}{R_1 R_2 + 1} \right. \\ &+ \left. \frac{\varphi \sigma_1 (1 - R_1)}{R_1 R_2 + 1} \right\} + O\left(\frac{1}{l^2}\right). \end{aligned} \quad (5.16)$$

Equating the terms proportional to  $l$ , (5.16) yields

$$\sigma_0 \sim \underbrace{\frac{1}{\varphi} \frac{C}{H_{vap}} \frac{1}{k} \frac{R_1 R_2 + 1}{R_1 (R_2 + 1)} \left\{ \frac{1}{S_0^* - 1} - Q_{liq} \right\}}_{\text{first term}} - \underbrace{\frac{1 - R_1 R_2 R_3}{R_2 + 1} \frac{1}{\varphi}}_{\text{second term}}. \quad (5.17)$$

The above dispersion relation for short waves has the same interpretation as for the isothermal steady state (4.43), except that the cooling parameter  $Q_{liq}$  appears instead of the ratio of temperature contrast  $\Theta_0$ , and the reciprocal of the Stefan number  $H_{vap}$  appears instead of  $H_{liq}$ . The first term (with negative sign), which represents the diffusive heat transport process, has a stabilising effect, whereas

the second term (with positive sign when liquid is above vapour, i.e.  $R_3 < 0$ ), which represents the buoyancy force, has a destabilising effect on the liquid-vapour interface (see Section 4.1). Thus, the competition between the horizontal diffusion (first term in 5.17) and the buoyancy force (second term in 5.17) will determine the nature of the liquid-vapour interface for short-wave perturbations.

Assuming that the first and second terms balance each other, i.e. marginal stability ( $\sigma_0 = 0$ ) and solving (5.17) for  $R_3$  enables us to find a conditional expression for the critical Rayleigh number for infinite wave numbers,

$$R_3^{crit} \sim R_{3,\infty}^{crit} = \frac{2}{H_{vap}} \frac{Q_{liq}}{k} \frac{C}{R_1} \frac{1}{R_2} \frac{R_1 R_2 + 1}{R_1 - 1}, \quad \text{as } l \rightarrow \infty. \quad (5.18)$$

In the light of (5.18) the following three cases can now be distinguished

1. If the Rayleigh number  $|R_3| > |R_{3,\infty}^{crit}|$  and  $R_3 < 0$  then the configuration with liquid above vapour is unstable ( $\sigma_0 > 0$ ) to short-wave perturbations.
2. If the Rayleigh number  $R_3 = R_{3,\infty}^{crit}$ , then the system is neutrally stable ( $\sigma_0 = 0$ ) for infinite wave numbers.
3. If the Rayleigh number  $|R_3| < |R_{3,\infty}^{crit}|$  and  $R_3 < 0$ ; or if  $R_3 > 0$ , then the system is asymptotically stable ( $\sigma_0 < 0$ ) for infinite wave numbers.

Figure 5.2 illustrates the effects of the critical Rayleigh number on the short wavelength disturbances. As was predicted analytically above, if the Rayleigh number is less than the critical Rayleigh number, then the system is stable to short-wave perturbations. As the Rayleigh number increases the system becomes more unstable: this instability is a reflection of buoyancy effects, which is because the heavier fluid is overlying the lighter fluid (see Section 4.1.1). Note that in all the cases plotted, short waves are the last to become unstable.

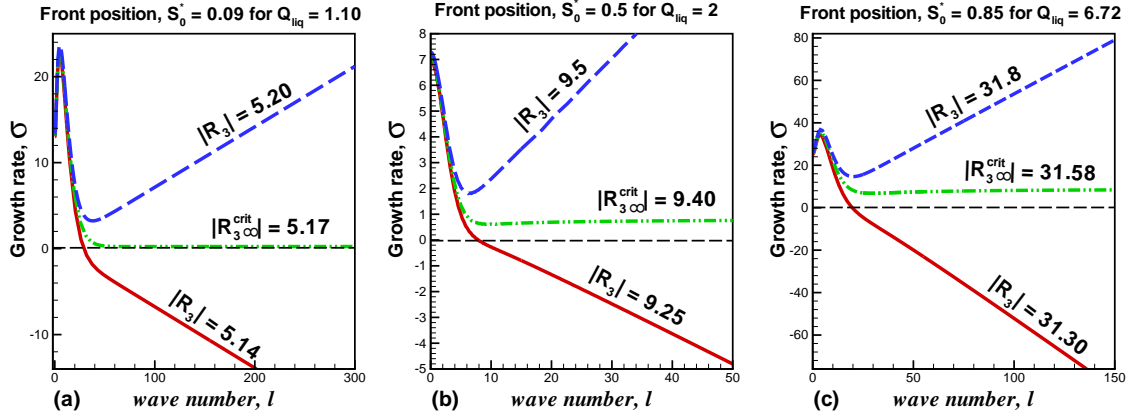


Figure 5.2: Short wave disturbances of the liquid-vapour interface with no through flow and a constant heat flux at the liquid boundary, where  $R_1 = 0.0006$ ,  $R_2 = 8.75$ ,  $\varphi = 0.38$ ,  $H_{vap} = 41.17$ ,  $C = 2.02$  and  $k = 4$

### 5.2.5.2 Onset of instability at $l = 0$

Assuming marginal stability ( $\sigma = 0$ ) and using  $S_0^*$  from (5.6), the critical Rayleigh number for zero wave number is obtained by taking the limit of (5.15) as  $l \rightarrow 0$ ,

$$R_{3,0}^{crit} \approx \frac{2C Q_{liq} (R_1 R_2 (Q_{liq} - 1) + 1)}{R_1 R_2 (2C(Q_{liq} - 1) + k(1 + 2H_{vap})) (R_1 - 1)}. \quad (5.19)$$

The above expression for  $R_{3,0}^{crit}$  contains all the physical parameters associated with the problem, such as the cooling parameter  $Q_{liq}$ , the density ratio  $R_1$ , the conductivity ratio  $k$ , the dynamic viscosity ratio  $R_2$ , the specific heat ratio  $C$  and the reciprocal of the Stefan number for vapour phase  $H_{vap}$ . As for short waves, (5.19) shows that the stability of the liquid-vapour interface is conditional. If  $|R_3| < |R_{3,0}^{crit}|$  with  $R_3 < 0$ , then the interface is stable to long-wave perturbations.

### 5.2.5.3 Onset of instability for medium wave numbers

The critical Rayleigh numbers for zero and infinite wave numbers (5.19) and (5.18) are functions of various parameters of the problem, in particular the dimensionless cooling flux  $Q_{liq}$  and the density ratio  $R_1$ . So, the difference between these critical

Rayleigh numbers is used to find appropriate values for the heat flux  $Q_{liq}$  and the density ratio  $R_1$  in order to locate regions of parameter space where transition may occur first for intermediate wave numbers. Figure 5.3 suggests how we can choose appropriate values for the density ratio  $R_1$  and the heat flux  $Q_{liq}$  for which the difference between the critical Rayleigh numbers for zero and infinite wave numbers is approximately zero.

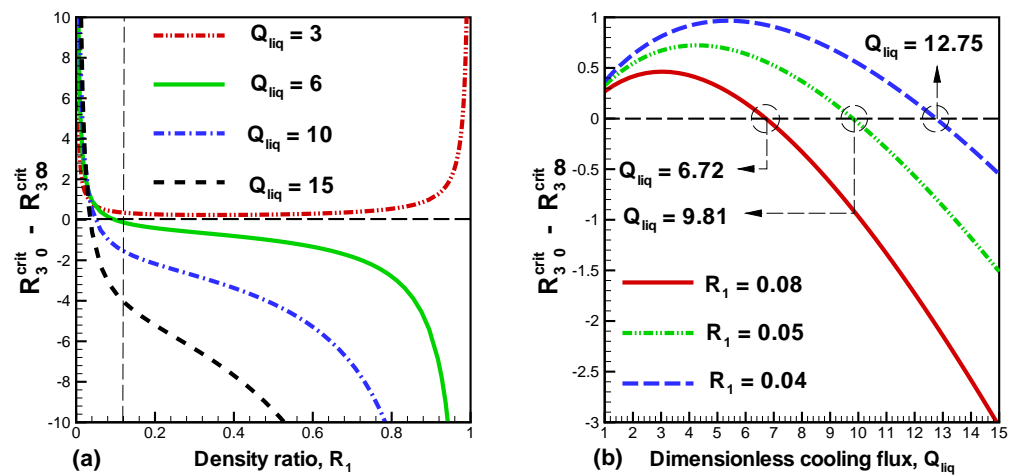


Figure 5.3: The difference between the critical Rayleigh numbers for zero and infinite wave numbers vs (a) the density ratio  $R_1$  and (b) the dimensionless heat flux  $Q_{liq}$ , where  $R_2 = 8.75$ ,  $H_{vap} = 7$ ,  $C = 1.96$ , and  $k = 4$ . Note that  $R_3 < 0$  (liquid above vapour).

The physically appropriate value of the density ratio  $R_1$  is 0.0006 (see Section 2.7), but for plotting purposes it is convenient to choose a somewhat higher value. Figure 5.3 (a) suggests that the qualitative behaviour of the stability problem is the same for all sufficiently small values of  $R_1$ : we will consider several values of  $R_1$  in the range  $(0, 1)$ .

Figure 5.3 (b) shows how a critical value for  $Q_{liq}$  can be located once  $R_1$  has been set. Where the line crosses the axis is where the short-wave instability replaces the

long-wave instability. Close to this critical value of  $Q_{liq}$  (see Figure 5.3 (b)), we might get (i) spontaneous transition as in Il'ichev & Tsyppkin [31], or (ii) a finite most unstable wavenumber.

The dispersion relation (5.15) is solved for the roots in the case of marginal stability, i.e.,  $\sigma = 0$ . The roots are obtained numerically and the results are presented in Figure 5.4 for the critical values of  $Q_{liq}$ . This indicates that there exists a critical Rayleigh number for intermediate wavelengths that results in unstable perturbations at the liquid-vapour interface. Furthermore, as the density ratio increases, the critical Rayleigh number becomes smaller; as  $Q_{liq}$  increases, the critical Rayleigh number gets larger. So, a higher heat flux has a stabilising effect. It is clear that the transition to instability occurs for medium wavelength. For zero and infinite wave numbers the front is marginally stable at the same value of  $R_3$ , because we have chosen  $Q_{liq}$  in such a way to ensure this happens.

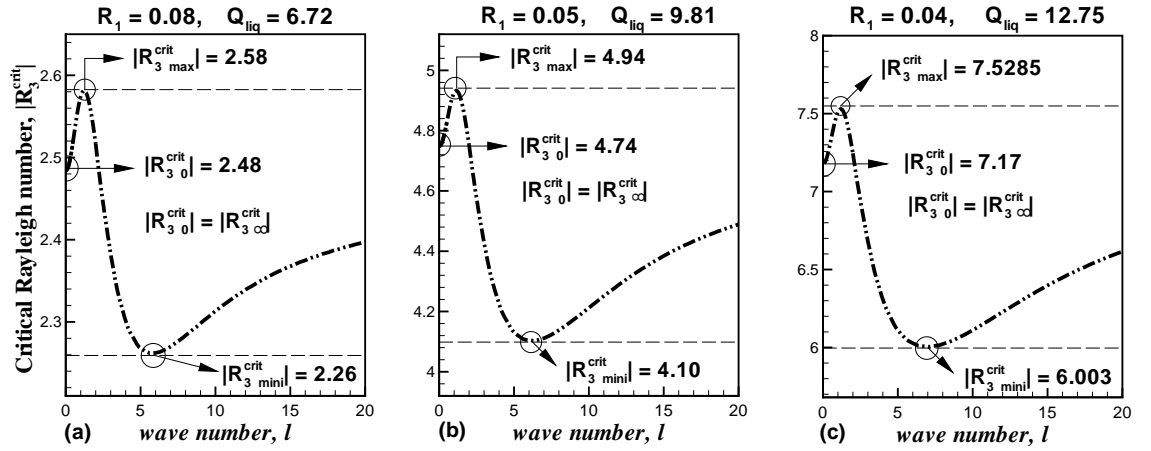


Figure 5.4: The critical Rayleigh number  $R_3^{crit}$  versus wave number  $l$  for the dimensionless heat flux  $Q_{liq}$ , for various values of  $R_1$ . Here  $R_2 = 8.75$ ,  $H_{vap} = 7$ ,  $E_1 = 1$ ,  $E_2 = 1$ ,  $C = 1.96$ ,  $\varphi = 0.38$  and  $k = 4$ . Note that  $R_3 < 0$  (liquid above vapour).

In Figure 5.4,  $R_{3,mini}^{crit}$  and  $R_{3,max}^{crit}$  are defined as being the smallest and largest magnitude of the Rayleigh numbers, respectively, for which we have  $\sigma = 0$  for

some wave number  $l$ .

The behavior of the dispersion relation for the three different combinations of the proposed critical values of  $Q_{liq}(R_1)$  (see Figure 5.3 (b)) is illustrated in Figures 5.6 and 5.5. As was discussed above, the transition to instability occurs first for medium-wave perturbations. Figure 5.5 confirms that for the minimum critical Rayleigh number (see Figure 5.4 for  $R_{3,crit}^{mini}$ ) the liquid-vapour interface is marginally stable. In this medium-wave region, an increase in the critical Rayleigh number will cause further instability of the liquid-vapour front. Figure 5.5 shows that a stable liquid over vapour configuration is possible if  $|R_3| < |R_{3,crit}^{mini}|$ .

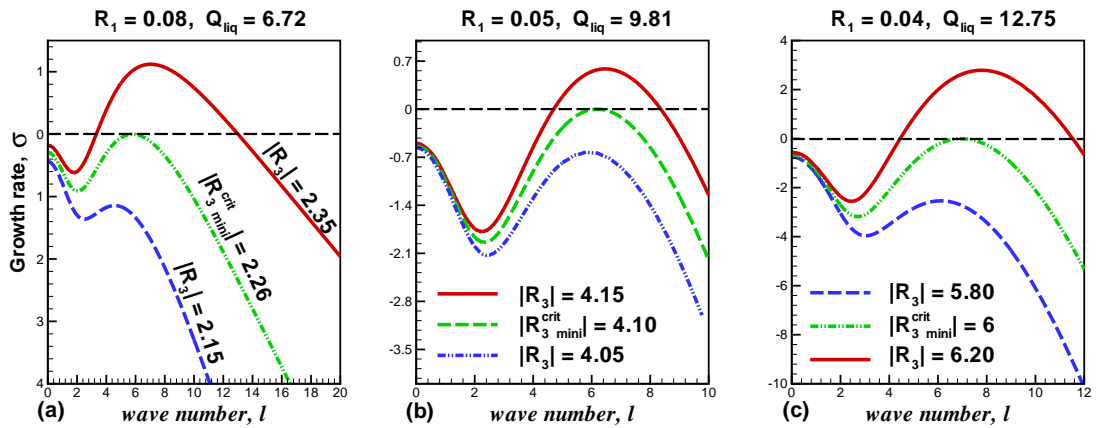


Figure 5.5: Medium wavelength disturbances of the liquid-vapour interface with no through flow and a constant heat flux condition.

Figure 5.6 shows that when  $R_3^{crit} = R_{3,max}^{crit}$ , the system is marginally stable to medium waves, whereas the zero and short-wave perturbations are unstable.

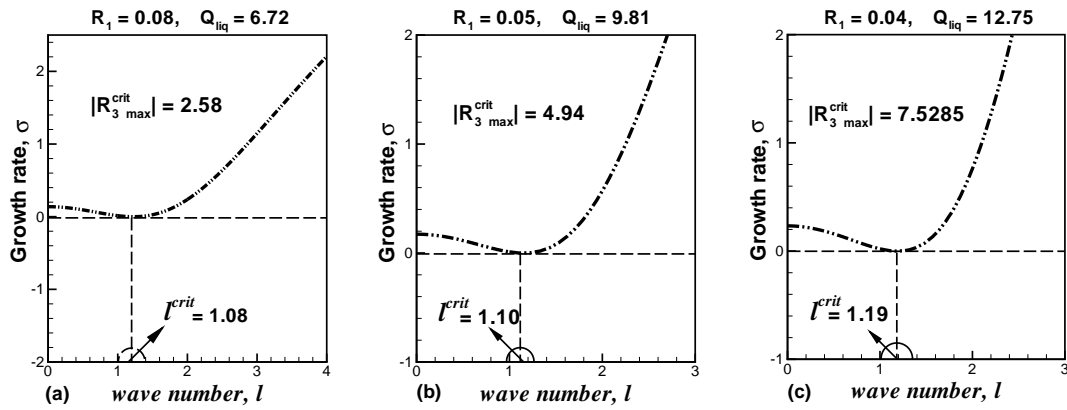


Figure 5.6: The long wavelength behaviour of the liquid-vapour interface with no through flow and a constant heat flux condition when the critical Rayleigh number  $R_3^{crit} = R_{3,max}^{crit}$ . For  $R_{3,max}^{crit}$  see the text.

### 5.2.6 Special cases

From the dispersion equation (5.15), three different special cases are derived in the same manner as in Section 4.3.6. The key variation in these cases is the assumption of different modes of heat transport (see Table 5.1).

Boundary conditions	Basic state	Perturbed state
Flux at the top and fixed temperature at the bottom with fixed pressure	no through flow	Only diff in the entire system Adv & diff in the liquid phase Adv & diff in the vapour phase

Table 5.1: List of problems under consideration with fixed flux condition

The asymptotic conditions on critical Rayleigh numbers for long wavelengths for the above different cases are given in Table 5.2. These asymptotic conditions can be used as a convenient starting point for the stability analysis and we can use them to explore the dependence on various parameters.

Critical Rayleigh number, $ R_{3,0}^{crit} $	Modes of heat transport
$\frac{C Q_{liq} (R_1 R_2 (Q_{liq} - 1) + 1)}{R_1 R_2 k H_{vap} (R_1 - 1)}$	Only diff in the entire system
$\frac{C Q_{liq} (R_1 R_2 (Q_{liq} - 1) + 1)}{R_1 R_2 (C(Q_{liq} - 1) + k H_{vap}) (R_1 - 1)}$	Adv & diff in the liquid phase
$\frac{2 C Q_{liq} (R_1 R_2 (Q_{liq} - 1) + 1)}{R_1 R_2 k (2 H_{vap} + 1) (R_1 - 1)}$	Adv & diff in the vapour phase
$\frac{2 C Q_{liq} (R_1 R_2 (Q_{liq} - 1) + 1)}{R_1 R_2 (2 C(Q_{liq} - 1) + k (1 + 2 H_{vap})) (R_1 - 1)}$	Adv & diff in the entire system

Table 5.2: List of critical Rayleigh numbers for long-wave perturbations with fixed flux condition

For all the above cases, the condition on critical Rayleigh numbers for short-wave perturbations ( $R_{3,\infty}^{crit}$ ) is the same as (5.18), because horizontal diffusion dominates over advection for short-wave length disturbances (for physical mechanisms see Section 4.1). The same observations were made for the isothermal steady state (see Section 4.3.6.4).

Following the same procedure as in Section 5.2.5.3, the difference between the critical Rayleigh numbers for short (5.18) and long wavelengths (see Table 5.2) has been used to find the appropriate values for the heat flux  $Q_{liq}$  and the density ratio  $R_1$ . The results for  $R_{3,0}^{crit} - R_{3,\infty}^{crit}$  are plotted in Figure 5.7 (a), where the different curves are the different modes of heat transport. Figure 5.7 (a) suggests that, as in Figure 5.3 (a), the qualitative behaviour is the same for all sufficiently small  $R_1$ . We take  $R_1 = 0.04$  for plotting purposes. This is then used to find the critical

value for the cooling parameter  $Q_{liq}$  (see Figure 5.7 (b)).

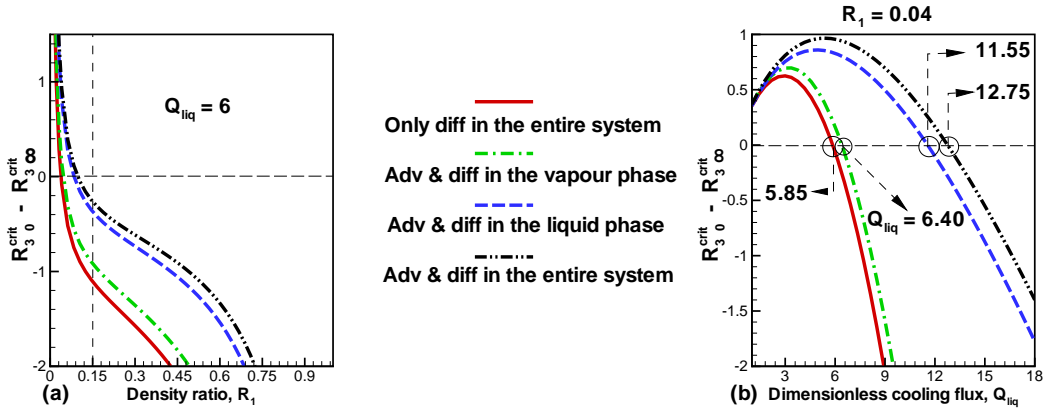


Figure 5.7: The difference between the critical Rayleigh numbers for zero and infinite wave numbers vs (a) the density ratio  $R_1$  and (b) the heat flux  $Q_{liq}$  for the different modes of heat transport, where  $R_2 = 8.75$ ,  $H_{vap} = 7$ ,  $C = 1.96$ ,  $k = 4$  and  $\varphi = 0.38$ .

The dispersion relation equations for the different modes of heat transport in Table 5.1 are obtained from (5.15) (dispersion equation for a system with advection and diffusion in both phases). Then, in the case of marginal stability, i.e.,  $\sigma = 0$ , the stability results are presented in Figure 5.8 for the suggested critical values of  $Q_{liq}$  (see Figure 5.7 (b)). The results in Figure 5.8 for the different heat transport processes (see Table 5.1) are broadly in agreement with those in Figure 5.4 for the problem with advective and diffusive transport in both phases. The transition to instability happens for medium wavelengths.

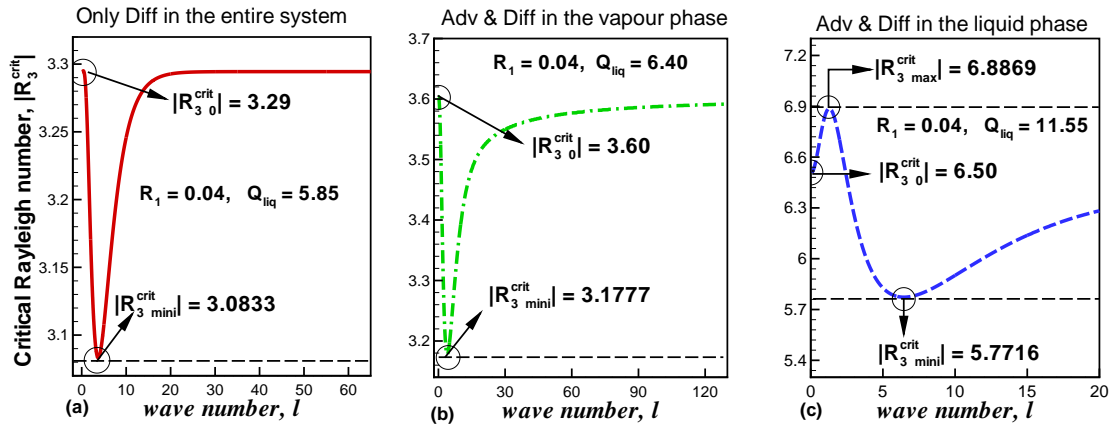


Figure 5.8: The dependence of  $|R_3^{crit}|$  on the wave number  $l$  for the different modes of heat transport (see Table 5.1), where  $R_1 = 0.04$ ,  $R_2 = 8.75$ ,  $H_{vap} = 7$ ,  $C = 1.96$ ,  $k = 4$ ,  $E_1 = 1$ ,  $E_2 = 1$  and  $\varphi = 0.38$ .

It will be interesting to know whether advection is essential to such a configuration (steady state with no through flow). For this, we have used the values of the critical Rayleigh numbers for medium and long wavelengths given in Figure 5.8 for each individual heat transport process. The medium-wave unstable behaviour of the liquid-vapour interface with and without heat advection is presented in Figure 5.9. Figure 5.9 shows typical results for the dependence of growth rate ( $\sigma$ ) on the wave number ( $l$ ) for constant heat flux  $Q_{liq}$  and for different Rayleigh numbers (for the values of  $Q_{liq}$ ,  $R_1$  and  $R_3$  see Figure 5.8).

Figure 5.9 (a) shows that the system with pure diffusion becomes unstable to medium waves when  $|R_3| \approx 3.0833$ . For the same values of  $Q_{liq}$ ,  $R_1$  and  $R_3$ , the dispersion relations for the remaining three combinations of heat transport processes are plotted for comparison. It is clear that when the system with pure diffusion is marginally stable then the configurations with advection are unstable to both long and medium-wave perturbations. The short-wave perturbations are stable with and without advection for this particular set of parameters.

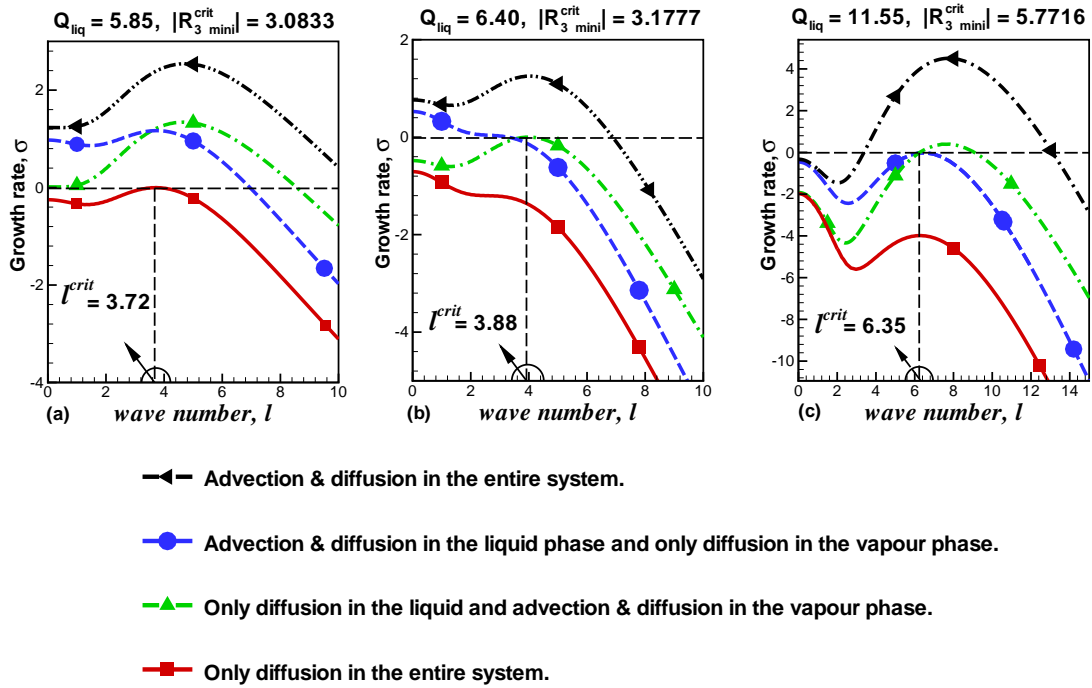


Figure 5.9: Medium wavelength disturbances of the system with and without advection and a fixed flux condition at the liquid boundary. The values of  $|R_{3,mini}^{crit}|$ ,  $Q_{liq}$  and the other parameters for (a), (b) and (c) are adapted from figure 5.8 (a), (b) and (c), respectively.

Figure 5.9 (b) shows the results for the value of  $R_3$  at which the system with advection and diffusion in the vapour phase and pure diffusion in the liquid phase is marginally stable. In comparison with the remaining configurations, the system with pure diffusion is stable for all waves. The system with advection and diffusion in the liquid phase and pure diffusion in the vapour phase is unstable to long waves, whereas the system with advection and diffusion in both phases is unstable to both long and medium waves. As before, the short-wave perturbations are stable with and without advection.

Figure 5.9 (c) shows that the system with advection and diffusion in the liquid phase and pure diffusion in the vapour phase becomes unstable to medium-wave

perturbations when  $|R_3| \approx 5.7716$ . The systems with advection and diffusion in the vapour phase and in both phases are unstable to medium waves only.

The results for the transition to instability for zero-wave perturbations of the different cases given in Table 5.1 are plotted in Figure 5.10. A curious feature of Figures 5.9 and 5.10 is that long-wave perturbations are more unstable when advection is included in the liquid phase but not in the vapour phase, whereas the opposite is true for short-wave perturbations. We have not so far been able to explain this physically.

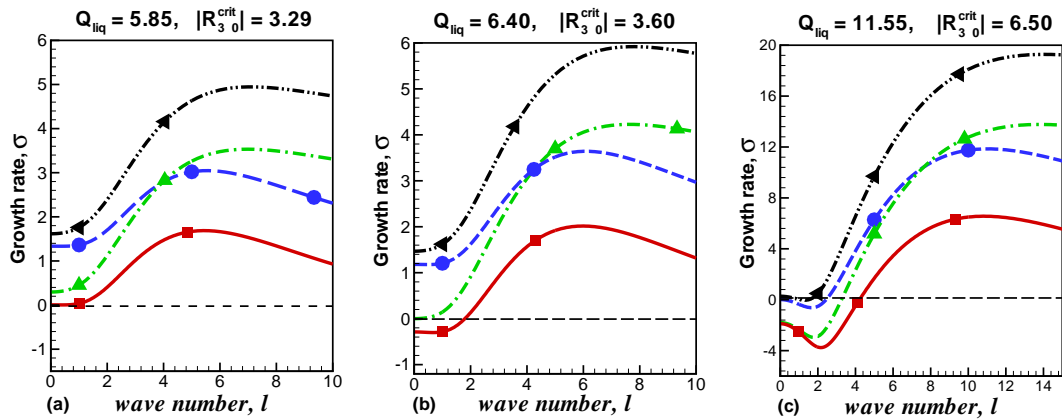


Figure 5.10: Long wavelength disturbances of the system with and without advection and a fixed flux condition at the liquid boundary. The critical values of  $|R_{3,0}^{crit}|$  and  $Q_{liq}$  and the other parameters for (a), (b) and (c) are adapted from figure 5.8 (a), (b) and (c), respectively.

The overall feature of these special cases is that the transition to instability occurs for medium waves both with and without heat advection. The same observations were made for the steady state with no through flow and isothermal boundary conditions (see Section 4.3.6.4). Furthermore, advective heat transport is not essential for instability, but it encourages the unstable behaviour.

A particularly interesting aspect of this problem is that we found maximum and minimum values of  $R_3$  for which the system is marginally stable for medium waves.

In the steady state with isothermal conditions, we have not seen this behaviour, although we cannot rule it out for some parameter regime that we have not investigated. For the moment, as far as we know it occurs only for this particular configuration (steady state with a constant flux condition).

### 5.3 Stability with non-zero through flow

In this section, we will discuss the stability of a base state with fixed temperature at the vapour boundary and a constant heat flux at the liquid boundary, with non-zero through flow. The competition between the effects of cooling and the viscosity difference in such configurations means that multiple front positions are possible (see Section 3.1.2). We will investigate the stability of each position of the liquid-vapour interface using the bifurcation diagram to guide us as in Section 4.4.

#### 5.3.1 Steady state solution

The detailed mathematical formulation of the steady-state through flow problem, and its solution, have been discussed in Section 3.1.2. We found exact solutions for the base state and confirmed the results given by Rubin & Schweitzer [68], that for a constant heat flux there may be up to three steady-state front positions. The bifurcation diagram 5.11 shows that in the intervals  $|R_3| \in [0, 34.093)$ ,  $|R_3| \in (0.23, 34.093)$  and  $|R_3| \in (0.23, 45]$ , the liquid-vapour interface  $S_0^*$  has low, middle and upper branch solutions, respectively. We will analyse the stability of the liquid-vapour interface, following the direction of the arrows as shown in Figure 5.11.

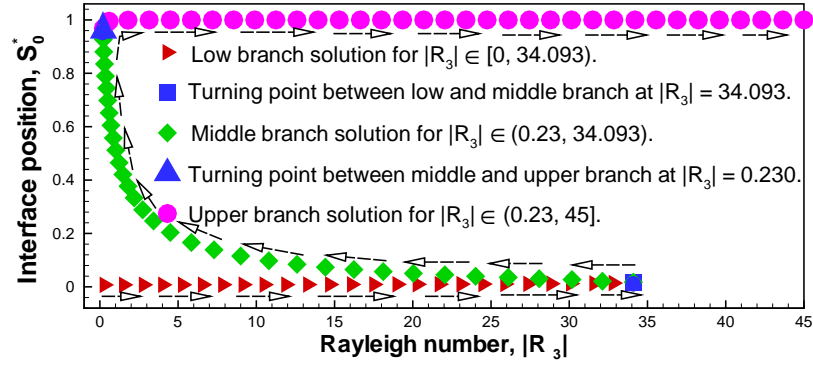


Figure 5.11: A bifurcation diagram for the liquid-vapour front  $S_0^*$  with a constant heat flux at the liquid boundary, where  $R_1 = 0.0006$ ,  $R_2 = 8.75$ ,  $C = 2.01$ ,  $k = 4$ ,  $H_{vap} = 41.17$ ,  $Pec_i = -160$ ,  $Q_{liq} = 1.45$ ,  $R = 22.11$  and  $R_3 \leq 0$ . See text for explanation of arrows.

### 5.3.2 Perturbed state

The first order formulation of the two dimensional, time-dependent flow with time dependent mass flux across the liquid-vapour interface has been given in detail in (4.30). The perturbed time dependent advective and diffusive heat flow in both phases (liquid and vapour) is governed by

$$\begin{aligned}
 E_1 \frac{\partial \Theta_{liq}^1}{\partial t^*} + \frac{Pec_i F(S_0^*) C}{k} \frac{\partial \Theta_{liq}^1}{\partial x^*} - \frac{\partial \Lambda_1}{\partial x^*} \frac{d\Theta_{liq}^0}{dx^*} &= \nabla^{*2} \Theta_{liq}^1, \\
 \frac{E_2 k R_1}{C} \frac{\partial \Theta_{vap}^1}{\partial t^*} + Pec_i F(S_0^*) \frac{\partial \Theta_{vap}^1}{\partial x^*} - \frac{R_1 R_2 k}{C} \frac{\partial \Pi_1}{\partial x^*} \frac{d\Theta_{vap}^0}{dx^*} &= \nabla^{*2} \Theta_{vap}^1.
 \end{aligned} \tag{5.20}$$

The corresponding perturbed thermal boundary conditions and the time dependent heat jump condition across the liquid-vapour interface  $S_0^*$  will remain the same as given in (5.8) and (5.9), respectively.

### 5.3.3 The eigenvalue problem

The details of the eigenvalue problem and its solution for eigenfunctions of the pressure profile in both phases have been given in Section 4.4.3. The first order

temperature profiles (5.20) and the corresponding boundary conditions (5.8) are expanded using the normal mode expansion (4.34), giving

$$\begin{aligned} & \left( \frac{d^2}{dx^{*2}} - \frac{Pec_i F(S_0^*) C}{k} \frac{d}{dx^*} - E_1 \sigma - l^2 \right) \phi_{liq} \\ & \quad + M_1 \exp \left( \frac{Pec_i F(S_0^*) C x^*}{k} \right) \frac{d\Psi}{dx^*} = 0, \\ & \frac{d\phi_{liq}}{dx^*} \Big|_{x^*=0} = 0, \quad \phi_{liq}(S_0^*) = -M_2 \Phi, \\ & \left( \frac{d^2}{dx^{*2}} - Pec_i F(S_0^*) \frac{d}{dx^*} - \frac{E_2 k R_1}{C} \sigma - l^2 \right) \phi_{vap} \\ & \quad + \frac{R_1 R_2 k}{C} N_2 \exp(Pec_i F(S_0^*) (x^* - 1)) \frac{d\Sigma}{dx^*} = 0, \end{aligned} \tag{5.21}$$

$$\phi_{vap}(1) = 0, \quad \phi_{vap}(S_0^*) = -N_4 \Phi,$$

where

$$\left. \begin{aligned} M_1 &= \frac{Q_{liq} Pec_i}{k} \left[ H_{vap} + \frac{1}{1 - \exp(Pec_i)} \right], \\ M_2 &= M_1 \exp \left( \frac{Pec_i F(S_0^*) C}{k} S_0^* \right). \end{aligned} \right\} \tag{5.22}$$

The solution of (5.21) for the temperature eigenfunction in the liquid phase is

$$\begin{aligned} \phi_{liq}(x^*) &= \frac{1}{f_1 f_5 f_6 M_4} \left\{ f_1 f_6 M_1 M_4 C_3 \exp(x^*(\omega_0 - 1)) + \left[ M_8 \cosh \left( \frac{\gamma_3 x^*}{2} \right) \right. \right. \\ & \left. \left. + 4 M_7 \omega_0 \sinh \left( \frac{\gamma_3 x^*}{2} \right) \right] \exp \left( \frac{x^* \omega_0}{2} \right) - f_1 f_5 M_1 M_4 C_3 l \exp(x^*(\omega_0 + 1)) \right\}, \end{aligned} \tag{5.23}$$

where

$$M_3 = \exp(\omega_0 S_0^*), \quad M_4 = f_1 \gamma_3 - \omega_0 f_4, \quad M_5 = f_5 \gamma_3 \Phi M_2 f_6,$$

$$M_6 = f_6 f_7 - f_3 f_5, \quad M_7 = \frac{M_1 C_3 l}{4} \{ 4 f_1 f_2 (E_1 \sigma + l^2) + M_6 \},$$

$$M_8 = - \left[ M_5 + M_1 C_3 l \{ 4 f_1 f_4 \omega_0 (E_1 \sigma + l^2) + \gamma_3 M_6 \} \right].$$

The expressions for  $\gamma_3$  and the various  $f_i$  are given in (4.69). Since we have considered a fixed temperature at the vapour boundary, the solution of (5.21) for the temperature eigenfunction in the vapour phase will remain the same as (4.69).

### 5.3.4 Dispersion analysis

The relationship between the growth rate  $\sigma$  and the wave number  $l$  is obtained by using the energy balance across the liquid-vapour interface. The substitution of the normal mode expansion (4.34) into (5.9) leads to

$$\varphi \sigma \Phi = \left\{ \frac{C}{H_{vap}} \left[ \frac{1}{k} \left\{ \Phi \frac{d^2 \Theta_{vap}^0}{dx^{*2}} + \frac{d\phi_{vap}}{dx^*} \right\} - \left\{ \Phi \frac{d^2 \Theta_{liq}^0}{dx^{*2}} + \frac{d\phi_{liq}}{dx^*} \right\} \right] - \frac{d\Psi}{dx^*} \right\}_{x^*=S_0^*}. \quad (5.24)$$

From the basic state we know that

$$\left. \begin{aligned} \frac{d^2 \Theta_{liq}^0}{dx^{*2}} \Big|_{x^*=S_0^*} &= M_2 \frac{Pec_i F(S_0^*) C}{k}, \\ \frac{d^2 \Theta_{vap}^0}{dx^{*2}} \Big|_{x^*=S_0^*} &= N_4 Pec_i F(S_0^*). \end{aligned} \right\} \quad (5.25)$$

Substituting (5.25) into (5.24) yields

$$\varphi \sigma \Phi = \left\{ \frac{C}{H_{vap}} \left[ \frac{1}{k} \left\{ \frac{d\phi_{vap}}{dx^*} + \Phi N_4 Pec_i F(S_0^*) \right\} - \left\{ \frac{d\phi_{liq}}{dx^*} + \Phi M_2 \frac{Pec_i F(S_0^*) C}{k} \right\} \right] - \frac{d\Psi}{dx^*} \right\}_{x^*=S_0^*}, \quad (5.26)$$

which can be solved numerically for values of the dimensionless growth rate  $\sigma$ . The numerical and asymptotic solutions of the dispersion equation (5.26) are analysed in the  $(Q_{liq}, R_3)$  parameter space, where  $|R_3|$  is the bifurcation parameter and  $Q_{liq}$  is the cooling parameter as before. The numerical and asymptotic methods used for analysing the dispersion relation  $\sigma(l)$  have been discussed in detail in Section 4.4.5.

### 5.3.5 Asymptotic analysis

The asymptotic analysis of the dispersion function  $\mathbb{E} \equiv \text{LHS}(5.26) - \text{RHS}(5.26)$  will help to explain the stability behaviour for short-wave perturbations. The details of the asymptotic method have been given in Section 4.4.5.2.

We have assumed an asymptotic solution of the form  $\sigma = \sigma^* l$  as  $l \rightarrow \infty$ . An explanation of this ansatz lies in the numerical observations of the dispersion function  $\mathbb{E}$  which suggest that the growth rate  $\sigma$  behaves linearly for large  $l$ .

Following the same procedure as in Section 4.4.5.2, all the exponential and hyperbolic terms in the expression  $\mathbb{E}$  are rewritten in terms of  $\alpha_1 \equiv \exp(l)$  and  $\alpha_2 \equiv \exp(S_0^* l)$  multiplied by appropriate asymptotic expansions in powers of  $1/l$ . The combinations of  $\alpha_1$  and  $\alpha_2$  which appear in the expansion of  $\mathbb{E}$  are

$$\begin{aligned} \alpha_2 \alpha_1^5 &\equiv \exp(S_0^* l) \exp(5l), & \alpha_2^2 \alpha_1^4 &\equiv \exp(2 S_0^* l) \exp(4l), \\ \alpha_2^3 \alpha_1^3 &\equiv \exp(3 S_0^* l) \exp(3l), & \alpha_2^3 \alpha_1^5 &\equiv \exp(3 S_0^* l) \exp(5l), \\ \alpha_2^4 \alpha_1^4 &\equiv \exp(4 S_0^* l) \exp(4l), & \alpha_2^5 \alpha_1^3 &\equiv \exp(5 S_0^* l) \exp(3l), \\ \alpha_2^5 \alpha_1^5 &\equiv \exp(5 S_0^* l) \exp(5l), & \alpha_2^6 \alpha_1^4 &\equiv \exp(6 S_0^* l) \exp(4l), \\ \alpha_2^7 \alpha_1^3 &\equiv \exp(7 S_0^* l) \exp(3l). \end{aligned}$$

From the above combinations, it is clear that the terms  $\alpha_2 \alpha_1^5$ ,  $\alpha_2^2 \alpha_1^4$ ,  $\alpha_2^3 \alpha_1^3$ ,  $\alpha_2^3 \alpha_1^5$ ,  $\alpha_2^4 \alpha_1^4$  and  $\alpha_2^5 \alpha_1^3$  compared to  $\alpha_2^5 \alpha_1^5$  are small. Comparing the remaining terms  $\alpha_2^5 \alpha_1^5$ ,  $\alpha_2^6 \alpha_1^4$  and  $\alpha_2^7 \alpha_1^3$ , since  $\alpha_1 > \alpha_2$ , we conclude that  $\alpha_2^5 \alpha_1^5$  is the largest term. Thus expanding the coefficient of  $\exp(5 S_0^* l) \exp(5l)$  in inverse powers of  $l$ , we get the leading term in the expansion which is

$$\mathbb{E} \sim f(\sigma^*; \text{other parameters}) l \exp(5 S_0^* l) \exp(5l).$$

Finally, we set  $f$  equal to zero and solved numerically for  $\sigma^*$ . The asymptotic results for the low and the middle branch front positions are plotted in Figure 5.12. The low branch solution in the interval  $|R_3| \in (9.525, 34.093)$  is unstable to both medium and short-wave perturbations. The middle branch solution for the liquid-vapour front in the interval  $|R_3| \in (0.7365, 34.093)$  is unstable to all perturbations. The asymptotic growth rate  $\sigma^*$  for the upper branch is not shown because it is always negative and hence stable to short-wave perturbations.

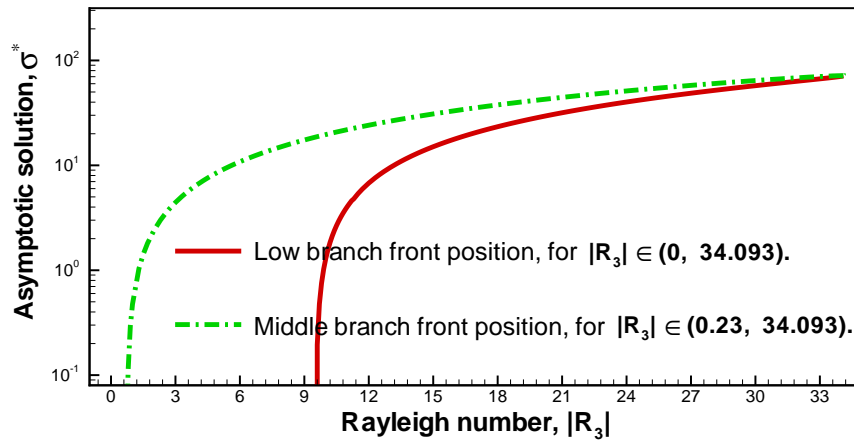


Figure 5.12: Asymptotic solution for the low and middle branch front positions.

### 5.3.6 Numerical results for $\sigma(l)$

The dispersion relation (5.26) is analysed following the bifurcation diagram 5.11. The roots of  $\sigma(l)$  are obtained numerically using [Maple](#) for the three different branch front positions and the results are presented in the following sections.

#### 5.3.6.1 Unstable low branch solution

The bifurcation diagram, Figure 5.11, shows that the liquid-vapour interface has a low branch solution in the interval  $|R_3| \in [0, 34.093)$ . This low branch solution

corresponds to a strong flow from vapour into liquid (see Section 3.1.2).

The behaviour of the dispersion relation for the low branch solution is illustrated in Figure 5.13. Figure 5.13 (b) shows that the medium wavelength perturbations to the low branch front position are unstable with and without buoyancy. This shows that apparently Saffman-Taylor fingering is causing an instability. It is natural to ask how gravitationally stable this needs to be to overcome the viscous fingering instability. So, we considered some positive values for  $R_3$  and found that the system is stable when  $R_3 \approx 43.715$ . The stability results for positive Rayleigh numbers (vapour above liquid) are presented in Figure 5.13 (a). The physical mechanism associated with Saffman-Taylor instability is discussed in Section 5.3.7. Figure 5.13 (c) illustrates the effects of the Rayleigh number on the short wavelength disturbances and shows that transition to instability for infinite wave numbers is possible, but only for large Rayleigh numbers compared to medium wave instability.

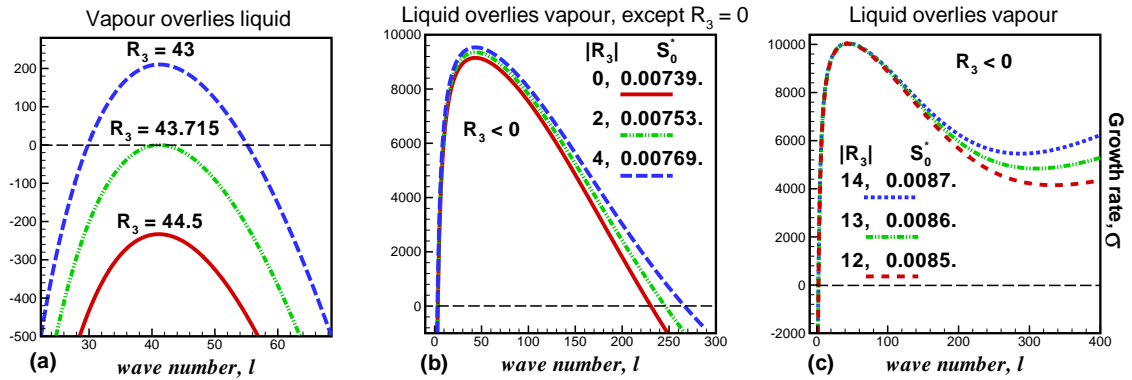


Figure 5.13: Stability plots of the low branch solution of  $S_0^*$  with a fixed flux condition.

The asymptotic results for the low branch solution are compared with the numerical results in Figure 5.14. Figure 5.14 shows that for short-wave perturbations, the asymptotic and the numerical results are in agreement for  $|R_3| > |R_{3,\infty}^{crit}|$  but not necessarily for values of  $|R_3|$  close to or less than  $|R_{3,\infty}^{crit}|$ .

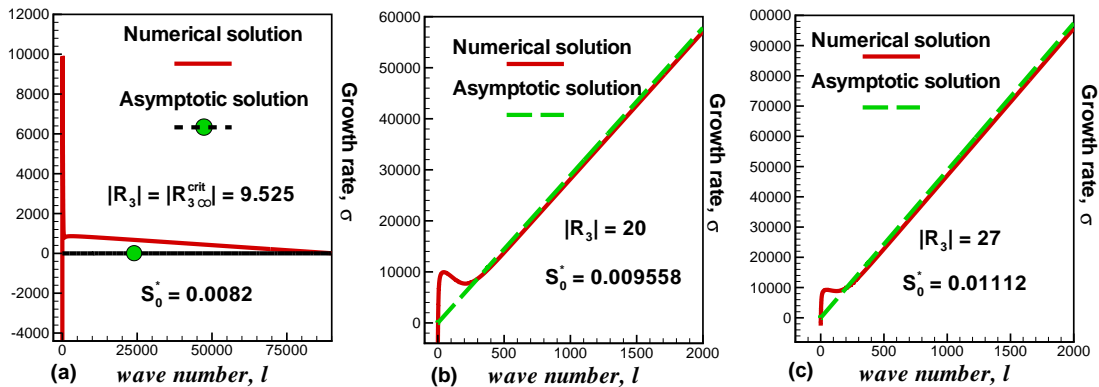


Figure 5.14: Comparison between the numerical and asymptotic solutions for the low branch solution of  $S_0^*$  with a fixed flux condition.

### 5.3.6.2 Unstable middle branch solution

Figure 5.15 shows that  $\sigma(l = 0)$  passes through zero precisely at the turning point between the middle and upper branches (see the equivalent behaviour in Section 4.4.6.2). The middle branch front position under discussion corresponds to  $|R_3| \in (0.23, 34.093)$  (see the bifurcation diagram, Figure 5.11).

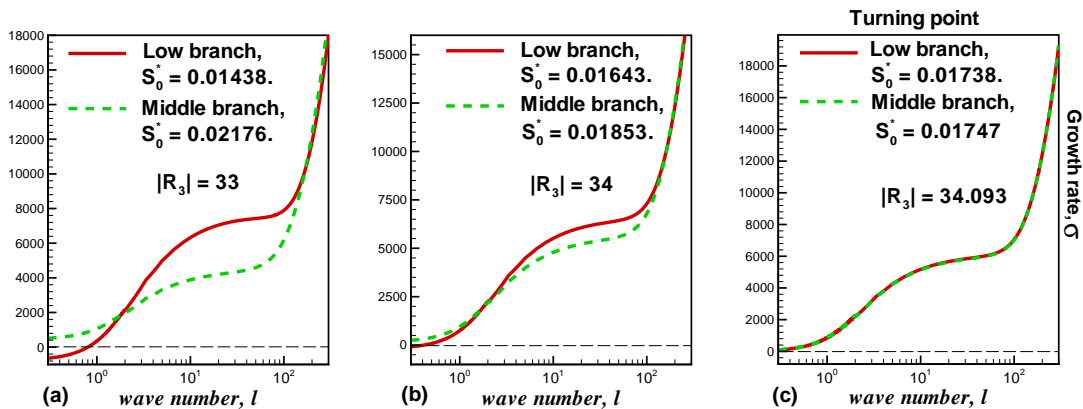


Figure 5.15: Behaviour of the low and middle branch near the turning point at  $|R_3| \approx 34.093$ . The log scale is used for better visualisation.

Between the turning point and  $|R_3| \approx 0.7365$  (corresponding to  $S_0^* \approx 0.601$ ) the

middle branch is unstable to all perturbations. At  $|R_3| \approx 0.7365$ , the short-wave perturbations become stable (see Figure 5.16 (d)). Figure 5.16 (d) shows that as  $|R_3|$  decreases the front position  $S_0^*$  on the middle branch increases and the short-wave perturbations become stable. This contrasts with the middle branch front position with the isothermal boundary conditions, which is unstable to all disturbances (see Section 4.4.6.2).

The asymptotic solutions for the middle branch are presented in Figures 5.16 (a), (b) and (c). The asymptotic solutions and the numerical solutions for the middle branch front position agree well.

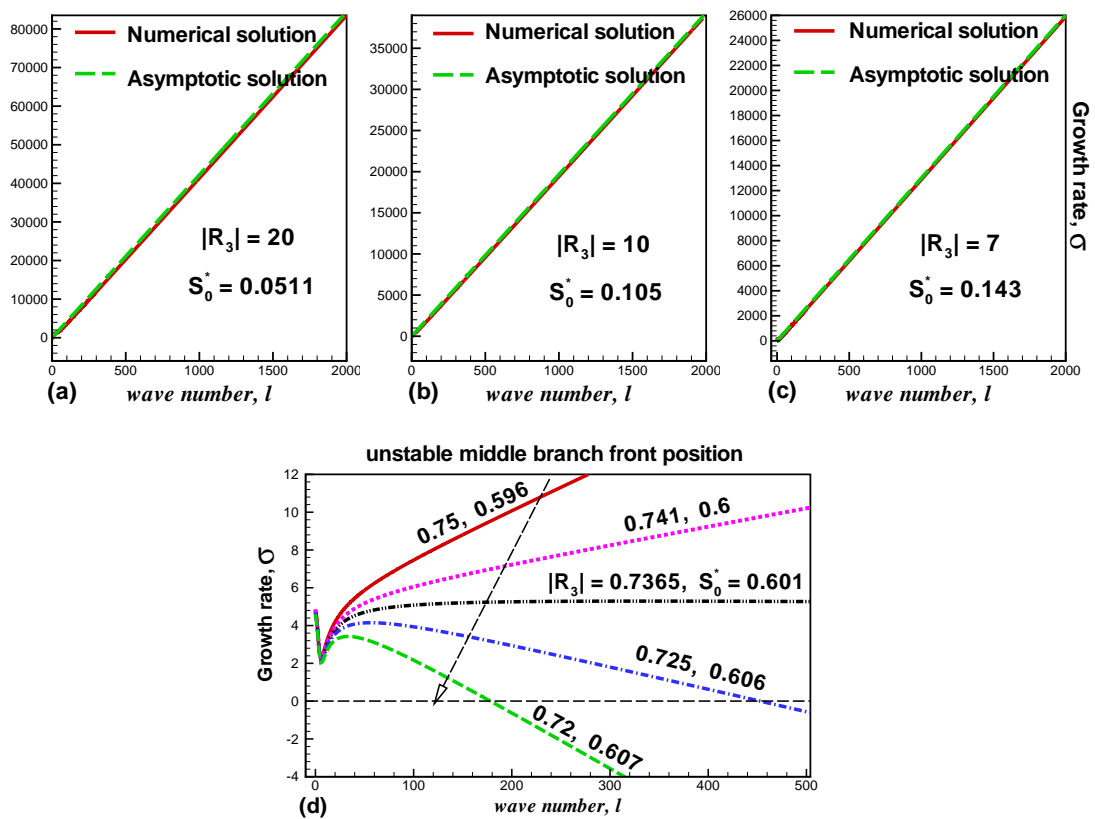


Figure 5.16: Stability plots for the middle branch front position and comparison with asymptotic solution.

### 5.3.6.3 Stable upper branch solution

The bifurcation diagram, Figure 5.11, shows that the interface  $S_0^*$  has an upper branch solution in the interval  $|R_3| \in (0.23, 45]$ . In the neighborhood of the turning point between the middle and upper branch at  $|R_3| \approx 0.230899$ , the upper branch is stable to all perturbations (see Figures 5.17 (a), (b) and (c)). In comparison, the upper branch front position for the isothermal boundary conditions, first becomes stable to zero-wave perturbations, then to short-wave perturbations and finally becomes stable to all perturbations depending on the controlling parameter, the Rayleigh number  $|R_3|$  (see Section 4.4.6.3). Figure 5.17 shows that the upper branch front position is stable to all wavelengths.

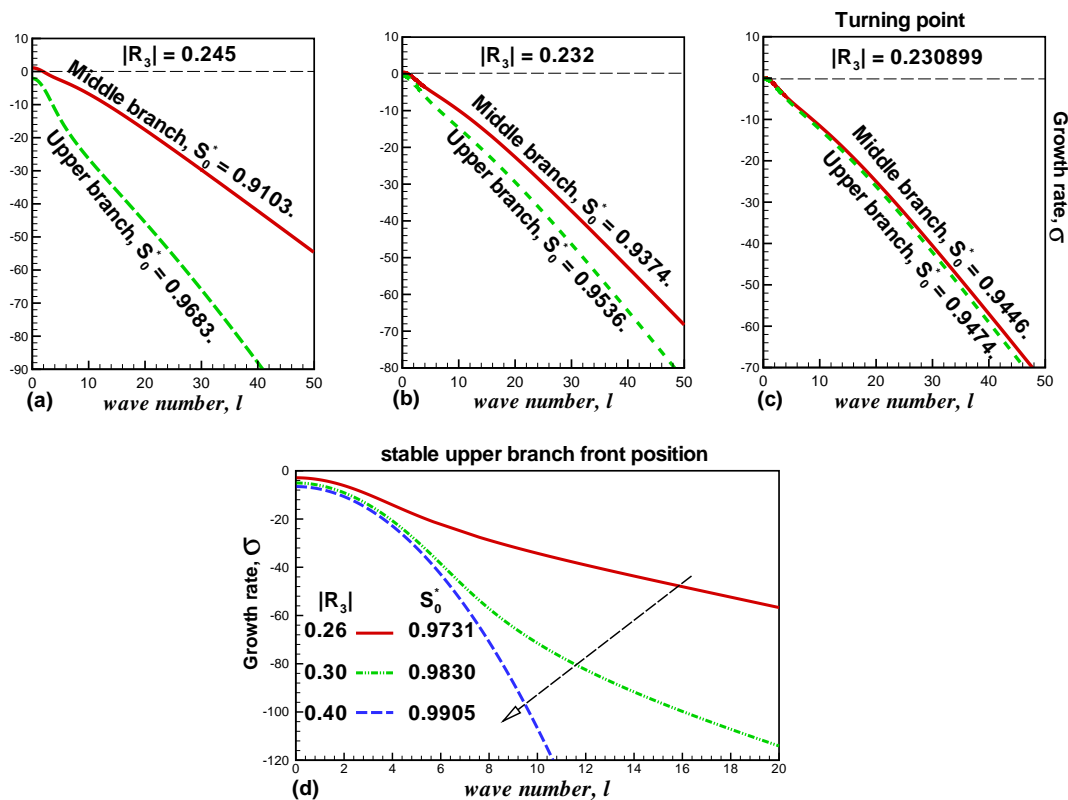


Figure 5.17: Stability plots of the upper branch front position with a fixed flux condition.

### 5.3.7 Rubin and Schweitzer [68] revisited

In the absence of gravity, i.e.  $R_3 = 0$ , the transcendental equation (3.32) describes a porous configuration in which fluid flows horizontally from a vapour phase into a liquid phase with a fixed heat flux condition at the liquid boundary (see Figure 5.18). In Section 3.1.2, we have shown that the liquid-vapour interface in such configuration has three front positions.

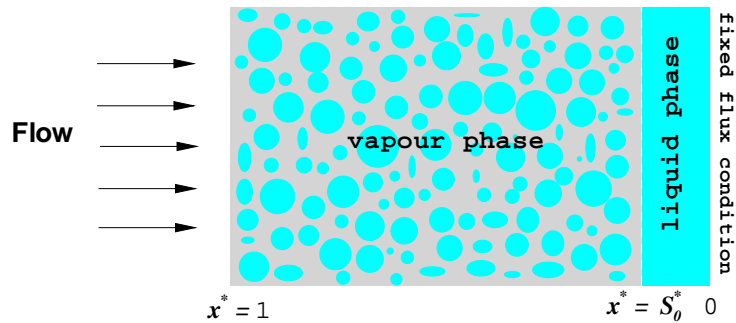


Figure 5.18: A horizontal configuration in which the porous layer is mostly filled with vapour.

Rubin & Schweitzer [68] have also proposed such a basic state and carried out a quasi-one-dimensional stability analysis. They made two simplifications. The first is to consider only one dimensional stability, which is equivalent to taking the zero-wave number limit. Secondly, they simplified the equations by assuming that the temperature profiles in both phases (liquid and vapour) are known beforehand, which is a quasi-steady-state temperature profile (equivalent to neglecting the timescale for thermal diffusion within each phase). The zero-wave number limit is perfectly legitimate, but it is not obvious that the second simplification is correct. We therefore compare Rubin & Schweitzer's [68] analysis with the limiting case  $l = 0$  of our two dimensional analysis, to examine the validity of this quasi-steady-state temperature profile assumption.

Rubin & Schweitzer [68] also suggested that the middle front position is unstable, whereas the upper and lower front positions are stable. As a special case of the through flow problem discussed earlier, we have investigated the two dimensional stability of the proposed horizontal flow model. The results of the three front positions are discussed using the bifurcation diagram 5.19, where the cooling flux  $Q_{liq}$  is now the new bifurcation parameter.

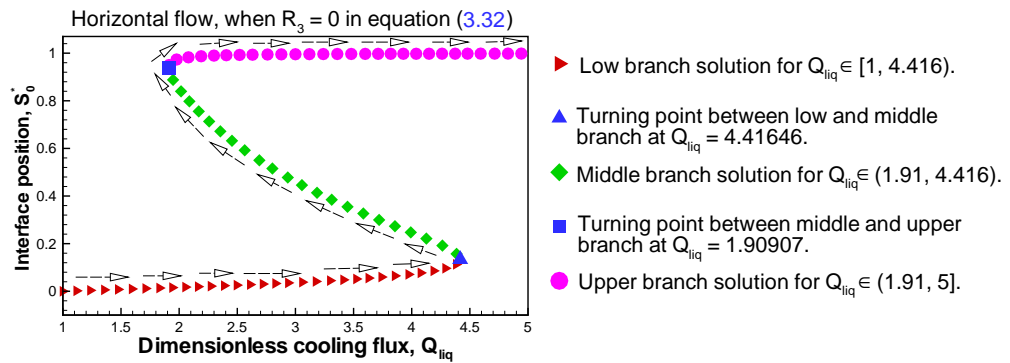


Figure 5.19: The bifurcation diagram for the liquid-vapour interface  $S_0^*$ , when  $R_3 = 0$  and  $Q_{liq}$  is the bifurcation parameter.

In Section 5.3.6.1 we mentioned the Saffman-Taylor instability for medium-wave perturbations. The same instability occurs here (see Figure 5.20). From Figures 5.13 (a), (b) and 5.20 (a) it is clear that for different liquid and vapour viscosities with and without gravity, the low branch front position is stable to both short and long wavelength perturbations since  $\sigma < 0$ . The long wavelength perturbations (small  $l$ ) are stabilised by vertical diffusion, whereas the short wavelength perturbations (large  $l$ ) are stabilised by horizontal diffusion (for explanation see Section 4.1). However, medium wavelength perturbations are unstable.

To understand the unstable behaviour of the low branch solution to medium-wave perturbations, we have relaxed the assumption of different viscosities and considered that the liquid and the vapour have the same viscosity. For  $R = 1$ , the transcendental equation (3.32) has a unique position for the liquid-vapour front.

Figure 5.20 (b) shows that this unique front position is stable to all perturbations suggesting that the viscosity contrast is essential for instability.

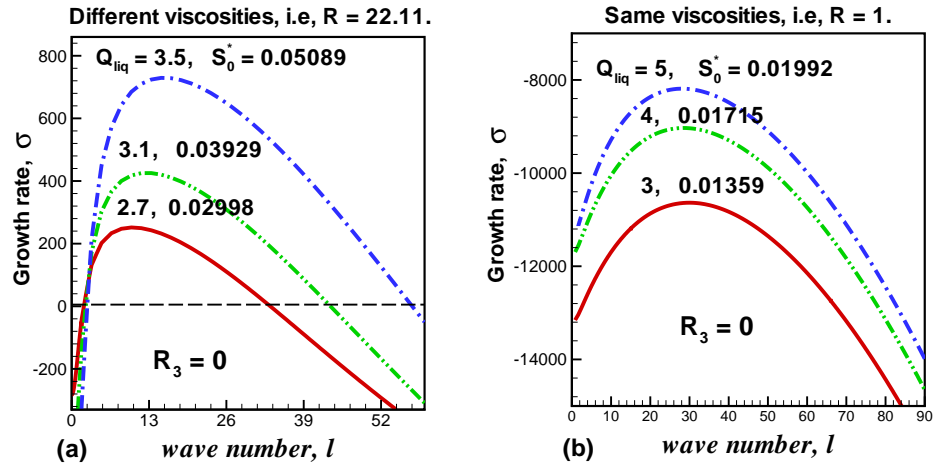


Figure 5.20: Stability plots of the low branch solution of  $S_0^*$  when  $R_3 = 0$ .

Furthermore, the low branch solution corresponds to a configuration in which the porous layer is mostly filled with vapour, and there is a strong flow from (less viscous) vapour into (more viscous) liquid (for schematic see Figure 5.18). Thus, the medium wavelength instability is of the Saffman-Taylor type, i.e., due to a less viscous fluid displacing a more viscous fluid (also see Section 4.1.1). This unstable behaviour of the low branch front position is in contrast with Rubin & Schweitzer's [68] "quasi-steady-state" one dimensional stability results.

The stability behaviour in the neighborhood of the turning point between the low and middle branch shows that both branches are unstable (see Figure 5.21), although the middle branch is always stable to long-wave perturbations. As was mentioned earlier, the low branch is unstable to medium-wave perturbation only because of the viscous fingering. Our results for the middle branch agree with Rubin & Schweitzer's [68], but their study lacks any detailed analysis of the dispersion relation.

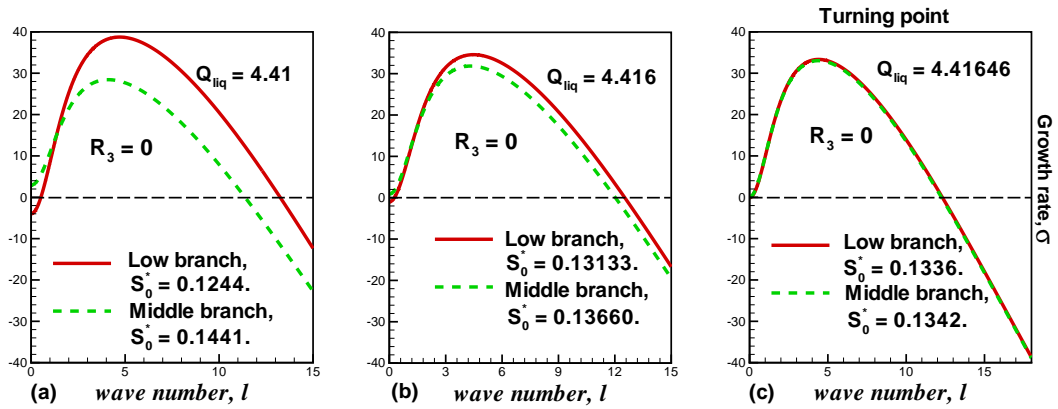


Figure 5.21: Stability plots of the middle branch solution of  $S_0^*$  when  $R_3 = 0$ .

The bifurcation diagram, Figure 5.19, shows that the turning point between the middle and upper branches is at  $Q_{liq} = 1.91$ . Figures 5.17 and 5.22 shows that the middle and upper branch front position behave in the same way in the neighborhood of the turning point with and without gravitational effects and that the upper branch front is stable to all perturbations. This stable behaviour of the upper branch is in agreement with Rubin & Schweitzer’s [68] results.

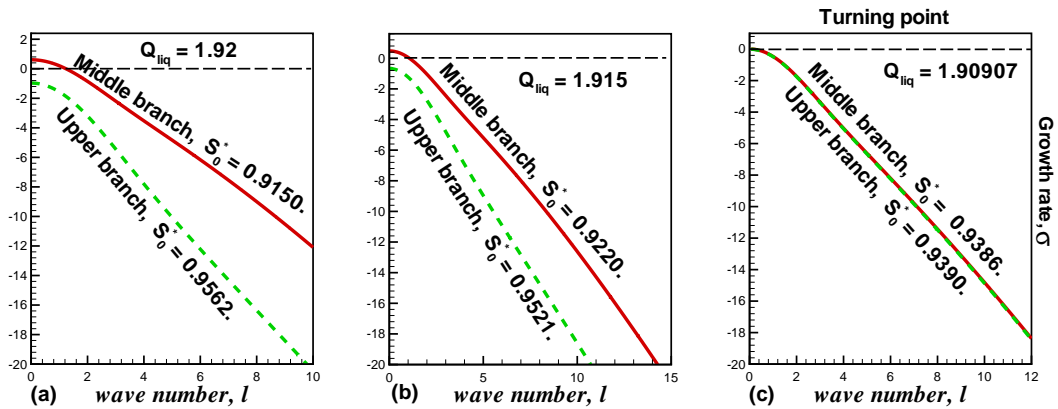


Figure 5.22: Stability plots of the upper branch solution of  $S_0^*$  when  $R_3 = 0$ .

### 5.3.8 Summary of our findings

Figure 5.23 summarises our findings for the interface with non-zero through flow, in the particular parameter regime investigated here.

- (i) For  $|R_3| \lesssim 0.23$  : There is only one front position, which is unstable to medium-waves only. This medium-wave instability on the low branch has been identified as Saffman-Taylor instability.
- (ii) When  $0.23 \lesssim |R_3| \lesssim 0.7365$  : There are three front positions and only the high- $S_0^*$  position is stable. The intermediate branch is unstable to both medium and short wave perturbations, whereas the low- $S_0^*$  position is unstable to medium-waves only.
- (iii) When  $0.7365 \lesssim |R_3| \lesssim 9.525$  : There are three front positions. The low branch has the viscous fingering instability. The middle branch is unstable to all perturbations, whereas the upper branch is stable.
- (iv) When  $9.525 \lesssim |R_3| \lesssim 34.093$  : There are three front positions and only the upper branch is stable. The low branch experience both the Saffman-Taylor and the Rayleigh-Taylor instabilities. The middle branch is unstable to all perturbations.
- (v) For  $|R_3| \gtrsim 34.093$  : There is only one front position, which is stable.

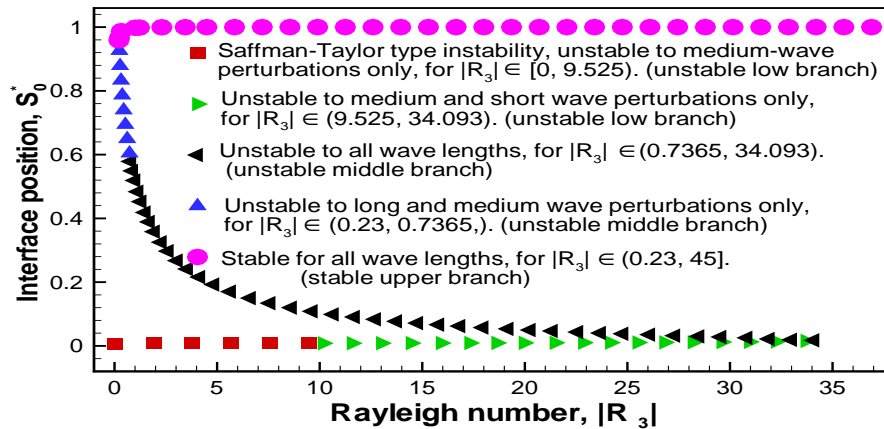


Figure 5.23: Identification of stable and unstable behaviour of the liquid-vapour interface with a fixed flux condition.

## 5.4 Summary and conclusions

In this chapter we used two dimensional linear stability methods to study the behaviour of a liquid-vapour interface in a porous medium with a heat constant flux condition at the liquid boundary. The unperturbed state in such configurations was analysed with and without through flow.

### 5.4.1 Basic state with no through flow

In Section 5.2, we carried out the stability analysis of a diffusive steady state. We found out that in the absence of advection, the liquid-vapour interface has a unique position. The stability results showed that the interface becomes unstable first to medium-wave perturbations. We were able to find conditions on the critical Rayleigh numbers for both long and short wavelengths.

### 5.4.2 Basic state with through flow

In Section 5.3, we discussed the two dimensional stability of the most interesting configuration, in which the advective steady state with or without gravity has mul-

tiple positions. We revisited Rubin & Schweitzer's [68] work as a special case and suggested that the low branch solution of the horizontal flow has Saffman-Taylor type instability.

We have shown that the low branch solution of the basic state with through flow becomes unstable first to medium-wave perturbations (Saffman-Taylor instability) and then to short-wave perturbations (Rayleigh-Taylor instability) as the Rayleigh number increases. The middle and upper branches are unstable and stable, respectively.

Finally, we have discussed the stability results presented by Rubin & Schweitzer [68]. We found that the low branch position is unstable. But Rubin & Schweitzer [68], focusing on the long-wave limit and neglecting the thermal diffusion timescale, had suggested that the low branch position was stable. The middle and upper branches are unstable and stable, respectively, which agrees with Rubin & Schweitzer's [68] one dimensional stability results.

# Chapter 6

## Conclusions and possible extensions

### 6.1 Summary

In this thesis, we have investigated vertical heat transfer and flow across a horizontal porous layer with various combinations of boundary conditions.

In Chapter 3, we have thoroughly investigated possible one-dimensional steady states and confirmed the findings of earlier work [68] that multiple steady states are available when there is a heat flux condition on one boundary (Section 3.1.1). We have also demonstrated that in addition to this, multiple steady states are possible with fixed-temperature conditions on both boundaries when the pressure difference across the layer is specified, due to competition between thermal and hydrostatic effects (Section 3.1.2).

Also in Chapter 4, we have explored in some detail the stability properties of these steady states. In particular, we have investigated the circumstances under which “spontaneous” transitions to instability are possible [31], the mechanisms

contributing to stability and instability, and the changes in stability along the bifurcation curve when multiple steady states are available (Section 4.4).

The “spontaneous” transition of Il’ichev & Tsyarkin [31] is shown to be a very unusual case, depending not only on the front position but also on the neglect of advective heat transport. It does not, however, depend on the temperature–pressure condition applied at the front (Section 4.3.6.2).

The mechanisms contributing to stability are essentially thermal: horizontal and vertical diffusion, the latter controlled by the fixed temperature at the phase-change front. Although the Rayleigh–Taylor (buoyancy-driven) mechanism is the dominant contributor to instability, a Saffman–Taylor viscous fingering effect also becomes important when there is a strong throughflow from less viscous vapour into more viscous liquid.

Contrary to the conclusions of Rubin & Schweitzer [68], it is not straightforward to describe stability changes along the bifurcation curve: the upper and lower branches are not necessarily stable nor the middle branch unstable (Section 5.3). This applies even to perturbations in the limit of zero wavenumber (Section 5.3.7).

These findings contribute to a more complete understanding of the conditions under which “water-over-steam” configurations may develop in geothermal reservoirs.

## 6.2 Possible extensions

### 6.2.1 Numerical work

It would be valuable to develop numerical methods to solve the nonlinear governing equations, both in one dimension in order to confirm the existence of steady states and to investigate problems with less idealised boundary conditions, and in two or

three dimensions in order to investigate the stability properties.

One common approach is to use a mixed-phase model (Section 1.2.2.1, [1, 2, 48, 65, 72, 73, 80, 84]). Apart from the complex nature of the flow (which may involve vertical and horizontal counterflow), identifying a limit of the governing equations in which they reduce to a sharp-front model is not straightforward, and so direct comparison with stability analysis is not available.

Another approach, which has been widely employed to model Stefan problems with a liquid–solid transition, is the enthalpy method. This method is used to reformulate the Stefan problem in terms of a single energy conservation equation for the entire solution domain [15, 52, 87–89, 91].

The standard enthalpy approach is to define a function  $E(T)$  which is the total heat energy per unit mass as follows

$$E(T) = \begin{cases} c_{liq} (T - T_{ref}) : & \text{for } T < T_S \text{ (liquid phase),} \\ c_{vap} (T - T_S) + \lambda + c_{liq} (T_S - T_{ref}) : & \text{for } T > T_S \text{ (vapour phase),} \end{cases} \quad (6.1)$$

where  $c$  is the specific heat,  $T_{ref}$  is a reference temperature below  $T_S$ ,  $T_S$  is the phase change temperature and  $\lambda$  is the latent heat. Meanwhile the volumetric heat capacity is given by

$$(\rho c) = \begin{cases} (\rho c)_{liq} : & \text{for } T < T_S \text{ (liquid phase),} \\ (\rho c)_{vap} : & \text{for } T > T_S \text{ (vapour phase).} \end{cases} \quad (6.2)$$

Note that in most applications of this method, the densities of the two phases are taken to be the same. The function  $E(T)$  allows for a single domain conservation of enthalpy (the sum of sensible and latent heats). In one dimension, this equation is

$$\frac{\partial \rho E}{\partial t} + \frac{\partial (\rho u E)}{\partial x} = \frac{\partial}{\partial x} \left( k_m \frac{\partial T}{\partial x} \right).$$

Integrating the above conservation of enthalpy over a small region around the phase change front  $S$  yields

$$\begin{aligned} \int_{S^-}^{S^+} \frac{\partial(\rho E)}{\partial t} dx + [\rho u E]_{S^-}^{S^+} &= \left[ k_m \frac{\partial T}{\partial x} \right]_{S^-}^{S^+}, \\ \Rightarrow \lambda \rho_{vap} \left( u_{vap} - \frac{dS}{dt} \right) + E_{liq}(S^-) \left[ -\rho_{vap} \frac{dS}{dt} + \rho_{liq} \frac{dS}{dt} + \rho_{vap} u_{vap} - \rho_{liq} u_{liq} \right] \\ &= k_{m,vap} \frac{\partial T}{\partial x} \Big|_{S^+} - k_{m,liq} \frac{\partial T}{\partial x} \Big|_{S^-}. \end{aligned}$$

In the above transformation, the coefficient of the enthalpy function  $E_{liq}(S^-)$  is

$$\frac{dS}{dt} (\rho_{liq} - \rho_{vap}) - (\rho_{liq} u_{liq} - \rho_{vap} u_{vap}) = 0,$$

by mass conservation, so the integrated equation at the phase front reduces to

$$\lambda \rho_{vap} \left( u_{vap} - \frac{dS}{dt} \right) = k_{m,vap} \frac{\partial T}{\partial x} \Big|_{S^+} - k_{m,liq} \frac{\partial T}{\partial x} \Big|_{S^-}.$$

This is the Stefan condition at the liquid-vapour interface (see Section 2.6.1.1). The advantage of using such a reformulation is that the condition to explicitly locate the phase change interface is removed.

Once the problem is reformulated, a standard numerical approach such as finite difference and finite element methods can be employed [13]. Mackenzie & Robertson [45] proposed an adaptive moving mesh method based on a smoothed enthalpy-temperature relationship. The idea is to smooth the enthalpy-temperature relationship to take away the jump condition at the phase change interface and then use the adaptive moving mesh to attain some sort of accuracy [5, 45, 46].

However, for vapour-liquid phase changes there is a problem with this method, which is that there is a non-unique relationship between  $T$  and  $\rho E$  when the densities, and thus the volumetric heat capacities, of liquid and vapour are very different. This is crucial: there is a unique relationship between  $T$  and  $E$ , but the

quantity that we track is actually  $\rho E$  (the heat per unit volume), and this is not uniquely related to  $T$  when  $\rho_{vap} < \rho_{liq}$ .

The variations of  $E$  and  $\rho E$  with temperature  $T$  are shown in Figure 6.1. Figure 6.1 shows that at the phase change temperature  $T_S$ , the enthalpies of liquid and vapour phases are 1 and 2, respectively: there is a positive jump of enthalpy equal to the latent heat. But the jump in  $\rho E$  is negative because of the drop in density.

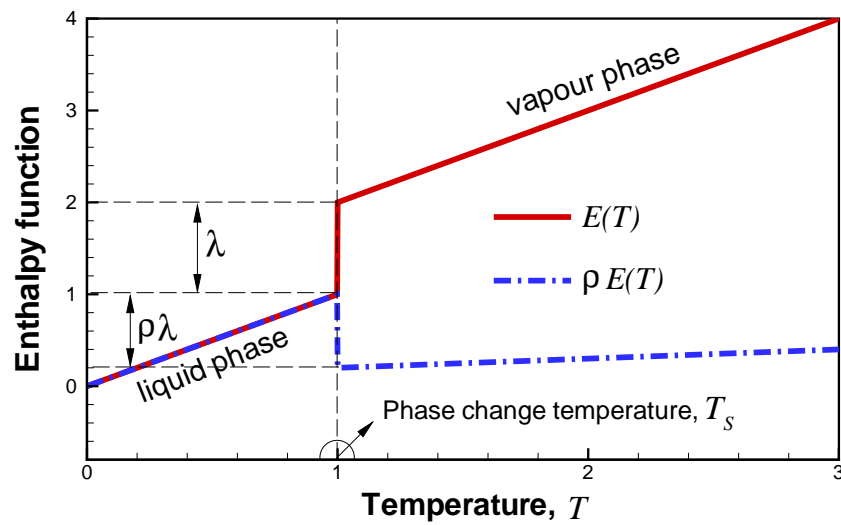


Figure 6.1: The negative jump of the enthalpy  $\rho E$  as a function of temperature  $T$ , where  $\rho_{liq} = 1$ ,  $\rho_{vap} = 0.1$ ,  $c_{liq,vap} = 1$ ,  $\lambda = 1$ ,  $T_S = 1$  and  $T_{ref} = 0$ .

The other alternative line of attack would seem to be a front-tracking method. A method which require to track the phase change front explicitly, which makes the location of the front central to the accuracy of the method [10, 13, 35, 75, 79].

## 6.2.2 Analytical work

It would also be interesting to investigate the stability of non-stationary solutions. In Section 3.2, a self-similar solutions to a one-dimensional problem were discussed, and these could be taken as the base states for a stability analysis. The self-similar

solutions are stationary when written in terms of the similarity variable  $\eta = x/\sqrt{t}$ . Hence, classical linear stability theory can be applied in the similarity coordinates [6, 61].

Allowing for the presence of dissolved minerals, either with a temperature controlled solubility [62] or which accumulate at the phase-change front when the fluid vaporises [32]. This would introduce an extra scalar field, which would be subject to advection and diffusion at different rates from the temperature and would also affect the fluid density, and would presumably make throughflow a more important influence on stability.

# Appendix A

## Determination of minimum heat output

We will determine the minimum heat flux necessary at  $x = 0$  to cause the front to approach  $x = 0$ . The situation we are after is where the front position  $S \rightarrow 0$ , i.e. liquid region is infinitesimally thin (but still exists, so a latent heat contribution is required).

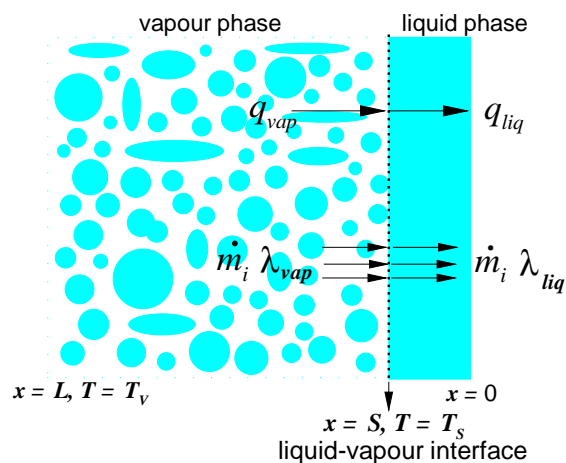


Figure A.1: Energy balance across a liquid-vapour interface.

The energy conservation across the liquid-vapour interface as illustrated in Figure A.1 yields

$$q_{vap} - q_{liq} = -\lambda \dot{m}_i, \quad (\text{A.1})$$

where  $\dot{m}_i$  is the reference mass flux (see (3.16)),  $\lambda = \lambda_{vap} - \lambda_{liq}$  is the latent heat. From Fourier's law  $q_{vap} = -k_{m,vap} \frac{dT_{vap}}{dx}$ , where  $k_{m,vap}$  is the thermal conductivity of the vapour phase. Moreover,  $q_{liq}$  is the minimum heat flux required at  $x = 0$  to cause the front to approach the liquid boundary, so (A.1) yields

$$\left. \frac{dT_{vap}}{dx} \right|_{x=0} = -\frac{1}{k_{m,vap}} (q_{liq} - \lambda \dot{m}_i), \quad (\text{A.2})$$

In the above constant heat flux condition at the liquid boundary,  $q_{liq}$  is still the unknown minimum heat flux. For this, the governing energy equation is

$$k_{m,vap} \frac{d^2 T_{vap}}{dx^2} - c_{p,vap} \dot{m}_i \frac{dT_{vap}}{dx} = 0, \quad 0 < x < L, \quad (\text{A.3})$$

with a constant temperature  $T = T_V$  at the vapour boundary (see Figure A.1). Integrating (A.3) subject to the appropriate boundary conditions yields the temperature distribution

$$T_{vap}(x) = T_V + \frac{1}{\dot{m}_i c_{p,vap}} (q_{liq}^{mini} - \lambda \dot{m}_i) [\exp(Pec_i) - \exp(Pec_i x^*)], \quad (\text{A.4})$$

where  $Pec_i$  is the reference Peclet number based on reference mass flux (see (3.17)) and  $x^* = x/L$ . Evaluating (A.4) at  $x = 0$ , with the condition that  $T_{vap}(0) = T_S$ , so the front is at the boundary, we get

$$q_{liq}^{mini} = \frac{Pec_i k_{vap}}{c_{p,vap} L} \left[ \lambda + \frac{c_{p,vap} (T_V - T_S)}{1 - \exp(Pec_i)} \right]. \quad (\text{A.5})$$

The heat flux condition for the case with no through flow is obtained by taking the limit of (A.5) as  $Pec_i \rightarrow 0$ , yielding

$$q_{liq}^{mini} \rightarrow \frac{k_{vap} (T_V - T_S)}{L}, \quad \text{as } Pec_i \rightarrow 0. \quad (\text{A.6})$$

# Appendix B

## Derivation of Rayleigh-Taylor instability in a porous medium

We consider the flow of a pair of incompressible fluids in a porous medium<sup>1</sup>. The vertical upward coordinate is denoted by  $x$ , with  $y$  and  $z$  being parallel to the horizontal interface which separates the two fluids. The denser fluid of density  $\rho_{liq}$  lies below the lighter fluid of density  $\rho_{vap} (< \rho_{liq})$  in a uniform gravitational field  $g$ . Note that we can invert the system by taking  $g < 0$ , i.e. liquid above vapour. Initially the interface which separates the two fluids is flat at  $x = 0$ .

As the medium is porous, the fluid flow is governed by Darcy's law (for a detailed discussion of flow in a porous medium see Chapter 2)

$$\vec{u}_i = -\frac{K_i}{\mu_i} \text{grad}(p_i + \rho_i g x), \text{ where } i = liq, vap, \quad (\text{B.1})$$

where  $x$  is the vertical axis with gravity  $g$ . The density and viscosity of the fluid are denoted as  $\rho$  and  $\mu$ , where  $K$  is the permeability, and where  $liq$  denotes the liquid (lower fluid) and  $vap$  denotes the vapour (upper fluid).

---

<sup>1</sup>Note that this derivation is adapted from [41, p. 823 - 829] for direct reference purposes, and has been obtained in the most suitable dimensionless form for our analysis.

The velocity potential is

$$\phi_i = -\frac{K_i}{\mu_i}(p_i + \rho_i g x), \text{ where } i = \text{liq, vap.} \quad (\text{B.2})$$

So on each side of the interface we have

$$\vec{u}_i = \text{grad } \phi_i, \text{ where } i = \text{liq, vap,} \quad (\text{B.3})$$

where

$$\phi = \begin{cases} \phi_{\text{liq}} & (x > h, \text{ liquid}) \\ \phi_{\text{vap}} & (x < h, \text{ vapour}). \end{cases} \quad (\text{B.4})$$

Let us introduce a small perturbation  $h(y, z, t)$  at the interface such that the front position originally at  $x = 0$  is translated to the new position  $x = h(y, z, t)$  with  $h = O(\epsilon)$  and  $\epsilon \ll 1$ . Hence the considered perturbation is

$$\Phi(x, y, z, t) = x - h(y, z, t), \text{ with } h(y, z, t) = \exp(i(l y + m z) + \sigma t), \quad (\text{B.5})$$

where  $\sigma$  is the growth rate,  $l$  and  $m$  are the wave numbers.

In the present analysis, we seek to determine the fate of the perturbed interface. So we will perturb the velocity and the pressure by using the following perturbed equations and keeping in mind that in the basic state the fluid has uniform velocity  $V$ ,

$$\vec{u}_i = V + \epsilon \vec{U}_i \quad (\text{B.6})$$

$$p_i = P_0 + \epsilon P_1, \text{ where } i = \text{liq, vap.} \quad (\text{B.7})$$

So, we have

$$\vec{U}_i = \nabla \phi_i, \text{ where } i = \text{liq, vap,} \quad (\text{B.8})$$

where the velocity potential satisfies Laplace's equation

$$\nabla^2 \phi_i = 0, \text{ where } i = \text{liq, vap,} \quad (\text{B.9})$$

The kinematic condition which must be satisfied by the disturbed velocity is

$$\frac{\partial \phi_i}{\partial x} = \varphi \frac{\partial x}{\partial t} + \frac{\partial \phi_i}{\partial y} \frac{\partial x}{\partial y} + \frac{\partial \phi_i}{\partial z} \frac{\partial x}{\partial z}, \text{ at } x = h, \text{ where } i = liq, vap, \quad (\text{B.10})$$

where  $\varphi$  is the porosity. Also (B.10) gives

$$\frac{\partial \phi_{liq}}{\partial x} = \frac{\partial \phi_{vap}}{\partial x} = \varphi \sigma \exp(i(l y + m z) + \sigma t). \quad (\text{B.11})$$

An appropriate form for the solutions of (B.9) for the potential functions is

$$\phi_{liq}(x, y, z, t) = F_{liq}(x, t) \exp[i(l y + m z)], \quad (\text{B.12})$$

$$\phi_{vap}(x, y, z, t) = F_{vap}(x, t) \exp[i(l y + m z)],$$

which gives

$$\frac{\partial^2 F_i}{\partial x^2} - (l^2 + m^2) F_i = 0, \text{ where } i = liq, vap. \quad (\text{B.13})$$

Solving (B.13) gives

$$F_{liq}(x, t) = G_{liq}(t) \exp \left[ -(l^2 + m^2)^{\frac{1}{2}} x \right], \quad x > 0, \quad (\text{B.14})$$

$$F_{vap}(x, t) = G_{vap}(t) \exp \left[ (l^2 + m^2)^{\frac{1}{2}} x \right], \quad x < 0.$$

Now substituting (B.14) into (B.12) we obtain

$$\phi_{liq}(x, y, z, t) = G_{liq}(t) \exp[i(l y + m z)] \exp \left[ -(l^2 + m^2)^{\frac{1}{2}} x \right], \quad x > 0, \quad (\text{B.15})$$

$$\phi_{vap}(x, y, z, t) = G_{vap}(t) \exp[i(l y + m z)] \exp \left[ (l^2 + m^2)^{\frac{1}{2}} x \right], \quad x < 0.$$

Thus the kinematic boundary condition (B.10) with  $x = 0$  yields

$$G_{liq}(t) = -G_{vap}(t) = -\frac{\varphi \sigma}{\sqrt{l^2 + m^2}} \exp(\sigma t). \quad (\text{B.16})$$

Hence

$$\begin{aligned} \phi_{liq}(x, y, z, t) &= -\frac{\varphi \sigma}{\sqrt{l^2 + m^2}} \exp(\sigma t) \exp[i(l y + m z)] \\ &\quad \exp \left[ -(l^2 + m^2)^{\frac{1}{2}} x \right], \quad x > 0, \end{aligned} \quad (\text{B.17})$$

$$\begin{aligned} \phi_{vap}(x, y, z, t) &= \frac{\varphi \sigma}{\sqrt{l^2 + m^2}} \exp(\sigma t) \exp[i(l y + m z)] \\ &\quad \exp \left[ (l^2 + m^2)^{\frac{1}{2}} x \right], \quad x < 0. \end{aligned}$$

The final condition that must be satisfied is pressure continuity at the interface. From (B.2) the pressure can be written in terms of the potential as

$$\begin{aligned} p_{liq} &= -\frac{\mu_{liq}}{K_{liq}} \Phi_{liq} - \rho_{liq} g x, \\ p_{vap} &= -\frac{\mu_{vap}}{K_{vap}} \Phi_{vap} - \rho_{vap} g x. \end{aligned} \quad (\text{B.18})$$

Now the perturbed form of the potential function is

$$\begin{aligned} \Phi_{liq} &= V x + \epsilon \phi_{liq}, \\ \Phi_{vap} &= V x + \epsilon \phi_{vap}, \end{aligned} \quad (\text{B.19})$$

where  $V$  is the velocity of the fluids and also the interface between them, if the steady state is of uniform velocity, it will lead to the [69] instability. Hence the pressure continuity condition at the interface gives

$$\frac{\mu_{liq}}{K_{liq}} (V x + \epsilon \phi_{liq}) + \rho_{liq} g x = \frac{\mu_{vap}}{K_{vap}} (V x + \epsilon \phi_{vap}) + \rho_{vap} g x. \quad (\text{B.20})$$

Substituting (B.17) into (B.20) we have

$$\begin{aligned} &\frac{\mu_{liq}}{K_{liq}} \left\{ V x - \frac{\epsilon \varphi \sigma}{\sqrt{l^2 + m^2}} \exp(\sigma t) \exp[i(l y + m z)] \exp \left[ -(l^2 + m^2)^{\frac{1}{2}} x \right] \right\} \\ &+ \rho_{liq} g x = \rho_{vap} g x + \\ &\frac{\mu_{vap}}{K_{vap}} \left\{ V x + \frac{\epsilon \varphi \sigma}{\sqrt{l^2 + m^2}} \exp(\sigma t) \exp[i(l y + m z)] \exp \left[ (l^2 + m^2)^{\frac{1}{2}} x \right] \right\}, \end{aligned} \quad (\text{B.21})$$

where

$$x = \epsilon \exp(\sigma t) \exp[i(l x + m y)] \ll 1.$$

This gives

$$\frac{\mu_{liq}}{K_{liq}} \left\{ V - \frac{\varphi \sigma}{\sqrt{l^2 + m^2}} \right\} - \rho_{liq} g = \frac{\mu_{vap}}{K_{vap}} \left\{ V + \frac{\varphi \sigma}{\sqrt{l^2 + m^2}} \right\} - \rho_{vap} g \quad (\text{B.22})$$

Solving (B.22) for the growth rate  $\sigma$  we obtain

$$\left( \frac{\mu_{liq}}{K_{liq}} + \frac{\mu_{vap}}{K_{vap}} \right) \frac{\varphi \sigma}{\sqrt{l^2 + m^2}} = \left( \frac{\mu_{liq}}{K_{liq}} - \frac{\mu_{vap}}{K_{vap}} \right) V - (\rho_{liq} - \rho_{vap}) g. \quad (\text{B.23})$$

The dispersion equation (B.23) shows that the system is unstable, i.e.,  $\sigma > 0$  if and only if

$$\left( \frac{\mu_{liq}}{K_{liq}} - \frac{\mu_{vap}}{K_{vap}} \right) V - (\rho_{liq} - \rho_{vap}) g > 0. \quad (\text{B.24})$$

Otherwise the system is stable, i.e.,  $\sigma < 0$ . In the case when the densities of both fluids are equal, i.e.,  $\rho_{liq} = \rho_{vap}$ , and the ratio of the viscosity to the permeability is larger for the upper fluid than for the lower fluid, then the system is unstable. The dispersion equation (B.23) is in the generalized form, if we consider the 2D problem, i.e.,  $l = 0$  or  $m = 0$ , then we have

$$\left( \frac{\mu_{liq}}{K_{liq}} + \frac{\mu_{vap}}{K_{vap}} \right) \frac{\varphi \sigma}{l} = \left( \frac{\mu_{liq}}{K_{liq}} - \frac{\mu_{vap}}{K_{vap}} \right) V - (\rho_{liq} - \rho_{vap}) g. \quad (\text{B.25})$$

If we assume that  $K = K_{liq} = K_{vap}$  and use the dimensional quantities (3.15) and (3.20), then (B.25) will take the dimensionless form

$$\hat{\sigma} = \left\{ \frac{R_2 - 1}{R_2 + 1} V^* - \frac{1 - R_1}{1 + R_2} R_2 R_3 \right\} \frac{\hat{l}}{\varphi}, \quad (\text{B.26})$$

where the dimensionless parameters are

$$\hat{\sigma} = \frac{\sigma \rho_{liq} c_{p,liq} L^2}{k_{m,liq}}, \quad \hat{l} = Ll. \quad (\text{B.27})$$

# Appendix C

## Formulation of the basic state with specified mass flux

The basic state of a geothermal system is assumed to be steady and independent of the horizontal variable  $y^*$ , so  $\Lambda_0$ ,  $\Theta_{liq}^0$ ,  $\Pi_0$  and  $\Theta_{vap}^0$  are all functions of  $x^*$  only. The velocity profile is assumed to be advective and conductive, so (4.16) gives

$$\text{Pressure profile} \quad \left\{ \begin{array}{l} \frac{\partial \omega_0}{\partial x^*} = 0, \quad \frac{\partial \Omega_0}{\partial x^*} = 0, \\ \omega_0 = - \left( \frac{\partial \Lambda_0}{\partial x^*} + R_3 \right), \\ \Omega_0 = - \frac{R_1 R_2 k}{C} \left( \frac{\partial \Pi_0}{\partial x^*} + R_1 R_3 \right). \end{array} \right. \quad (\text{C.1})$$

Substituting  $\omega_0$  and  $\Omega_0$  into the continuity equation yields

$$\left. \begin{array}{l} \frac{d^2 \Lambda_0}{dx^{*2}} = 0, \quad \Lambda_0(S_0^*) = \Pi_0(S_0^*) = P_{S_0}^*, \\ \frac{d^2 \Pi_0}{dx^{*2}} = 0, \quad \Lambda_0(0) = P_L^*, \quad \Pi_0(1) = P_V^*, \\ \left\{ R_1 R_2 \frac{d\Pi_0}{dx^*} - \frac{d\Lambda_0}{dx^*} \right\}_{x^*=S_0^*} = R_3 (1 - R_1^2 R_2). \end{array} \right\} \quad (\text{C.2})$$

In the above equations  $R_1 R_2 = R$ , where  $R_1$  is the ratio of densities,  $R_2$  is the ratio of dynamic viscosities and  $R$  is the ratio of kinematic viscosities.

The solutions of (C.2) are

$$\left. \begin{aligned} \Lambda_0(x^*) &= \left\{ \frac{P_S^* - P_L^*}{S_0^*} \right\} x^* + P_L^*, \\ \Pi_0(x^*) &= \left\{ \frac{P_V^* - P_S^*}{1 - S_0^*} \right\} x^* - \frac{S_0^* P_V^* - P_S^*}{1 - S_0^*}, \\ P_{S^*}^* &= \frac{R S_0^* P_V^* + P_L^* (1 - S_0^*)}{R S_0^* + 1 - S_0^*} - \frac{R_3 (1 - S_0^*) S_0^* (1 - R_1 R)}{R S_0^* + 1 - S_0^*}. \end{aligned} \right\} \quad (\text{C.3})$$

Using  $P_{S^*}^*$  and substituting  $\Lambda_0(x^*)$  and  $\Pi_0(x^*)$  into (C.1) yields

$$\omega_0 = -\frac{R}{R S_0^* + 1 - S_0^*} [(P_V^* - P_L^*) + R_3 \{S_0^* (1 - R_1) + R_1\}], \quad (\text{C.4})$$

and

$$\Omega_0 = -\frac{R k}{C (R S_0^* + 1 - S_0^*)} [(P_V^* - P_L^*) + R_3 \{S_0^* (1 - R_1) + R_1\}]. \quad (\text{C.5})$$

Now here two limiting cases can be considered.

1. If the interface is at  $x^* = 1$ , then  $S_0^* = 1$ , which means that the medium is filled with liquid (water). The reference Peclet number which is based on the resulting flow rate can be obtained by substituting  $S_0^* = 1$  into (C.4).

$$Pec_{i,liq} = -[(P_V^* - P_L^*) + R_3]. \quad (\text{C.6})$$

2. Secondly, if the interface is at  $x^* = 0$ , then  $S_0^* = 0$ , thus the porous layer is filled with vapour only. Substituting  $S_0^* = 0$  into (C.5) yields the following Peclet number based on a vapour filled medium.

$$Pec_{i,vap} = -\frac{R k}{C} [(P_V^* - P_L^*) + R_1 R_3]. \quad (\text{C.7})$$

In our study we have taken the reference case to be a vapour filled medium and for convenience we refer to the Peclet number as  $Pec_i$ .

Since the mass flux has been specified then

$$\begin{aligned}
\omega_0 &= -\frac{R}{R S_0^* + 1 - S_0^*} \left[ \underbrace{(P_V^* - P_L^*) + R_1 R_3 + R_3 S_0^* (1 - R_1)}_{\text{eqn. (C.7)}}, \right], \\
\omega_0 &= -\frac{R}{R S_0^* + 1 - S_0^*} \left[ \left\{ -\frac{C Pec_i}{k R} \right\} + R_3 S_0^* (1 - R_1) \right], \\
\omega_0 &= \underbrace{\frac{1}{R S_0^* + 1 - S_0^*}}_{=F_1(S_0^*)} \frac{C}{k} Pec_i \left[ 1 - R S_0^* \underbrace{\frac{R_3 k (1 - R_1)}{C Pec_i}}_{=G_1} \right], \\
\omega_0 &= \frac{C}{k} Pec_i \underbrace{F_1(S_0^*) [1 - R S_0^* G_1]}_{=F(S_0^*)}, \\
\omega_0 &= \frac{C}{k} Pec_i F(S_0^*). \tag{C.8}
\end{aligned}$$

and

$$\begin{aligned}
\Omega_0 &= -\frac{R k}{C (R S_0^* + 1 - S_0^*)} \left[ \underbrace{(P_V^* - P_L^*) + R_1 R_3 + R_3 S_0^* (1 - R_1)}_{\text{eqn. (C.7)}}, \right], \\
\Omega_0 &= -\frac{R k}{C (R S_0^* + 1 - S_0^*)} \left[ \left\{ -\frac{C Pec_i}{k R} \right\} + R_3 S_0^* (1 - R_1) \right]. \\
\Omega_0 &= Pec_i F(S_0^*). \tag{C.9}
\end{aligned}$$

The temperature distribution in the basic state of a geothermal system is assumed to be advective and conductive, so (4.18) gives the energy equations in the liquid and vapour phases.

$$\text{Temperature profile} \quad \begin{cases} \omega_0 \frac{\partial \Theta_{liq}^0}{\partial x^*} = \frac{\partial^2 \Theta_{liq}^0}{\partial x^{*2}}, \\ \Omega_0 \frac{\partial \Theta_{vap}^0}{\partial x^*} = \frac{\partial^2 \Theta_{vap}^0}{\partial x^{*2}}. \end{cases} \tag{C.10}$$

Substituting  $\omega_0$  and  $\Omega_0$  from (C.8) and (C.9) into (C.10) yields

$$\left. \begin{aligned} \frac{d^2\Theta_{liq}}{dx^{*2}} - \frac{C Pec_i F(S_0^*)}{k} \frac{d\Theta_{liq}}{dx^*} &= 0, \\ \frac{d^2\Theta_{vap}}{dx^{*2}} - Pec_i F(S_0^*) \frac{d\Theta_{vap}}{dx^*} &= 0. \end{aligned} \right\} \quad (C.11)$$

The solutions for the temperature profiles (C.11) are obtained and discussed for two different sets of boundary conditions: (i) constant temperature at the lower boundary  $x = 0$  and (ii) constant heat flux  $q_{liq}$  at  $x = 0$  in Sections 3.1.1 and 3.1.2, respectively.

# Appendix D

## Pressure continuity condition at the phase change front

The pressure condition at a sharp interface can be obtained by simply considering continuity of pressure across the phase change interface.

$$P_{liq}^*(S^*, y^*, t^*) = P_{vap}^*(S^*, y^*, t^*), \quad (\text{D.1})$$

where  $P_{liq}^*$  and  $P_{vap}^*$  represent the pressures for the liquid and vapour phases. The dimensionless front position is denoted by  $S^*$ . Now we will linearize (D.1) using the following perturbation equations

$$P_{liq}^* = \Lambda_0 + \epsilon \Lambda_1, \quad P_{vap}^* = \Pi_0 + \epsilon \Pi_1, \quad S^* = S_0^* + \epsilon S_1^*(y^*, t^*), \quad (\text{D.2})$$

which yields

$$\begin{aligned} & \Lambda_0(S_0^* + \epsilon S_1^*, y^*, t^*) + \epsilon \Lambda_1(S_0^* + \epsilon S_1^*, y^*, t^*) \\ &= \Pi_0(S_0^* + \epsilon S_1^*, y^*, t^*) + \epsilon \Pi_1(S_0^* + \epsilon S_1^*, y^*, t^*). \end{aligned} \quad (\text{D.3})$$

A Taylor-series expansion of (D.3) about the unperturbed interface  $S_0^*$  leads to

$$\begin{aligned} & \Lambda_0(S_0^*, y^*, t^*) + \epsilon S_1^* \left. \frac{\partial \Lambda_0}{\partial x^*} \right|_{x^*=S_0^*} + \epsilon \left\{ \Lambda_1(S_0^*, y^*, t^*) + \epsilon S_1^* \left. \frac{d\Lambda_1}{dx^*} \right|_{x^*=S_0^*} \right\} \\ & = \Pi_0(S_0^*, y^*, t^*) + \epsilon S_1^* \left. \frac{\partial \Pi_0}{\partial x^*} \right|_{x^*=S_0^*} + \epsilon \left\{ \Pi_1(S_0^*, y^*, t^*) + \epsilon S_1^* \left. \frac{d\Pi_1}{dx^*} \right|_{x^*=S_0^*} \right\}. \end{aligned} \quad (\text{D.4})$$

Equating the terms proportional to  $\epsilon^0$  in (D.4) gives the following pressure continuity condition in the unperturbed state.

$$\Lambda_0(S_0^*, y^*, t^*) = \Pi_0(S_0^*, y^*, t^*). \quad (\text{D.5})$$

The pressure continuity condition in the perturbed state is obtained by equating the terms proportional to  $\epsilon^1$  in (D.4) and retaining the first order terms in  $\epsilon$  yields

$$\Lambda_1(S_0^*) + S_1^* \left. \frac{d\Lambda_0}{dx^*} \right|_{x^*=S_0^*} = \Pi_1(S_0^*) + S_1^* \left. \frac{d\Pi_0}{dx^*} \right|_{x^*=S_0^*}. \quad (\text{D.6})$$

In the above equation (D.6),  $\frac{d\Lambda_0}{dx^*}$  and  $\frac{d\Pi_0}{dx^*}$  denote the unperturbed pressure gradients in the liquid and in the vapour phase, respectively. In our analysis of the basic state of a geothermal system we considered the following two cases.

1. In the first case we assumed that the fluid is stationary, i.e,  $\omega_0 = \Omega_0 = 0$  then (C.1) leads to

$$\left. \begin{aligned} \left. \frac{d\Lambda_0}{dx^*} \right|_{x^*=S_0^*} &= -R_3, \\ \left. \frac{d\Pi_0}{dx^*} \right|_{x^*=S_0^*} &= -R_1 R_3. \end{aligned} \right\} \quad (\text{D.7})$$

Substituting (D.7) into (D.6) gives

$$\Lambda_1(S_0^*) = \Pi_1(S_0^*) + S_1^* R_3 (1 - R_1). \quad (\text{D.8})$$

Equation (D.8) represents the relationship between the pressures on either side of the phase change front.

2. In the second case we considered fluid flow in the basic state. (C.3) and (C.7) leads to

$$\left. \begin{aligned} \frac{d\Lambda_0}{dx^*} \Big|_{x^*=S_0^*} &= -F_1(S_0^*) \left\{ \frac{C}{k} Pec_i + S_0^* R_1 R R_3 - S_0^* R_3 + R_3 \right\}, \\ \frac{d\Pi_0}{dx^*} \Big|_{x^*=S_0^*} &= -F_1(S_0^*) \left\{ \frac{C}{k R} Pec_i + S_0^* R_1 R R_3 - S_0^* R_3 + R_1 R_3 \right\}. \end{aligned} \right\} \text{(D.9)}$$

Substituting (D.9) into (D.6) yields

$$\Lambda_1(S_0^*) = \Pi_1(S_0^*) + S_1^* N_0, \quad \text{(D.10)}$$

where

$$N_0 = F_1(S_0^*) \frac{C}{k} \frac{Pec_i}{R} \left\{ (R - 1) + \frac{k R R_3 (1 - R_1)}{C Pec_i} \right\}.$$

Equation (D.10) denotes the pressure continuity condition across the interface in the perturbed state with through flow.

# Appendix E

## Procedure for continuation method in Maple

We present a Maple procedure to implement a crude continuation method, which should be able to track along a solution curve once the implicit plot has suggested its location. This procedure was used to generate the plots presented in section 4.4.6. Taking the growth rate  $\sigma = \sigma_{\text{guess}}$  as the initial guess it finds  $\sigma(l_{\text{mini}})$ ; it then increments  $l$  (wave number) at each step and searches for  $\sigma$  in an interval (of width proportional to  $2\delta$ ) around the previous output value for  $\sigma$ . It returns a plot of  $\sigma(l)$ , and the output values are also written to a specified file.

```
> with(Statistics):  
>  $\mathcal{E} \equiv \text{LHS}(4.72) - \text{RHS}(4.72)$ :  
>  $\mathcal{E}_1 := \text{subs}(\Theta_0 = C * \text{RHS}(4.59), \mathcal{E})$ :  
> proc( $R_3, iS, l_{\text{mini}}, l_{\text{max}}, nl, l_{\text{guess}}, \delta, \text{digits}, \text{filout}$ ) global  $S_0 i$ ;  
local  $i, li, \sigma_i, l_{\text{data}}, \sigma_{\text{data}}, \text{fd}$ ;  
 $\text{fd} := \text{open}(\text{filout}, \text{WRITE})$ ;  
    Digits := digits;
```

```

Sout( $R_3$ );
 $\sigma_i :=$  fsolve(subs(parvals union  $R_3 = R_3, S_0 = S_{0i}[iS], l_{\text{mini}}, \mathbb{E}_1) = 0, \sigma =$ 
 $\sigma_{\text{guess}}$ );
 $l_{\text{data}} := [l_{\text{mini}}]$ ;
 $\sigma_{\text{data}} := [\sigma_i]$ ;
fprintf(fd, "%f \n",  $l_{\text{mini}}, \sigma_i$ );
for i from 1 to  $nl$  do
 $l_i :=$  evalf( $l_{\text{mini}} + (l_{\text{max}} - l_{\text{mini}}) * i / nl$ );
 $\sigma_i :=$  fsolve(subs(parvals union  $R_3 = R_3, S_0 = S_{0i}[iS], l = l_i, \mathbb{E}_1) = 0,$ 
 $\sigma = \sigma_i - \delta * \text{abs}(\sigma_i) .. \sigma_i + \delta * \text{abs}(\sigma_i)$ );
 $l_{\text{data}} := [\text{op}(l_{\text{data}}), l_i]$ ;
 $\sigma_{\text{data}} := [\text{op}(\sigma_{\text{data}}), \sigma_i]$ ;
fprintf(fd, "%f \n",  $l_i, \sigma_i$ );
od;
close(fd);
return(LineChart( $\sigma_{\text{data}}, x^* \text{coords} = l_{\text{data}}$ ));
end:

```

In the above procedure “parvals” is used as abbreviation for the different parameters (for the numerical values see Table 2.2).

# Bibliography

- [1] P. Amili and Y. C. Yortsos. Stability of heat pipes in vapor-dominated systems. *International Journal of Heat and Mass Transfer*, 47:1233 – 1246, 2004.
- [2] H. H. Bau and K. E. Torrance. Boiling in low-permeability porous materials. *International Journal of Heat and Mass Transfer*, 25:45 – 55, 1982.
- [3] J. Bear. *Dynamics of Fluids in Porous Media*. American Elsevier , New York, 1972.
- [4] J. Bear and J-M. Buchlin. *Modelling and applications of transport phenomena in porous media*. Kluwer Academic Publishers Group, USA, 1981.
- [5] G. Beckett, J. A. Mackenzie, and M. L. Robertson. A moving mesh finite element method for the solution of two-dimensional Stefan problems. *Journal of Computational Physics*, 168(2):500 – 518, 2001.
- [6] A. J. Bernoff and T. Witelski. Stability and dynamics of self-similarity in evolution equations. *Journal of Engineering Mathematics*, 66:11–31, 2010.
- [7] M. G. Blocher, G. Zimmermann, I. Moeck, W. Brandt, A. Hassanzadegan, and F. Magri. 3D numerical modeling of hydrothermal processes during the life time of a deep geothermal reservoir. *Geofluids*, 10:406 – 421, 2010.

- [8] G. Bodvarsson, K. Pruess, and M. Lippmann. Modeling of geothermal systems. *Journal of Petroleum Technology*, 38(9):1007–1021, 1986.
- [9] C. Bonacina, G. Comini, A. Fasano, and M. Primicerio. Numerical solution of phase change problems. *International Journal of Heat and Mass Transfer*, 16:1825 – 1832, 1973.
- [10] L. J. Bridge. *Computational interface capturing methods for phase change in porous media*. PhD in Mathematics, The University Of British Columbia, 2006.
- [11] V. P. Carey. *Liquid-Vapor Phase-Change Phenomena*. Taylor & Francis, Inc, New York, 2007.
- [12] A. O. P. Chiareli, H. E. Huppert, and M. G. Worster. Segregation and flow during the solidification of alloys. *Journal of Crystal Growth*, 139:134 – 146, 1994.
- [13] J. Crank. *Free and Moving Boundary Problems*. Clarendon Press, London, 1984.
- [14] H. Darcy. *Les Fontaines*. Victor Dalmont, Paris, 1856.
- [15] A. W. Date. A strong enthalpy formulation for the Stefan problem. *International Journal of Heat and Mass Transfer*, 34(9):2231 – 2235, 1991.
- [16] M. H. Dickson and M. Fanelli. *Geothermal Energy*. John Wiley & Sons, New York, 1995.
- [17] C. Doughty and K. Pruess. A semianalytical solution for heat-pipe effects near high-level nuclear waste packages buried in partially saturated geological media. *International Journal of Heat and Mass Transfer*, 31:79 – 90, 1988.

- [18] P. G. Drazin. *Introduction to Hydrodynamic Stability*. Cambridge University press, Cambridge, 2002.
- [19] J. E. Eastwood and T. J. T. Spanos. Stability of a stationary steam-water front in a porous medium. *Transport in Porous Media*, 14:1 – 21, 1994.
- [20] M. A. Grant. Mapping Kamojang reservoir. *Geothermal Resources Council Transactions*, 3:271 – 274, 1979.
- [21] M. A. Grant. Geothermal reservoir modeling. *Geothermics*, 12:251 – 263, 1983.
- [22] M. A. Grant. Mathematical modelling of Wairakei geothermal field. *The ANZIAM Journal*, 50:426 – 434, 2009.
- [23] M. A. Grant and P. F. Bixley. *Geothermal Reservoir Engineering*. Elsevier Science & Technology, USA, 2011.
- [24] S. C. Gupta. *The classical Stefan problem: basic concepts, modelling and analysis*. Elsevier, Netherlands, 2003.
- [25] J. Hager and S. Whitaker. Vapor–liquid jump conditions within a porous medium: Results for mass and energy. *Transport in Porous Media*, 40:73 – 111, 2000.
- [26] K. T. Harris, A. Haji-Sheikh, and A. G. A. Nnanna. Phase-change phenomena in porous media - a non-local thermal equilibrium model. *International Journal of Heat and Mass Transfer*, 44:1619 – 1625, 2001.
- [27] T. Hiroakia. On the stability of vapor film in pool film boiling. *International Journal of Heat and Mass Transfer*, 31:129 – 134, 1988.

- [28] A. Il'ichev and G. Tsypkin. Catastrophic transition to instability of evaporation front in a porous medium. *European Journal of Mechanics B/Fluids*, 27:665 – 677, 2008.
- [29] A. Il'ichev and G. Tsypkin. Instabilities of uniform filtration flows with phase transition. *Journal of Experimental and Theoretical Physics*, 107:699 – 711, 2008.
- [30] A. Il'ichev and G. Tsypkin. Influence of advective transfer of energy on stability of water over steam in geothermal systems. *Doklady Physics*, 56:227–231, 2011.
- [31] A. T. Il'ichev and G. G. Tsypkin. Transition to instability of the interface in geothermal systems. *European Journal of Mechanics B/Fluids*, 24:491 – 501, 2005.
- [32] A. T. Il'ichev, G. G. Tsypkin, D. Pritchard, and C. N. Richardson. Instability of the salinity profile during the evaporation of saline groundwater. *Journal of Fluid Mechanics*, 614:87 – 104, 2008.
- [33] S. E. Ingebritsen and M. L. Sorey. Vapor-dominated zones within hydrothermal systems: Evolution and natural state. *Journal of Geophysical Research*, 93:13,635 – 13,655, 1988.
- [34] E. Javierre, C. Vuik, F. J. Vermolen, and S. van der Zwaag. A comparison of numerical models for one-dimensional Stefan problems. *Journal of Computational and Applied Mathematics*, 192:445–459, 2006.
- [35] W. DeLima-Silva Jr. and L. C. Wrobel. A front-tracking BEM formulation for one-phase solidification/melting problems. *Engineering Analysis with Boundary Elements*, 16(2):171 – 182, 1995.

- [36] C. Karcher and U. Muller. Convection in a porous medium with solidification. *Fluid Dynamics Research*, 15:25 – 42, 1995.
- [37] M. Kaviany. Laminar flow through a porous channel bounded by isothermal parallel plates. *International Journal of Heat and Mass Transfer*, 28:851 – 858, 1985.
- [38] M. Kaviany. *Principles of Heat Transfer in Porous Media*. Springer-Verlag Inc, New York, 1995.
- [39] M. Kutz. *Mechanical Engineers' Handbook*. John Wiley & Sons, 1998.
- [40] A. Lagarde. Considérations sur le transfert de chaleur en milieux poreux. *Revue de l'Institute Francais du Petrole*, 20:383–445, 1965.
- [41] L. G. Leal. *Advanced Transport Phenomena: Fluid Mechanics and Convective Transport Processes*. Cambridge University Press, New York, 2007.
- [42] H. Lein and R. S. Tankin. Natural convection in porous media-II. Freezing. *International Journal of Heat and Mass Transfer*, 35(1):187 – 194, 1992.
- [43] J. W. Lund. Direct utilization of geothermal energy resources worldwide 2005. *Proceedings World Geothermal Congress*, pages 22–29, 2005.
- [44] J. W. Lund and D. H. Freeston. World-wide direct uses of geothermal energy 2000. *Geothermics*, 30(1):29 – 68, 2001.
- [45] J. A. Mackenzie and M. L. Robertson. The numerical solution of one-dimensional phase change problems using an adaptive moving mesh method. *Journal of Computational Physics*, 161:537, 2000.

- [46] J. A. Mackenzie and M. L. Robertson. A moving mesh method for the solution of the one-dimensional phase field equations. *Journal of Computational Physics*, 181:526 – 544, 2002.
- [47] S. Madruga, C. Perez-Garc, G. Lebon, and E. T. S. Ingenieros. Convective instabilities in two superposed horizontal liquid layers heated laterally. *Physical Review E*, 68, 2003.
- [48] J. C. Martin, R. E. Wegner, and F. J. Kelsey. One-dimensional convective and conductive geothermal heat flow. *Proceedings, Second Workshop Geothermal Reservoir Engineering*, 1:3, 1976.
- [49] R. M. M. Mattheij, S. W. Rienstra, and J. H. M. ten Thijsse Boonkamp. *Partial differential equations: modeling, analysis, computation*. Society for Industrial and Applied Mathematics, Philadelphia, PA, USA, 2005.
- [50] A. Minissale. The Larderello geothermal field: a review. *Earth-Science Reviews*, 31:133 – 151, 1991.
- [51] A. S. Mujumdar. *Handbook of Industrial Drying*. CRC Press, Taylor & Francis Group, LLC, Boca Raton, Florida, USA, third edition, 2007.
- [52] B. Nedjar. An enthalpy-based finite element method for nonlinear heat problems involving phase change. *Computers & Structures*, 80(1):9 – 21, 2002.
- [53] D. A. Nield. Estimation of the stagnant thermal conductivity of saturated porous media. *International Journal of Heat and Mass Transfer*, 34(6):1575 – 1576, 1991.

- [54] D. A. Nield. A note on the modeling of local thermal non-equilibrium in a structured porous medium. *International Journal of Heat and Mass Transfer*, 45:4367 – 4368, 2002.
- [55] D. A. Nield and A. Bejan. *Convection in Porous Media*. Springer-Verlag, New York, 1992.
- [56] M. J. O’Sullivan, A. Yeh, and W. I. Mannington. A history of numerical modelling of the Wairakei geothermal field. *Geothermics*, 38:155 – 168, 2009.
- [57] O. Ozen. *Effect of vapor dynamics on interfacial instabilities*. PhD in Chemical engineering, University Of Florida, 2004.
- [58] O. Ozen, D. Johnson, and R. Narayanan. Observations on interfacial convection in multiple layers without and with evaporation. *Lecture Notes in Physics*, 628:59 – 77, 2003.
- [59] C. H. Panzarella, S. H. Davis, and S. G. Bankoff. Nonlinear dynamics in horizontal film boiling. *Journal of Fluid Mechanics*, 402:163 – 194, 2000.
- [60] I. Pestov. Modelling structured geothermal systems: Application of dimensional methods. *Mathematical and Computer Modelling*, 25(7):43 – 63, 1997.
- [61] D. Pritchard. The linear stability of double-diffusive miscible rectilinear displacements in a Hele-Shaw cell. *European Journal of Mechanics - B/Fluids*, 28(4):564 – 577, 2009.
- [62] D. Pritchard and C. N. Richardson. The effect of temperature-dependent solubility on the onset of thermosolutal convection in a horizontal porous layer. *Journal of Fluid Mechanics*, 571:59 – 95, 2007.

- [63] A. Prosperetti. Boundary conditions at a liquid-vapour interface. *Meccanica*, 14(1):34 – 47, 1979.
- [64] K. Pruess. Numerical modeling of geothermal systems. *Mathematical Modeling of Fluid Flow and Heat Transfer*, (3):27 – 46, 2002.
- [65] P. S. Ramesh and K. E. Torrance. Stability of boiling in porous media. *International Journal of Heat and Mass Transfer*, 33:1895 – 1908, 1990.
- [66] L. Rayleigh. Investigation of the character of the equilibrium of an incompressible heavy fluid of variable density. *Proceedings of the London Mathematical Society*, 14:170 – 177, 1883.
- [67] G. Rousseaux, A. De Wit, and M. Martin. Viscous fingering in packed chromatographic columns: linear stability analysis. *Journal of Chromatography A*, 1149:254 – 273, 2007.
- [68] A. Rubin and S. Schweitzer. Heat transfer in porous media with phase change. *International Journal of Heat and Mass Transfer*, 15:43 – 60, 1972.
- [69] P. G. Saffman and G. I. Taylor. The penetration of a fluid into a porous medium or Hele-Shaw cell containing a more viscous liquid. *Proceedings of the Royal Society of London, Series A*, 245:312 – 329, 1958.
- [70] A. Sahli, C. Moyne, and D. Stemmelen. Boiling stability in a porous medium heated from below. *International Journal of Heat and Mass Transfer*, 82:527 – 545, 2010.
- [71] B. Sarler. Stefan’s work on solid-liquid phase changes. *Engineering Analysis with Boundary Elements*, 16:83 – 92, 1995.

- [72] C. Satik, M. Parlak, and Y. C. Yortsos. A study of steady-state steam-water counterflow in porous media. *International Journal of Heat and Mass Transfer*, 34:1755 – 1771, 1991.
- [73] G. Schubert and J. M. Straus. Steam-water counterflow in porous media. *Journal of Geophysical Research*, 84:1621 – 1628, 1979.
- [74] T. M. Shaw. Drying as an immiscible displacement process with fluid counterflow. *Physical Review Letters*, 59(15):1671 – 1674, Oct 1987.
- [75] W. Shyy, H. S. Udaykumar, and S.-J. Liang. An interface tracking method applied to morphological evolution during phase change. *International Journal of Heat and Mass Transfer*, 36(7):1833 – 1844, 1993.
- [76] A. Solomon. A note on the Stefan number in slab melting and solidification. *Letters in Heat and Mass Transfer*, 8:229 – 235, 1981.
- [77] J. M. Straus and G. Schubert. Gravitational stability of water over steam in vapor-dominated geothermal systems. *Journal of Geophysical Research*, 85:6505 – 6512, 1980.
- [78] J. M. Straus and G. Schubert. One-dimensional model of vapor-dominated geothermal systems. *Journal of Geophysical Research*, 86:9433 – 9438, 1981.
- [79] E. Tayfun and Tezduyar. Interface-tracking and interface-capturing techniques for finite element computation of moving boundaries and interfaces. *Computer Methods in Applied Mechanics and Engineering*, 195(23-24):2983 – 3000, 2006.
- [80] K. E. Torrance. Phase-change heat transfer in porous media. *Heat Transfer*, 1:181 – 188, 1986.

- [81] J. Tracey. Penetrative convection and multi-component diffusion in a porous medium. *Advances in Water Resources*, 22(4):399 – 412, 1998.
- [82] A. H. Truesdell and D. E. White. Production of super-heated steam from vapor-dominated geothermal reservoirs. *Geothermics*, 2:154 – 173, 1973.
- [83] G. Tsypkin and A. Il'ichev. Gravitational stability of the interface in water over steam geothermal reservoirs. *Transport in Porous Media*, 55:183 – 199, 2004.
- [84] K. S. Udell. Heat transfer in porous media heated from above with evaporation, condensation, and capillary effects. *Journal of Heat Transfer*, 105(3):485 – 492, 1983.
- [85] K. S. Udell. Heat transfer in porous media considering phase change and capillarity—the heat pipe effect. *International Journal of Heat and Mass Transfer*, 28:485 – 495, 1985.
- [86] K. Vafai and S. J. Kim. Forced convection in a channel filled with a porous medium: an exact solution. *ASME Journal of Heat Transfer*, 111:1103 – 1106, 1989.
- [87] V. Voller and M. Cross. Accurate solutions of moving boundary problems using the enthalpy method. *International Journal of Heat and Mass Transfer*, 24(3):545 – 556, 1981.
- [88] V. R. Voller. An implicit enthalpy solution for phase change problems: with application to a binary alloy solidification. *Applied Mathematical Modelling*, 11(2):110 – 116, 1987.

- [89] V. R. Voller. An enthalpy method for modeling dendritic growth in a binary alloy. *International Journal of Heat and Mass Transfer*, 51(3-4):823 – 834, 2008.
- [90] V. R. Voller. A numerical method for the Rubinstein binary-alloy problem in the presence of an under-cooled liquid. *International Journal of Heat and Mass Transfer*, 51:696 – 706, 2008.
- [91] V. R. Voller and L. Shadabi. Enthalpy methods for tracking a phase change boundary in two dimensions. *International Communications in Heat and Mass Transfer*, 11:239 – 249, 1984.
- [92] D. E. White, L. J. P. Muffler, and A. H. Truesdell. Vapor-dominated hydrothermal systems compared with hot water systems. *Economic Geology*, 66:75 – 97, 1971.
- [93] Y. Yano and T. Ishido. Numerical modeling of the evolution of two-phase zones under a fractured caprock. *Geothermics*, 24:507 – 521, 1995.
- [94] R. M. Young. Phase transitions in one-dimensional steady state hydrothermal flows. *Journal of Geophysical Research*, 101:18,011 – 18,022, 1996.
- [95] R. M. Young. Classification of one-dimensional steady-state two-phase geothermal flows including permeability variations-I. Theory and special cases. *International Journal of Heat and Mass Transfer*, 41:3919 – 3935, 1998.